nature nanotechnology

NOVEMBER 2012 VOL 7 NO 11
www.nature.com/naturenanotechnology

AFM in cancer diagnosis

GRAPHENE
Conductance of a single nanoribbon

MOLECULAR MACHINES
Defying microscopic reversibility

METAL DICHALCOGENIDES
Semiconductors in 2D

Probing the determinants of cellular elasticity by AFM

Inauguraldissertation
zur
Erlangen der Würde eines Doktors der Philosophie
vorgelegt der
Philosophisch-Naturwissenschaftlichen Faklutät
der Universität Basel

von
Marija Plodinec
Aus Staro Cice, Kroatien

Basel, 2012

Genehmigt von der Philosophisch-Naturwissenschaftlichen Fakultät
auf Antrag von

Prof. Dr. Ueli Aebi
Prof. Dr. Harald Herrmann
PD Dr. Cora-Ann Schoenenberger

Basel, den 14. December 2010

Prof. Dr. Martin Spiess
Dekan der Philosophisch Naturwissen-
Schaftlichen Fakultät

This thesis is dedicated
to Marko, Jana and Leon

Abstract

Cells within tissues continuously encounter mechanical challenges to which they respond by remodelling their cytoskeleton. Cellular interactions as well as the microenvironment regulate the cell's mechanical response under physiological and pathological conditions. An overview of the functional aspects associated with cell cytoskeleton, extracellular matrix (ECM) components and mechanical properties in health and disease is provided in Chapter 1. Atomic force microscopy (AFM) provides the ability to image, measure and mechanically manipulate major cytoskeletal and ECM components that contribute to the mechanical properties of cells and tissues, as will be presented in Chapter 2. Intermediate filaments (IFs) are one of the three main cytoskeletal components, and are essential determinants of cell shape and cytoskeletal integrity. In particular, they are considered the key responsive elements to extreme forces and deformations in living cells. However, their contribution to physiological nanoscale forces has received little attention. This has prompted us to employ a combined AFM/optical microscopy approach to examine the contribution of the vimentin IF network to the mechanical response of rat fibroblasts at high sensitivity and spatial resolution under near-physiological conditions (Chapter 3). To specifically target and modulate the vimentin network, fibroblasts were transfected with GFP-desmin variants. Depending on the variant desmin, transfectants were either softer or stiffer than untransfected fibroblasts. These findings demonstrated that specific alterations in the IF filament structure and architecture have a direct impact on the nanomechanical properties of cells. Despite its unique potential for probing cellular nanomechanics under physiological conditions (Chapters 2 and 3), AFM has so far not been applied to three-dimensional (3D) culture models or intact tumor tissues, which more accurately reflect the *in vivo* characteristics of cancer. As a first step towards this goal, we have systematically investigated nanomechanical changes associated with tumorigenic transformation and hypoxia in 3D culture models (Chapter 4). AFM stiffness maps from 3D spheroids showed that tumor spheroids were softer than their normal counterparts. In particular, the core was significantly softer than peripheral regions. To test whether nanomechanical properties could be measured in complex, organized tissues, we extended our studies to intact mammary tumor tissues ex vivo. The nanomechanical response of mammary tissues from a transgenic mouse model for human breast carcinoma and from human patient biopsies is presented in Chapter 5. AFM measurements revealed a gradual softening from the periphery to the core in human and murine cancer tissues while stromal tissue at the tumor periphery was stiffer than the underlying tumor. Comparison of the nanomechanical signature of human tissue samples with the corresponding histopathological diagnosis suggested a high ratio of soft versus stiff regions to be an indication of a more aggressive phenotype. Taken together, data presented in this thesis provide evidence that the nanomechanical properties may be used as a diagnostic marker for tumorigenesis.

Table of Contents

List of Figures

Chapter 1

General introduction

1.1 Cell mechanics

The field of cell mechanics studies the relationship between forces and deformations when these are applied to cells. The nature of the cell and tissue-associated forces can be parallel, such as the shear stress induced by blood flow in vessels, or perpendicular, such as the compressive or tensile stress induced by load bearing from the surrounding microenvironment (Figure 1-1; Butcher, Alliston et al. 2009). According to this simplified definition, measurements of cell mechanics reflect the properties of cell stiffness and viscoelasticity, although the term cell mechanics is often used in a much broader sense. For instance, cell traction forces, which are the contractile forces and deformations that cells actively exert on their substrates, are also considered in cell mechanics. While the concepts of cell stiffness and viscoelasticity apply to all cells, cell traction forces require the presence of a substrate and can only be applied by adherent cells.

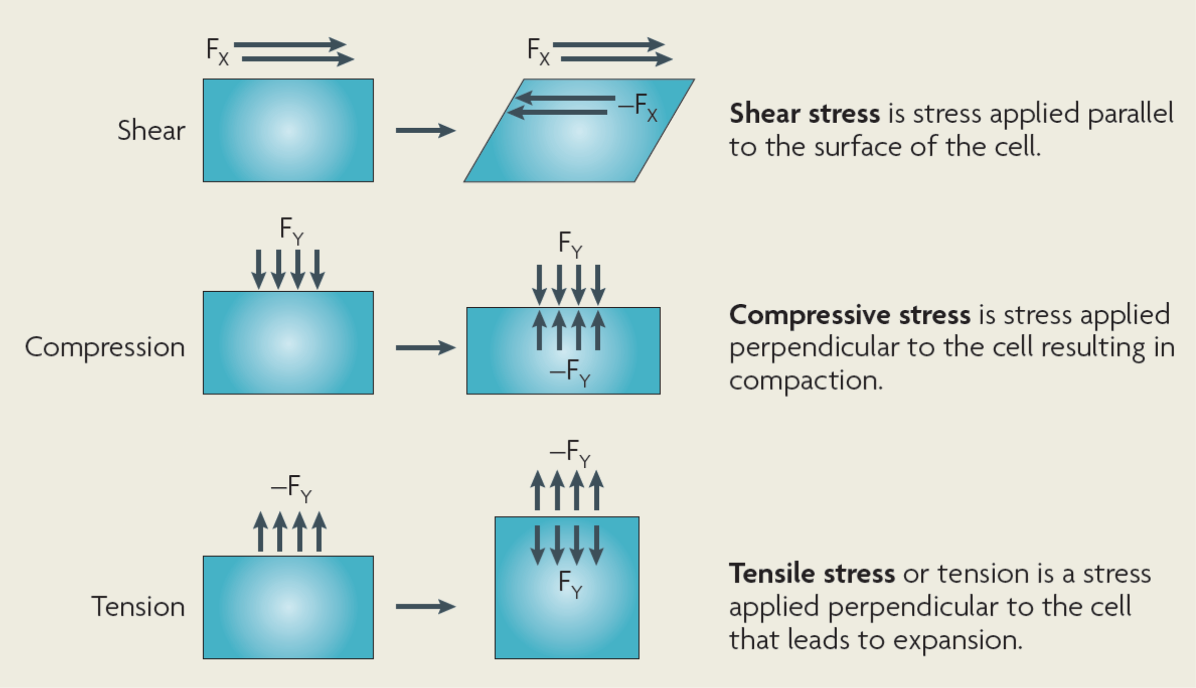

Figure 1-1. Schematics of different forces experienced by a cell. On the left are the forces that cells feel during normal physiological processes such as shear, compression, and tension. According to Newton's third law, cells mechanically respond to the applied force until a balance of forces is achieved. Reproduced from (Butcher, Alliston et al. 2009).

The mechanical behaviour of cells cultured on solid support is primarily determined by three main components: the plasma membrane, the nucleus, and the internal cytoskeleton (Figure 1-2).

Because nucleus constitutes a large fraction of the total cell volume, it can play an important role in mechanical measurements. The nuclear contributions are significant if the measurement technique probes the overall rather than the local surface properties of the cell. The nucleus is physically connected to the cytoskeleton and mechanical perturbations of the cell extend from its membrane to the nucleus via actin and vimentin filaments. The mechanical regulation of nuclear size could play a crucial role in functions such as DNA synthesis by changing the degree of DNA condensation or transcription (Dahl, Engler et al. 2005).

The semipermeable plasma membrane, composed of a lipid bilayer and transmembrane and surface proteins, provides a protective barrier for the cell while simultaneously mediating interactions with its external environment (Kusumi and Sako 1996).

The cytoskeleton is a meshwork of biopolymers that provide structural support to the cell and stabilize the cell shape. As such, it is the main determinant of cell viscoelasticity, besides its role in various other functions such as intracellular trafficking, cell division, or migration. The three main components of the cell cytoskeleton are actin microfilaments (AF), intermediate filaments (IF) and microtubules (MT) along with their associated proteins.

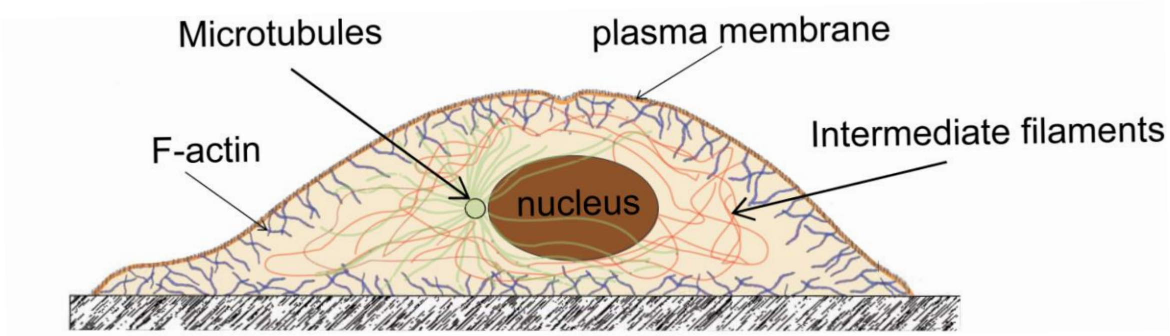

Figure 1-2. Main cellular structures that govern cell mechanical behaviour: plasma membrane, nucleus, and cytoskeleton filaments.

1.2 Measuring mechanical properties of living cells

The simplest way to assess mechanical properties of a cell is to measure stiffness, which can be quantified by obtaining the ratio between cell stress and strain after a given deformation. This ratio is termed as Young's modulus or simply elastic modulus (*E)* and it measured in units of kPa (N/m^2). It has been measured that all cells are extremely soft ranging from 0.1 kPa to 40 kPa depending on a cell type. For comparison, artificial rubber polymers have elastic modulus of 10^3-10^4 kPa. There are different explanations for the broad range of cell stiffness values reported in the literature, even for the same cell type (Table 1; Janmey and McCulloch 2007). First, different measuring techniques probe cell stiffness in different cell regions and at different length scales. Given cell heterogeneity, this can result in greatly varying values for *E*. Second, different cell/probe contact models and cell mechanical models also affect *E* values. Finally, the viscoelasticity of cells can lead to differences in calculated stiffness as a function of the time scale of the measurement. All cells (adherent and non-adherent) exhibit viscoelastic behaviour causing the relationship between stress and strain in any measurement to depend on the time scale of the measurement (Janmey, Winer et al. 2009).

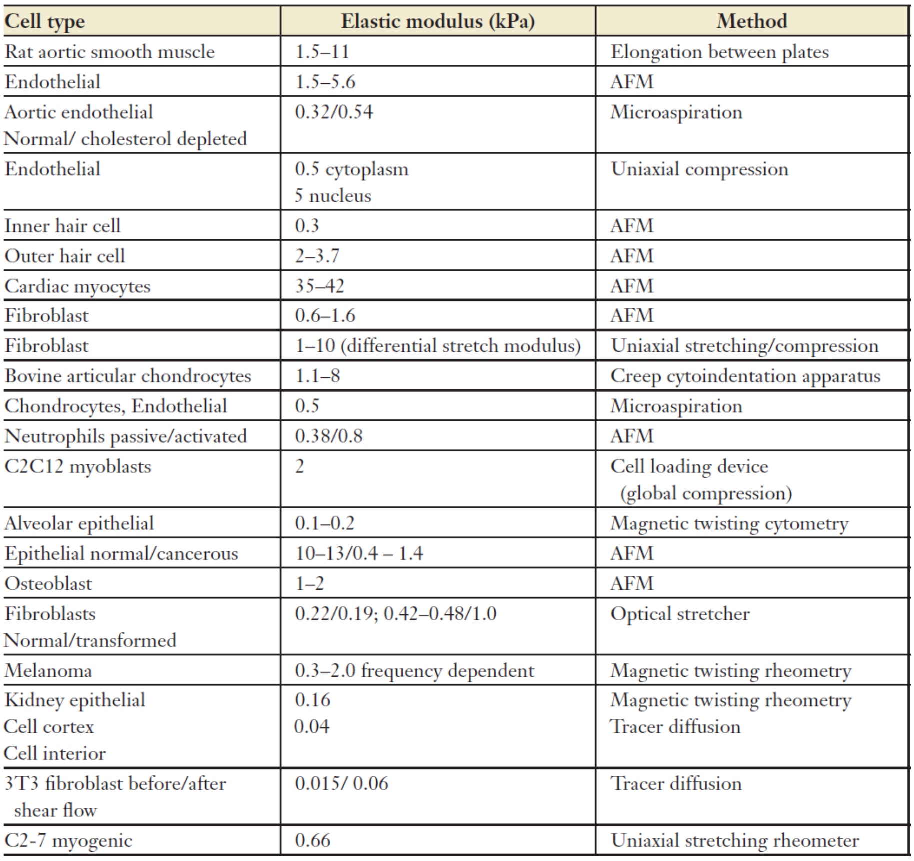

Cell type	Elastic modulus (kPa)	Method
Rat aortic smooth muscle	1.5–11	Elongation between plates
Endothelial	1.5–5.6	AFM
Aortic endothelial Normal/ cholesterol depleted	0.32/0.54	Microaspiration
Endothelial	0.5 cytoplasm 5 nucleus	Uniaxial compression
Inner hair cell	0.3	AFM
Outer hair cell	2–3.7	AFM
Cardiac myocytes	35–42	AFM
Fibroblast	0.6–1.6	AFM
Fibroblast	1–10 (differential stretch modulus)	Uniaxial stretching/compression
Bovine articular chondrocytes	1.1–8	Creep cytoindentation apparatus
Chondrocytes, Endothelial	0.5	Microaspiration
Neutrophils passive/activated	0.38/0.8	AFM
C2C12 myoblasts	2	Cell loading device (global compression)
Alveolar epithelial	0.1–0.2	Magnetic twisting cytometry
Epithelial normal/cancerous	10–13/0.4 – 1.4	AFM
Osteoblast	1–2	AFM
Fibroblasts Normal/transformed	0.22/0.19; 0.42–0.48/1.0	Optical stretcher
Melanoma	0.3–2.0 frequency dependent	Magnetic twisting rheometry
Kidney epithelial Cell cortex Cell interior	 0.16 0.04	 Magnetic twisting rheometry Tracer diffusion
3T3 fibroblast before/after shear flow	0.015/ 0.06	Tracer diffusion
C2-7 myogenic	0.66	Uniaxial stretching rheometer

Table 1. Comparison of elastic moduli measured for single cells in culture (reproduced from (Janmey and McCulloch 2007).

1.2.1 Techniques for quantifying mechanical properties of cells

A number of techniques have been developed to mechanically probe single cells and biological materials (Figure 1-3; Suresh 2007). In the following, the main techniques used to quantify cell mechanical properties along with how they have been used are summarized. A more detailed description can be found in corresponding review articles (Kasza, Rowat et al. 2007; Suresh 2007).

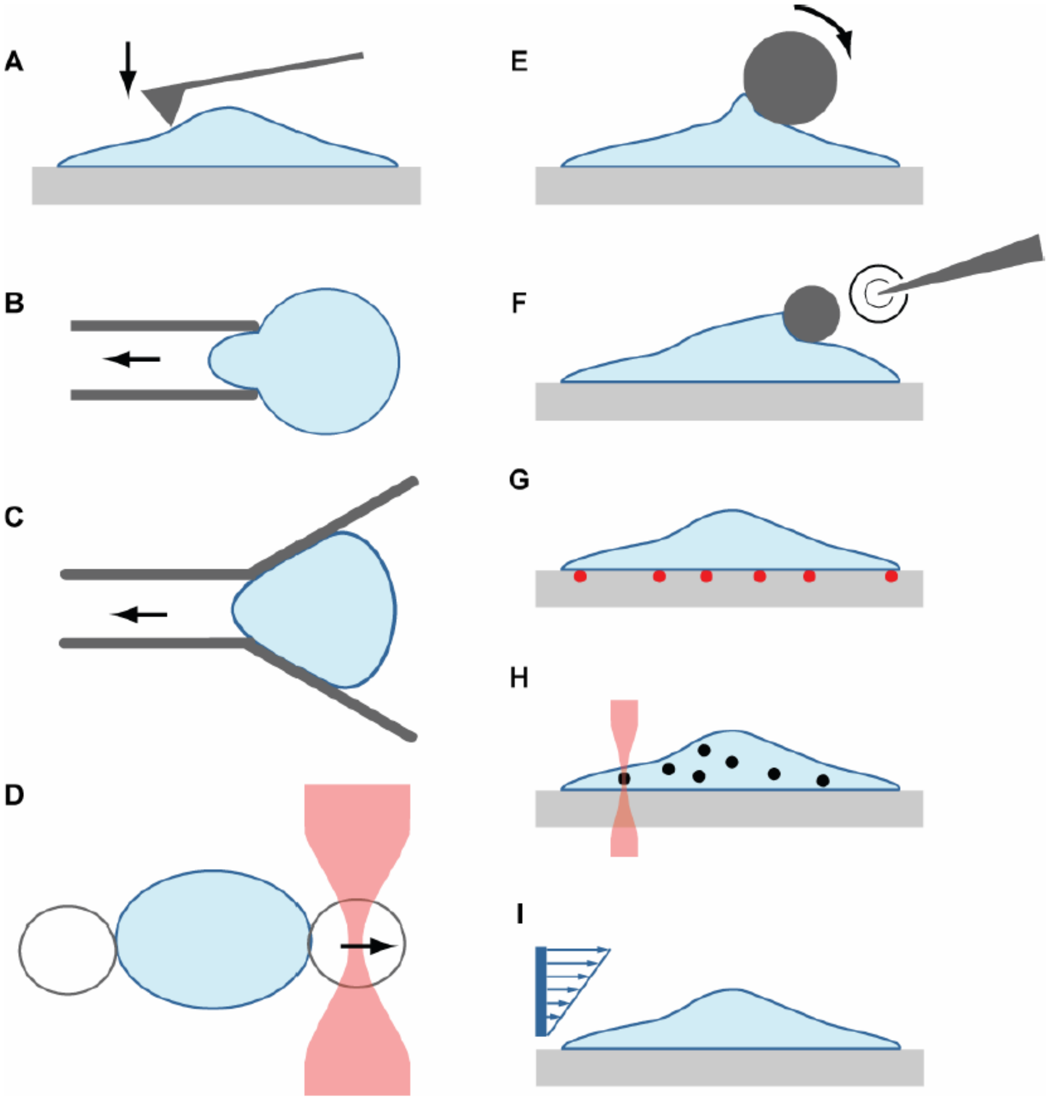

Figure 1-3. Single-cell measurement techniques. (A) Atomic Force Microscopy, (B) Micropipette Aspiration, (C) Microfluidics, (D) Optical Trap, (E) Magnetic Twisting Cytometry, (F) Magnetic Tweezers, (G) Force Traction Microscopy, (H) Laser Tracking Microscopy and Two Point Microrheology, (I) Shear Flow. Modified from (Suresh 2007).

1.2.2 Atomic Force Microscopy

Atomic force microscopy (AFM) (Binnig, Quate et al. 1986)offers precise imaging and mechanical measurement of biological cells and proteins. It was originally devised as an alternative to scanning tunnelling microscopy, which is able to image surfaces by forming a tunnelling current between a probe and a conducting surface. Through use of a flexible microfabricated cantilever probe instead of a current probe has the advantage of being able to operate in liquids, which is essential for interacting with living cells. In addition to the flexible cantilever, the basic components of any AFM include a laser diode focused onto the tip of the reflecting backside of the cantilever, a position-sensitive detector to collect the reflected laser beam, and a piezoelectrically controlled nano-positioner (piezo) in x,y, and z.

AFM has been extensively used to measure mechanical properties of living cells (Radmacher 2007). This is usually achieved by pressing a probe (the tip at the end of the flexible cantilever) at a constant rate at a given site against the cell and recording the cantilever deflection. The amount of force felt by the cantilever, as the tip approaches, contacts and indents the cell surface is measured by a force curve. The slope of each force curve represents sample stiffness. AFM can measure cell deformation at a single point or over the entire cell surface by recording a 2D array of force curves in a force-volume mode.

1.2.3 Micropipette aspiration

Micropipette aspiration has been extensively used to determine mechanical properties of non-adherent (Berk and Evans 1991; Discher, Mohandas et al. 1994) and adherent cells (Guilak, Ting-Beall et al. 1999). During micropipette aspiration, a portion of membrane and cytoplasm of the cell are drawn into a pipette by differential pressure. Sensitivity of this technique is limited by accurate measurements of pressure (~ 0.1 Pa) and visual tracking via optical microscopy of the cell membrane as it is aspirated into the micropipette (~25 nm) (Hochmuth 2000).

This technique can be used to describe an apparent membrane tension and cytoplasmic viscosity using the liquid droplet model, in which the cell is assumed to be a viscous fluid-filled bag with a constant surface tension (Herant, Marganski et al. 2003; Merenda, Rohner et al. 2007). When the cell forms a hemispherical projection into the micropipette, Laplace’s law can be used to determine the membrane tension of the cell. Cell viscosity can be also determined by measuring the flow rate of a cell into a micropipette. Micropipette aspiration has been also used to quantify the viscoelastic properties of cells (Trickey, Vail et al. 2004). Challenges of measuring cell deformability with micropipette aspiration include adhesion between the cell and the micropipette and clogging of the micropipette.

1.2.4 Microfluidics

Microfluidics can measure cell deformation by forcing cells through small channels. By controlling flow rate or pressure, varying forces can be applied to the cell. In addition, the high-throughput nature of microfluidics enables for a much larger sample size than other single cell techniques. In general, a microfluidic system is built by fabricating a master mold on a silicon wafer using traditional microfabrication techniques (reviewed in (Beebe, Mensing et al. 2002)). Then, a polydimethylsiloxane (PDMS) polymer is poured on top of the master mold. PDMS molds have several properties advantageous for biological studies including permeability to gases, optical transparency, reproducibility, and nanometer-level fidelity to the original mold.

Most of microfluidics systems use parallel microchannels to measure cell deformation. However, precisely quantifying values such as Young’s modulus or viscosity are difficult as cell diameters and loading conditions vary. Instead, readouts reported are transit time, change in pressure (Ward, Faivre et al. 2005), clogging time (Shevkoplyas, Yoshida et al. 2006; Higgins, Eddington et al. 2007), cell velocity (Tsukada, Sekizuka et al. 2001), changes in surface area to volume ratio (Gifford, Frank et al. 2003), cell stretching and deformability ratio (Tsukada, Sekizuka et al. 2001; Guck, Schinkinger et al. 2005) .

1.2.5 Optical Trap

Optical traps, also called optical tweezers, laser traps, or laser tweezers, have enabled basic biophysical measurements of motor proteins, DNA, and enzymes (Lang, Fordyce et al. 2003). Optical traps depend on the momentum of photons to hold microscopic particles in place. When light interacts with a particle, the photons exert a radiation pressure on the object. When the laser light is transmitted through a particle of high refractive index, the photons have a change in momentum due to the refraction from entering and exiting the particle. This change in momentum creates a restoring force on the particle towards the greatest photon flux, which is towards the focus of the laser beam (Peters, van Kooyk et al. 1999). The laser can be controlled with galvanometer driven mirrors, acousto-optic deflectors, or by moving the sample stage. Position of the particle in the trap can be tracked with video tracking, quadrant photodiodes, or by a position sensitive detector (Kuo 2001). Optical traps generally apply forces between 1-100 pN, and are not able to apply forces over 100 pN without thermally damaging cells which allows measuring local forces at very high sensitivity but makes them incapable of accessing cell heterogeneity.

Optical traps have been used to determine membrane elasticity, cell motility, cell spreading, adhesion forces, and cytoskeleton mechanics (Schinkinger, Wottawah et al. 2004; Lim, Zhou et al. 2006). Finally, a modified optical trap, called a cell stretcher, has been used as a high throughput method to measure cell deformability for diagnostic purposes (Guck, Schinkinger et al. 2005).

1.2.6 Magnetic Tweezers

Magnetic tweezers can apply forces from a few piconewtons (pN) to tens of nanonewtons (nN) on small magnetic particles via a magnetic needle. Particles that are used with magnetic tweezers are typically superparamagnetic, meaning that the particles acquire a magnetic moment only when they are in an external magnetic field (Tanase, Biais et al. 2007). The needle can be either a permanent or electromagnet. The advantage of using an electromagnet is that the magnetic field can be turned on and off without moving the needle. When the magnetic needle applies a magnetic field on the particle, the particle is pulled towards the needle. Translation of the particle is optically tracked by a microscope and image analysis software.

The technique was originally used on cells by Bausch *et al.* to probe local cellular viscoelastic parameters (Bausch, Ziemann et al. 1998). More recently, it has been also used to study mechanotransduction by applying loads onto focal adhesion sites in cells (Matthews, Overby et al. 2004; Matthews, Overby et al. 2006).

1.2.7 Magnetic Twisting Cytometry

Magnetic twisting cytometry (MTC), like magnetic tweezers, also involves the application of a magnetic field to cell-bound particles. Unlike magnetic tweezers, MTC uses ferromagnetic beads (ranging from 1-10 μm in diameter), which maintain their magnetic moment even after the disappearance of a magnetic field (Lele, Sero et al. 2007). To apply a torque, the particles are exposed to a strong and brief magnetic force from a horizontal Helmholtz coil, which aligns the magnetic dipoles horizontally, making the particles permanent magnets. Subsequently, a weaker magnetic field is applied with a vertical Helmholtz coil, which twists the beads and applies a shear force to the bound receptors (Lenormand and Fredberg 2006).

This field can be applied in a step or an oscillation, enabling measurement of the storage and loss modulus of a cell. Bead movement can be tracked optically for single particles (Fabry, Maksym et al. 2001) or with a magnetometer for average particle rotation (Lele, Sero et al. 2007). Originally devised by Crick to study the physical properties of cytoplasm (Crick 1950; Crick and Hughes 1950), MTC has been extensively used to investigate cell rheology (Fabry, Maksym et al. 2001; Lenormand, Millet et al. 2004); Lenormand et al. 2004; (Trepat, Deng et al. 2007) et al. 2007), coupling of adhesion molecules to the cytoskeleton (Wang 1998), mechanotransduction (Chen, Fabry et al. 2001), and intracellular stress transmission via the cytoskeleton (Wang, Hu et al. 2007).

1.2.8 Particle Microrheology

By passively observing Brownian motion of injected or endogenous particles within cells, local viscoelastic moduli of the cytoplasm can be measured (Wirtz 2009). For example, the Wirtz group has reported tracking of 100 nm particles that have been microinjected with a balistic particle delivery system (Panorchan, Lee et al. 2007). The mean square displacement (MSD) of the particles was then tracked by video microscopy and appropriate software. The complex viscoelastic modulus G^* was extracted from the MSD using the Stokes-Einstein relation where the elastic modulus G' and viscous modulus G'' are the real and imaginary components of G^*, respectively (Panorchan, Lee et al. 2007).

In this approach, particle size strongly affects measurements of local viscoelasticity, as larger particles will be trapped in the mesh of the cytoskeleton. This technique also revealed that viscoelastic properties can vary more than ten times within an individual cell and that the viscosity of the leading edge of a fibroblast is ten times higher than that of the trailing edge (Tseng, Kole et al. 2002; Kole, Tseng et al. 2005).

1.2.9 Traction Force Microscopy

Traction force microscopy aims at measuring forces that an adherent cell exerts on its microenvironment. Upon contact with a substrate, the cell assembles distinct focal adhesion sites that mediate cell attachment. The cell’s internal cytoskeleton interacts with these focal adhesions and contracts thereby exerting traction forces on the substrate. These forces play an important role in cell motility, cytokinesis, and cytoskeleton remodelling. Cell traction forces were first observed by placing fibroblasts on a thin silicone substrate. The cells furrowed the substrate due to the contractile forces within the cell (Wang, Lin et al. 2007). Current techniques employ thin gels of collagen, gelatine, or polyacrylamide with sub-micron fluorescent beads embedded within the gels or placed on the surface. (Wang, Ostuni et al. 2002). By comparing the bead positions under no load conditions to the pattern after cell contraction, a deformation map of the substrate is obtained from which a stress map can be derived.

An alternative method for measuring traction forces was developed by microfabricating arrays of narrow PDMS posts (Tan, Tien et al. 2002). As cells adhere to the post tops, they contract, causing the posts to deflect. Traction force can then be determined by cantilever beam equations and by measuring cantilever deflection with optical microscopy.

1.2.10 Shear Flow

The shear flow of fluid over cells has been shown to have significant effects on cellular mechanotransduction. For example, mechanosensitive ion channels that are sensitive to shear across the cell membrane have been implicated in mechanotransduction (Alenghat, Nauli et al. 2004). Generally, shear stress is applied by parallel plate flow chambers with fully developed laminar flow in the region under observation. By increasing the flow rate, the shear stress is also increased. Cells have been shown to respond to shear stress by altering their cytoskeletal architecture (Helmke, Rosen et al. 2002; Davies, Zilberberg et al. 2003; Helmke, Rosen et al. 2003).

1.3 Modelling the cell as a material

One of the main challenges in data interpretation lies in employing an adequate model of cell mechanics. There are several different models commonly used, including traditional viscoelastic, power law or soft glass, tensegrity, and poroelasticity models. Each research group appears to favour one model over the other (Ingber 2003; Hoffman, Massiera et al. 2006; Stamenovic, Rosenblatt et al. 2007). Since, living cell is a highly complex material and the experimental data may fit several models, it is important to select a model according to the aim of the experiment.

1.3.1 Tensegrity

In an attempt to associate cell structure with mechanical behaviour, Ingber et al. proposed the tensegrity model 17 years ago (Ingber 1993). Tensegrity system maintains its three-dimensional structure by a network of struts in compression and cables in tension (Fuller 1961). Ingber extended this concept to the cell, proposing that actin and intermediate filaments are cables in tension, while microtubules correspond to struts in compression (Ingber 2003; Ingber 2003). This model has been extensively propagated by Ingber and colleagues over the years (Stamenovic, Fredberg et al. 1996; Ingber 1997; Maniotis, Bojanowski et al. 1997; Chen and Ingber 1999; Stamenovic and Ingber 2009). For example, work by Ning Wang's laboratory has shown that local perturbation of a cell results in heterogeneous distal responses thought to be mediated by the actin cytoskeleton (Hu, Chen et al. 2003; Luo, Xu et al. 2008). Using "laser scissors" to ablate actin stress fibres of cultured endothelial cells, Kumar *et al.* were able to show that individual stress fibers are actively tensed (Kumar, Maxwell et al. 2006). In addition, Brangwynne *et al.* have shown that microtubules can bear significantly higher loads within cells than *in vitro* due to lateral reinforcement by the surrounding cellular structure (Brangwynne, MacKintosh et al. 2006), thus serving as the compressive "struts" of the tensegrity model.

The notion that cells have cytoskeleton structures in tension and compression is by now widely accepted, however, this model fails to predict or address viscoelastic properties of cells.

1.3.2 Poroelasticity

Recent work suggests that cells behave like a poroelastic material (Charras, Yarrow et al. 2005;Charras, Mitchison et al. 2009). Poroelastic model provides a prediction of the spatiotemporal connections between cytoskeleton components within a cell by treating it as a biphasic material with a tightly meshed elastic cytoskeleton network within a viscous cytosol (Charras, Yarrow et al. 200 5). Introduced by Biot to predict settling of porous soil (Biot and Clingan 1941), poroelasticity theory has also been used to explain the mechanical behaviour of biological materials such as bone (Cowin 1998), soft tissues (Pena, Bolton et al. 1998) and collagen gels (Chandran and Barocas 2004). When the material is locally deformed, the elastic phase remodels, creating a localized increase in pressure of the interstitial fluid, whose flow is impeded by the dense network. Over time, the fluid flows radially away from the site of perturbation, causing continuous deformations until the pressure equilibrates. Charras *et al.* tested the model by applying poroelasticity theory to explain blebbing behaviour in cells and predicted an increasing equilibration time with distance from perturbation (Charras, Yarrow et al. 2005) while others tested the model directly on data obtained from combined atomic force microscopy-particle tracking measurements (Rosenbluth, Crow et al. 2008).

1.3.3 Traditional viscoelastic models

Traditional viscoelastic models have been the basis of cell mechanics research. These models include springs and dashpots in series and parallel as well as elastic membranes. Much of the original work was focused on blood cell deformability (Chien, Sung et al. 1992), as blood cell mechanics clearly affect cell flow through the vascular system. For adherent cells, the standard linear solid model has been commonly used to determine cell viscoelasticity (Koay, Shieh et al. 2003; Hemmer, Nagatomi et al. 2009).

Studies based on AFM techniques generally employ a simplified elastic model because of indenter shape complexity (pyramid or sphere) and the shared feature of constant rate experiments (Radmacher 2007;Sirghi, Ponti et al. 2008). When comparing stiffness measurements across experiments, loading rates need to be considered, as fast loading rates will make a cell appear stiffer then slow loading rates (Rosenbluth, Lam et al. 2006). Additionally, employing AFM-based creep experiments, a viscous term can be quantified as well (Mahaffy, Park et al. 2004; Darling, Zauscher et al. 2006).

1.3.4 Power law and soft glassy rheology

While traditional viscoelastic models predict a characteristic timescale of relaxation, power law models do not. Instead they quantify stiffness as a function of frequency: $G' = f x$, with G' being the elastic modulus, f the frequency, and x the power law exponent. Power law rheology for cells was first suggested by (Tsai and Hammer 1997). Since then, power law behaviour has been reported with a variety of techniques, including AFM (Tsai, Waugh et al. 1996; Alcaraz, Buscemi et al. 2003) Power-law response has led to the suggestion that a cell behaves as a soft glass, similar to foams or colloids (Lenormand and Fredberg 2006; (Trepat, Deng et al. 2007). Soft glassy rheology (SGR) is a conceptual model that classifies a material as having the disordered state of a liquid but the rigidity of a solid. Glassy behaviour arises from a structure in which elements have to cross energy barriers that are large compared to thermal energy of the system and thus, they are trapped in a metastable state before reaching equilibrium (Fabry, Maksym et al. 2001).

Some studies disagree with the suggestion that cells behave as a soft glass, reasoning that SGR cannot explain stress induced stiffening (Hoffman, Massiera et al. 2006) or that relaxation follows multiple power law regimes instead of just one, which is in the SGR model (Stamenovic, Rosenblatt et al. 2007).

1.3.5 Implications and limitations of models

“Heidemann *et al.* compared cell mechanics literature to the ‘The Blind Men and the Elephant’, a poem by John Godfrey Saxe based on an Indian tale, where each blind man touches a different part of the elephant and presents dramatically different interpretations of what exactly an elephant is like” (M.J. Rosenbluth, 2009) (Heidemann and Wirtz 2004).

While some work has tried to bring varying techniques together to present a unifying model (Hoffman, Massiera et al. 2006) most research is focused on one perspective or another (M.J. Rosenbluth, 2009). In addition, most material models of cells essentially consider cells as a passive material and do not address cell dynamics. Defining the specific aim of the research could hopefully guide a researcher which model to use.

Finally, for developing assays for diagnostic or screening purposes, a complete description of the mechanical properties of a cell may not be necessary rather a clear and reproducible method to assess relative differences in mechanical properties is far more important.

1.4 Cell cytoskeleton: structure, function and mechanics

Until the 1970s, living cell was modelled as viscous fluid surrounded by a stiff plasma membrane. The primary structural role of the cell was attributed to the cellular membrane (cellular cortex) and its mechanical dynamics to the viscous cytoplasm. Later, in the early 1980s, it was discovered that cells contain a cytoskeleton- cellular "skeleton" within the cytoplasm, a complex network of three major filament types which provides the structural support for maintaining cellular shape and enabling cellular motion.

1.4.1 Actin microfilaments

In the majority of eukaryotic cells, actin is the most abundant protein, accounting for about 5-10% of the total protein content. Actin plays a crucial role in many cellular processes including migration, contraction and cell division. Accordingly it has been of key interest since it was first described by Straub in 1941(Straub 1942). Globular actin monomers (G-actin) polymerize into two-stranded helical filaments (F-actin). The morphology of the actin filament is two long-pitch right handed helices as shown in Figure 1-4A. F-Actin filaments have a polar configuration (Schaller, Weber et al. 2010) where polymerization occurs rapidly at the (+) end of the microfilament and less rapidly at the (-) end, where in turn depolymerisation takes place predominantly. This effect is commonly called "treadmilling" (Kirschner 1980). Actin is "activated" in its ATP-bound form, and upon polymerization ATP hydrolysis occurs and actin assumes an ADP-bound state in the maturing filament.

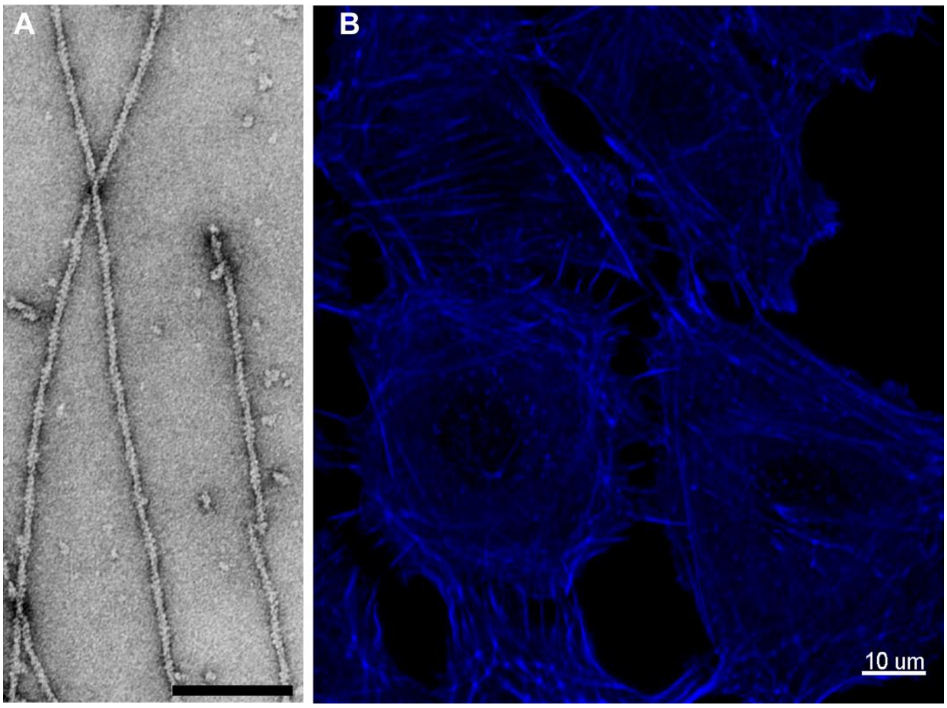

Figure 1-4. Actin filaments *in vitro* and *in vivo*. (A) Negatively stained preparations of MFs reveal helicity of F-actin with a distinct periodicity. Typical diameter of an individual filament is between 6-8 nm. Scale bar, 100 nm. (B) Dense meshwork of actin filaments and bundling of F-actin into stress fibres is resolved by staining cells with fluorescently tagged phalloidin) that specifically recognizes only polymerized actin. Scale bar, 10 µm.

Actin filaments exhibit diameter between 6-8 nm and a length up to 100 µm. A myriad of actin binding proteins (ABPs) regulate polymerization dynamics, filament length, and 3D actin organization *in vivo*. The morphology of actin networks varies depending on the location within the cell and the cell type. Different morphologies are necessary for normal cellular functions (structural stability, motility, mechanotransduction, etc.). The typical morphology of an F-actin cytoskeleton in a fibroblast cell is presented in Figure 1-4B. Eukaryotic cells express three classes of actin isoforms (α, β, γ), each with different functions and properties: the muscle-specific α-actinins associated with contraction in different types of muscle cells; nonmuscle cells express β- and γ-actin isoforms that form filamentous structures at the leading edge in lamellopodia and filopodia (Pantaloni, Le Clainche et al. 2001) and bundle into stress fibres. Dynamic reorganization of F-actin networks in different regions of a cell plays a crucial role during cell migration and division (Carlier and Pantaloni 1997).

The F-actin cytoskeleton is a key determinant of the cell’s shape and mechanical behaviour. Advances in quantitative approaches, imaging technology, molecular biology, and biochemistry have enabled rapid progress, both, in the control over F-actin cytoskeletal networks in living cells, and the ability to reconstitute F-actin networks *in vitro*. In particular, the mechanical properties of the actin cytoskeleton were investigated during several processes such as cell adhesion, migration and division (Bathe, Heussinger et al. 2008). Different microrheological studies have quantified in detail the mechanical behaviour (e.g. force deformation, shear moduli vs frequency, or shear moduli vs concentration) of actin filaments for both *in vitro* (Chaudhuri, Parekh et al. 2007; Luan, Lieleg et al. 2008; Lee, Ferrer et al. 2010) and *in vivo* (Gerthoffer 2005; Kumar, Maxwell et al. 2006) environments. Moreover, stiffness has been reported to decrease remarkably if the actin cytoskeleton is disrupted by treating cells with actin-binding drugs (such as cytochalasin or latrunculin) (Wakatsuki, Schwab et al. 2001). By using synthetic actin gels, it has been observed that the stiffness of the actin cytoskeleton is crucially dependent on the concentration of cross-linking proteins such as filamin and α-actinin (Wachsstock, Schwarz et al. 1994; Esue, Tseng et al. 2009).

Integration of numerous physical measurements performed *in vitro* with measurements on living cells should increase the understanding of how the dynamics and mechanics of individual macromolecules interact to give rise to the complex actin cytoarchitecture with its crucial functions for living cells. More detailed understanding of the mechanics of the actin cytoskeleton during the cellular protrusions and contractions can augment understanding of critical immunological responses (i.e. extravasation and migration) as well as actin polymerization regulation therapies for treating cancer (Buda and Pignatelli 2004; Tan, de Noronha et al. 2005; Rebillard, Jouan-Lanhouet et al. 2010).

1.4.2 Intermediate filaments (IFs)

Intermediate filaments (IFs) constitute a large, heterogeneous family of proteins. The members of the IF protein family are encoded by at least 70 genes (Herrmann, Strelkov et al. 2009). Despite their distinct primary amino acid sequences they share a common domain organization. Cytoplasmic IFs assemble in three major steps from a 45 nm long coiled-coil dimer as the elementary building block in a stranded-rope fashion. When assembled, IFs exhibit a diameter of about ~ 10 nm, (Parry, Strelkov et al. 2007) depending on the type of IF (Figure 1-5A).

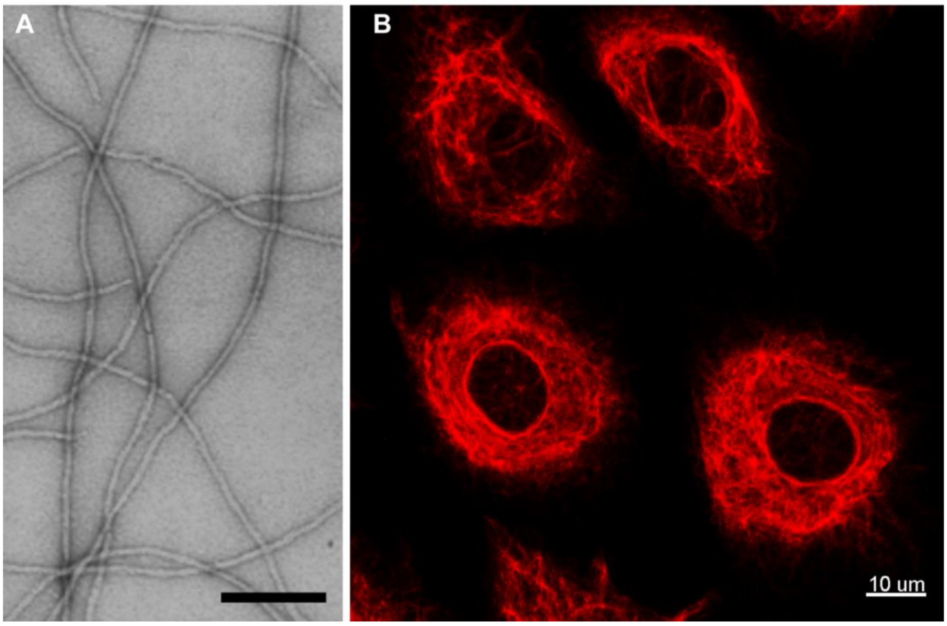

Figure 1-5. Intermediate filaments *in vitro* and *in vivo*. (A) Electron micrograph of *in vitro* assembled vimentin IF filament. Mature filaments exhibit a typical diameter of 10 nm. Scale bar, 100 nm. (B) Indirect immunofluorescence staining of vimentin cytoskeleton in rat fibroblasts reveals complex network formed by vimentin filaments that extends from the cell periphery to the outer nuclear membrane. Scale bar, 10 µm.

In contrast to actin and microtubules, IFs are considered the most flexible cytoskeleton polymers, important for cell architecture as well as cellular and nuclear stability (Herrmann, Strelkov et al. 2009). Recently, it has been suggested that IFs are very efficient both as stress buffers and as signalling scaffolds even for high abundance signalling molecules (Eriksson, Dechat et al. 2009). IFs are differentially expressed during embryonic development and cell differentiation and have distinct tissue – specific functions both in the healthy and diseased state. For instance, keratin heteropolymers are abundant in epithelial cells and provide structural support to hair and nails. Vimentin filaments are the most widely distributed IFs in nature, found in endothelial cells, leukocytes, fibroblasts, and myoblasts ((Herrmann, Bar et al. 2007). Higher metazoan cells express two distinct types of IFs in parallel; cytoplasmic IFs and in the nucleus lamins. Cytoplasmic IFs form a cage-like structure of thin filaments around the nucleus (Figure 1.5B). In vivo contour lengths of intermediate filaments have been observed to range from 10-20 µm (Fudge, Gardner et al. 2003) .

Most of the knowledge about the biophysical properties of IFs results from studying vimentin and desmin IFs. For example, disruption of vimentin filaments with acrylamide or calyculin A was reported to reduce stiffness in non-attached T lymphocytes (Brown, Hallam et al. 2001) and in attached fibroblasts and endothelial cells (Wang and Stamenovic 2000). These measurements showed that vimentin-deficient cells are softer than control cells, suggesting that vimentin makes a significant contribution to cell stiffness. The viscoelastic behaviour of IFs *in vitro* has been examined by rheological methods (Butler, Tolic-Norrelykke et al. 2002; Tolic-Norrelykke and Wang 2005). In particular it was demonstrated that IFs exhibit a property called strain stiffening, i.e., upon application of stress to the filament suspension it becomes more viscoelastic (Storm, Pastore et al. 2005; Lin, Yao et al. 2010). In contrast, MFs and MTs break under increasing strain because their persistence length is larger compared to IFs. Persistence lengths for vimentin can vary from 0.3-3 µm depending on the measurement technique (Mucke, Kreplak et al. 2004; Ackbarow and Buehler 2009; Mucke, Klenin et al. 2009). Similar values are observed for desmin IFs (Hohenadl, Storz et al. 1999). The lower persistence length of IF compared to that of F-actin filaments is caused by the presence of flexible linker regions within the coiled-coil dimer and also due to axial slipping between dimers within the filaments (Rogers, Herrmann et al. 1996). The coiled-coil dimer structure enables the IF to have a Young's modulus on the order of E ~6MPa (calculated from persistence length and diameter measurements) (Wagner, Rammensee et al. 2007). Moreover, nanomechanical properties of individual vimentin and desmin IFs adsorbed on mica measured by AFM revealed that individual filaments can be stretched up to 3.5 fold and that IFs can carry a high tensile strength of approximately 180 MPa (Kreplak, Bar et al. 2005; Guzman, Jeney et al. 2006; Kreplak, Herrmann et al. 2008).

IFs are involved in human diseases in several contexts. An important hallmark of all primary IF disorders, is an altered mechanical response from the cellular to the tissue level as for example skin blistering in epidermolysis bullosa, muscle degradation in myopathies and damage to nucleus shape and mechanical stability in laminopathies (Omary 2009). In addition, a recent work from Kreplak and Bar (Kreplak and Bar 2009) has shown that filaments *in vitro* exhibiting desminopathic mutations have significantly altered mechanical phenotype when compared to the wild type filaments.

1.4.3 Microtubules

Microtubules are formed by the polymerization of α- and β-tubulin heterodimers, which form hollow cylinders of approximately 14 nm inner and 25 nm outer diameters that can be more than 100 µm long (Figure 1-6A). These cylinders have a distinct polarity, with a plus end that recruits additional dimers faster than the minus end (Margolis and Wilson 1998). Their Young’s modulus has been estimated to be between 0.8 - 1.9 GPa (Deriu, Enemark et al. 2007).

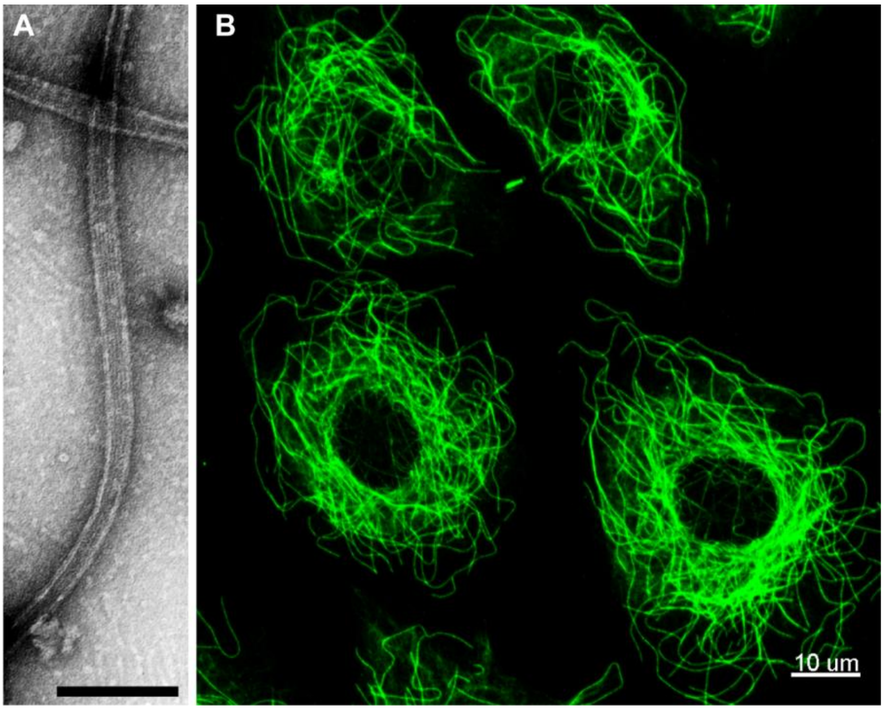

Figure 1-6. Microtubules *in vitro* and *in vivo*. (A) Ultrastructural analysis of microtubules assembled in *vitro* shows are negatively stained and examined by transmission electron microscopy. Tubular structures with an outer diameter of approximately 25 nm are seen. Scale bar, 100 nm. (B) Indirect immunofluorescence staining of microtubule cytoskeleton in rat fibroblasts reveals filaments that are radially extending from microtubule organizing center termed centrosome. Scale bar, 10 µm.

In addition to serving as tracks along which cargo is transported within the cell, microtubules are involved in moving cellular structures such as chromosomes, mitotic spindles and other organelles within living cells (Rodionov, Gyoeva et al. 1993; Vantard, Cowling et al. 2000). This is achieved by attaching one end of microtubules to the respective structures, so the microtubules polymerize and depolymerize while the structures are pushed or pulled. Microtubule ends have three important properties: 1) plus and minus ends have different structures, 2) they undergo biochemical transition upon GTP hydrolysis and 3) they form distinct targets for the binding of specific proteins (Spittle and Cassimeris 1996; Nguyen, Chari et al. 1997; Shea 1997). These different properties render microtubules a molecular machine, which switches between growing and shrinking modes (Desai and Mitchison 1997). Each mode is associated with a specific end-structure with which end-binding proteins interact to modulate dynamics and couple the dynamic properties of microtubules to the movement of cellular structures. The amount of microtubules present in cells is much smaller than that of microfilaments, and their respective organizations are very different. While microfilaments arrange to form the actin cortex (in non-adherent cells) or actin bundles in adherent cells, microtubules predominantly radiate individually from a nucleating centre called the centrosome (Keating and Borisy 1999) (Figure 1-5B).

Microtubules interact with other cytoskeletal filaments through cross-linking proteins such as plakins at cellular junctions (Sonnenberg and Liem 2007) and microtubule actin cross-linking factor (MACF) (Leung, Sun et al. 1999). Besides crosslinking and bundling microtubules, MT-associated proteins can modulate their rigidity and stability.

Mechanical properties (flexural rigidity, persistence length, etc.) have been measured via a variety of empirical methods that examine bending and buckling of individual microtubules (Kasas and Dietler 2007). Together, the experimental data show that microtubules are the stiffest of all three cytoskeleton polymers and have the most complex assembly and disassembly dynamics. Their persistence length is ~5 mm which means that single microtubules can form tracks that are almost linear and span the whole length of metazoan cells (Gittes, Mickey et al. 1993; Venier, Maggs et al. 1994; Kurz and Williams 1995). On the other hand, MTs are known to buckle under compressive loads in living cells (Das, Levine et al. 2008). Although the role of microtubules in determining mechanical properties of living cells is considered remarkably smaller than that of actin or intermediate filaments, microtubules alone or in networks represent essentially interesting structures for potential nano-and bioengineering applications (Hawkins, Mirigian et al. 2010).

1.5 Mechanical properties of tissues

Tissues are composed of various cell types, extracellular matrix (ECM) proteins and other components with each exhibiting unique mechanical properties such as elasticity, viscosity, viscoelasticity, tensile strength and stiffness (Ingber 1993). These physical properties collectively define the material properties of the tissue and dictate how it will respond to mechanical signals and how it will sense and transmit force. Mechanical forces are crucial in normal tissue-specific development, while disruption in tissue structure and force balance leads to various diseases. For example major mechanical stimulus to the fetal lung growth is tension induced by fetal breathing movements (Kitterman 1996). Also during embryo development, the normal morphogenic movements generate compressive stress that affects the physical shape of the embryo (Farge 2003). Other examples are mechanical tension induced hypertrophic response in cardiac myocytes (Sadoshima and Izumo 1997), and hemodynamic forces as regulators for vascular endothelial gene expression (Resnick, Yahav et al. 1997).

A balance of forces is required to maintain homeostasis in a tissues, including bone (Burr, Robling et al. 2002) and cartilage (Grodzinsky, Levenston et al. 2000). For instance, exercise affects joint loading, and thus increases proteoglycan content of articular cartilage, whereas reduced mobility leads to loss of proteoglycan content and promotes osteoarthritis (Haapala, Lammi et al. 1996; Bird, Platt et al. 2000). Similarly, while laminar shear stress induced by blood flow allows normal artery maturation, turbulent shear stress may lead to atherosclerosis (Davies, Remuzzi et al. 1986). Furthermore, mechanical forces of the same type can produce different responses depending on the magnitude, duration and application mode of loading. One specific example is the effect of compressive stiffness on the extracellular biosynthesis of chondrocytes. *In vitro* studies have shown that static compression on chondrocyte-seeded constructs or cartilage explants inhibits ECM biosynthesis (Chen and Sah 1998), while dynamic compression stimulates ECM biosynthesis (Kisiday, Jin et al. 2004).

Methods that were initially developed for single cell mechanics, have been readily used to measure mechanical properties of tissues, as for example tension (Dzamba, Jakab et al. 2009), compression (Forgacs, Foty et al. 1998), shear testing (Samani, Bishop et al. 2003) and AFM (Plodinec, Loparic et al. ; Stolz, Raiteri et al. 2004). These studies and many others have revealed that individual cellular constituents, ECM and their interactions govern the mechanical response of a tissue.

1.5.1 Extracellular matrix (ECM)

A substantial volume of most tissues comprises extracellular space, which is mostly filled by complex network of macromolecules constituting the extracellular matrix (ECM). This matrix is composed of a variety of proteins and polysaccharides that are secreted locally by cells and assembled into an organized meshwork surrounding the cells that produced them. In most tissues ECM is frequently more abundant than the amount of cells embedded, and it determines the tissue's mechanical properties. The amounts of ECM present in different organs vary greatly, while it is found abundantly in cartilage and bone, an insignificant amount is found in brain and spinal cord (Levental, Georges et al. 2007). Variations in the relative amount of ECM per cell and its organization give rise to a remarkable diversity of forms, each tailored to the functional requirements of that particular tissue. The vertebrate ECM was once thought to mainly serve as inert scaffold to stabilize the physical structure of tissue. However, it is becoming clear that the matrix has a far more active and complex role in regulating the activities of cells by influencing their survival, development, migration, proliferation, shape, and function (Huang and Ingber 2005).

The ECM is composed of a great variety of molecules that include: 1) proteoglycan and glycosaminoglycan gels (GAGs) and 2) fibrous proteins including collagen family, fibronectin, elastin and laminin (Rosso, Giordano et al. 2004). The proteoglycan molecules in a connective tissue form a highly hydrated gel in which the fibrous proteins are embedded (Kiani, Chen et al. 2002).

The proteoglycan gel resists compressive forces while allowing the rapid diffusion of nutrients, hormones, and metabolites between the blood and tissue cells (Kiani, Chen et al. 2002). The collagen fibers contribute to tensile strength and organize the matrix. In general, collagen is the most abundant protein in the body that comprises a heterogeneous class of proteins with different mechanical and functional properties.

Collagen types I, II and III are the most abundant collagens of the human body that form fibrils responsible for the tensile strength of the tissue (Rosso, Giordano et al. 2004). Other collagens, such as types IV, VII, IX, and X are found associated with collagen fibrils comprising the basal lamina (Montesano, Orci et al. 1983). The elastin fibers as the name says provide the tissue with flexibility and elasticity. They play a crucial role in the mechanical behaviour of tissues, such as for example skin, at small stresses and small deformations (Oxlund, Manschot et al. 1988). In particular, they are responsible for the recoiling mechanism after a stress or a deformation has been applied.

Elastins are synthesized by fibroblasts and smooth muscle cells (Brooke, Bayes-Genis et al. 2003).

Fibronectin is a glycoprotein that circulates in a soluble form in the plasma and in an insoluble form it localizes to the ECM (Magnusson and Mosher 1998). Soluble fibronectin is polymerized into ECM fibrils through a cell-mediated process which requires coordinated interactions between integrin receptors and the actin cytoskeleton (Magnusson and Mosher 1998). The active assembly of fibronectin into the ECM controls the later deposition, organization and retention of several other ECM molecules including collagen I (Pereira, Rybarczyk et al. 2002; Sottile and Hocking 2002). Fibronectin polymerization also increases cytoskeletal organization and mechanical tension generated by cells (Hocking, Sottile et al. 2000). Together with collagen fibronectin plays a crucial role in determining the mechanical strength of tissues. Importantly, in most connective tissues, above mentioned matrix macromolecules are largely secreted by cells termed fibroblasts (Figure 1-7; Kalluri and Zeisberg 2006).

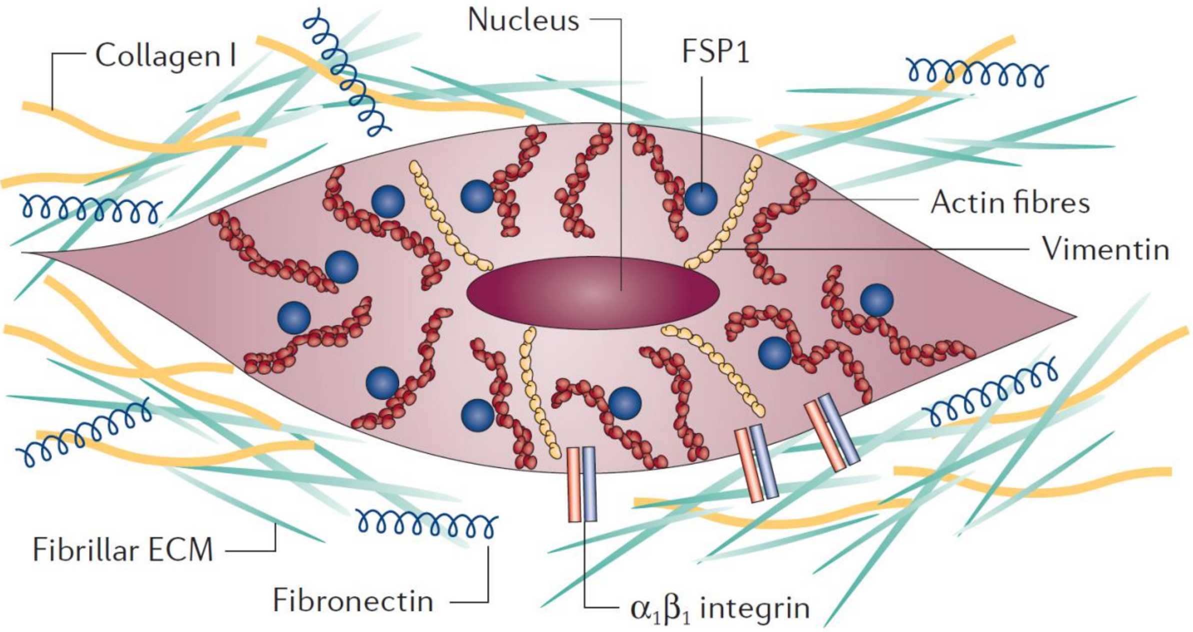

Figure 1-7. Fibroblast cell embedded within the extracellular matrix (ECM) of the connective tissue. ECM secreted by fibroblasts consists largely of type I collagen and fibronectin. Fibroblasts interact with their surrounding microenvironment through integrins such as $\alpha_1\beta_1$ integrin. Typically fibroblasts exhibit prominent actin and vimentin cytoskeleton. Reproduced from (Kalluri and Zeisberg 2006).

The basal lamina is a specialized type of ECM. It is a 60 – 100 nm thick sheet meshwork of ECM components collagen IV and laminin. The multiple interactions between these two components connect and stabilize the overall structure of the basal lamina (Yurchenco and Orear 1994). Both type IV collagen and laminin also bind to specific an important class of cell-adhesion molecules (CAMs) present in the plasma membrane (Yurchenco and Orear 1994). Basal lamina is often confused with the basement membrane, and the term is used inconsistently in the literature. It is important to note that the actual basement membrane is the fusion of two laminae, the basal lamina and the reticular lamina (Vracko 1974). The basement membrane is associated with epithelial, endothelial cells and muscle cells and separates these cells from the underlying connective tissue (Hofmann, Voss et al. 1984). The basement membrane also determines cell polarity, influences cell metabolism, organize the proteins in adjacent plasma membranes, promote cell survival, proliferation, or differentiation, and serve as specific highways for cell migration (Welling, Zupka et al. 1995). In terms of mechanical properties, the basic structure comprising the basement membrane is a collagen IV scaffold which provides basement membrane with nonlinear elastic properties, modest to high tensile strength and elastic support (Welling, Zupka et al. 1995) . It is important in tissue regeneration after injury and acts as a mechanical barrier for cancer progression (Sund, Xie et al. 2004).

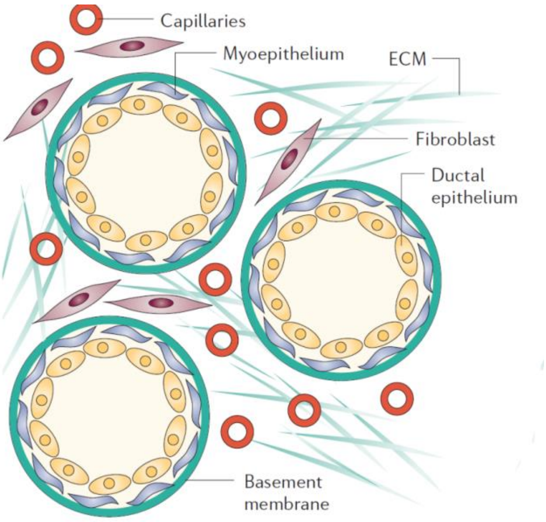

Figure 1-8. Schematic representation of a basement membrane lining the epithelium of a normal breast. In a normal female breast, the ductal epithelium and the underlying myoepithelial cells are separated by a basement membrane from the surrounding connective tissue comprised of ECM, fibroblasts and capillaries. Modified from (Kalluri and Zeisberg 2006).

1.5.2 Tissue mechanics and mechano-transduction

Cells sense and convert mechanical cues into biochemical responses. Studies of mechanotransduction examine how mechanical forces influence intracellular signalling and subsequent behaviour of cells. Numerous techniques have been used systematically to study the molecular basis of cellular mechanotransduction, as for example micro-contact printing, magnetic twisting cytometry, magnetic pulling cytometry, optical and magnetic tweezers and traction force microscopy (Lele, Sero et al. 2007). Results of these experiments have shown that the cellular response to mechanical forces is intrinsically coupled to the internal organization of the cytoskeleton and cell adhesion to surrounding cells and ECM (Chen, Tan et al. 2004). Several mechanosensors that respond to different magnitudes and types of force have been identified, as for example mechano-sensory apparatus of the auditory hair bundle and the primary cilia in tubular epithelial cells (Praetorius and Spring 2005; Fettiplace and Hackney 2006). Alternatively, intracellular signalling cascades can be activated by force induced spatial reorganization of cell surface receptors such as integrin clustering (Paszek, Boettiger et al. 2009) and spatial restriction of Ephrin receptors (Plodinec and Schoenenberger ; Salaita, Nair et al. 2010).

Interaction of cells with the ECM through cell-cell and cell-ECM junctions plays a key role in tissue formation and mechanical response. Cells can sense external forces via cell junctions, leading to a global remodelling of their cytoskeleton elements (Gao, Sotomayor et al. 2006). Overall, cell junctions are classified into three functional groups: 1) occluding junctions, 2) communicating junctions, and 3) anchoring junctions.

1.5.3 Occluding junctions

Occluding junctions serve as selective permeability barriers, separating fluids on either side that have a different chemical composition. These junctions are called tight junctions in vertebrates and septate junctions in invertebrates (Madara and Dharmsathaphorn 1985).

1.5.4 Communicating junction

A different kind of junction, termed a communicating junction or gap junction, enables chemical signalling between cells in animal tissues (Makowski, Caspar et al. 1984). These junctions allow inorganic ions and other small water-soluble molecules to pass directly from the cytoplasm of one cell to the cytoplasm of an adjacent cell, thereby coupling the cells both electrically and chemically. Sharing of small metabolites and ions by cells via gap junctions provides a mechanism for coordinating the activities of individual cells and for smoothing out small random fluctuations in molecular concentrations (Tepass and Hartenstein 1994). Cell coupling via gap junctions also seems to be important for embryogenesis, since coupled cells tend to behave as a cooperative assembly and follow a similar developmental pathway (Haefliger, Krattinger et al. 2006).

1.5.5 Anchoring junctions

Anchoring junctions are type of junctions found abundantly in animal tissues that are subjected to severe mechanical stress, such as heart, muscle, etc. They are of great importance for tissue mechanical properties since these junctions facilitate communication between cells and the external environment via physical forces (Lecuit and Lenne 2007) . Anchoring junctions are composed of two main classes of proteins: intracellular anchor proteins and transmembrane adhesion proteins (Fenteany, Janmey et al. 2000). Intracellular anchor proteins lie on the cytoplasmic face of the plasma membrane and connect the junctional complex to either actin filaments or intermediate filaments (Dudek and Garcia 2001).

Transmembrane adhesion proteins have a cytoplasmic tail that binds to one or more intracellular anchor proteins and an extracellular domain that interacts with either the ECM or the extracellular domains of specific transmembrane adhesion proteins on another cell (Qin, Vinogradova et al. 2004). Anchoring junctions include both the adherens junctions and desmosomes that hold cells together by cadherins known as a major type of cell adhesion molecule (Takeichi 1990). Focal adhesions (FA) and hemidesmosomes bind cells to the extracellular matrix and are formed by transmembrane adhesion proteins of the integrin family (Figure 1-9; Ingber 2003), (Kornberg, Earp et al. 1992). Actin network mediates the formation of adherens junctions and FAs (Perez-Moreno, Jamora et al. 2003), whereas the intermediate filament network mediates the formation of desmosomes and hemidesmosomes (Green and Jones 1996).

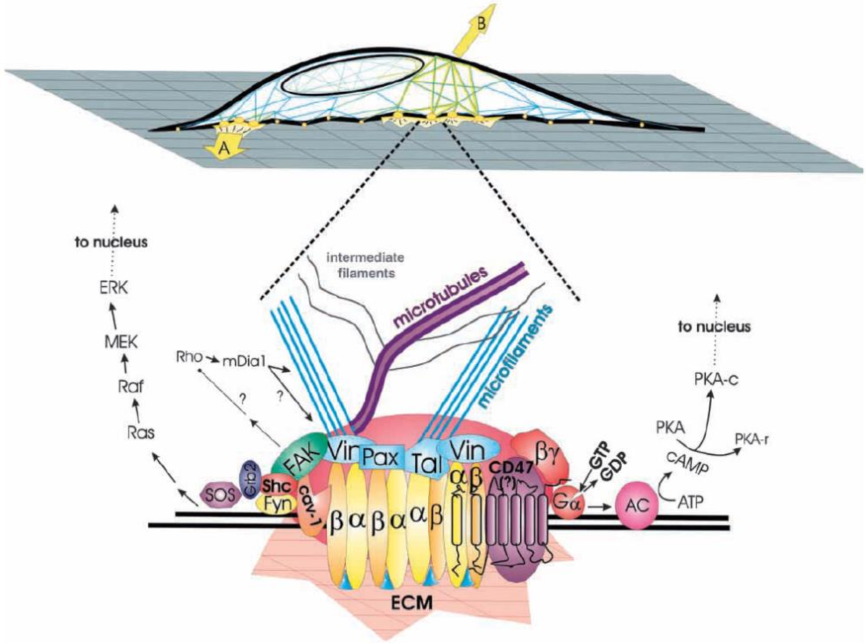

Figure 1-9. Schematic diagram of how forces applied via ECM (A) or directly to the cell surface (B) transmit across integrins and focal adhesions to induce a biochemical response, respectively. Forces (A) concentrated within the focal adhesion can stimulate clustering of dimeric (α,β) integrin receptors and induce recruitment of focal adhesion proteins (e.g. vinculin (Vin), paxillin (Pax), talin (Tal)) that connect to cytoskeletal structures (actin filaments and microtubules), thereby activating integrin-associated signalling cascades, such as focal adhesion kinase (FAK). Cell distortion induced by forces (B) increase intracellular tension, which is transmitted to focal adhesions through the cytoskeleton. Reproduced from (Ingber 2003).

Molecular principles behind these different kinds of anchoring junctions are similar. FAs are a highly specialized type of attachment between cells and the ECM which allows cells not only to adhere but to pull on their microenvironment and thereby respond to its stiffness (Discher, Janmey et al. 2005). Focal contacts also transduce signals from the ECM to the inside of the cell (Geiger, Bershadsky et al. 2001) through a kinase, called focal adhesion kinase (FAK) which responds to the extracellular environment (Sieg, Hauck et al. 1999). In this manner, ECM regulates the survival, growth, proliferation, morphology, movement, and differentiation of cells through focal adhesions (Geiger, Bershadsky et al. 2001). Furthermore, the interaction between ECM and cytoskeleton is reciprocal (Roskelley, Srebrow et al. 1995).

Most cells are anchorage dependent thus to survive, proliferate, and function properly they need to attach to the ECM (Schwartz and Assoian 2001). On the other hand, regulated degradation of ECM macromolecules is crucial to a variety of important biological processes, such as cell migration. For example, extracellular proteolytic enzymes secreted locally by cells degrade matrix components and facilitate cell migration (Friedl and Wolf 2009). In conclusion, accumulating data demonstrate that cell-generated forces play broad roles in regulating cell growth, migration and differentiation as well as cell-cell and cell-ECM communication and spatial organization of cells and tissues (Engler, Humbert et al. 2009; Jaalouk and Lammerding 2009). Externally applied and cell-generated forces operate in coordinated manner to maintain cell and tissue structure and homeostasis which becomes disrupted in pathological conditions such as cancer.

1.6 Tissue mechanics and cancer

In general, cancer is a disease characterized by uncontrolled growth of abnormal cells which have undergone DNA mutation. The most commonly mutated gene in human tumors is p53, which is a tumor suppressor gene promoting arrest in G1 and G2 checkpoints of the cell cycle, apoptosis and DNA repair in response to damaged DNA (Lee 1995). The accumulation of DNA mutations promotes the development of cancers. For instance leukemias are cancers of white blood cells, which do not form solid tumors, but circulate in the blood vessels. However, 85% of human cancers form solid tumors, such as sarcomas, carcinomas and adenocarcinomas (Jemal, Siegel et al. 2008).These solid tumors transform over time from a benign cell mass into a malignant phenotype. Eventually, those malignant cells will spread to other parts of the body (metastasis) and become fatal. Cancer research has historically focused primarily on studying the role of genetic and biochemical changes in tumor progression. Only in recent years, the importance of mechanical properties in tumor biology has been increasingly appreciated. In growing solid tumors, cancer cells experience many different types of forces due to the uncontrolled cell proliferation in a confined space (Butcher, Alliston et al. 2009; Kumar and Weaver 2009).

Indeed, cancer cells in tumor tissue have been shown to experience 1) matrix stiffening due to abundant deposit of collagenous fibers synthetized by activated stromal myofibroblasts (Shao, Nguyen et al. 2000), 2), increased interstitial pressure due to a leaky vasculature and poor lymphatic drainage (Boucher and Jain 1992; Less, Posner et al. 1992) and 3) increased compressive stress due to the expanding tumor mass (Helmlinger, Netti et al.

1997; Cheng, Tse et al. 2009). Correspondingly as cancer cells escape from the tumor and get into blood vessels or lymphatic system, increased hydrostatic pressures enhance tumor cell adhesion to epithelium or ECM (Basson, Yu et al. 2000; Downey, Alwan et al. 2006). These data suggest that tumor cells exhibit very different mechanical properties than their normal counterparts. Studies with isolated cancer cells suggest that they become increasingly compliant as they transform, such that highly metastatic tumor cells are less stiff than normal cells (Cross, Jin et al. 2008). However, these measurements were conducted in culture and the mechanical properties of cells *in situ* and in culture can be very different. On the other hand, recent studies have shown that the viscoelasticity of living cells can be substantially modified by biochemical factors present in the context of a three-dimensional (3D) tissue environment (Plodinec et. al., unpublished) such as heterotypic cell-cell interactions (Khaldoyanidi, Glinsky et al. 2003), localized effects of the vasculature (Almqvist, Bhatia et al. 2004) and the ECM (Khaldoyanidi, Glinsky et al. 2003; Paszek, Zahir et al. 2005). Also, cancer cells are hypersensitive to ECM stiffness and exhibit elevated actomyosin-generated contractility when compared to normal cells (Baker, Bonnecaze et al. 2009; Lam, Cao et al. 2010).

Taken together, these results suggest that the intrinsic cytoskeletal behaviour of cancer cells, interactions with ECM and local microenvironmental conditions contribute to heterogeneous tumor phenotype. Notably, cytoskeleton, ECM organization (Kakkad, Solaiyappan et al. 2010) and tumor stiffness vary dramatically within the same tumor (Plodinec et.al., unpublished) providing a provocative explanation for some of the variability noted within a cancerous tissue *in vivo*. Discrepancies found between studies using isolated cancer cells and *in situ* analysis underscore the influence of the tissue microenvironment on cellular mechanical properties and the intrinsic differences of the mechanical properties between normal and transformed cells.

1.6.1 Hypoxia in cancer

Hypoxia is defined as a state of reduced oxygen (O2) availability or decreased O2 partial pressure below critical thresholds, thus restricting or even abolishing the function of organs, tissues, or cells. There is clear evidence that these hypoxic thresholds can vary widely, although an upper limit of 35 mmHg is set (Hockel and Vaupel 2001). Relative low partial oxygen pressure is a common feature of many solid tumours. Cancer cells become hypoxic because of the rapid proliferation within the tumor mass and the limited diffusion distance (i.e. 100-200 μm; dependent on the vasculature), as they outgrow the local blood supply (Brown and Giaccia 1998). Tumour hypoxia is a powerful driving force for malignant progression and has been identified as an adverse prognostic factor, since number of clinical studies have firmly established that hypoxia is associated with impaired response to both radiotherapy and chemotherapy (Hockel and Vaupel 2001; Vaupel and Mayer 2007). The latter effect is due to two main reasons: 1) poor perfusion and restricted drug access to hypoxic areas and 2) hypoxia-dependent adaptive changes in gene expression which probably play the major role in altered tumor response (Tredan, Galmarini et al. 2007).

1.6.1.1 Hypoxia-inducible factor-1 (HIF-1) structure and function

Hypoxic stress, induced by a decrease in O2 partial pressure below 5% (40 mmHg) activates the transcription factor Hypoxia-inducible factor-1(HIF-1), a heterodimer composed of an inducible, oxygen-sensitive α subunit and a constitutively expressed β subunit (Figure 1-10, (Brahimi-Horn and Pouyssegur 2007).

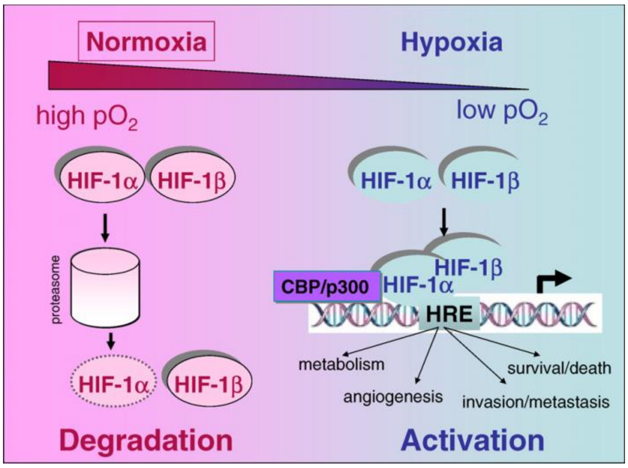

Figure 1-10. Degradation and activation of HIF-1 transcription factor in normoxia and hypoxia. The transcription factor HIF is composed of an alpha and beta subunit. Under atmospheric levels of oxygen (normoxia) the HIF-1α and HIF-1β subunits are constitutively expressed. Whereas HIF-1α is rapidly degraded by the 26S proteasomal system, HIF-1β remains constant. In contrast, under low levels of oxygen (hypoxia) HIF-1a escapes degradation, associates with HIF-1b and together they bind to hypoxia-response elements (HRE) in target genes. Reproduced from (Brahimi-Horn and Pouyssegur 2007).

Generally, HIF-1 is responsible for the transcription of more than 100 putative genes in hypoxic environments (Figure 1-11, (Semenza 2003) which occurs both during normal development and several pathophysiological conditions such as cancer (Semenza 2003).

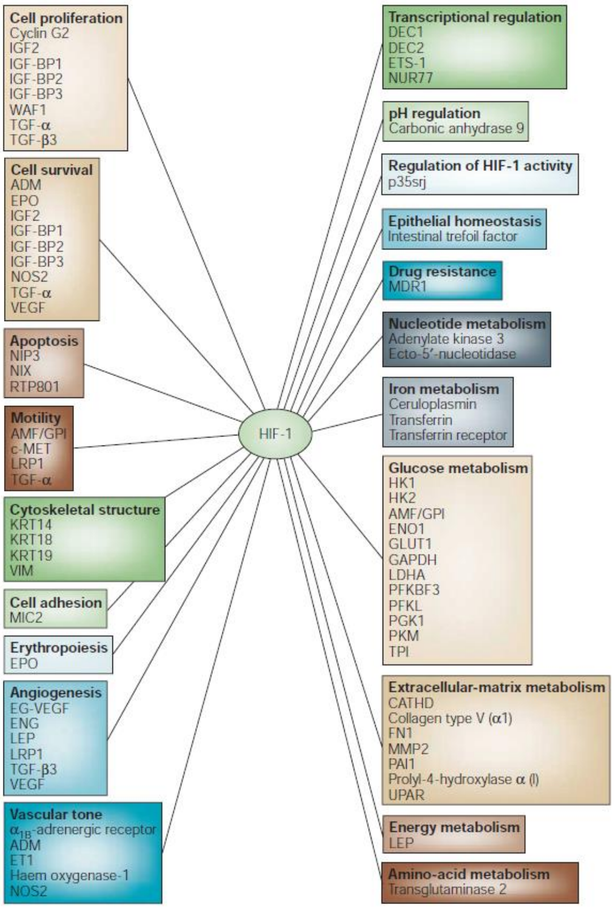

Figure 1-11. Genes that are transcriptionally activated by HIF-1. Reproduced from (Semenza 2003).

HIF-1 dependent pathways are involved in the control of cellular proliferation since hypoxia induces the expression of growth factors stimulating cell proliferation, such as PDGF, TGF-α and IGF2 (Mullerat, Deroide et al. 2003). Also under hypoxic conditions a switch occurs from aerobic metabolism to anaerobic glycolysis. HIF-1 regulates the expression of enzymes that are necessary for the glycolysis and glucose transporters such as GLUT1 and GLUT3, mediating glucose uptake by the cells (Zagorska and Dulak 2004). HIF-1 activates angiogenesis, via enhanced expression of the vascular growth factors ANG2 (angiopoeitin-2) and VEGF, encoded by one of the best HIF-1 target genes (Ferrara, Gerber et al. 2003). Under hypoxic conditions apoptosis is induced following HIF-1-dependent accumulation of p53, which results in selection of cells carrying mutations in *p53* and/or other genes involved in apoptosis control, making tumour cells less prone to drug-induced cell death. In addition, HIF-1 has been shown to downregulate the expression of pro-apoptotic genes in human cancer cells, thereby shifting the balance even further towards cell survival (Flamant, Notte et al. 2010). In addition, under hypoxia an increase is observed in telomerase activity, an enzyme essential to sustain the immortality of tumour cells (Nishi, Nakada et al. 2004). Hypoxia induces activation of anaerobic glycolysis and increased expression of type IX carbonic anhydrase which result in production of lactic acid and carbon dioxide causing high intracellular acidity relative to the extracellular space. This in turn contributes to tumour invasion by activating a number of proteases dependent on acidic pH Thus hypoxic cells, in contrast to normal cells, are able to escape and thus survive from a relatively acidic microenvironment (Pouyssegur and Mechta-Grigoriou 2006).

1.6.1.2 Hypoxia and cancer mechanics

Hypoxia stimulates cell adhesion and migration and ECM remodelling, and can cooperate with ECM stiffness to collectively influence cell behaviour (Erler, Bennewith et al. 2009). In addition to induced oncogene expression and DNA mutation rate, hypoxia could drive tumor progression through cytoskeleton and ECM remodelling. Previous studies have shown that hypoxia influences rearrangement of vimentin cytoarchitecture (Liu, Guevara et al. 2010) and promotes actin polymerization thus increase in cell stiffness (An, Pennella et al. 2005). Hypoxia increases ECM biosynthesis (Tamamori, Ito et al. 1997), fibrillar deposition (Kukacka, Bibova et al. 2007) and remodelling through overexpression of matrix remodelling enzymes (Le, Denko et al. 2004). Also, micro-array analysis revealed a correlation between lysyl oxidase (LOX) and hypoxia in human tumor cells (Denko, Fontana et al. 2003). Hypoxia induced LOX was shown to induce covalent- crosslinking of collagens and elastins, hence increasing tensile strength in living cells (Kagan and Li 2003). Consistent with this finding a recent study has shown that LOX dependent collagen-crosslinking of the mammary fat pad promotes collagen fibrinogenesis, gland stiffening and malignant progression (Levental, Yu et al. 2009). Interestingly, another very recent study demonstrates that within the same solid tumor, normoxic regions exhibited a dense mesh of collagen fibers, whereas much less and structurally altered collagen fibers were detected in hypoxic tumor regions consistently with increased LOX expression in hypoxic regions (Kakkad, Solaiyappan et al. 2010).

Indeed, structural and mechanical heterogeneity observed within solid tumor and discrepancies in published data signify at the same time the importance and the intricacy of the relationship between tumor hypoxia, cytoskeleton, ECM and mechanical response within tumor tissue.

1.6.2 Three-dimensional (3D) tumor models

Microenvironment and tissue architecture of tumors are significant regulators of cellular phenotype and functions with respect to malignant progression. These factors seem to determine the biochemical and molecular response of cancer cells to external cues. For small avascular tumors, the microenvironment can be closely reproduced in i*n vitro* model systems (Hirschhaeuser, Menne et al. 2010). Unfortunately, most of the *in vitro* experiments in the field of tumor biology were performed with monolayer cultures since they are easy and convenient to handle. However, although they provide a valuable model to study distinct functions, monolayer cultures insufficiently reflect the tumor pathobiology due to the lack of stroma components, extracellular matrix and fundamental geometric differences between two-dimensional (2D) cultures and three-dimensional (3D) solid tumors.

As already mentioned, the three-dimensional organisation of cells provides a complex network of cell-cell and cell-matrix interactions relevant for distribution and function of hormones, growth factors and nutrients influencing cellular differentiation, proliferation and survival. A 3D architecture of tumor cells needs to be generated *in vitro* to reflect the multicellular microenvironment when investigating tumor cell physiology and response to therapeutic agents. In order to approach this problem, 3D cell culture models were developed where tumor cells were cultured within gels, in scaffolds or as cellular multilayers (Pampaloni, Reynaud et al. 2007). The 3D architecture allows both the homologues and heterologous co-cultivation of tumor cells with fibroblast, immune and endothelial cells, enabling the investigation of tumor/stroma interaction effects in vitro (Kunz-Schughart, Heyder et al. 2001) .

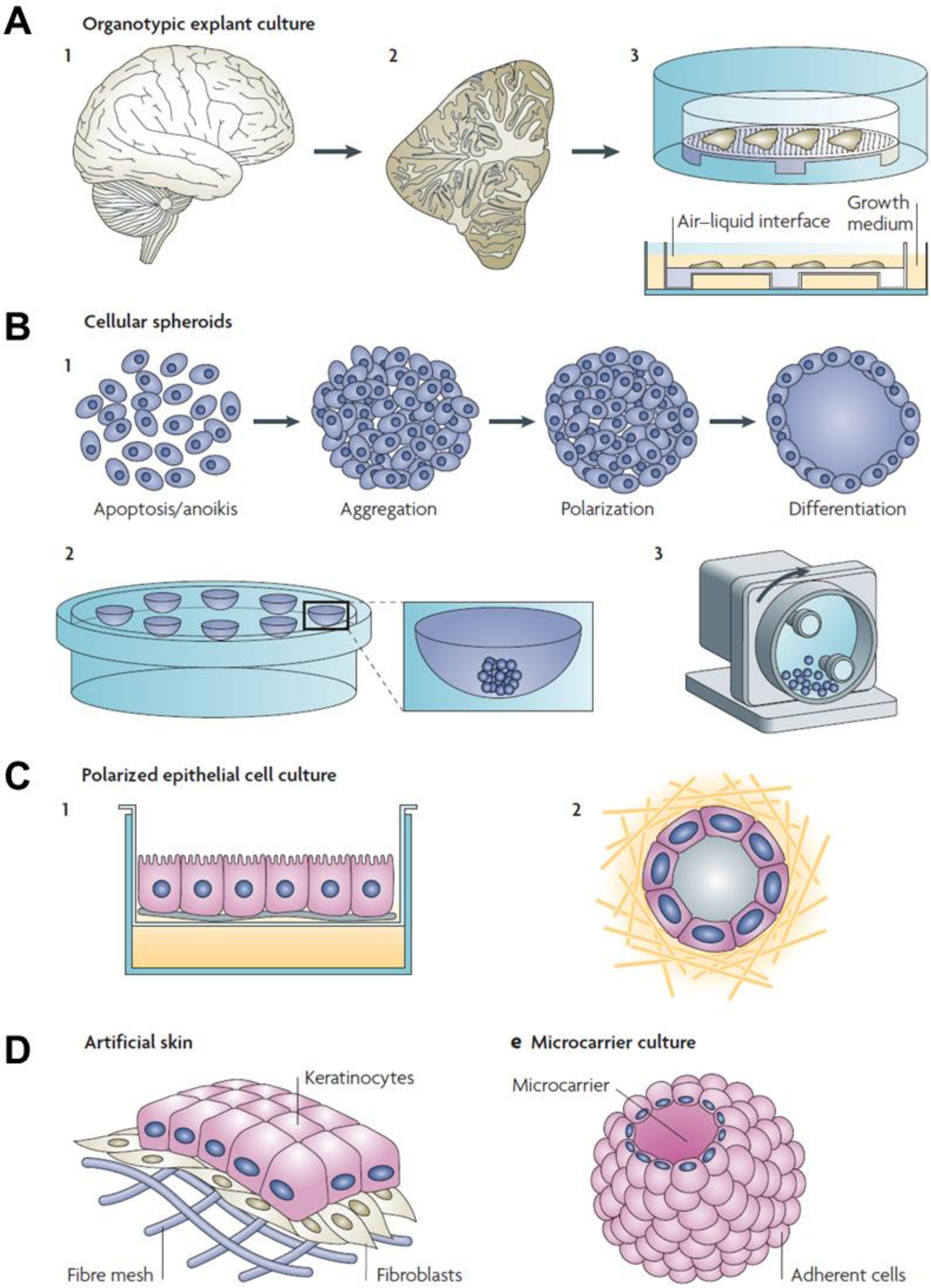

Figure 1-12. Schematic representation of three-dimensional (3D) culture models. (A) In an organotypic explant culture dissected organ slices are placed on porous substrates, supported by a metal grid and cultured at the air–liquid growth medium interface. (B) Cellular spheroids are shaped by aggregating cells from cell suspension into large aggregates on contact-inhibited surfaces. (C) Polarized epithelial cell cultures grown at the air–medium interface on porous membranes form polarized monolayers. (D) For artificial skin, primary fibroblasts are cultured in petri dishes and are subsequently seeded onto a biodegradable fibre mesh. After several weeks in culture, keratinocytes are placed onto the new dermal tissue and form an epidermal layer. (E) Microscaled materials (microcarriers) derived from dextran, gelatine, glycosaminoglycans and other porous polymers can be used as a 3D support for the culture of anchorage-dependent animal cell lines. Reproduced from (Pampaloni, Reynaud et. al. 2007).

1.6.2.1 The multicellular spheroid model and similarities to tumors

Multicellular spheroids consist of only one cell type and exhibit an intermediate complexity between an organotypic culture and real tissue because they do not integrate the influence of stromal components but maintain the three-dimensional architecture of tumors. This is evident by increased intercellular contacts and tight junctions leading to molecule transport limitations and the establishment of hypoxic and nutrient deprived regions. This is a very important property, because in contrast to monolayer cultures (even grown on a physiological ECM substrates), the spheroid model allows for establishing oxygen and nutrient gradients similarly as solid tumors *in vivo* (Mueller-Klieser 2000) . Therefore, multicellular spheroids have long been accepted as an *in vitro* model for solid tumors that mimic biological properties of micrometastases and vessel distal regions of tumors (Mueller-Klieser 2000). The similarity of the response patterns to radiation and therapy of tumors and tumor spheroids indicated the potential of the spheroid model to mimic tumor biology *in vitro* (Sutherla.Rm, Inch et al. 1970).

Tumor cells grown as spheroids synthesize and deposit matrix proteins with similar quantities and structural arrangement to those observed *in vivo* which is not detected in monolayer cultures (Nederman, Norling et al. 1984). Gene expression is also altered in cells grown as spheroids compared to monolayer cultures. For example, in a differential gene expression array study analysing metastatic melanoma cells, more than 100 genes were significantly upregulated in spheroids compared to their monolayer counterpart (Ghosh, Spagnoli et al. 2005). Growth kinetics described for solid tumors *in vivo* is similar to those observed in spheroids. A phase of exponential growth is followed by a decline in growth rate, associated with the accumulation of non-proliferating, hypoxic and in the later stage necrotic cells important for the vascularization process (Gimbrone, Cotran et al. 1972).

In fact, experiments performed on tumor spheroids showing that oxygen diffusion limits tumor spheroid growth flagged the way for the angiogenesis hypothesis (Folkman and Moscona 1978). Oxygen diffusion was shown to be constant regardless of spheroid size and is comparable to the diffusion detected in solid tumors (Muellerklieser 1984). Similar to avascular areas in tumors, nutrient and oxygen limitations as well as the accumulation of waste metabolites lead to the establishment of hypoxia and acidosis in core regions of spheroids (Groebe and Muellerklieser 1991). In the majority of the spheroids however, necrosis preceded hypoxia or no necrosis was detectable although oxygen pressure measured was close to 0 mm Hg (Mueller-Klieser 2000). This suggests that a limitation of oxygen supply is not always the single cause of necrosis and conversely detection of hypoxia is not necessarily an indicator for necrosis. Moreover, observations that spheroids from different tumor tissue origins cultivated under similar conditions displayed the onset of necrosis at different, individual spheroid sizes indicate that cell death depends on additional specific, properties of the tumor cell itself (Hirschhaeuser, Menne et al. 2010).

1.6.2.2 Methods to generate spheroids

Various culture techniques are used to generate spheroids (Santini and Rainaldi 1999). In the spinner (Sutherland and Durand 1984) and the gyratory rotation technique (Moscona 1961) trypsinized cells are placed in a culture vessel with a magnetic stirrer inhibiting cell attachment to the substrate and favouring cell-cell adhesion. In a more recently developed technique spheroids are grown in a hanging drop of an inverted micro-plate (Kelm, Timmins et al. 2003).

A most common and simple approach to the cultivation of MCTS is a liquid overlay. In the liquid-overlay technique, trypsinized cells are placed on dishes covered with a thin film of agar agarose, Poly (2- hydroxyethyl) methacrylate (Poly-HEMA), or fabricated from non-adherent materials (e.g., polystyrene Petri dishes) and a cell suspension is then layered over top (Carlsson and Yuhas 1984). PolyHEMA hydrogels exhibit physical properties similar to living tissues (high water content, soft and rubbery consistency, hydrophility, water permeability and low interfacial tension). PolyHEMA is well known to prevent cellular adhesion and spreading (Folkman and Moscona 1978). Because the coating prevents cell attachment to the dish, cells can grow only in 3D and individual cells give rise to aggregates or spheroid colonies. Although widely used this method is limited by either long cultivation time, formation of unequal-size spheroids, or difficult mechanical accessibility.

Simple modifications of the general approach can be employed to address some of these issues. Controlled aggregation of individual MCTS can be achieved by cultivation in 96-well plates coated with PolyHEMA (all cells contributing to one MCTS in each well) and using shakers to facilitate the cell suspension.

1.6.2.3 Mechanical properties of tumor spheroids

Mechanical properties of a tissue are highly relevant for tumor development and progression. Multicellular spheroids are established as a fundamental tool for studying the role of microenvironment in tumor cell physiology and therapeutic problems associated with metabolic and proliferative gradients in a 3D cellular context (Rodriguez-Enriquez, Gallardo-Perez et al. 2008; Hirschhaeuser, Menne et al. 2010). Development of optimized and novel biochemical and optical methods has significantly contributed to our understanding of the biochemical environment of *in vitro* tumor models, as for example hypoxia and low pH (Koike, McKee et al. 2002; Pampaloni, Reynaud et al. 2007). However, due to a lack of effort and techniques to measure the mechanical properties of tumor spheroids, the influence of biochemical factors such as hypoxia on the mechanical response of avascular tumor models is poorly understood.

The heterogeneity of a tumor makes the spatial quantification of mechanical properties even more challenging. Only few studies addressed the question of the effect of compressive stress produced by cells on their microenvironment (Helmlinger, Netti et al. 1997) and the effect of local stress on the growth dynamic within the spheroid (Helmlinger, Netti et al. 1997; Cheng, Tse et al. 2009). Their findings suggest that the mechanical heterogeneity of the confining tissue can guide morphological changes in tumor growth by inducing apoptosis in regions of high compressive stress and allowing proliferation in regions of low stress, thus controlling the tumor growth in a rigid environment. However, it should be taken into consideration that tumor spheroids confined in agarose or agar gels, cannot degrade the gel. It is plausible that such mechanical restriction opposed on expanding tumor cells alters their properties inversely than found *in vivo*. *In vivo,* tumor cells under stress (low oxygen) manage to degrade the ECM which allows them to escape and invade neighbouring tissues and ultimately metastasize to distant organs (Storz, Doppler et al. 2009). In this respect, it important that both the spheroid growth and mechanical studies are performed in physiologically confined microenvironment.

1.7 Tissue mechanics and breast cancer

1.7.1 Normal mammary gland function and tumorigenesis

Mammary gland consists of ductal cells, milk producing alveolar epithelial cells which are embedded in stromal connective tissue and the mammary fat pad. Mammary epithelial cells organize into three-dimensional structures, which are strongly dependent on a polarized morphology, specialized cell-cell contacts and the attachment to an underlying basement membrane (Figure 1-13; Butcher, Alliston et al. 2009). Cell-cell and cell-ECM adhesive interactions regulate functions of normal mammary gland and are critical for maintenance of tissue homeostasis (Naylor, Li et al. 2005; Kass, Erler et al. 2007). Mechanical forces and signalling from neighbouring cells and ECM regulate cellular organization and are prerequisite for the proper control of cell proliferation, survival, differentiation, migration and milk protein secretion (Rodriguezboulan and Salas 1989; Bissell, Weaver et al. 2001).

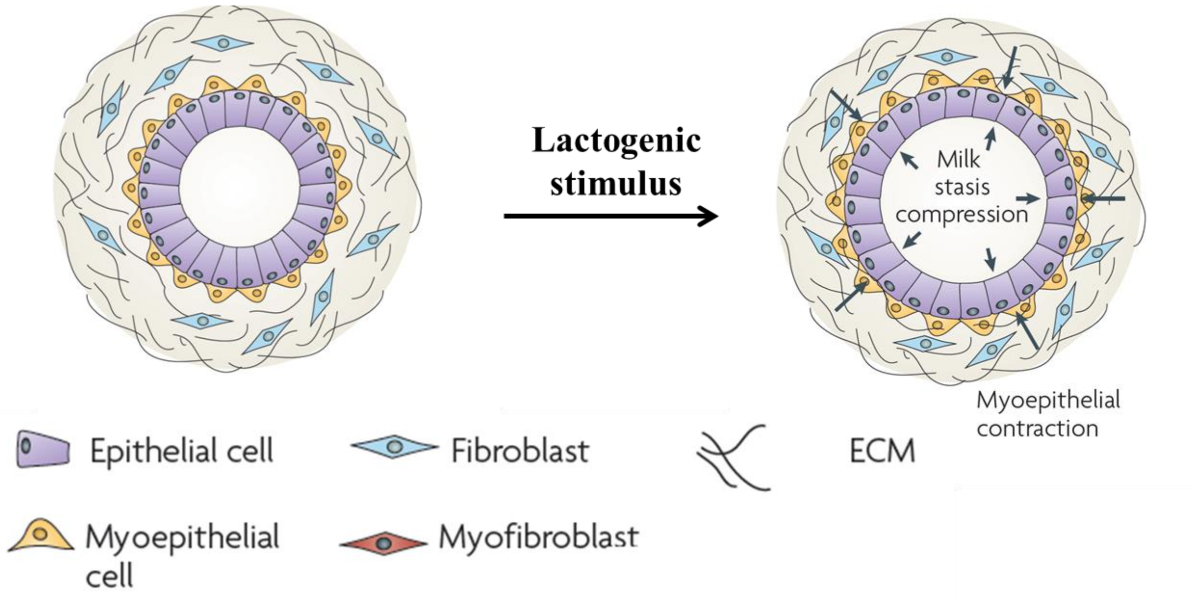

Figure 1-13. The normal mammary gland acts as a mechanically active tissue. The developing breast is subjected to a number of forces that facilitate its normal function. During lactation the normal breast experiences compressive stress on the luminal epithelial cells and the basement membrane due to the accumulation of milk and alveolar enlargement. Upon sucking and oxytocin stimulation, epithelial cells encounter inward tensile stress as the myoepithelium contracts to force the milk out of the alveolar sacs. In the absence of this stimulus, milk will accumulate within the acinus and eventually exert an outward projecting compressive force on the surrounding epithelium. This compressive force is opposed by a compensatory inward projecting resistance force. Chronic exposure to these forces induces apoptotic cues so that the gland undergoes involution accompanied by extensive remodelling of the epithelium and stroma. Modified from (Butcher, Alliston et al. 2009).

Normal tissue structure and mechanical equilibrium are disrupted during tumor initiation and progression. Because the behaviour, structure and organization within the tissue are continuously changing as the cancer progresses, the mechanical properties also evolve. In breast, the mechanical characteristics in a 1) hyperplasia (benign lesion), 2) carcinoma *in situ* (primary tumor), 3) invasive lesion (invasion to surrounding tissues) and 4) metastatic lesion (invasion to distant organs) can be very different (Figure 1-14; Butcher, Alliston et al. 2009).

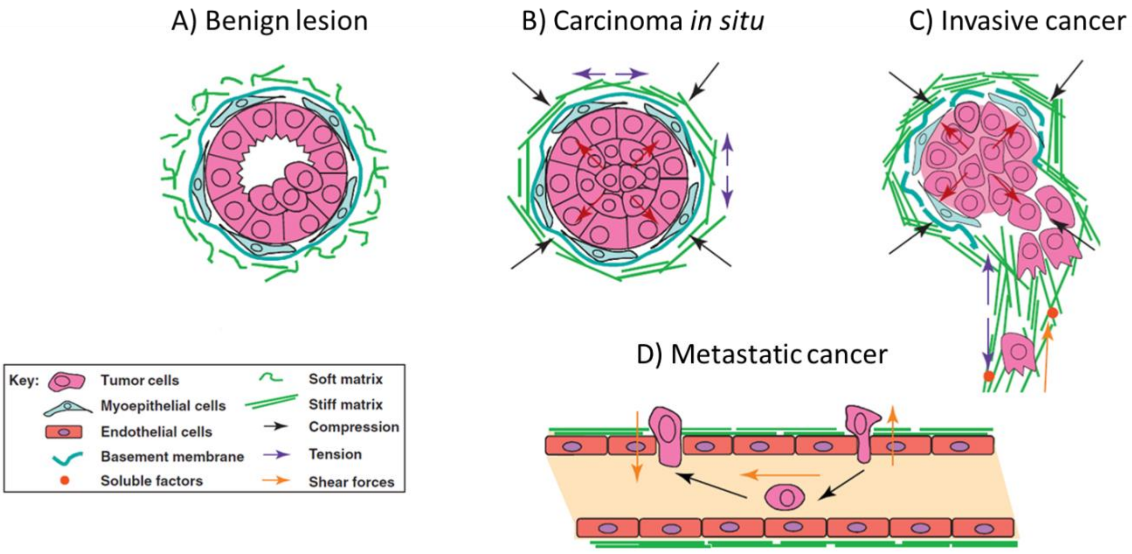

Figure 1-14. Breast cancer progression is associated with continuous alterations in tissue and cell mechanics. (A) In hyperplastic lesions, cells gradually lose polarity and grow into the luminal space. The myoepithelial cell layer and the basement membrane remain intact. (B) In carcinoma *in situ* lesions, cell polarity is lost and the lumen is filled by neoplastic cells that exhibit uncontrolled growth in confined volume. In this case only the basement membrane still remains intact. (C) In invasive lesions, tumor cells break down the basement membrane and invade into the interstitial ECM. As tumor cells invade through the basement membrane and ECM, they experience a range of different forces. (D) During intravasation and extravasation, tumor cells experience forces, as for example shear, from blood flow and neighbouring cells, which facilitate their transport in and out of the vessels. Modified from (Butcher, Alliston et al. 2009).

1.7.1.1 Benign lesion

A hyperplastic (benign) lesion typically involves loss normal cell polarization and organization, disruption of cell-cell and cell-ECM adhesions which results in altered mechanical response (Plodinec et. al., unpublished) and mechano-sensing and transduction (Schwartz and DeSimone 2008). In particular hyperplastic lesion is characterized by increased matrix deposition, cell proliferation and thickening of the basement membrane, which altogether contribute to tissue stiffening (Ingber 2008). The most important property of benign lesions is that they do not experience biochemical and/or mechanical signals that facilitate invasion to nearby tissues or spread to other parts of the body and cells remain confined within the myoepithelium.

1.7.1.2 Carcinoma *in situ*

Carcinoma *in situ* is characterized by uncontrolled cell growth due to genetic and epigenetic alterations and reduced cell death within an intact basement membrane and interstitial ECM (Anderson, Weaver et al. 2006). In addition, cancer cells exhibit pleomorphic characteristics, hence vary in size and shape, often including multinucleate giant cells with atypical nuclei

(Elston and Ellis 1991). Uncontrolled cell growth and consequently the increase in tumor mass within the restricted volume lead to elevated compression on the surrounding ECM (Sarntinoranont, Rooney et al. 2003). Also due to the tumor growth, biochemical factors such as intratumoral hypoxia can further contribute to mechanical changes. In response to hypoxia, tumor and stromal cells secrete various soluble factors, facilitating matrix remodelling including basement membrane breakdown and angiogenesis, which overall endorse cell invasion (Tlsty and Coussens 2006).

1.7.1.3 Invasive cancer

Local tumor invasion is an early step in the complex process of tumor dissemination (Fidler 1978). In invasive tumor cell-cell interactions further decrease and tumor cells disseminate through damaged basement membrane and interstitial ECM (Sugarbaker 1993). Invading cells are accompanied by surrounding stromal cells (fibroblasts and macrophages) and migrate by degrading the matrix following biochemical gradients towards the circulatory system (Wyckoff, Jones et al. 2000; Condeelis and Pollard 2006). Various mechanical forces such as interstitial compression, shear and ECM tension can guide the direction and rate of tumor cell migration (Kumar and Weaver 2009). In particular, they influence cell cytoskeleton remodelling, resulting in stiffness decrease and allowing cancer cells to overcome boundaries between different tissues and intravasate vessels (Fritsch, Hockel et al. 2010).

1.7.1.4 Metastatic cancer

During intravasation and transportation in the bloodstream and/or lymphatic flow tumor cells are exposed to shear forces and hydrodynamic flow which promote their transport and enable interactions with leukocytes and endothelial cells to permit extravasation (Liang, Slattery et al. 2008). Cancer cells display organ specific-metastasis which can depend on the intrinsic genetics of tumor cells, the affinity of tissues to host metastatic cells and the pattern of circulation within the tissue (Nguyen, Bos et al. 2009). Breast cancer commonly spreads to the regional lymph nodes, bones, lungs, liver, or brain (Muller, Homey et al. 2001). In general, cells can selectively grow on and within specific substrates according to their mechanical properties (Discher, Janmey et al. 2005). In this respect, organ specific mechanical properties can contribute to the preferential migration, attachment, survival and proliferation of cancer cells in specific organs (Kostic, Lynch et al. 2009; Pathi, Kowalczewski et al. 2010).

1.7.2 Mouse models of breast cancer

Our understanding of breast cancer progression and metastasis has greatly profited from the use of genetically modified mouse models and advanced transplantation techniques. A number of mouse models exist that allow for the systematic and reproducible study of breast cancer growth and metastasis (Vargo-Gogola and Rosen 2007). Unfortunately, only few of these mouse models reflect the complexity of human breast cancers, especially their progression to metastasis (Robles and Varticovski 2008).

1.7.2.1 MMTV-PyMT mouse model

One of the best-characterized models for breast cancer progression is the MMTV-PyMT model. In this model, the expression of the oncoprotein, polyoma middle T antigen (PyMT mice) is controlled and restricted by the mouse mammary tumor virus (MMTV) only to the mammary epithelium (Guy, Cardiff et al. 1992). PyMT is a protein attached to the plasma membrane, encoded by the small DNA polyoma virus and not expressed in human breast cells. Nevertheless, it a powerful oncogene because it regulates several signalling pathways such as *Src* family, *ras* and PI3 kinase pathways, that are altered in human breast cancers (Dankort and Muller 2000). In addition, in PyMT mice mammary glands, the expression of PyMT is found to be associated with an increased *c-myc* level, a gene located in one of the three amplified chromosomal regions found in human primary breast cancer (Guy, Cardiff et al. 1992; Brison 1993). Detailed histological, biochemical and molecular analysis has shown that PyMT model has many similarities with human breast cancer. Tumor formation and progression are characterized by four stages: 1) hyperplasia, 2), carcinoma *in situ*, 3) invasive cancer and 4) metastatic cancer (Lin, Jones et al. 2003). In the PyMT model onset of tumor and its behaviour is hormonally regulated by loss of estrogen and progesterone receptors (ERs and PRs respectively) and overexpression of human epidermal growth factor receptor 2 (Her2/neu) and cyclin D1, similarly to human breast cancers with poor prognosis (Lapidus, Nass et al. 1998; Menard, Tagliabue et al. 2000) . Furthermore, during progression to malignancy these mice exhibit altered expression of integrin-β which plays an important role in regulating cell proliferation, differentiation, and apoptosis of normal mammary epithelium (Bissell, Radisky et al. 2002). Indeed, studies have shown that MMTV-PyMT mice are characterized by short latency, a high penetrance, and a high incidence of lung metastasis (Lin, Nguyen et al. 2001). Also, the same study showed that the kinetics of tumor progression is reproducible and occurs independently of pregnancy.

Taken together, these studies indicate that the PyMT model recapitulates many processes found in human breast cancers, not only morphologically but also in the expression pattern of biomarkers associated with poor prognosis. Therefore, MMTV-PyMT mouse model of mammary carcinogenesis represents a powerful tool for investigating the fundamental mechanisms associated with tumor progression and metastases in human breast cancer.

1.7.3 Breast cancer diagnostics

Breast cancer is the most frequently diagnosed form of cancer and the second leading cause of dead in Western women (http://www.who.int/cancer/detection/breastcancer/en/). While primary tumor is not a deadly disease, occurrence of local and/or distant metastasis significantly decreases therapy options and consequently the life expectancy (Polyak 2007). Therefore, early, accurate and fast diagnostic procedures are crucial for enabling optimal treatment. Currently, typical clinical examination comprises manual palpation and breast ultrasound, usually a mammography and if necessary also magnetic resonance imaging. In case of suspicious, palpable and non-palpable lesions (www.acr.org) an invasive diagnostic procedure using a biopsy tool is mandatory to rule out or to confirm the diagnosis of breast cancer. Subsequently, a histopathological examination of surgically removed tissue sample is performed which is considered as the gold standard for the diagnosis of malignancy in any organ system. However, the disadvantage of the histology is that it is slow because the sample preparation requires between 2-5 days depending on the particular staining procedure. In addition, multiple studies in various cancers have demonstrated discrepancy rates of up to 30% with an average of approximately 10%. A "discrepancy" happens when one pathologist renders a diagnosis and another pathologist looks at the same material and renders a different opinion (Gupta and Layfield 2000). Therefore, the general aim is to develop objective and quantitative cancer detection methods.

1.7.3.1Mechanical markers of breast cancer

The difference in mechanical properties between normal and abnormal breast tissue has long been recognized (Bassler 1996). Many researchers have proposed non-invasive macroscopic techniques for examining breast tissues that rely upon imaging and acquiring quantitative stiffness contrasts (Garra, Cespedes et al. 1997; Zhu, Jiang et al. 2008; Kumm, Chau et al. 2010).

Elastography is a technique that uses the stiffness differences to detect the tumors in the breast by providing quantitative modulus results. In elastography, external static compression (ultrasound elastography) or harmonic shear waves (magnetic resonance elastography) are applied to the tissue for stimulation. The resulting tissue displacements are then monitored using ultrasound (ultrasound elastography) (Hiltawsky, Kruger et al. 2001) or MRI(Lawrence, Mahowald et al. 2000). These displacements are then used to reconstruct tissue stiffness. Using ultrasound elastography the Young's (elastic) modulus of the tissues can be measured. The Young's modulus is measured by using the strain values before and after compressing the tissue by a known amount and comparing the time difference between the pre and post compression states (Hiltawsky, Kruger et al. 2001). Using magnetic resonance elastography, shear modulus of the tissue can be measured (Sinkus, Siegmann et al. 2007). Acoustic shear waves are sent to the tissue, and an MRI based method is used to image the propagation of the waves inside the tissue. Ultrasound elastography has the advantage of detecting the invisible lesions that cannot be detected using regular ultrasound (Zhi, Ou et al. 2007) . But it has the limitation of detecting various scattered lesions. Magnetic resonance elastography has a limitation of detecting small lesions (Mariappan, Glaser et al. 2010). Both, the ultrasound elastography and the MRI elastography have been recently introduced into clinical application.

Whereas these macroscopic methods visualize the mechanical response of the tissue within a breast, other microscopic *ex vivo* techniques are starting to emerge. They employ portable indentation devices that apply either uniaxial cyclic compression or punch indentation to measure mechanical response of a breast biopsy in ambient conditions (Hansma, Yu et al. 2009). In order to estimate the relative elastic modulus of the tissue from the indention measurements, different types of tissue are compared (tumor, normal, benign, fat, etc.). Unfortunately, these techniques do not possess high enough resolution to detect and evaluate heterogeneous behaviour of malignant breast tumors which would be the crucial improvement to current diagnostic accuracy.

Recent developments in atomic force microscopy (AFM) have allowed probing mechanical properties of human cartilage biopsies at a nanoscopic level under physiological conditions (Stolz, Gottardi et al. 2009). Although AFM stiffness measurements have started to provide important insights into the mechanical properties of human normal and cancer cells (Cross, Jin et al. 2007), the majority of information is obtained on cultured cells which lack cell-cell and cell-ECM interactions that occur during breast cancer development and progression. Hence, establishing an AFM setup for measuring nanomechanical properties of breast biopsies under native conditions might provide accurate, reliable and fast diagnostic method for breast cancer.

1.8 References

Ackbarow, T. and M. J. Buehler (2009). "Molecular Mechanics of Stutter Defects in Vimentin Intermediate Filaments." Experimental Mechanics 49(1): 79-89.

Alcaraz, J., L. Buscemi, et al. (2003). "Microrheology of human lung epithelial cells measured by atomic force microscopy." Biophysical Journal 84(3): 2071-2079.

Alenghat, F. J., S. M. Nauli, et al. (2004). "Global cytoskeletal control of mechanotransduction in kidney epithelial cells." Experimental Cell Research 301(1): 23-30.

Almqvist, N., R. Bhatia, et al. (2004). "Elasticity and adhesion force mapping reveals real-time clustering of growth factor receptors and associated changes in local cellular rheological properties." Biophysical Journal 86(3): 1753-1762.

An, S. S., C. M. Pennella, et al. (2005). "Hypoxia alters biophysical properties of endothelial cells via p38 MAPK- and Rho kinase-dependent pathways." American Journal of Physiology-Cell Physiology 289(3): C521-C530.

Anderson, A. R. A., A. M. Weaver, et al. (2006). "Tumor morphology and phenotypic evolution driven by selective pressure from the microenvironment." Cell 127(5): 905-915.

Baker, E. L., R. T. Bonnecaze, et al. (2009). "Extracellular Matrix Stiffness and Architecture Govern Intracellular Rheology in Cancer." Biophysical Journal 97(4): 1013-1021.

Bassler, R. (1996). "Diseases of the breast." Pathologe 17(1): 92-97.

Basson, M. D., C. F. Yu, et al. (2000). "Effects of increased ambient pressure on colon cancer cell adhesion." Journal of Cellular Biochemistry 78(1): 47-61.

Bathe, M., C. Heussinger, et al. (2008). "Cytoskeletal bundle mechanics." Biophysical Journal 94(8): 2955-2964.

Bausch, A. R., F. Ziemann, et al. (1998). "Local measurements of viscoelastic parameters of adherent cell surfaces by magnetic bead microrheometry." Biophysical Journal 75(4): 2038-2049.

Beebe, D. J., G. A. Mensing, et al. (2002). "Physics and applications of microfluidics in biology." Annual Review of Biomedical Engineering 4: 261-286.

Berk, D. and E. Evans (1991). "Detachment of Agglutinin-Bonded Red-Blood-Cells .3. Mechanical Analysis for Large Contact Areas." Biophysical Journal 59(4): 861-872.

Binnig, G., C. F. Quate, et al. (1986). "Atomic Force Microscope." Physical Review Letters 56(9): 930-933.

Biot, M. A. and F. M. Clingan (1941). "Consolidation settlement of a soil with an impervious top surface." Journal of Applied Physics 12(7): 578-581.

Bird, J. L. E., D. Platt, et al. (2000). "Exercise-induced changes in proteoglycan metabolism of equine articular cartilage." Equine Veterinary Journal 32(2): 161-163.

Bissell, M. J., D. C. Radisky, et al. (2002). "The organizing principle: microenvironmental influences in the normal and malignant breast." Differentiation 70(9-10): 537-546.

Bissell, M. J., V. Weaver, et al. (2001). "The structural basis of tissue-specific signaling in normal and malignant breast." Molecular Biology of the Cell 12: 1A-1A.

Boucher, Y. and R. K. Jain (1992). "Microvascular Pressure Is the Principal Driving Force for Interstitial Hypertension in Solid Tumors - Implications for Vascular Collapse." Cancer Research 52(18): 5110-5114.

Brahimi-Horn, M. C. and J. Pouyssegur (2007). "Oxygen, a source of life and stress." Febs Letters 581(19): 3582-3591.

Brangwynne, C. P., F. C. MacKintosh, et al. (2006). "Microtubules can bear enhanced compressive loads in living cells because of lateral reinforcement." Journal of Cell Biology 173(5): 733-741.

Brison, O. (1993). "Gene Amplification and Tumor Progression." Biochimica Et Biophysica Acta 1155(1): 25-41.

Brooke, B. S., A. Bayes-Genis, et al. (2003). "New insights into elastin and vascular disease." Trends in Cardiovascular Medicine 13(5): 176-181.

Brown, J. M. and A. J. Giaccia (1998). "The unique physiology of solid tumors: Opportunities (and problems) for cancer therapy." Cancer Research 58(7): 1408-1416.

Brown, M. J., J. A. Hallam, et al. (2001). "Rigidity of circulating lymphocytes is primarily conferred by vimentin intermediate filaments." Journal of Immunology 166(11): 6640-6646.

Buda, A. and M. Pignatelli (2004). "Cytoskeletal network in colon cancer: from genes to clinical application." International Journal of Biochemistry & Cell Biology 36(5): 759-765.

Burr, D. B., A. G. Robling, et al. (2002). "Effects of biomechanical stress on bones in animals." Bone 30(5): 781-786.

Butcher, D. T., T. Alliston, et al. (2009). "A tense situation: forcing tumour progression." Nature Reviews Cancer 9(2): 108-122.

Butler, J. P., I. M. Tolic-Norrelykke, et al. (2002). "Traction fields, moments, and strain energy that cells exert on their surroundings." American Journal of Physiology-Cell Physiology 282(3): C595-C605.

Carlier, M. F. and D. Pantaloni (1997). "Control of actin dynamics in cell motility." Journal of Molecular Biology 269(4): 459-467.

Carlsson, J. and J. M. Yuhas (1984). "Liquid-Overlay Culture of Cellular Spheroids." Recent Results in Cancer Research 95: 1-23.

Chandran, P. L. and V. H. Barocas (2004). "Microstructural mechanics of collagen gels in confined compression: Poroelasticity, viscoelasticity, and collapse." Journal of Biomechanical Engineering-Transactions of the Asme 126(2): 152-166.

Charras, G. T., T. J. Mitchison, et al. (2009). "Animal cell hydraulics." Journal of Cell Science 122(18): 3233-3241.

Charras, G. T., J. C. Yarrow, et al. (2005). "Non-equilibration of hydrostatic pressure in blebbing cells." Nature 435(7040): 365-369.

Chaudhuri, O., S. H. Parekh, et al. (2007). "Reversible stress softening of actin networks." Nature 445(7125): 295-298.

Chen, A. C. and R. L. Sah (1998). "Effect of static compression on proteoglycan biosynthesis by chondrocytes transplanted to articular cartilage in vitro." Journal of Orthopaedic Research 16(5): 542-550.

Chen, C. S. and D. E. Ingber (1999). "Tensegrity and mechanoregulation: from skeleton to cytoskeleton." Osteoarthritis and Cartilage 7(1): 81-94.

Chen, C. S., J. Tan, et al. (2004). "Mechanotransduction at cell-matrix and cell-cell contacts." Annual Review of Biomedical Engineering 6: 275-302.

Chen, J. X., B. Fabry, et al. (2001). "Twisting integrin receptors increases endothelin-1 gene expression in endothelial cells." American Journal of Physiology-Cell Physiology 280(6): C1475-C1484.

Cheng, G., J. Tse, et al. (2009). "Micro-Environmental Mechanical Stress Controls Tumor Spheroid Size and Morphology by Suppressing Proliferation and Inducing Apoptosis in Cancer Cells." Plos One 4(2): -.

Chien, S., L. P. A. Sung, et al. (1992). "Red-Cell Membrane Elasticity as Determined by Flow Channel Technique." Biorheology 29(5-6): 467-478.

Condeelis, J. and J. W. Pollard (2006). "Macrophages: Obligate partners for tumor cell migration, invasion, and metastasis." Cell 124(2): 263-266.

Cowin, S. C. (1998). "Bone fluid poroelasticity." Poromechanics: 391-396

Crick, F. H. C. (1950). "The Physical Properties of Cytoplasm - a Study by Means of the Magnetic Particle Method .2. Theoretical Treatment." Experimental Cell Research 1(4): 505-533.

Crick, F. H. C. and A. F. W. Hughes (1950). "The Physical Properties of Cytoplasm - a Study by Means of the Magnetic Particle Method .1. Experimental." Experimental Cell Research 1(1): 37-80.

Cross, S. E., Y. S. Jin, et al. (2007). "Nanomechanical analysis of cells from cancer patients." Nature Nanotechnology 2(12): 780-783.

Cross, S. E., Y. S. Jin, et al. (2008). "AFM-based analysis of human metastatic cancer cells." Nanotechnology 19(38): -.

Dahl, K. N., A. J. Engler, et al. (2005). "Power-law rheology of isolated nuclei with deformation mapping of nuclear substructures." Biophysical Journal 89(4): 2855-2864.

Dankort, D. L. and W. J. Muller (2000). "Signal transduction in mammary tumorigenesis: a transgenic perspective." Oncogene 19(8): 1038-1044.

Darling, E. M., S. Zauscher, et al. (2006). "Viscoelastic properties of zonal articular chondrocytes measured by atomic force microscopy." Osteoarthritis and Cartilage 14(6): 571-579.

Das, M., A. J. Levine, et al. (2008). "Buckling and force propagation along intracellular microtubules." Epl 84(1): -.

Davies, P. F., A. Remuzzi, et al. (1986). "Turbulent Fluid Shear-Stress Induces Vascular Endothelial-Cell Turnover Invitro." Proceedings of the National Academy of Sciences of the United States of America 83(7): 2114-2117.

Davies, P. F., J. Zilberberg, et al. (2003). "Spatial microstimuli in endothelial mechanosignaling." Circulation Research 92(4): 359-370.

Denko, N. C., L. A. Fontana, et al. (2003). "Investigating hypoxic tumor physiology through gene expression patterns." Oncogene 22(37): 5907-5914.

Deriu, M. A., S. Enemark, et al. (2007). "Tubulin: from atomistic structure to supramolecular mechanical properties." Journal of Materials Science 42(21): 8864-8872.

Desai, A. and T. J. Mitchison (1997). "Microtubule polymerization dynamics." Annual Review of Cell and Developmental Biology 13: 83-117.

Discher, D. E., P. Janmey, et al. (2005). "Tissue cells feel and respond to the stiffness of their substrate." Science 310(5751): 1139-1143.

Discher, D. E., N. Mohandas, et al. (1994). "Molecular Maps of Red-Cell Deformation - Hidden Elasticity and in-Situ Connectivity." Science 266(5187): 1032-1035.

Downey, C., K. Alwan, et al. (2006). "Pressure stimulates breast cancer cell adhesion independently of cell cycle and apoptosis regulatory protein (CARP)-1 regulation of focal adhesion kinase." American Journal of Surgery 192(5): 631-635.

Dudek, S. M. and J. G. N. Garcia (2001). "Cytoskeletal regulation of pulmonary vascular permeability." Journal of Applied Physiology 91(4): 1487-1500.

Dzamba, B. J., K. R. Jakab, et al. (2009). "Cadherin Adhesion, Tissue Tension, and Noncanonical Wnt Signaling Regulate Fibronectin Matrix Organization." Developmental Cell 16(3): 421-432.

Elston, C. W. and I. O. Ellis (1991). "Pathological Prognostic Factors in Breast-Cancer .1. The Value of Histological Grade in Breast-Cancer - Experience from a Large Study with Long-Term Follow-Up." Histopathology 19(5): 403-410.

Engler, A. J., P. O. Humbert, et al. (2009). "Multiscale Modeling of Form and Function." Science 324(5924): 208-212.

Eriksson, J. E., T. Dechat, et al. (2009). "Introducing intermediate filaments: from discovery to disease." Journal of Clinical Investigation 119(7): 1763-1771.

Erler, J. T., K. L. Bennewith, et al. (2009). "Hypoxia-Induced Lysyl Oxidase Is a Critical Mediator of Bone Marrow Cell Recruitment to Form the Premetastatic Niche." Cancer Cell 15(1): 35-44.

Esue, O., Y. Tseng, et al. (2009). "alpha-Actinin and Filamin Cooperatively Enhance the Stiffness of Actin Filament Networks." Plos One 4(2): -.

Fabry, B., G. N. Maksym, et al. (2001). "Signal transduction in smooth muscle - Selected contribution: Time course and heterogeneity of contractile responses in cultured human airway smooth muscle cells." Journal of Applied Physiology 91(2): 986-994.

Farge, E. (2003). "Mechanical induction of twist in the Drosophila foregut/stomodeal primordium." Current Biology 13(16): 1365-1377.

Fenteany, G., P. A. Janmey, et al. (2000). "Signaling pathways and cell mechanics involved in wound closure by epithelial cell sheets." Current Biology 10(14): 831-838.

Ferrara, N., H. P. Gerber, et al. (2003). "The biology of VEGF and its receptors." Nature Medicine 9(6): 669-676.

Fettiplace, R. and C. M. Hackney (2006). "The sensory and motor roles of auditory hair cells." Nature Reviews Neuroscience 7(1): 19-29.

Fidler, I. J. (1978). "Tumor Heterogeneity and Biology of Cancer Invasion and Metastasis." Cancer Research 38(9): 2651-2660.

Flamant, L., A. Notte, et al. (2010). "Anti-apoptotic role of HIF-1 and AP-1 in paclitaxel exposed breast cancer cells under hypoxia." Molecular Cancer 9: -.

Folkman, J. and A. Moscona (1978). "Role of Cell-Shape in Growth-Control." Nature 273(5661): 345-349.

Forgacs, G., R. A. Foty, et al. (1998). "Viscoelastic properties of living embryonic tissues: a quantitative study." Biophysical Journal 74(5): 2227-2234.

Friedl, P. and K. Wolf (2009). "Proteolytic interstitial cell migration: a five-step process." Cancer and Metastasis Reviews 28(1-2): 129-135.

Fritsch, A., M. Hockel, et al. (2010). "Are biomechanical changes necessary for tumour progression?" Nature Physics 6(10): 730-732.

Fudge, D. S., K. H. Gardner, et al. (2003). "The mechanical properties of hydrated intermediate filaments: Insights from hagfish slime threads." Biophysical Journal 85(3): 2015-2027.

Gao, M., M. Sotomayor, et al. (2006). "Molecular mechanisms of cellular mechanics." Physical Chemistry Chemical Physics 8(32): 3692-3706.

Garra, B. S., E. I. Cespedes, et al. (1997). "Elastography of breast lesions: Initial clinical results." Radiology 202(1): 79-86.

Geiger, B., A. Bershadsky, et al. (2001). "Transmembrane extracellular matrix-cytoskeleton crosstalk." Nature Reviews Molecular Cell Biology 2(11): 793-805.

Gerthoffer, W. T. (2005). "Actin cytoskeletal dynamics in smooth muscle contraction." Canadian Journal of Physiology and Pharmacology 83(10): 851-856.

Ghosh, S., G. C. Spagnoli, et al. (2005). "Three-dimensional culture of melanoma cells profoundly affects gene expression profile: A high density oligonucleotide array study." Journal of Cellular Physiology 204(2): 522-531.

Gifford, S. C., M. G. Frank, et al. (2003). "Parallel microchannel-based measurements of individual erythrocyte areas and volumes." Biophysical Journal 84(1): 623-633.

Gimbrone, M. A., R. S. Cotran, et al. (1972). "Tumor Dormancy in-Vivo by Prevention of Neovascularization." Journal of Experimental Medicine 136(2): 261-&.

Gittes, F., B. Mickey, et al. (1993). "Flexural Rigidity of Microtubules and Actin-Filaments Measured from Thermal Fluctuations in Shape." Journal of Cell Biology 120(4): 923-934.

Green, K. J. and J. C. R. Jones (1996). "Desmosomes and hemidesmosomes: Structure and function of molecular components." Faseb Journal 10(8): 871-881.

Grodzinsky, A. J., M. E. Levenston, et al. (2000). "Cartilage tissue remodeling in response to mechanical forces." Annual Review of Biomedical Engineering 2: 691-+.

Groebe, K. and W. Muellerklieser (1991). "Distributions of Oxygen, Nutrient, and Metabolic Waste Concentrations in Multicellular Spheroids and Their Dependence on Spheroid Parameters." European Biophysics Journal 19(4): 169-181.

Guck, J., S. Schinkinger, et al. (2005). "Optical deformability as an inherent cell marker for testing malignant transformation and metastatic competence." Biophysical Journal 88(5): 3689-3698.

Guilak, F., H. P. Ting-Beall, et al. (1999). "Viscoelastic properties of intervertebral disc cells - Identification of two biomechanically distinct cell populations." Spine 24(23): 2475-2483.

Gupta, D. and L. J. Layfield (2000). "Prevalence of inter-institutional anatomic pathology slide review - A survey of current practice." American Journal of Surgical Pathology 24(2): 280-284.

Guy, C. T., R. D. Cardiff, et al. (1992). "Induction of Mammary-Tumors by Expression of Polyomavirus Middle T-Oncogene - a Transgenic Mouse Model for Metastatic Disease." Molecular and Cellular Biology 12(3): 954-961.

Guzman, C., S. Jeney, et al. (2006). "Exploring the mechanical properties of single vimentin intermediate filaments by atomic force microscopy." Journal of Molecular Biology 360(3): 623-630.

Haapala, J., M. J. Lammi, et al. (1996). "Coordinated regulation of hyaluronan and aggrecan content in the articular cartilage of immobilized and exercised dogs." Journal of Rheumatology 23(9): 1586-1593.

Haefliger, J. A., N. Krattinger, et al. (2006). "Connexin43-dependent mechanism modulates renin secretion and hypertension." Journal of Clinical Investigation 116(2): 405-413.

Hansma, P., H. Yu, et al. (2009). "The tissue diagnostic instrument." Rev Sci Instrum 80(5): 054303.

Hawkins, T., M. Mirigian, et al. (2010). "Mechanics of microtubules." Journal of Biomechanics 43(1): 23-30.

Heidemann, S. R. and D. Wirtz (2004). "Towards a regional approach to cell mechanics." Trends in Cell Biology 14(4): 160-166.

Helmke, B. P., A. B. Rosen, et al. (2002). "Flow-induced strain focusing in the endothelial cytoskeleton." Second Joint Embs-Bmes Conference 2002, Vols 1-3, Conference Proceedings: 321-322
2682.

Helmke, B. P., A. B. Rosen, et al. (2003). "Mapping mechanical strain of an endogenous cytoskeletal network in living endothelial cells." Biophysical Journal 84(4): 2691-2699.

Helmlinger, G., P. A. Netti, et al. (1997). "Solid stress inhibits the growth of multicellular tumor spheroids." Nature Biotechnology 15(8): 778-783.

Hemmer, J. D., J. Nagatomi, et al. (2009). "Role of Cytoskeletal Components in Stress-Relaxation Behavior of Adherent Vascular Smooth Muscle Cells." Journal of Biomechanical Engineering-Transactions of the Asme 131(4): -.

Herant, M., W. A. Marganski, et al. (2003). "The mechanics of neutrophils: Synthetic modeling of three experiments." Biophysical Journal 84(5): 3389-3413.

Herrmann, H., H. Bar, et al. (2007). "Intermediate filaments: from cell architecture to nanomechanics." Nature Reviews Molecular Cell Biology 8(7): 562-573.

Herrmann, H., S. V. Strelkov, et al. (2009). "Intermediate filaments: primary determinants of cell architecture and plasticity." Journal of Clinical Investigation 119(7): 1772-1783.

Higgins, J. M., D. T. Eddington, et al. (2007). "Sickle cell vasoocclusion and rescue in a microfluidic device." Proceedings of the National Academy of Sciences of the United States of America 104(51): 20496-20500.

Hiltawsky, K. M., M. Kruger, et al. (2001). "Freehand ultrasound elastography of breast lesions: Clinical results." Ultrasound in Medicine and Biology 27(11): 1461-1469.

Hirschhaeuser, F., H. Menne, et al. (2010). "Multicellular tumor spheroids: An underestimated tool is catching up again." Journal of Biotechnology 148(1): 3-15.

Hochmuth, R. M. (2000). "Micropipette aspiration of living cells." Journal of Biomechanics 33(1): 15-22.

Hockel, M. and P. Vaupel (2001). "Tumor hypoxia: Definitions and current clinical, biologic, and molecular aspects." Journal of the National Cancer Institute 93(4): 266-276.

Hocking, D. C., J. Sottile, et al. (2000). "Stimulation of integrin-mediated cell contractility by fibronectin polymerization." Journal of Biological Chemistry 275(14): 10673-10682.

Hoffman, B. D., G. Massiera, et al. (2006). "The consensus mechanics of cultured mammalian cells." Proceedings of the National Academy of Sciences of the United States of America 103(27): 10259-10264.

Hofmann, H., T. Voss, et al. (1984). "Localization of Flexible Sites in Thread-Like Molecules from Electron-Micrographs - Comparison of Interstitial, Basement-Membrane and Intima Collagens." Journal of Molecular Biology 172(3): 325-343.

Hohenadl, M., T. Storz, et al. (1999). "Desmin filaments studied by quasi-elastic light scattering." Biophysical Journal 77(4): 2199-2209.

Hu, S. H., J. X. Chen, et al. (2003). "Intracellular stress tomography reveals stress focusing and structural anisotropy in cytoskeleton of living cells." American Journal of Physiology-Cell Physiology 285(5): C1082-C1090.

Huang, S. and D. E. Ingber (2005). "Cell tension, matrix mechanics, and cancer development." Cancer Cell 8(3): 175-176.

Ingber, D. E. (1993). "Cellular Tensegrity - Defining New Rules of Biological Design That Govern the Cytoskeleton." Journal of Cell Science 104: 613-627.

Ingber, D. E. (1993). "Extracellular-Matrix, Cellular Mechanics, and Tissue-Development." Journal of Cellular Biochemistry: 149-149.

Ingber, D. E. (1997). "Tensegrity: The architectural basis of cellular mechanotransduction." Annual Review of Physiology 59: 575-599.

Ingber, D. E. (2003). "Tensegrity I. Cell structure and hierarchical systems biology." Journal of Cell Science 116(7): 1157-1173.

Ingber, D. E. (2003). "Tensegrity II. How structural networks influence cellular information processing networks." Journal of Cell Science 116(8): 1397-1408.

Ingber, D. E. (2008). "Can cancer be reversed by engineering the tumor microenvironment?" Seminars in Cancer Biology 18(5): 356-364.

Jaalouk, D. E. and J. Lammerding (2009). "Mechanotransduction gone awry." Nature Reviews Molecular Cell Biology 10(1): 63-73.

Janmey, P. A. and C. A. McCulloch (2007). "Cell mechanics: Integrating cell responses to mechanical stimuli." Annual Review of Biomedical Engineering 9: 1-34.

Janmey, P. A., J. P. Winer, et al. (2009). "The Hard Life of Soft Cells." Cell Motility and the Cytoskeleton 66(8): 597-605.

Jemal, A., R. Siegel, et al. (2008). "Cancer statistics, 2008." Ca-a Cancer Journal for Clinicians 58(2): 71-96.

Kagan, H. M. and W. D. Li (2003). "Lysyl oxidase: Properties, specificity, and biological roles inside and outside of the cell." Journal of Cellular Biochemistry 88(4): 660-672.

Kakkad, S. M., M. Solaiyappan, et al. (2010). "Hypoxic Tumor Microenvironments Reduce Collagen I Fiber Density." Neoplasia 12(8): 608-617.

Kalluri, R. and M. Zeisberg (2006). "Fibroblasts in cancer." Nature Reviews Cancer 6(5): 392-401.

Kasas, S. and G. Dietler (2007). "Techniques for measuring microtubule stiffness." Current Nanoscience 3(1): 85-96.

Kass, L., J. T. Erler, et al. (2007). "Mammary epithelial cell: Influence of extracellular matrix composition and organization during development and tumorigenesis." International Journal of Biochemistry & Cell Biology 39(11): 1987-1994.

Kasza, K. E., A. C. Rowat, et al. (2007). "The cell as a material." Current Opinion in Cell Biology 19(1): 101-107.

Keating, T. J. and G. G. Borisy (1999). "Centrosomal and non-centrosomal microtubules." Biology of the Cell 91(4-5): 321-329.

Kelm, J. M., N. E. Timmins, et al. (2003). "Method for generation of homogeneous multicellular tumor spheroids applicable to a wide variety of cell types." Biotechnology and Bioengineering 83(2): 173-180.

Khaldoyanidi, S. K., V. V. Glinsky, et al. (2003). "MDA-MB-435 human breast carcinoma cell homo- and heterotypic adhesion under flow conditions is mediated in part by Thomsen-Friedenreich antigen-galectin-3 interactions." Journal of Biological Chemistry 278(6): 4127-4134.

Kiani, C., L. Chen, et al. (2002). "Structure and function of aggrecan." Cell Research 12(1): 19-32.

Kirschner, M. W. (1980). "Implications of Treadmilling for the Stability and Polarity of Actin and Tubulin Polymers Invivo." Journal of Cell Biology 86(1): 330-334.

Kisiday, J. D., M. S. Jin, et al. (2004). "Effects of dynamic compressive loading on chondrocyte biosynthesis in self-assembling peptide scaffolds." Journal of Biomechanics 37(5): 595-604.

Kitterman, J. A. (1996). "The effects of mechanical forces on fetal lung growth." Clinics in Perinatology 23(4): 727-&.

Koay, E. J., A. C. Shieh, et al. (2003). "Creep indentation of single cells." Journal of Biomechanical Engineering-Transactions of the Asme 125(3): 334-341.

Koike, C., T. D. McKee, et al. (2002). "Solid stress facilitates spheroid formation: potential involvement of hyaluronan." British Journal of Cancer 86(6): 947-953.

Kole, T. P., Y. Tseng, et al. (2005). "Intracellular mechanics of migrating fibroblasts." Molecular Biology of the Cell 16(1): 328-338.

Kornberg, L., H. S. Earp, et al. (1992). "Cell-Adhesion or Integrin Clustering Increases Phosphorylation of a Focal Adhesion-Associated Tyrosine Kinase." Journal of Biological Chemistry 267(33): 23439-23442.

Kostic, A., C. D. Lynch, et al. (2009). "Differential Matrix Rigidity Response in Breast Cancer Cell Lines Correlates with the Tissue Tropism." Plos One 4(7): -.

Kreplak, L. and H. Bar (2009). "Severe Myopathy Mutations Modify the Nanomechanics of Desmin Intermediate Filaments." Journal of Molecular Biology 385(4): 1043-1051.

Kreplak, L., H. Bar, et al. (2005). "Exploring the mechanical behavior of single intermediate filaments." Journal of Molecular Biology 354(3): 569-577.

Kreplak, L., H. Herrmann, et al. (2008). "Tensile properties of single desmin intermediate filaments." Biophysical Journal 94(7): 2790-2799.

Kukacka, J., J. Bibova, et al. (2007). "Protein remodeling of extracellular matrix in rat myocardium during four-day hypoxia: the effect of concurrent hypercapnia." General Physiology and Biophysics 26(2): 133-142.

Kumar, S., I. Z. Maxwell, et al. (2006). "Viscoelastic retraction of single living stress fibers and its impact on cell shape, cytoskeletal organization, and extracellular matrix mechanics." Biophysical Journal 90(10): 3762-3773.

Kumar, S. and V. Weaver (2009). "Mechanics, malignancy, and metastasis: The force journey of a tumor cell." Cancer and Metastasis Reviews 28(1-2): 113-127.

Kumm, T., A. Chau, et al. (2010). "Diagnostic Performance of Elastography in the Evaluation of Lesions Referred for Breast Biopsy: Combined Use of Color Elastogram and Strain Ratio Assessment." American Journal of Roentgenology 194(5): -.

Kunz-Schughart, L. A., P. Heyder, et al. (2001). "A heterologous 3-D coculture model of breast tumor cells and fibroblasts to study tumor-associated fibroblast differentiation." Experimental Cell Research 266(1): 74-86.

Kuo, S. C. (2001). "Using optics to measure biological forces and mechanics." Traffic 2(11): 757-763.

Kurz, J. C. and R. C. Williams (1995). "Microtubule-Associated Proteins and the Flexibility of Microtubules." Biochemistry 34(41): 13374-13380.

Kusumi, A. and Y. Sako (1996). "Cell surface organization by the membrane skeleton." Current Opinion in Cell Biology 8(4): 566-574.

Lam, W. A., L. Cao, et al. (2010). "Extracellular matrix rigidity modulates neuroblastoma cell differentiation and N-myc expression." Molecular Cancer 9: -.

Lang, M., P. Fordyce, et al. (2003). "Combined fluorescence & force microscopy." Biophysical Journal 84(2): 301a-301a.

Lapidus, R. G., S. J. Nass, et al. (1998). "The loss of estrogen and progesterone receptor gene expression in human breast cancer." Journal of Mammary Gland Biology and Neoplasia 3(1): 85-94.

Lawrence, A. J., J. L. Mahowald, et al. (2000). "Magnetic resonance elastography of breast cancer." Radiology 214(2): 612-613.

Le, Q. T., N. C. Denko, et al. (2004). "Hypoxic gene expression and metastasis." Cancer and Metastasis Reviews 23(3-4): 293-310.

Lecuit, T. and P. F. Lenne (2007). "Cell surface mechanics and the control of cell shape, tissue patterns and morphogenesis." Nature Reviews Molecular Cell Biology 8(8): 633-644.

Lee, E. Y. H. P. (1995). "Tumor-Suppressor Genes and Their Alterations in Breast-Cancer." Seminars in Cancer Biology 6(3): 119-125.

Lee, H., J. M. Ferrer, et al. (2010). "Passive and active microrheology for cross-linked F-actin networks in vitro." Acta Biomaterialia 6(4): 1207-1218.

Lele, T. P., J. E. Sero, et al. (2007). "Tools to study cell mechanics and mechanotransduction." Cell Mechanics 83: 443-+.

Lenormand, G. and J. J. Fredberg (2006). "Deformability, dynamics, and remodeling of cytoskeleton of the adherent living cell." Biorheology 43(1): 1-30.

Lenormand, G., E. Millet, et al. (2004). "Linearity and time-scale invariance of the creep function in living cells." Journal of the Royal Society Interface 1(1): 91-97.

Less, J. R., M. C. Posner, et al. (1992). "Interstitial Hypertension in Human Tumors .4. Interstitial Hypertension in Human Breast and Colorectal Tumors." Cancer Research 52(22): 6371-6374.

Leung, C. L., D. M. Sun, et al. (1999). "Microtubule actin cross-linking factor (MACF): A hybrid of dystonin and dystrophin that can interact with the actin and microtubule cytoskeletons." Journal of Cell Biology 147(6): 1275-1285.

Levental, I., P. C. Georges, et al. (2007). "Soft biological materials and their impact on cell function." Soft Matter 3(3): 299-306.

Levental, K. R., H. M. Yu, et al. (2009). "Matrix Crosslinking Forces Tumor Progression by Enhancing Integrin Signaling." Cell 139(5): 891-906.

Liang, S., M. J. Slattery, et al. (2008). "Hydrodynamic shear rate regulates melanoma-leukocyte aggregation, melanoma adhesion to the endothelium, and subsequent extravasation." Annals of Biomedical Engineering 36(4): 661-671.

Lim, C. T., E. H. Zhou, et al. (2006). "Experimental techniques for single cell and single molecule biomechanics." Materials Science & Engineering C-Biomimetic and Supramolecular Systems 26(8): 1278-1288.

Lin, E. Y., J. G. Jones, et al. (2003). "Progression to malignancy in the polyoma middle T oncoprotein mouse breast cancer model provides a reliable model for human diseases." American Journal of Pathology 163(5): 2113-2126.

Lin, E. Y., A. V. Nguyen, et al. (2001). "Colony-stimulating factor 1 promotes progression of mammary tumors to malignancy." Journal of Experimental Medicine 193(6): 727-739.

Lin, Y. C., N. Y. Yao, et al. (2010). "Origins of Elasticity in Intermediate Filament Networks." Physical Review Letters 104(5): -.

Liu, T. G., O. E. Guevara, et al. (2010). "Regulation of vimentin intermediate filaments in endothelial cells by hypoxia." American Journal of Physiology-Cell Physiology 299(2): C363-C373.

Luan, Y., O. Lieleg, et al. (2008). "Micro- and macrorheological properties of isotropically cross-linked actin networks." Biophysical Journal 94(2): 688-693.

Luo, Y. Z., X. Xu, et al. (2008). "A multi-modular tensegrity model of an actin stress fiber." Journal of Biomechanics 41(11): 2379-2387.

Madara, J. L. and K. Dharmsathaphorn (1985). "Occluding Junction Structure-Function Relationships in a Cultured Epithelial Monolayer." Journal of Cell Biology 101(6): 2124-2133.

Magnusson, M. K. and D. F. Mosher (1998). "Fibronectin - Structure, assembly, and cardiovascular implications." Arteriosclerosis Thrombosis and Vascular Biology 18(9): 1363-1370.

Mahaffy, R. E., S. Park, et al. (2004). "Quantitative analysis of the viscoelastic properties of thin regions of fibroblasts using atomic force microscopy." Biophysical Journal 86(3): 1777-1793.

Makowski, L., D. L. D. Caspar, et al. (1984). "Gap Junction Structures .6. Variation and Conservation in Connection Conformation and Packing." Biophysical Journal 45(1): 208-218.

Maniotis, A. J., K. Bojanowski, et al. (1997). "Mechanical continuity and reversible chromosome disassembly within intact genomes removed from living cells." Journal of Cellular Biochemistry 65(1): 114-130.

Margolis, R. L. and L. Wilson (1998). "Microtubule treadmilling: what goes around comes around." Bioessays 20(10): 830-836.

Mariappan, Y. K., K. J. Glaser, et al. (2010). "Magnetic Resonance Elastography: A Review." Clinical Anatomy 23(5): 497-511.

Matthews, B. D., D. R. Overby, et al. (2004). "Mechanical properties of individual focal adhesions probed with a magnetic microneedle." Biochemical and Biophysical Research Communications 313(3): 758-764.

Matthews, B. D., D. R. Overby, et al. (2006). "Cellular adaptation to mechanical stress: role of integrins, Rho, cytoskeletal tension and mechanosensitive ion channels." Journal of Cell Science 119(3): 508-518.

Menard, S., E. Tagliabue, et al. (2000). "Role of HER2 gene overexpression in breast carcinoma." Journal of Cellular Physiology 182(2): 150-162.

Merenda, F., J. Rohner, et al. (2007). "Micro-optics for optical trapping in microfluidics - art. no. 66440P." Optical Trapping and Optical Micromanipulation Iv 6644: P6440-P6440 660.

Montesano, R., L. Orci, et al. (1983). "Invitro Rapid Organization of Endothelial-Cells into Capillary-Like Networks Is Promoted by Collagen Matrices." Journal of Cell Biology 97(5): 1648-1652.

Moscona, A. (1961). "Rotation-Mediated Histogenetic Aggregation of Dissociated Cells - a Quantifiable Approach to Cell Interactions in Vitro." Experimental Cell Research 22: 455-&.

Mucke, N., K. Klenin, et al. (2009). "Filamentous Biopolymers on Surfaces: Atomic Force Microscopy Images Compared with Brownian Dynamics Simulation of Filament Deposition." Plos One 4(11): -.

Mucke, N., L. Kreplak, et al. (2004). "Assessing the flexibility of intermediate filaments by atomic force microscopy." Journal of Molecular Biology 335(5): 1241-1250.

Mueller-Klieser, W. (2000). "Tumor biology and experimental therapeutics." Critical Reviews in Oncology Hematology 36(2-3): 123-139.

Muellerklieser, W. (1984). "Method for the Determination of Oxygen-Consumption Rates and Diffusion-Coefficients in Multicellular Spheroids." Biophysical Journal 46(3): 343-348.

Muller, A., B. Homey, et al. (2001). "Involvement of chemokine receptors in breast cancer metastasis." Nature 410(6824): 50-56.

Mullerat, J., F. Deroide, et al. (2003). "Proliferation and p53 expression in anal cancer precursor lesions." Anticancer Research 23(3C): 2995-2999.

Naylor, M. J., N. Li, et al. (2005). "Ablation of beta 1 integrin in mammary epithelium reveals a key role for integrin in glandular morphogenesis and differentiation." Journal of Cell Biology 171(4): 717-728.

Nederman, T., B. Norling, et al. (1984). "Demonstration of an Extracellular-Matrix in Multicellular Tumor Spheroids." Cancer Research 44(7): 3090-3097.

Nguyen, D. X., P. D. Bos, et al. (2009). "Metastasis: from dissemination to organ-specific colonization." Nature Reviews Cancer 9(4): 274-U65.

Nguyen, H. L., S. Chari, et al. (1997). "Overexpression of full- or partial-length MAP4 stabilizes microtubules and alters cell growth." Journal of Cell Science 110: 281-294.

Nishi, H., T. Nakada, et al. (2004). "Hypoxia-inducible factor 1 mediates upregulation of telomerase (hTERT)." Molecular and Cellular Biology 24(13): 6076-6083.

Omary, M. B. (2009). ""IF-pathies": a broad spectrum of intermediate filament-associated diseases." Journal of Clinical Investigation 119(7): 1756-1762.

Oxlund, H., J. Manschot, et al. (1988). "The Role of Elastin in the Mechanical-Properties of Skin." Journal of Biomechanics 21(3): 213-218.

Pampaloni, F., E. G. Reynaud, et al. (2007). "The third dimension bridges the gap between cell culture and live tissue." Nature Reviews Molecular Cell Biology 8(10): 839-845.

Panorchan, P., J. S. H. Lee, et al. (2007). "Probing cellular mechanical responses to stimuli using ballistic intracellular nanorheology." Cell Mechanics 83: 115-+.

Pantaloni, D., C. Le Clainche, et al. (2001). "Cell biology - Mechanism of actin-based motility." Science 292(5521): 1502-1506.

Parry, D. A. D., S. V. Strelkov, et al. (2007). "Towards a molecular description of intermediate filament structure and assembly." Experimental Cell Research 313(10): 2204-2216.

Paszek, M. J., D. Boettiger, et al. (2009). "Integrin Clustering Is Driven by Mechanical Resistance from the Glycocalyx and the Substrate." Plos Computational Biology 5(12): -.

Paszek, M. J., N. Zahir, et al. (2005). "Tensional homeostasis and the malignant phenotype." Cancer Cell 8(3): 241-254.

Pathi, S. P., C. Kowalczewski, et al. (2010). "A Novel 3-D Mineralized Tumor Model to Study Breast Cancer Bone Metastasis." Plos One 5(1): -.

Pena, A., M. D. Bolton, et al. (1998). "Cellular poroelasticity: A theoretical model for soft tissue mechanics." Poromechanics: 475-480

Pereira, M., B. J. Rybarczyk, et al. (2002). "The incorporation of fibrinogen into extracellular matrix is dependent on active assembly of a fibronectin matrix." Journal of Cell Science 115(3): 609-617.

Perez-Moreno, M., C. Jamora, et al. (2003). "Sticky business: Orchestrating cellular signals at adherens junctions." Cell 112(4): 535-548.

Peters, I. M., Y. van Kooyk, et al. (1999). "3D single-particle tracking and optical trap measurements on adhesion proteins." Cytometry 36(3): 189-194.

Plodinec, M., M. Loparic, et al. "Imaging articular cartilage tissue using atomic force microscopy (AFM)." Cold Spring Harb Protoc 2010: pdb prot5499.

Plodinec, M. and C. A. Schoenenberger "Spatial organization acts on cell signaling: how physical force contributes to the development of cancer." Breast Cancer Res 12(4): 308.

Polyak, K. (2007). "Breast cancer: origins and evolution." Journal of Clinical Investigation 117(11): 3155-3163.

Pouyssegur, J. and F. Mechta-Grigoriou (2006). "Redox regulation of the hypoxia-inducible factor." Biological Chemistry 387(10-11): 1337-1346.

Praetorius, H. A. and K. R. Spring (2005). "A physiological view of the primary cilium." Annual Review of Physiology 67: 515-529.

Qin, J., O. Vinogradova, et al. (2004). "Integrin bidirectional signaling: a molecular view." Plos Biology 2(6): 726-729.

Radmacher, M. (2007). "Studying the mechanics of cellular processes by atomic force microscopy." Cell Mechanics 83: 347-372.

Rebillard, A., S. Jouan-Lanhouet, et al. (2010). "Cisplatin-induced apoptosis involves a Fas-ROCK-ezrin-dependent actin remodelling in human colon cancer cells." European Journal of Cancer 46(8): 1445-1455.

Resnick, N., H. Yahav, et al. (1997). "Endothelial gene regulation by laminar shear stress." Analytical and Quantitative Cardiology 430: 155-164.

Robles, A. I. and L. Varticovski (2008). "Harnessing genetically engineered mouse models for preclinical testing." Chemico-Biological Interactions 171(2): 159-164.

Rodionov, V. I., F. K. Gyoeva, et al. (1993). "Microtubule-Dependent Control of Cell-Shape and Pseudopodial Activity Is Inhibited by the Antibody to Kinesin Motor Domain." Journal of Cell Biology 123(6): 1811-1820.

Rodriguez-Enriquez, S., J. C. Gallardo-Perez, et al. (2008). "Energy metabolism transition in multi-cellular human tumor spheroids." Journal of Cellular Physiology 216(1): 189-197.

Rodriguezboulan, E. and P. J. I. Salas (1989). "External and Internal Signals for Epithelial-Cell Surface Polarization." Annual Review of Physiology 51: 741-754.

Rogers, K. R., H. Herrmann, et al. (1996). "Characterization of disulfide crosslink formation of human vimentin at the dimer, tetramer, and intermediate filament levels." Journal of Structural Biology 117(1): 55-69.

Rosenbluth, M. J., A. Crow, et al. (2008). "Slow Stress Propagation in Adherent Cells." Biophysical Journal 95(12): 6052-6059.

Rosenbluth, M. J., W. A. Lam, et al. (2006). "Force microscopy of nonadherent cells: A comparison of leukemia cell deformability." Biophysical Journal 90(8): 2994-3003.

Roskelley, C. D., A. Srebrow, et al. (1995). "A Hierarchy of Ecm-Mediated Signaling Regulates Tissue-Specific Gene-Expression." Current Opinion in Cell Biology 7(5): 736-747.

Rosso, F., A. Giordano, et al. (2004). "From cell-ECM interactions to tissue engineering." Journal of Cellular Physiology 199(2): 174-180.

Sadoshima, J. and S. Izumo (1997). "The cellular and molecular response of cardiac myocytes to mechanical stress." Annual Review of Physiology 59: 551-571.

Salaita, K., P. M. Nair, et al. (2010). "Restriction of Receptor Movement Alters Cellular Response: Physical Force Sensing by EphA2." Science 327(5971): 1380-1385.

Samani, A., J. Bishop, et al. (2003). "Measuring the elastic modulus of ex vivo small tissue samples." Physics in Medicine and Biology 48(14): 2183-2198.

Santini, M. T. and G. Rainaldi (1999). "Three-dimensional spheroid model in tumor biology." Pathobiology 67(3): 148-157.

Sarntinoranont, M., F. Rooney, et al. (2003). "Interstitial stress and fluid pressure within a growing tumor." Annals of Biomedical Engineering 31(3): 327-335.

Schaller, V., C. Weber, et al. (2010). "Polar patterns of driven filaments." Nature 467(7311): 73-77.

Schinkinger, S., F. Wottawah, et al. (2004). "Feeling for cells with light." Optical Trapping and Optical Micromanipulation 5514: 170-178

Schwartz, M. A. and R. K. Assoian (2001). "Integrins and cell proliferation: regulation of cyclin-dependent kinases via cytoplasmic signaling pathways." Journal of Cell Science 114(14): 2553-2560.

Schwartz, M. A. and D. W. DeSimone (2008). "Cell adhesion receptors in mechanotransduction." Current Opinion in Cell Biology 20(5): 551-556.

Semenza, G. L. (2003). "Targeting HIF-1 for cancer therapy." Nature Reviews Cancer 3(10): 721-732.

Shao, Z. M., M. Nguyen, et al. (2000). "Human breast carcinoma desmoplasia is PDGF initiated." Oncogene 19(38): 4337-4345.

Shea, T. B. (1997). "Phospholipids alter tau conformation, phosphorylation, proteolysis, and association with microtubules: Implication for tau function under normal and degenerative conditions." Journal of Neuroscience Research 50(1): 114-122.

Shevkoplyas, S. S., T. Yoshida, et al. (2006). "Direct measurement of the impact of impaired erythrocyte deformability on microvascular network perfusion in a microfluidic device." Lab on a Chip 6(7): 914-920.

Sieg, D. J., C. R. Hauck, et al. (1999). "Required role of focal adhesion kinase (FAK) for integrin-stimulated cell migration." Journal of Cell Science 112(16): 2677-2691.

Sinkus, R., K. Siegmann, et al. (2007). "MR elastography of breast lesions: Understanding the solid/liquid duality can improve the specificity of contrast-enhanced MR mammography." Magnetic Resonance in Medicine 58(6): 1135-1144.

Sirghi, L., J. Ponti, et al. (2008). "Probing elasticity and adhesion of live cells by atomic force microscopy indentation." European Biophysics Journal with Biophysics Letters 37(6): 935-945.

Sonnenberg, A. and R. K. H. Liem (2007). "Plakins in development and disease." Experimental Cell Research 313(10): 2189-2203.

Sottile, J. and D. C. Hocking (2002). "Fibronectin polymerization regulates the composition and stability of extracellular matrix fibrils and cell-matrix adhesions." Molecular Biology of the Cell 13(10): 3546-3559.

Spittle, C. S. and L. Cassimeris (1996). "Mechanisms blocking microtubule minus end assembly: Evidence for a tubulin dimer-binding protein." Cell Motility and the Cytoskeleton 34(4): 324-335.

Stamenovic, D., J. J. Fredberg, et al. (1996). "A microstructural approach to cytoskeletal mechanics based on tensegrity." Journal of Theoretical Biology 181(2): 125-136.

Stamenovic, D. and D. E. Ingber (2009). "Tensegrity-guided self assembly: from molecules to living cells." Soft Matter 5(6): 1137-1145.

Stamenovic, D., N. Rosenblatt, et al. (2007). "Rheological Behavior of living cells is timescale-dependent." Biophysical Journal 93(8): L39-L41.

Stolz, M., R. Gottardi, et al. (2009). "Early detection of aging cartilage and osteoarthritis in mice and patient samples using atomic force microscopy." Nature Nanotechnology 4(3): 186-192.

Stolz, M., R. Raiteri, et al. (2004). "Dynamic elastic modulus of porcine articular cartilage determined at two different levels of tissue organization by indentation-type atomic force microscopy." Biophysical Journal 86(5): 3269-3283.

Storm, C., J. J. Pastore, et al. (2005). "Nonlinear elasticity in biological gels." Nature 435(7039): 191-194.

Storz, P., H. Doppler, et al. (2009). "FOXO3a Promotes Tumor Cell Invasion through the Induction of Matrix Metalloproteinases." Molecular and Cellular Biology 29(18): 4906-4917.

Straub, F. B. (1942). "Purification of malic acid dehydrase and the significance of cell structure in dehydrogenation." Hoppe-Seylers Zeitschrift Fur Physiologische Chemie 275: 63-72.

Sugarbaker, P. H. (1993). "Metastatic Inefficiency - the Scientific Basis for Resection of Liver Metastases from Colorectal-Cancer." Journal of Surgical Oncology: 158-160.

Sund, M., L. Xie, et al. (2004). "The contribution of vascular basement membranes and extracellular matrix to the mechanics of tumor angiogenesis." Apmis 112(7-8): 450-462.

Suresh, S. (2007). "Biomechanics and biophysics of cancer cells." Acta Biomaterialia 3(4): 413-438.

Sutherla.Rm, W. R. Inch, et al. (1970). "Multi-Component Radiation Survival Curve Using an in-Vitro Tumour Model." International Journal of Radiation Biology and Related Studies in Physics Chemistry and Medicine 18(5): 491-&.

Sutherland, R. M. and R. E. Durand (1984). "Growth and Cellular Characteristics of Multicell Spheroids." Recent Results in Cancer Research 95: 24-49.

Takeichi, M. (1990). "Cadherins - a Molecular Family Important in Selective Cell-Cell Adhesion." Annual Review of Biochemistry 59: 237-252.

Tamamori, M., H. Ito, et al. (1997). "Stimulation of collagen synthesis in rat cardiac fibroblasts by exposure to hypoxic culture conditions and suppression of the effect by natriuretic peptides." Cell Biology International 21(3): 175-180.

Tan, C., R. G. de Noronha, et al. (2005). "Identification of a novel small-molecule inhibitor of the hypoxia-inducible factor 1 pathway." Cancer Research 65(2): 605-612.

Tan, J. L., J. Tien, et al. (2002). "Feel the force: Using a bed of needles to map single cell generated traction forces." Second Joint Embs-Bmes Conference 2002, Vols 1-3, Conference Proceedings: 1648-1649

2682.

Tanase, M., N. Biais, et al. (2007). "Magnetic tweezers in cell biology." Cell Mechanics 83: 473-493.

Tepass, U. and V. Hartenstein (1994). "The Development of Cellular Junctions in the Drosophila Embryo." Developmental Biology 161(2): 563-596.

Tlsty, T. D. and L. M. Coussens (2006). "Tumor stroma and regulation of cancer development." Annual Review of Pathology-Mechanisms of Disease 1(1): 119-150.

Tolic-Norrelykke, I. M. and N. Wang (2005). "Traction in smooth muscle cells varies with cell spreading." Journal of Biomechanics 38(7): 1405-1412.

Tredan, O., C. M. Galmarini, et al. (2007). "Drug resistance and the solid tumor microenvironment." Journal of the National Cancer Institute 99(19): 1441-1454.

Trepat, X., L. H. Deng, et al. (2007). "Universal physical responses to stretch in the living cell." Nature 447(7144): 592-+.

Trickey, W. R., T. P. Vail, et al. (2004). "The role of the cytoskeleton in the viscoelastic properties of human articular chondrocytes." Journal of Orthopaedic Research 22(1): 131-139.

Tsai, M. A. and D. A. Hammer (1997). "Rheology of rat basophilic leukemia cells." Annals of Biomedical Engineering 25(1): 62-68.

Tsai, M. A., R. E. Waugh, et al. (1996). "Changes in HL-60 cell deformability during differentiation induced by DMSO." Biorheology 33(1): 1-15.

Tseng, Y., T. P. Kole, et al. (2002). "Micromechanical mapping of live cells by multiple-particle-tracking microrheology." Biophysical Journal 83(6): 3162-3176.

Tsukada, K., E. Sekizuka, et al. (2001). "Direct measurement of erythrocyte deformability in diabetes mellitus with a transparent microchannel capillary model and high-speed video camera system." Microvascular Research 61(3): 231-239.

Vantard, M., R. Cowling, et al. (2000). "Cell cycle regulation of the microtubular cytoskeleton." Plant Molecular Biology 43(5-6): 691-703.

Vargo-Gogola, T. and J. M. Rosen (2007). "Modelling breast cancer: one size does not fit all." Nature Reviews Cancer 7(9): 659-672.

Vaupel, P. and A. Mayer (2007). "Hypoxia in cancer: significance and impact on clinical outcome." Cancer and Metastasis Reviews 26(2): 225-239.

Venier, P., A. C. Maggs, et al. (1994). "Analysis of Microtubule Rigidity Using Hydrodynamic Flow and Thermal Fluctuations." Journal of Biological Chemistry 269(18): 13353-13360.

Vracko, R. (1974). "Basal Lamina Scaffold-Anatomy and Significance for Maintenance of Orderly Tissue Structure." American Journal of Pathology 77(2): 314-346.

Wachsstock, D. H., W. H. Schwarz, et al. (1994). "Cross-Linker Dynamics Determine the Mechanical-Properties of Actin Gels." Biophysical Journal 66(3): 801-809.

Wagner, O. I., S. Rammensee, et al. (2007). "Softness, strength and self-repair in intermediate filament networks." Experimental Cell Research 313(10): 2228-2235.

Wakatsuki, T., B. Schwab, et al. (2001). "Effects of cytochalasin D and latrunculin B on mechanical properties of cells." Journal of Cell Science 114(5): 1025-1036.

Wang, J. H. C., J. S. Lin, et al. (2007). "Cell traction force microscopy." Advanced Bioimaging Technologies in Assessment of the Quality of Bone and Scaffold Materials: Techniques and Applications: 227-235

Wang, N. (1998). "Mechanical interactions among cytoskeletal filaments." Hypertension 32(1): 162-165.

Wang, N., S. H. Hu, et al. (2007). "Imaging stress propagation in the cytoplasm of a living cell." Cell Mechanics 83: 179-+.

Wang, N., E. Ostuni, et al. (2002). "Micropatterning tractional forces in living cells." Cell Motility and the Cytoskeleton 52(2): 97-106.

Wang, N. and D. Stamenovic (2000). "Contribution of intermediate filaments to cell stiffness, stiffening, and growth." American Journal of Physiology-Cell Physiology 279(1): C188-C194.

Ward, T., M. Faivre, et al. (2005). "Microfluidic flow focusing: Drop size and scaling in pressure versus flow-rate-driven pumping." Electrophoresis 26(19): 3716-3724.

Welling, L. W., M. T. Zupka, et al. (1995). "Mechanical-Properties of Basement-Membrane." News in Physiological Sciences 10: 30-35.

Wirtz, D. (2009). "Particle-Tracking Microrheology of Living Cells: Principles and Applications." Annual Review of Biophysics 38: 301-326.

Wyckoff, J. B., J. G. Jones, et al. (2000). "A critical step in metastasis: In vivo analysis of intravasation at the primary tumor." Cancer Research 60(9): 2504-2511.

Yurchenco, P. D. and J. J. Orear (1994). "Basal Lamina Assembly." Current Opinion in Cell Biology 6(5): 674-681.

Zagorska, A. and J. Dulak (2004). "HIF-1: the knowns and unknowns of hypoxia sensing." Acta Biochimica Polonica 51(3): 563-585.

Zhi, H., B. Ou, et al. (2007). "Comparison of ultrasound elastography, mammography, and sonography in the diagnosis of solid breast lesions." Journal of Ultrasound in Medicine 26(6): 807-815.

Zhu, Q. L., Y. X. Jiang, et al. (2008). "Real-time ultrasound elastography: Its potential role in assessment of breast lesions." Ultrasound in Medicine and Biology 34(8): 1232-1238.

Chapter 2

Atomic force Microscopy (AFM) for biological imaging and mechanical testing across length scales

Marija Plodinec[1], Marko Loparic[1] and Ueli Aebi[1*†]

[1]M.E. Müller Institute for Structural Biology, Biozentrum University of Basel,
Klingelbergstrasse 50/70, 4056 Basel, Switzerland

* Correspondence: ueli.aebi@unibas.ch

† Supported by two research grants from the Swiss National Science Foundation (to U.A.), and funds from the National Center of Competence in Research on 'Nanoscale Science' (SNF NCCR-Nano), the Swiss Nanoscience Institute, the M. E. Müller Foundation of Switzerland, and the Canton Basel-Stadt (all to U.A.).

2.1 Abstract

The Atomic force microscope (AFM) offers the researcher a unique opportunity to visualize, manipulate, and quantitatively assess structural and mechanical aspects of native biological samples with nanometer resolution. An unparalleled advantage of the AFM over other high-resolution microscopes is that biological specimens, ranging from tissues to cells to molecules, can be investigated in physiologically relevant aqueous environments. The AFM can be operated at 37°C, which makes it ideal for in situ cell or tissue studies. Combining an optical microscope with an AFM makes it possible to directly correlate structural/nanomechanical changes with optical/fluorescence images. This ability to simultaneously acquire structural and functional information is unprecedented in biology. This chapter provides instructional tips, methods, and protocols for studying biological samples by AFM. After introducing the basics of AFM, sample protocols are provided in which AFM is used to investigate cartilage, living cells, and collagen II. These protocols were chosen because they illustrate how AFM can be used to image and investigate the properties of a wide range of biological samples, specifically tissues, cells, and molecules, thus revealing the vast applicability of AFM in the life sciences.

2.2 Introduction: AFM basic operating principles

At the heart of the AFM lies a mechanical probe composed of a flexible cantilever with an ultrasharp tip at its free end (Figure 2-1) (Ludwig et al. 2008; Muller 2008). A standard mode of AFM operation (Schaffer et al. 1996) in biology is referred to as a contact mode. Here, a laser that reflects off the back of the AFM cantilever is used to monitor its bending as it is rasterscanned across a sample surface. Fluctuations in the reflected laser corresponding to surface features are monitored using a photodetector, while the force on the sample is held constant by a piezoelectric scanner. The force impinging the sample surface can be calculated by invoking Hooke‘s law, $F = k_c d$, where F is the force, k_c is the cantilever spring constant, and d is the cantilever deflection. The signals generated by either the cantilever deflection or the vertical piezoelectric-scanner displacement can be used to generate a three-dimensional image of the sample surface.

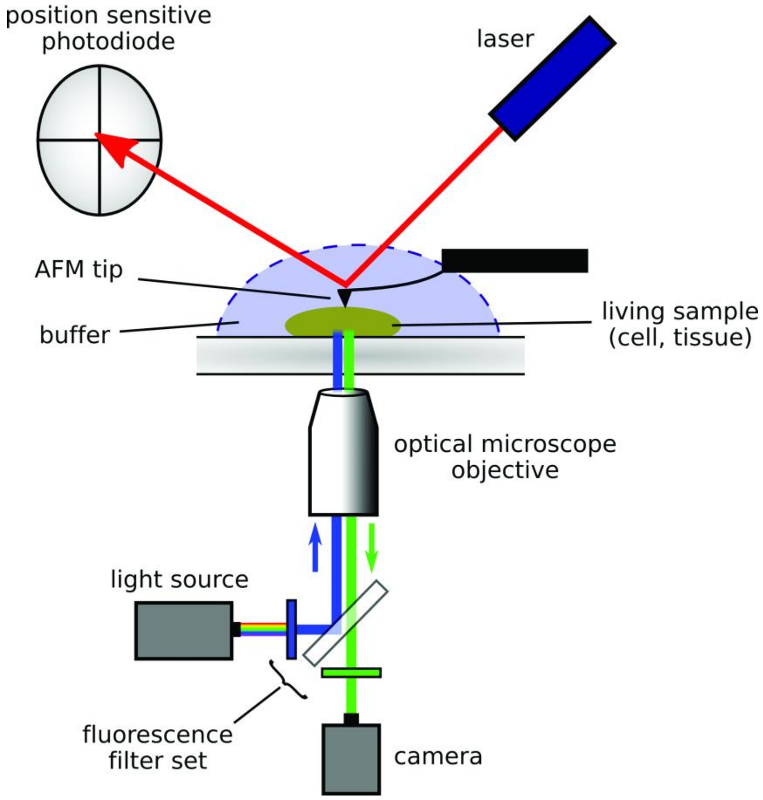

Figure 2-1. Schematic of the AFM–LM setup. The AFM is mounted on an inverted optical microscope equipped with a high-resolution objective. Illumination with a light source together with fluorescence filters allows for simultaneous fluorescence microscopy that is recorded via a CCD camera. The AFM probe scans the surface of living samples (cells, tissue) maintained in buffer or culture medium. Surface corrugations are recorded from a laser beam that is reflected from the spring (cantilever) onto a photodetector.

A cantilever deflection-generated image is called a deflection image, and a vertical piezoelectric-scanner displacement image is termed a topography image. More advanced operational modes, such as noncontact, intermittent contact (or tapping mode), and phase imaging, may also be employed (Boisgard et al. 2007).

2.2.1 Combining AFM with optical microscopy

Many state-of-the-art AFMs can be integrated with optical microscopes and simultaneously operated in bright-field optics, differential interference contrast, epifluorescence, total internal reflection fluorescence, or confocal microscopy (Haga et al. 2000; Lehenkari et al. 2000; Kellermayer et al. 2006; Madl et al. 2006). Whereas AFM provides high spatial resolution with the option to mechanically manipulate and measure biological samples, light microscopy (LM) offers high temporal resolution and the possibility of functional imaging using fluorescence. When combined, AFM and LM are complementary techniques that provide an unprecedented experimental platform for investigating biological structure and function in situ and in real time. In fact, advances in software development now allow regions of interest to be selected from the optical image and scanned by AFM (e.g., see Imaging and Mechanical Testing of Rat-2 Fibroblasts with the Bioscope II in Protocol 2).

The Microscope

A schematic of an AFM–LM setup is shown in Figure 2-1. This instrument consists of an AFM system mounted on top of an inverted optical microscope equipped with low- and high-magnification objectives and a high-sensitivity charge-coupled device (CCD) camera. In most integrated AFM–LM systems, the AFM is operated in the closed-loop mode, which uses high-resolution capacitors that precisely control the sample position and allow for fast zooming in on an area of interest without loss of scanning accuracy. The AFM is equipped with an infrared laser ($\lambda = 850$ nm) to avoid interference between the laser and the fluorescence signals. To reduce the effect of mechanical and acoustic vibrations (i.e., noise), the entire system is placed on a vibration isolation table.

Medium Control and Perfusion

A key advantage of the AFM is that the environmental conditions can be controlled to minimize changes to the native structure and function of the sample. In our setup (see Protocol 2), we have incorporated a syringe pump with a perfusion fluid cell to continuously replenish the appropriate growth medium. This maintains a physiological pH around the sample, provides fresh nutrients, and compensates for evaporation. The syringe at the input end is filled with sterile medium equilibrated to contain 5% CO2, which is pumped into the perfusion fluid cell via a ~1-m long, sterile extension tube. The output end is connected to a waste container and a mechanical vacuum pump via an ~1-m long, sterile extension tube.

Temperature Control

Small temperature changes can have profound effects on cell physiology, so they must be controlled. A heating plate with sensitivity up to 0.1°C can be directly incorporated in the AFM microscope stage. By heating only the sample and not the entire microscope, systemic imaging instabilities are avoided. Alternatively, and depending upon the configuration of the instrument, entire AFMs can be placed in a thermostatically controlled box not exceeding 30°C.

2.2.2 Probes suitable for working with biological samples

It is essential to choose the correct probe for each AFM experiment. The defining probe parameters are the cantilever spring constant and the radius of curvature of the tip (Rtip). The cantilever spring constant (k_c) determines the sensitivity of the AFM to the mechanical properties of the sample. *R*tip defines the image quality and resolution during scanning. Careful selection of the probe greatly enhances and optimizes the AFM measurements. Silicon-nitride cantilevers with *k*c values ranging from 0.01 N/m to 0.06 N/m are typically used for imaging and mechanical testing of biological material. Generally, these probes are sensitive to forces in the picoNewton (pN) and nanoNewton (nN) range. The smaller the value of *k*c, the more susceptible the cantilever will be to both mechanical and acoustic vibrations. Thus, the utmost care should be taken to reduce sources of noise.

Tip geometry is a crucial parameter to consider in AFM applications. For obtaining high-resolution images, oxide-sharpened tips made of silicon nitride with *R*tip values ranging from 5 nm to 20 nm are recommended (e.g., (MSNL) probes available from Veeco Instruments Inc.; http://www.veeco.com/). AFM tips can also be functionalized with different chemistries for use in special applications (Raab et al. 1999). When imaging high samples, such as cells, the height of the tip should be at least double as the cell height (typical cell height >6 μm) to prevent the cantilever from contacting the sample. High-resolution probes measure the local properties of the sample at the nanometer scale. To probe the bulk properties of the sample, glass spheres can be glued to the AFM cantilever (Protocol 4) (Ling et al. 2007). Although typical sphere diameters can be 5–10 μm, the size of the sphere depends greatly on the sample's fine structure.

It is important to experimentally determine the spring constant (e.g., by the thermal noise; Hutter and Bechhoefer 1993) and the sensitivity of each cantilever before starting AFM experiments. Measured values can differ from the nominal values given by the manufacturer and are crucial for accurate control of the force applied on the sample.

2.2.3 Mehanical testing of biological samples

In addition to imaging, AFM is ideally suited for measuring nanomechanical properties—such as stiffness in tension or compression, plasticity, and viscoelasticity—of biological samples under physiological conditions. Instead of raster-scanning the probe as is done during imaging, the AFM is engaged in force-curve or force-measurement mode (Figure 2-2). This involves varying the tip-to-sample separation (*Z*) over a single point such that the tip approaches and impinges the sample surface vertically and then retracts away from the surface. The cantilever displacement is continuously monitored as the tip-to-sample separation changes to produce force or load displacement curves. The slope (gradient) of each curve (Δforce/Δdisplacement) is a measure of the specimen's stiffness (Figure 2-2). A more advanced method of collecting force curves is termed force-volume mode or force mapping, which requires the acquisition of a user-specified number of force curves (in a two-dimensional array) over a given area. Besides controlling the velocity at which the force curves are acquired, a constant, well-defined maximum load can be maintained in all curves by defining a maximum tip deflection (i.e., a relative trigger threshold).

Using the force-volume mode, a spatial distribution of the stiffness on the sample surface can be created. The resulting stiffness measurements can be interpreted as the elastic modulus (also known as Young’s modulus) by calculating its stress-to-strain ratio. (Stress is defined as the force normalized by the cross-sectional area, while strain is the change in length divided by the initial length of the material.)

The remainder of this chapter presents protocols that demonstrate the types of biological samples that can be studied by AFM.

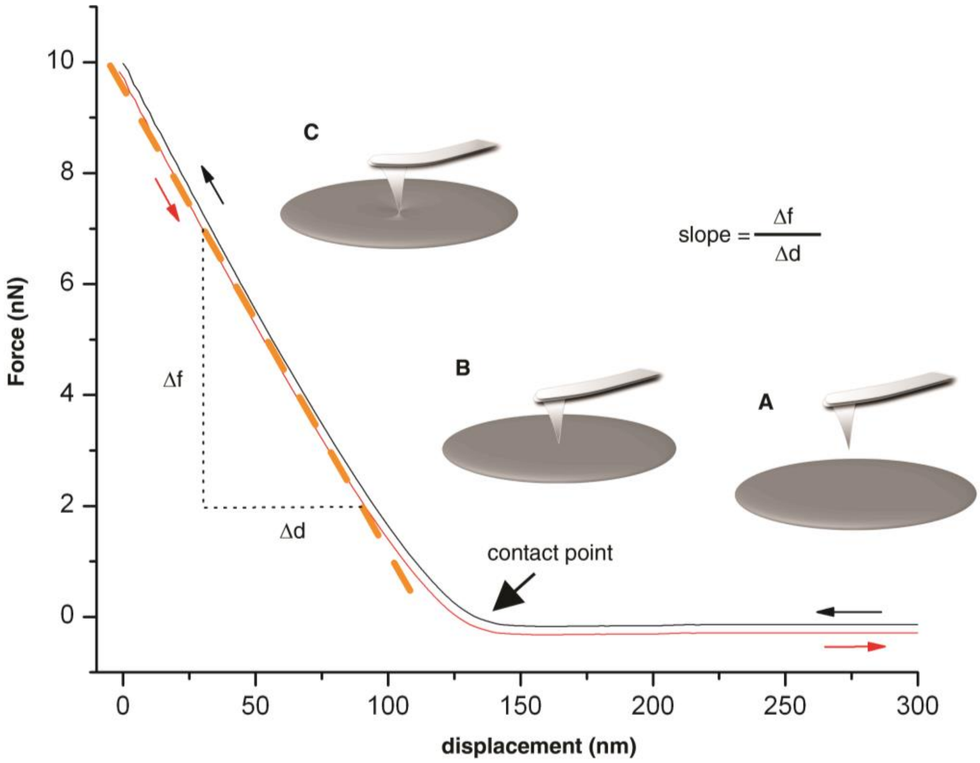

Figure 2-2. Force-curve measurements. During force measurements, the bending of the cantilever is monitored as the tip is brought into contact with the sample surface (black curve) and then retracted (red curve). (*A*) The cantilever is approaching the surface. (*B*) Contact is made with the sample surface. (*C*) Tip indents the sample and bends upward. Slope (orange dashed line) of the recorded force curve (Δforce/Δdisplacement) represents the sample stiffness.

2.3 Protocol 1

2.3.1 Imaging Articular Cartilage Tissue Using AFM

Cartilage is a complex avascular tissue composed of cells (chondrocytes) embedded in an extracellular matrix (ECM) consisting of 70%–80% water. The primary components of the ECM are negatively charged aggrecans and collagen II fibrils, which possess a characteristic, ordered threedimensional structure. The components interact to ensure that the cartilage is able to absorb shock and can function to protect the bone ends. An AFM can be used to examine structure–function relationships of cartilage at both micrometer and nanometer scales. When imaged at the micrometer scale with microspheres, only the ECM and chondrocytes can be distinguished. Correspondingly, mechanical testing of cartilage at the micrometer scale results in unimodal distribution of the stiffness because the bulk elastic property of the ECM is probed. In contrast, bare AFM tips are able to reveal the molecular components of the ECM at the nanometer scale. Mechanical testing at the nanometer scale reveals a bimodal distribution of the stiffness and reflects the distinct stiffness of the collagen network and the proteoglycan moiety. Here, the corresponding AFM image and force map reveal the distinct morphology of the collagen fibers and proteoglycan gel. Although, in principle, these experiments can be performed using any AFM, an AFM with tube scanners that have manual screws for tilting the sample is preferable because cartilage has macroscopically rough surface features. By manually tilting the probe over the sample, an optimal angle for tip approach can be achieved.

2.3.2 Related information

Within the ECM, collagen contributes predominantly to the shear and tensile strength of the cartilage, whereas aggrecans provide most of its compressive strength (Han et al. 2007; Pfeiffer et al. 2008). The ability of the AFM to operate in liquid makes it an ideal tool to assess the functionality of normal, diseased, or engineered articular cartilage (Stolz et al. 2004; Stolz et al. 2007). By employing bare tips and tips modified with microspheres (Protocol 4), AFM can be used to examine structure–function relationships at different length scales and architectural complexity (Figure 2-3).

2.3.3 Materials

Reagents

Articular cartilage (from knee joints of freshly slaughtered pigs; see Step 1)

Ringer's solution supplemented with a protease inhibitor cocktail (Complete, Boehringer-Mannheim, Mannheim, Germany)

Equipment

AFM

This experiment is carried out with a Nanoscope III (Multimode AFM, Veeco Instruments) equipped with a 120-µm scanner (J-Scanner) and a standard fluid cell. The microscope is placed on an antivibration isolation unit (JRS Scientific Instruments).

Biopsy needle (e.g., the Cage bone-marrow biopsy needle, 3.264-mm diameter, Medax, Italy)

Disk, stainless-steel (10-mm diameter)

Disk, Teflon (11-mm diameter, 0.25-mm thick)

Glue, fast-setting (e.g., Loctite 401)

Glue, Histoacryl tissue

Magnetic sample holder (Multimode AFM, Veeco Instruments)

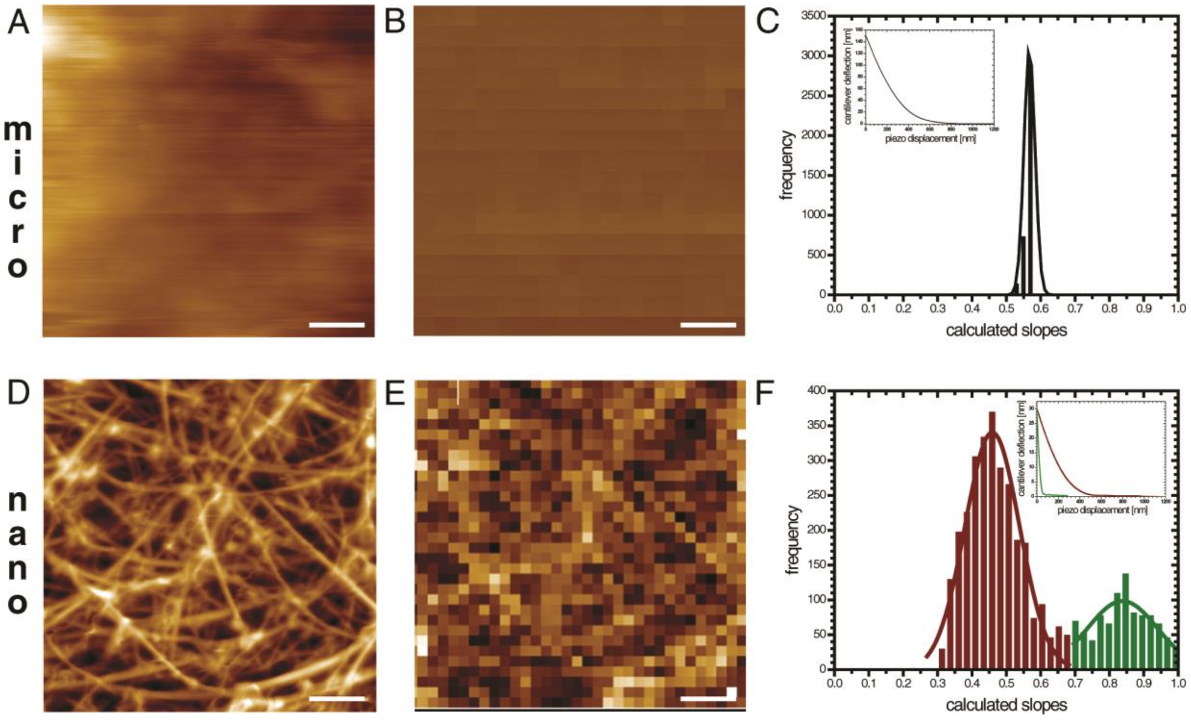

Figure 2-3. Imaging and mechanical testing of articular cartilage at micrometer and nanometer scales. Images and force-volume maps of cartilage are scaled to a height of 400 nm. (*A*) An image of articular cartilage recorded with a microsphere tip showing a nonstructured surface. Individual collagen fibrils are not revealed. (*B*) Force-volume map exhibiting a uniform microstiffness. (*C*) Uniform microstiffness falls into a narrow Gaussian distribution. (*Inset*) Slope of the averaged force curve was derived from the maximum of the Gaussian distribution. (*D*) Imaging of articular cartilage with a nanometer-sized tip resolves individual collagen fibrils. (*E*) The force-volume map recorded at the nanometer scale revealing the differential stiffness of individual collagen fibrils. (*F*) The slopes obtained from the individual force curves exhibit a bimodal distribution. (*Inset*) Two averaged force curves represent the stiff collagen fibrils in green and soft proteoglycan moiety in red.

2.3.4 Method

Preparation of Cartilage Specimens

1. Prepare porcine articular cartilage from knee joints of freshly slaughtered pigs within 1 h to 2 h postmortem. The knee joints from several animals can be collected and stored at 4°C in Ringer’s solution supplemented with a protease inhibitor cocktail until cartilage removal.
2. Using a clinical punch biopsy tool, obtain several adjacent osteochondral plugs (three to four samples) from the underlying bone of the medial and lateral femoral knee. Keep the cylindrical- shaped plugs in Ringer’s solution supplemented with a protease inhibitor cocktail at 4°C until measurement. Do not let the specimen dry out.
3. For each cartilage stiffness measurement, fix a Teflon disk (11-mm diameter, 0.25-mm thick) onto a 10-mm diameter stainless-steel disk with fast-setting glue. Next, glue the cartilage specimen from Step 2 onto the Teflon disk with Histoacryl tissue glue.

Imaging Articular Cartilage with AFM

4. Start the AFM software.
5. Mount the chip into the fluid cell.
6. Calibrate the cantilever sensitivity by obtaining a load-displacement curve on an infinitely stiff sample, such as clean glass (Hutter and Bechhoefer 1993).
7. Place the Teflon disk with the sample onto the magnetic sample holder.
8. Turn the screws that hold the AFM head high enough to avoid contact of the head with the sample surface.
9. Place the head on the screws above the sample, and attach springs from each side to secure the head. Make sure that you hold the head tightly while attaching the springs. When the head is properly attached, lower it until the probe is immersed in the fluid but is not touching the sample.
10. Align the laser spot on the tip. To center the reflected laser in the middle of the photodetector, adjust the vertical and horizontal signals to ~0.
11. Set the initial parameters for engaging the AFM, and move the tip toward the sample until the tip comes into contact with the sample surface.
12. Withdraw the probe slightly from the surface making certain that it remains submerged in the liquid. Let the microscope and probe equilibrate for at least 30 min.
13. After 30 min, repeat step 11. .

14. Set the scan frequency to ~0.7 Hz for imaging cartilage.

    Scanning parameters such as gains or scan frequency depend on the cantilever, sample, and microscope used. Optimal settings should be empirically determined for each experiment.

15. Initially, set a large scan area (~30–40 µm) to obtain an overview of the tissue. When the region of interest is located, reduce the scan area size to ~10 µm.

    After imaging the cartilage, the same buffer solution can be used for mechanical testing experiments. Once imaging of the selected area is complete, switch, without disengaging, to forcevolume mode. Set the loading frequency to 3 Hz, which is similar to the physiological frequency for cartilage loading inside the knee or hip joint (Popko et al. 1986).

2.4 Protocol 2

2.4.1 Imaging Fibroblast Cells Using AFM

AFM can be used to visualize the three major cytoskeletal components that contribute to the mechanical properties of the cell. These are actin microfilaments, intermediate filaments, and microtubules. In this protocol, rat embryonic fibroblasts expressing actin tagged with green fluorescent protein (GFP) are used to demonstrate this procedure.

RELATED INFORMATION

In Figure 2-4, the image produced by the AFM provides information about cell height, shape, and fine structures beneath the plasma membrane, while the fluorescence image identifies actin filaments. By correlating mechanical testing with AFM–LM imaging, the contributions of actin filaments to local differences in cell stiffness can be pinpointed precisely (Figure 5).

2.4.2 Materials

CAUTION: See Appendix for proper handling of materials marked with <!>

See the end of the chapter for recipes for reagents marked with <R>.

Reagents

Agarose gel, 1%
ATV solution <R>
cDNA, human β-actin cytoplasmic
DFCS (decomplemented fetal calf serum) culture medium <R>
PCR reagents
pEGFPC1 vector, BglII/EcoRI digested (BD Biosciences; GenBank accession #U55763)

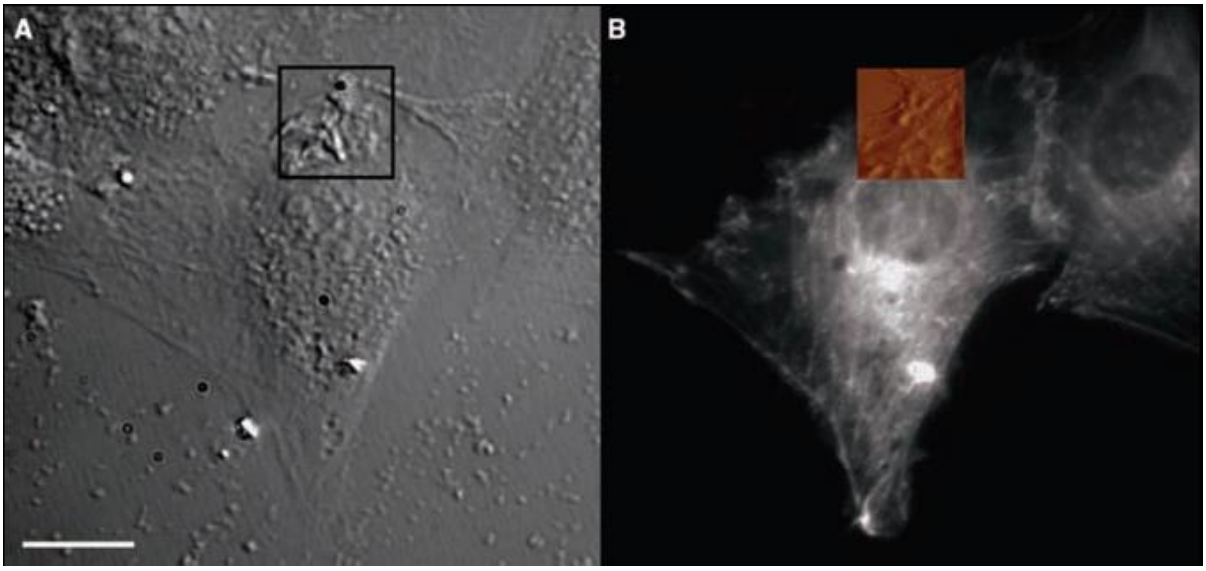

Figure 2-4. Combined AFM and optical imaging of GPF-actin-transfected Rat-2 embryonic fibroblasts. (*A*) Nuclear and cytoplasmic regions can be discerned in the DIC image of cells recorded with a 63× objective. The area selected for AFM imaging is boxed. (*B*) The corresponding fluorescence image reveals GFP-actin structures in transfected cells. The most prominent features are actin stress fibers. The direct overlay of the fluorescence image and AFM topography confirms that the filamentous structures correspond to actin filaments. Scale bar, 20 mm.

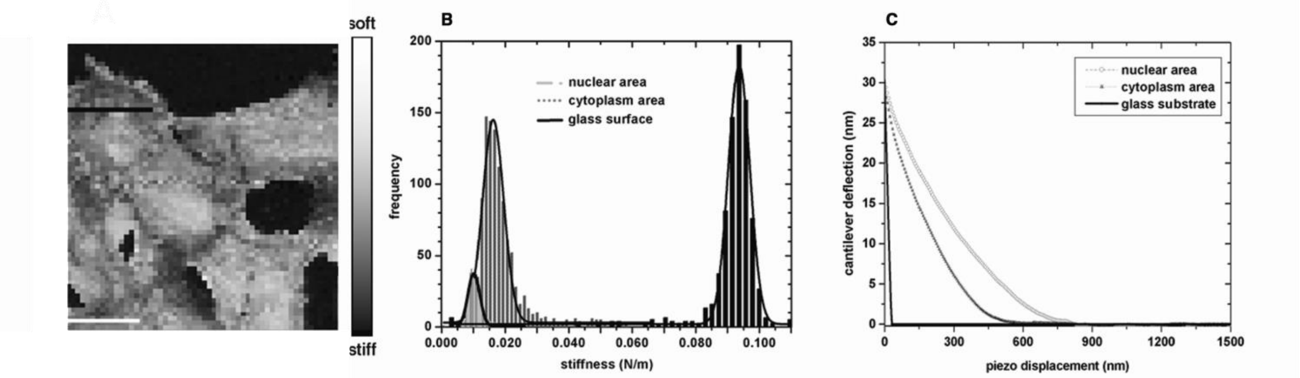

Figure 2-5. Cellular elasticity of Rat-2 fibroblasts mapped by AFM. (*A*) Force-volume map showing soft regions in white and stiff regions in black. Scale bar, 20 μm. (*B*) The force-volume map indicating that the nuclear area is softer than the cytoplasm. (*C*) Averaged curves for individual regions are derived from the histograms in (*B*).

Rat-2 cells, confluent in a T-25 culture flask

Rat-2 fibroblasts

Restriction enzymes, BamHI and EcoRI

Tissue culture medium, serum- and antibiotic-free (prewarmed to 37°C)

Transfection reagent (FuGENE 6; Roche)

Trypsin

Equipment

AFM

Bioscope II AFM system (BSII; Veeco Instruments) mounted on top of a DMI 6000 inverted optical microscope (Leica Microsystems) equipped with 10x, 63x, and 100x objectives and a Leica DC350FX (Leica Microsystems) CCD camera. To reduce mechanical and acoustic vibrations, the BS II system is placed on a vibration isolation table (Halcyonics Microscopy Workstation 1000).

AFM Miro software (Microscope image registration and overlay; Veeco Instruments)

Centrifuge, low speed

Culture dishes, 60-mm WillCo glass bottom (Intracel, Royston, UK)

Incubator, set at 5% CO2 and 37°C

Syringe pump

We use the Injectomat cp-PS syringe pump (Fresenius HemoCare GmbH, Germany).

Polymerase chain reaction (PCR)

Perfusion fluid cell

Sample holder, magnetic, for 60-mm culture dish (Veeco Instruments)

Tube, conical

Vacuum pump, mechanical (Alcatel Vacuum Products)

2.4.3 Method

Cloning the GFP-Actin Construct

1. Using PCR, insert a BamHI and an EcoRI restriction site at the 5′ and 3′ ends, respectively, of a human β-actin cytoplasmic cDNA.
2. Digest the amplified PCR fragment with BamHI and EcoRI restriction enzymes, and purify the DNA on a 1% agarose gel.
3. Extract the BamHI/EcoRI-actin fragment from the agarose gel, and ligate it into a pEGFPC1 vector digested with BglII and EcoRI.
4. Amplify the pEGFP-actin plasmid DNA, and purify it using standard molecular biology protocols.

Cell Culture

5. Trypsinize a confluent T-25 culture flask of Rat-2 cells with 2 mL of ATV solution at 37°C.

6. Resuspend the cells in 5 mL of DFCS culture medium, transfer them to a conical tube, and centrifuge the cells at 600*g* for 5 min.
7. Remove the supernatant. Break up the pellet by gently agitating the tube.
8. Resuspend the pellet in DFCS, count the cells, and adjust the cell number to 104 cells/mL.
9. Pipette 2 mL of the cell suspension into a 60-mm glass bottom culture dish.
10. Incubate at 37°C in a 5% CO2 incubator. Allow cells to attach to the dish for 24 h before transfection.

Transient Transfection Using FuGENE 6

11. Mix 4.5 μL of FuGENE 6 transfection reagent with serum and antibiotic-free medium (prewarmed to 37°C) and incubate for 4 min at room temperature. The volume of the medium depends on the concentration of the DNA (amount of DNA = 2.4 μg) but should add up to a final volume of 300 μL. Do not vortex the mixture!
12. Add 2.4 μg of pEGFP-actin DNA to the mixture, gently tap the microfuge tube, and incubate for 25 min at room temperature. Do not vortex!
13. Add the entire pEGFP-actin DNA/FuGENE mixture to a 60-mm dish containing Rat-2 fibroblasts in 1 mL DFCS medium and incubate at 37°C for 24 h in a 5% CO2 incubator.
14. Add fresh DFCS at 37°C shortly before performing AFM imaging and indentation testing experiments.

    This protocol can be used for other expression plasmids as well. Transfection protocols should be optimized for each construct.

Imaging and Mechanical Testing of Rat-2 Fibroblasts with the Bioscope II

15. Repeat Steps 4–6 as for Protocol 1.
16. Position the culture dish onto the stage, which has been preheated to 37°C. Secure the dish with a magnetic sample holder.
17. Mount the perfusion fluid cell onto the culture dish, and connect the tubes of the syringe pump to the corresponding ports of the perfusion fluid cell. Before proceeding, make sure that perfusion works properly and that there is no leaking.

    This arrangement continuously replenishes the growth medium, thus maintaining a physiological pH around the sample, providing fresh nutrients, and compensating for evaporation. The syringe at the input end is filled with sterile medium equilibrated to contain 5% CO2, which is pumped into the perfusion fluid cell via an ~1-m-long sterile extension tube. The output end is connected to a waste container and a mechanical vacuum pump via an ~1-m-long sterile extension tube.

18. Focus the cells with the optical microscope. Raise the AFM head high enough to avoid contact when you place it on top of the sample.
19. Align the laser spot onto the tip (see Fig. 1).

    Veeco Instruments provides an alignment accessory for the ATM that they call EasyAlign. Use a culture dish filled with the same medium as will be used for experiments because the laser spot shifts in different environments. When aligning the laser spot, the sum signal should be as high as possible (typically between 4 V and 8 V). To center the reflected laser in the middle of the photodetector, adjust the vertical and horizontal signals to ~0.

20. Place the scan head onto the base of the AFM. Maximize the laser signal again.
21. Use the optical microscope to navigate the AFM probe to an area of the glass culture dish lacking cells.
22. Set the initial parameters for engaging the AFM, and move the tip toward the sample until the tip comes into contact with the glass substrate.
23. Withdraw the probe slightly from the surface making certain that it remains submerged in the liquid. Let the microscope and probe equilibrate for at least 30 min.
24. Position the probe next to the cell of interest using a low-magnification objective (e.g., 10x) and with the optical microscope operating in transmitted light mode (e.g., differential interference contrast [DIC], phase contrast, or bright field).
25. Use the fluorescence mode to verify that the cell of interest is expressing the GFP-tagged actin.
26. Change to the high-magnification objective (in our case, a 63x air objective with a NA of 0.8). Record the DIC and fluorescence image of the selected area using a CCD camera.

    The best results are obtained by using a camera with high sensitivity for fluorescence because it has a superior signal-to-noise ratio (SNR) that allows for clear capture of weak fluorescence emissions. To avoid interference with the optical image, a filter specific for the infrared laser light should be inserted in the optical path.

27. Use the Miro software to combine optical and AFM images. Follow the guided calibration process.

    To record the exact tip position during calibration, overexpose the optical image until the tip on the cantilever is clearly visible.

28. Indicate the region of the cells that should be scanned by AFM. The optimal scan size for an area selected at 100x magnification should be ~20 μm or less. Do not set the starting point of the scan at a site over the cell nucleus because the nuclear region is relatively high and thus more susceptible to damage even at low scanning force. In the

beginning, scan parameters are not fully optimized, so it is always better to start scanning either at the cell periphery or at the substrate next to a cell of interest.

29. Engage the probe, and initiate scanning. Optimize the scanning parameters for live cell imaging. The ratio between integral and proportional gains should be around 3:1. If the gains are too high, periodic noise and high-pitched sound will interfere. For imaging living cells, the scan velocity should not exceed 30 μm/sec. At a higher scan velocity, the tip will damage the cell resulting in tip contamination and detachment of the cell from the substrate.

    After imaging, one can continue performing mechanical testing with the force-volume mode. We recommend collecting 32 x 32 or 64 x 64 arrays of curves per scan area with 512 points per scan line. The total number of curves will suffice for statistical calculations of mechanical properties. Scan frequency should be set to <1.5 Hz because higher frequency rates can cause irreversible damage to the cells. The recorded data can be directly exported for further analysis into LabVIEW, Origin, or Microsoft Excel.

2.5 Protocol 3

Imaging Collagen II Using AFM

Collagen II is a fibrous protein that assembles from basic tropocollagen subunits to form extracellular supramolecular fiber networks within cartilage tissue. Tropocollagen subunits of ~300 nm in length self-assemble first into pentameric uniform microfibrils, which fuse into bigger collagen fibrils that can range from 10 nm to 500 nm in diameter. The collagen fibrils display a characteristic 67-nm repeat because of the staggering of individual collagen molecules with respect to each other. This protocol demonstrates how to prepare collagen protein samples for analysis by AFM. It also describes the steps for generating AFM images of collagen samples during and after manipulation to analyze collagen self-assembly.

2.5.1 MATERIALS

CAUTION: See Appendix for proper handling of materials marked with <!>.

See the end of the chapter for recipes for reagents marked with <R>.

Reagents

Cartilage (from knee or hip joint of freshly slaughtered pigs; see Step 1)
Isopropanol <!>, 30%
MgCl2 <!>, 1 M
Muscovite mica or highly ordered pyrolytic graphite (HOPG)
Phosphate-buffered saline (PBS), ice-cold <R>

Ringer's solution, ice-cold, containing protease inhibitors

Sorensen's phosphate buffer, 133 mM (pH 7.2) <R>

After preparation of the buffer, add bovine hylauronidase (Sigma-Aldrich) to a final concentration of 1 mg/mL.

Equipment

Adhesive tape

AFM

This experiment is carried out with a JPK NanoWizard (JPK Instruments) mounted on a Zeiss Axiovert 135 TV inverted optical microscope, equipped with low- and high-resolution objectives and a Leica DC350FX CCD camera (Leica Microsystems). The entire system is placed on a vibration isolation table (JRS Scientific Instruments).

Homogenizer (e.g., Ultra-Turrax T25)

Nitrogen gas

Petri dish

Scalpel

Adhesive tape

2.5.2 Method

Extraction of Collagen II from Pig Knee or Hip Cartilage

All preparation steps should be carried out in a cold room at 4°C.

1. Obtain knee or hip joint from freshly slaughtered pigs, and immediately place in ice-cold Ringer's solution containing protease inhibitors for transport to the laboratory.

   The time between animal slaughtering and collagen extraction must not exceed more than a few hours, because chondrocytes deteriorate rapidly. Cell disruption releases enzymes, which, once activated, will have deleterious effects on the collagen structure.

2. Clean the surface of the joint with 30% isopropanol to remove debris and fatty tissue.
3. Remove the cartilage from the joint with a surgical scalpel and cut into small pieces. Cartilage is the glassy tissue at the proximal end of the knee or hip bones.

   To avoid potential contamination of the cartilage with collagens other than type II, which are present in the surrounding tissue, make sure that only the cartilage layer is removed. Because cartilage is avascular, any sign of blood dots on the bone-face side of the extracted part shows that layers beneath the cartilage were cut, and thus the sample is contaminated with other collagen molecules (e.g., collagen I, collagen X).

4. To remove proteoglycans (e.g., hyaluronic acid, chondroitin sulfate, or keratin sulfate) and chondrocytes, do the following:

i. Place cartilage pieces in a microfuge tube.

ii. Add 1 mL of 133 mM Sorensen's phosphate buffer (pH 7.2) containing 1 mg/mL bovine hylauronidase and incubate for ~12 h at 37°C.

iii. For complete digestion, replace the solution with fresh enzyme and incubate for an additional 12 h at 37°C.

iv. Repeat Step 4iii.

5. After hyaluronidase digestion, wash the remaining collagen matrix three times with ice-cold PBS to remove enzymes and digested molecules.
6. Place the collagen matrix in a Petri dish with ice-cold PBS, and with the scalpel, make cuts in a criss-cross pattern. Then shave off thin slices of the collagen matrix.
7. Homogenize the slices of collagen matrix in PBS at 4°C in a homogenizer at 11,000 rpm for 10 sec to obtain individual collagen fibrils.
8. Analyze the homogenate by sodium dodecyl sulfate-polyacrylamide gel electrophoresis (SDSPAGE) and immunoblotting to confirm that only collagen II is present.
9. Use collagen fibril suspension for AFM experiments, or store it at 4°C for up to 2 wk.

The density of collagen in the homogenate strongly depends on its origin and the condition of the cartilage tissue. For instance, extraction of collagen from adult human healthy cartilage will result in a higher density of collagen per cartilage weight compared with collagen extracted from osteoarthritic cartilage. Moreover, extraction of collagen from infant cartilage, heavily osteoarthritic cartilage, and tissue-engineered cartilage will, in general, require a smaller quantity of enzymes for digestion and shorter time and velocity of fragmentation. This is because the collagen from these sources is rather thin, between 20 nm and 80 nm diameter compared with >80 nm diameter in the adult healthy cartilage.

Stable Attachment of Collagen on the Substrate Surface for AFM

A prerequisite for obtaining good AFM images or reproducible curves in manipulation experiments is to first stabilize collagen on the surface of an appropriate substrate (e.g., mica or HOPG; see Fig. 6). Muscovite mica (phyllosilicate mineral of aluminum and potassium) is used as a common substrate in AFM because it is atomically flat and charged. HOPG is also atomically flat but has a nonpolar surface. Depending on the experiment, these substrates can be coated to increase their affinity for collagen. For attaching collagen noncovalently, coating the substrate with MgCl2 will suffice for stabilization.

10. Cleave off the surface layer of mica or HOPG with adhesive tape immediately before beginning each experiment. Make sure that the entire layer is uniformly removed.

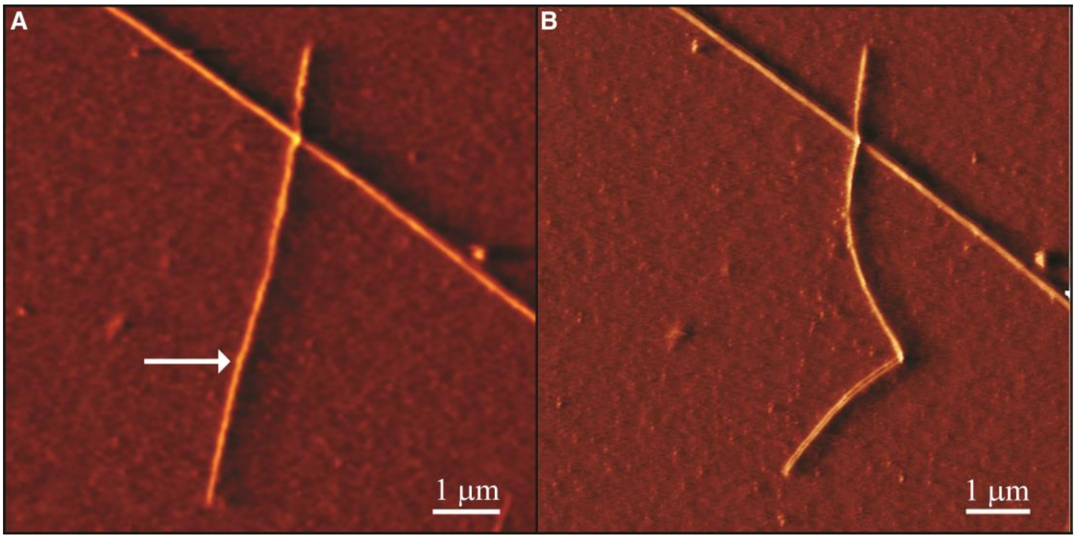

Figure 2-6. Manipulation of collagen fibrils. Images taken (*A*) before and (*B*) after manipulation. The white arrow indicates the site of manipulation. Scale bar, 1 μm.

11. Incubate the mica or HOPG in a solution of 1 M MgCl2 for 1 h at room temperature.
12. Wash three times with ultrapure water, and dry in a stream of nitrogen gas.
13. Incubate 10 μL of collagen suspension on the mica or HOPG substrate for 1 h at room temperature.
14. Gently wash three to five times with PBS to remove unattached collagen. This will prevent tip contamination and improve the AFM experiments.

    The appropriate cantilever for small-diameter collagen (<60 nm) is one with a low spring constant (usually 0.02–0.08 N/m). For imaging, we recommend V-shaped cantilevers. Generally the spatial resolution is improved if the ratio between the lateral and vertical spring constant is high. In particular, at the edges of collagen fibrils where the approach angle of the cantilever is very steep, a high lateral spring constant is advantageous. Cantilevers with low lateral spring constants are prone to instabilities resulting in noisy vertical signals, which will affect the image quality. For mechanical manipulation experiments, rectangular cantilevers are recommended over triangular ones because the former are more sensitive to lateral forces.

Imaging and Mechanical Manipulation of Collagen

15. Mount the cantilever in the cantilever holder. Place the specimen onto the sample holder and the cantilever holder onto the AFM head. With the specimen submerged in buffer solution, target the laser beam onto the front tip of the cantilever. Let the system equilibrate. Monitoring horizontal and vertical signals of the photodetector allows you to detect when the drift diminishes.

16. When the system has equilibrated, move the tip toward the surface of the sample. Because native collagen is fragile, apply minimal force (i.e., voltage), and retract the scanner after the initial contact. Then, with a minimal applied voltage, slowly extend the piezoelectric scanner to the contact point until the image appears.
17. As a general rule, set the gains as high as possible, until they reach the point of cantilever resonance, and then reduce gains just below the resonance frequency. The scan velocity for imaging largely depends on the sample. In the case of a hard or a very sticky sample, fast scanning in combination with high gains should yield good images. A relatively soft sample such as collagen requires a very low scanning velocity, typically 40 μm/sec.

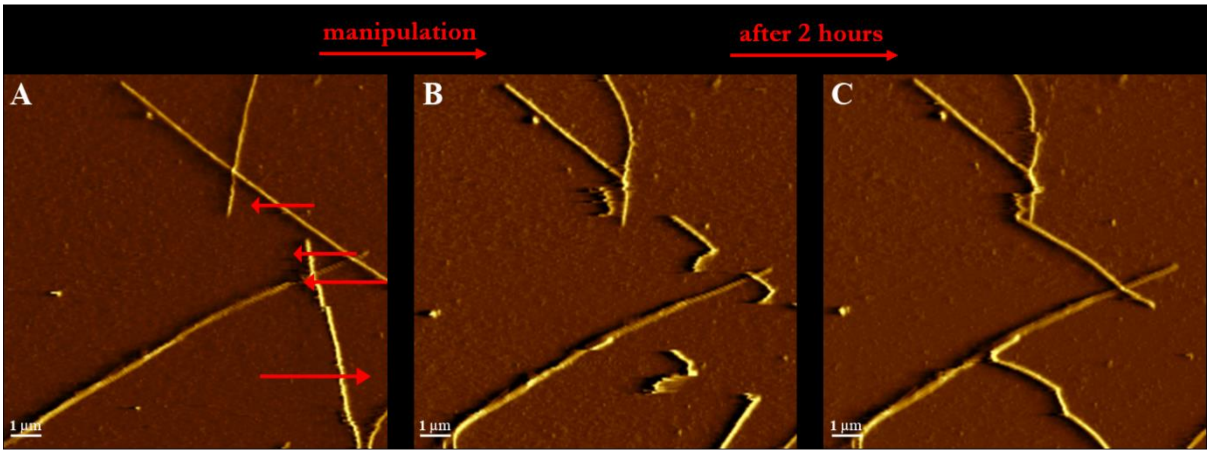

Figure 2-7. Time-lapse AFM showing mechanical disruption and reassembly of collagen fibrils. (*A*) Collagen fibrils attached to MgCl2-treated mica and imaged in PBS with a rectangular cantilever. The red arrows point to manipulation sites.(*B*) Mechanical manipulation leads to the disruption of collagen fibrils. (*C*) Self-assembly of new collagen fibrils occurs during a 2-h incubation in PBS saturated with tropocollagen. Scale bar, 1 μm.

18. For collagen, the recommended imaging procedure is to start with a large scan size (30 x 30 μm) at low resolution (128 x 128 pixels) to obtain an overview of the sample. Based on this, an area of interest is selected and subsequently scanned at a higher resolution (512 x 512-pixels or more).
19. In a mechanical manipulation experiment, align the collagen fibril of interest parallel to the cantilever. The scanning axis should then be perpendicular to the cantilever (Figs. 6 and 7).

In this manner, lateral bending of the cantilever dominates over vertical bending.

2.6 Protocol 4

Preparation of Microsphere Tips

For micrometer-scale imaging and mechanical testing, we use spherical indenters having a 10-μm diameter. A spherical indenter is prepared by gluing a hard borosilicate sphere to a tipless cantilever. For this purpose, we employ a stereomicroscope with a micromanipulator attachment. The spheres are cleaned prior to gluing to remove any contamination from their surfaces. Once cleaned, store the borosilicate spheres in absolute ethanol in a glass tube.

2.6.1 Materials

Reagents

Acetone <!>
Ethanol, 100% <!>
KOH<!>, 200 mM

Equipment

Borosilicate microspheres (Thermo Scientific,
Clean box
  See Step 19.
Coverslips, precleaned (24 x 60 mm; #1)
  See note to Step 8.
Epoxy glue, 30-min (e.g., Devcon)
Femtotips, sterile (Femtotip II, Eppendorf)
Micromanipulator (e.g., InjectMan NI 2, Eppendorf)
Sonicator (Sonorex RK 100, Bandelin electronic, Berlin, Germany)
Steel plate (see Fig. 8E)
Stereomicroscope (e.g., Axio Observer A1, Zeiss)
Tape, double-stick
Tipless cantilever (NSC12, MikroMasch) (Fig. 8)
Toothpicks

2.6.2 Method

Cleaning the Microspheres

1. Centrifuge the spheres three times for 5 sec each at 800*g* in double-distilled H2O. Use double-distilled H2O throughout the protocol.
2. Remove the H2O, and immerse the spheres in pure acetone.

3. Sonicate the spheres for 5 min in acetone.
4. Rinse the spheres three times with $H2O$ as in Step 1.
5. Remove the $H2O$, and sonicate the spheres for 20 min in 200 mM KOH.
6. Rinse the spheres three times with $H2O$ as in Step 1.
7. Remove the $H2O$, and sonicate the spheres for 5 min in 100% ethanol.
8. Stir the spheres in ethanol, and pipette ~20 µL of the suspension onto a precleaned microscope coverslip.

   Coverslips should be cleaned prior to Step 8 using the cleaning protocol in Steps 1–7. The centrifugation steps can be eliminated.

9. Allow the spheres to dry on the coverslip in a clean hood.

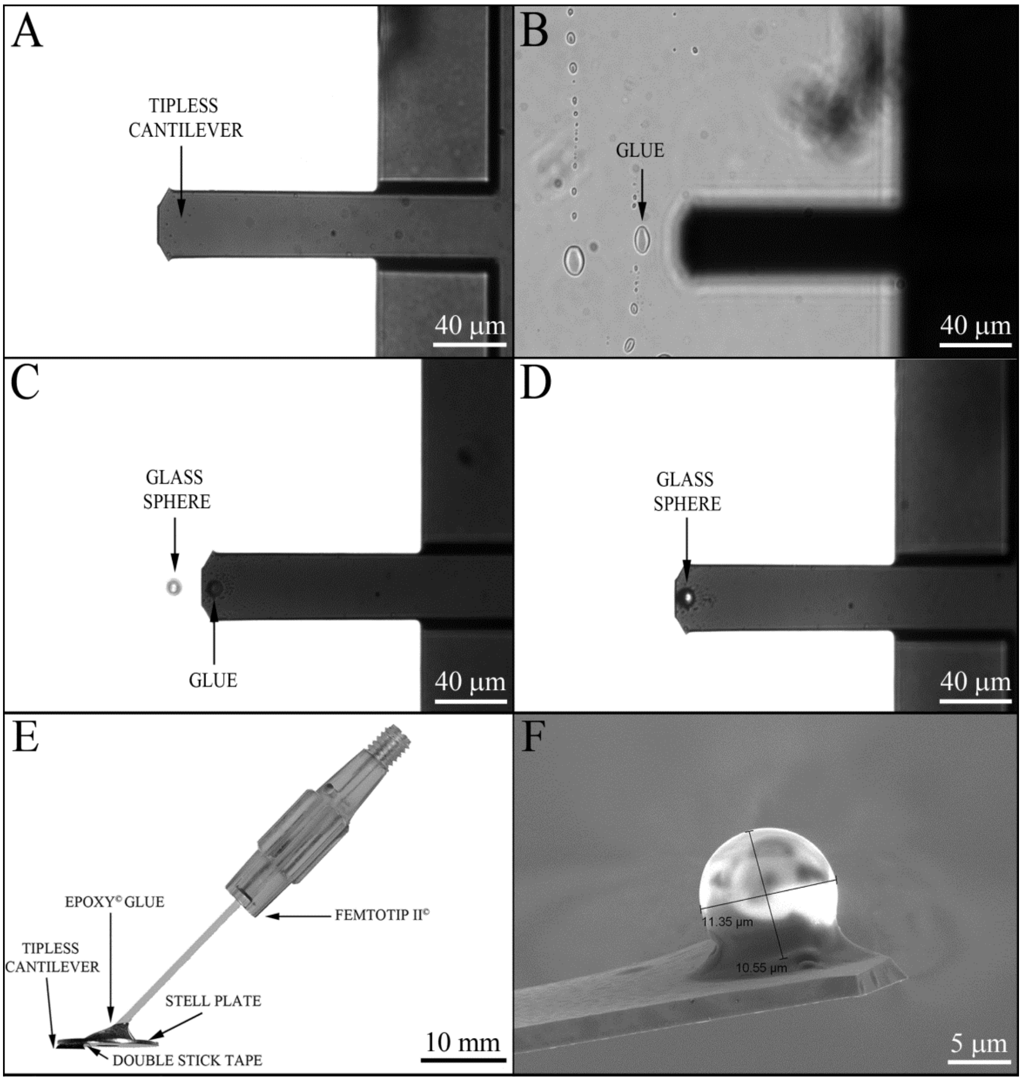

Figure 2-8. Gluing a glass microsphere onto a tipless cantilever. (*A*) Tipless cantilever before gluing. (*B*) Small drops of Epoxy glue and cantilever out of focus. (*C*) A small drop of glue is visible on the front of the cantilever while a glass sphere is positioned next to the cantilever. (*D*) A glass borosilicate microsphere is positioned and glued onto the front of the tipless cantilever. (*E*) Adapted Femtotip II tip for the gluing of the sphere. (*F*) Scanning electron microscope image of a glass microsphere glued to a tipless cantilever.

Preparation of the Adapted Femtotip

Perform Steps 10–19 under a stereomicroscope with a micromanipulator attachment (Fig. 8).

10. Cut a Femtotip II glass capillary 2 cm from the plastic holder.
11. Glue the glass capillary to a steel plate with epoxy glue. This is the adapted femtotip.
12. Attach double-stick tape to the lower side of the steel plate.
13. Position the tipless cantilever to the front part of the steel plate, and attach it with doublestick tape.

Gluing a Microsphere onto a Tipless Cantilever

14. Connect the adapted femtotip (Fig. 8A) to the micromanipulator holder.
15. Mix equal parts resin and hardener of a 30-min Epoxy glue.
16. Deposit a small drop of glue on the coverslip from the step 9 tilever to the middle of the field of view.
17. Position the cantilever on the edge of the glue, and slowly approach it until the cantilever contacts the glue. Retract the cantilever to remove excess glue.

    It is easy to control the amount of glue because the droplet is clearly visible. We recommend that the diameter of the glue droplet should not exceed one-third of the sphere diameter.
18. Lift the cantilever, and search for a sphere. Position the center of the cantilever above the sphere, and slowly approach the sphere until the glue droplet just contacts the sphere. If the glue droplet surrounds the sphere, the sphere is contaminated and the procedure needs to be repeated.
19. When the sphere is correctly glued, leave it to harden in a clean box at room temperature for at least 24 h before use.

2.7 Conclusions

We have used cartilage tissue, live fibroblast cells, and individual collagen assemblies to illustrate how AFM is applicable to a diversity of biological studies. By implementing imaging and mechanical measurements in physiological environments, the AFM has the unique ability to probe the topographical and mechanical properties of biological samples at the nanometer scale. The combination of AFM with optical techniques provides a powerful platform to address nanomechanical and biochemical effects simultaneously. Future technical developments in new fluorescent dyes and novel microscope developments—such as high-speed AFM imaging, AFM sensing, and actuation—will open new avenues in biomedicine and nanoscience.

2.8 Ackwnoledgements

The authors gratefully acknowledge Roderick Lim and Cora-Ann Schönenberger for their many valuable suggestions made during the preparation of this chapter and Janne Hyötylä for preparing Figure 1. This work was supported by two research grants from the Swiss National Science Foundation (to U.A.) and funds from the National Center of Competence in Research on ”Nanoscale Science,” the Swiss Nanoscience Institute, the M.E. Müller Foundation of Switzerland, and the Canton Basel-Stadt (all to U.A.).

Recipes

ATV Solution (0.05%)

NaCl	8 g
KCl <!>	0.4 g
NaHCO3	0.58 g
Glucose	1.1 g
EDTA <!> (ethylenediamine tetra-acetic acid)	0.2 g
Trypsin <!> (2.5%)	20mL

1. Dissolve the contents in 500 mL of dH2O. Adjust to a final volume of 1 L with dH2O.
2. Use HCl to adjust the pH to 7.4.
3. Incubate the solution at 37°C for at least 1 h to activate the trypsin.
4. Sterilize the solution through a 0.22-mm filter, prepare 50-mL aliquots, and store themat –20°C.

DFCS Culture Medium

Component	Final Concentration
Dulbecco's minimal essential medium	1x
L-Glutamine	2 mM
Penicillin	100 IU/mL
Streptomycin	100 mg/mL
Fetal calf serum	10%

Final volume is 500 mL.

Phosphate-buffered saline (10x)

Reagent	Quantity	Final concentration
NaCl	80 g	1.37 M
KCl <!>	2 g	27 mM
KH2PO4	2.4 g	20 mM
Na2HPO4	14.4 g	100 mM
H2O	to 1 L	

Sorensen's Phosphate Buffer (0.133M, pH 7.2)

Reagent	Quantity
Na2HPO4	18.89 g
KH2PO4	9.08 g
dH2O	1 L

Prepare 0.133 M stock solutions of both salts, and mix 71.5 mL of Na2HPO4 and 28.5 mL of KH2PO4 to obtain pH 7.2.

2.9 References

Boisgard, R., Aime, J.P., and Couturier, G. 2007. Dynamic operation modes of AFM: Non-linear behavior and theoretical analysis of the stability of the AFM oscillator. *International Journal of Non-Linear Mechanics* 42(4): 673-680.

Haga, H., Sasaki, S., Kawabata, K., Ito, E., Ushiki, T., and Sambongi, T. 2000. Elasticity mapping of living fibroblasts by AFM and immunofluorescence observation of the cytoskeleton. *Ultramicroscopy* 82(1-4): 253-258.

Han, L., Dean, D., Mao, P., Ortiz, C., and Grodzinsky, A.J. 2007. Nanoscale shear deformation mechanisms of opposing cartilage aggrecan macromolecules. *Biophysical Journal* 93(5): L23-L25.

Hutter, J.L. and Bechhoefer, J. 1993. Calibration of Atomic-Force Microscope Tips (Vol 64, Pg 1868, 1993). *Review of Scientific Instruments* 64(11): 3342-3342.

Kellermayer, M.S.Z., Karsai, A., Kengyel, A., Nagy, A., Bianco, P., Huber, T., Kulcsar, A., Niedetzky, C., Proksch, R., and Grama, L. 2006. Spatially and temporally synchronized atomic force and total internal reflection fluorescence microscopy for imaging and manipulating cells and biomolecules. *Biophys J* 91(7): 2665-2677.Lehenkari, P.P., Charras, G.T., Nykanen, A., and Horton, M.A. 2000. Adapting atomic force microscopy for cell biology. *Ultramicroscopy* 82(1-4): 289-295.

Ludwig, T., Kirmse, R., Poole, K., and Schwarz, U.S. 2008. Probing cellular microenvironments and tissue remodeling by atomic force microscopy. *Pflugers Archiv-European Journal of Physiology* 456(1): 29-49.

Madl, J., Rhode, S., Stangl, H., Stockinger, H., Hinterdorfer, P., Schutz, G.J., and Kada, G. 2006. A combined optical and atomic force microscope for live cell investigations. *Ultramicroscopy* 106(8-9): 645-651.

Muller, D.J. 2008. AFM: a nanotool in membrane biology. *Biochemistry* 47(31): 7986-7998.

Pfeiffer, E., Vickers, S.M., Frank, E., Grodzinsky, A.J., and Spector, M. 2008. The effects of glycosaminoglycan content on the compressive modulus of cartilage engineered in type II collagen scaffolds. *Osteoarthritis and Cartilage* 16(10): 1237-1244.

Popko, J., Mnich, Z., Wasilewski, A., and Latosiewicz, R. 1986. Topographic differences in the value of the 2 sec Elastic Modul in the cartilage tissue of the knee joint. *Beitr Orthop Traumatol* 33(10): 506-509.

Raab, A., Han, W.H., Badt, D., Smith-Gill, S.J., Lindsay, S.M., Schindler, H., and Hinterdorfer, P. 1999. Antibody recognition imaging by force microscopy. *Nature Biotechnology* 17(9): 902-905.

Schaffer, T.E., Cleveland, J.P., Ohnesorge, F., Walters, D.A., and Hansma, P.K. 1996. Studies of vibrating atomic force microscope cantilevers in liquid. *Journal of Applied Physics* 80(7): 3622-3627.

Stolz, M., Aebi, U., and Stoffler, D. 2007. Developing scanning probe-based nanodevices - stepping out of the laboratory into the clinic. *Nanomedicine-Nanotechnology Biology and Medicine* 3(1): 53-62.

Stolz, M., Raiteri, R., Daniels, A.U., VanLandingham, M.R., Baschong, W., and Aebi, U. 2004. Dynamic elastic modulus of porcine articular cartilage determined at two different levels of tissue organization by indentation-type atomic force microscopy. *Biophysical Journal* 86(5): 3269-3283.

Chapter 3

The nanomechanical properties of rat fibroblasts are modulated by interfering with the vimentin intermediate filament system

Marija Plodinec[1], Marko Loparic[1], Rosmarie Suetterlin[1], Harald Herrmann[2], Ueli Aebi[1], and Cora-Ann Schoenenberger[1,*]

[1]M.E. Müller Institute for Structural Biology, Biozentrum, University of Basel, 4056 Basel, Switzerland

[2] Department of Molecular Genetics, German Cancer Research Center, 69120 Heidelberg, Germany

[*]Correspondence: cora-ann.schoenenberger@unibas.ch

Keywords: cytoskeleton, intermediate filaments, vimentin, myopathies, atomic force microscopy, nanomechanics, stiffness, dynamic elastic modulus

3.1 Abstract

The contribution of the intermediate filament (IF) network to the mechanical response of cells has so far received little attention, possibly because the assembly and regulation of IFs are not as well understood as that of the actin cytoskeleton or of microtubules. The mechanical role of IFs has been mostly inferred from measurements performed on individual filaments or gels in vitro. In this study we employ atomic force microscopy (AFM) to examine the contribution of vimentin IFs to the nanomechanical properties of living cells under native conditions. To specifically target and modulate the vimentin network, Rat-2 fibroblasts were transfected with GFP-desmin variants. Cells expressing desmin variants were identified by the fluorescence microscopy extension of the AFM instrument. This allowed us to directly compare the nanomechanical response of transfected and untransfected cells at high spatial resolution by means of AFM. Depending on the variant desmin, transfectants were either softer or stiffer than untransfected fibroblasts. Expression of the non-filament forming GFP-DesL345P mutant led to a collapse of the endogenous vimentin network in the perinuclear region that was accompanied by localized stiffening. Correlative confocal microscopy indicates that the expression of desmin variants specifically targets the endogenous vimentin IF network without major rearrangements of other cytoskeletal components. By measuring functional changes caused by IF rearrangements in intact cells, we show that IFs play a crucial role in mechanical behavior not only at large deformations but also in the nanomechanical response of individual cells.

3.2 Introduction

Living cells are complex heterogeneous systems with specific viscoelastic properties that are dominated by the structure of the three main cytoskeleton components; actin microfilaments, intermediate filaments (IFs) and microtubules. Developments in atomic force microscopy (AFM) allowed for mechanical probing of small volumes such as individual cells (Radmacher, 2007). Mechanical measurements on living cells show that the disruption of the actin or microtubule cytoskeleton results in a decreased cellular stiffness (Rotsch and Radmacher, 2000; Pelling et al., 2007; Ofek et al., 2009). While these studies have provided insight into distinct roles of these cytoskeletal constituents on cellular mechanics, the contribution of the IF system remains elusive. The abundance of IFs in specific cells and the fact that they span the entire cell from the nucleus to the plasma membrane suggest that they play an important mechanical role by providing structural stability and/or by relaying mechanical signals (Steinbock, Nikolic et al. 2000). To date, most of the information on the mechanical function of IFs in cells is inferred from rheological measurements on vimentin, desmin and keratin gels in vitro (Janmey, 1991; Coulombe, 1998 ; Schopferer, 2009).These polymer gels exhibit highly nonlinear stress-strain relationships, characterized by a very low initial stiffness at small strains and relatively high stiffness at large strains. Molecular dynamics simulations support that IFs are rather compliant at low strain and stiffen when a high strain is applied (Qin, Kreplak et al. 2009).

Vimentin is the most widely distributed of all IF proteins. It is essential in early embryonic development and is a hallmark of mesenchymal cells, for example, fibroblasts, leukocytes, and endothelial cells. Interestingly, these cell types occur in tissues that experience extensive forces, such as shear, tension and compression (Wang, 2000; Brown, 2001; Brown, 2001). Moreover, vimentin is frequently overexpressed in many aggressive tumors (Prasad, Soldatenkov et al. 1999). The mechanical properties of vimentin have been examined by rheometry techniques in vimentin knock-out cells and in drug-treated cells (Sager 1989; Wang, Butler et al. 1993; Eckes, Dogic et al. 1998; Eckes, Martin et al. 1998; Wang and Stamenovic 2000). These studies indicate a significant role of the vimentin network at large deformation, whereas at small deformation, cellular mechanics appear to be unaffected by changes in vimentin.

Despite numerous human diseases that arise from single point mutations in IF genes the nanomechanical function of IFs in individual cells is still an enigma (Selcen, 2004). Mutations in the muscle-specific desmin, which belongs to the same class of IFs as vimentin, are associated with skeletal and cardiac myopathies. Interestingly, during development and differentiation of muscle cells, vimentin and desmin are co-expressed (Selcen, 2004). In addition, vimentin and desmin are able to copolymerize at all stages of filament assembly *in vitro* (Wickert, Mucke et al. 2005). Transfection experiments using different desmin mutations have shown that the mutant desmin interacts with the endogenous vimentin and affects the architecture of the IF network in the cell (Bar, Mucke et al. 2006; Bar, Goudeau et al. 2007).

Recently, the nanoscopic properties of individual vimentin and desmin filaments *in vitro* were examined by AFM (Kreplak and Fudge 2007; Kreplak, Herrmann et al. 2008). These AFM experiments have shown that individual IFs, both recombinant and authentic, are soft, extensible and very compliant. Although these properties might be reflected in the mechanics of living cells, IFs form a complex network within the cell and thus may exhibit a different elastic behavior compared to isolated filaments. Questions on the nanomechanical function of IFs in a cellular context have so far not been systematically addressed because tools to specifically target IFs have been missing. In this study, we have specifically modified the IF network in Rat-2 fibroblasts by expressing GFP-tagged wild-type desmin and desminopathic mutants and have compared the nanomechanical response of transfected and untransfected cells. For mechanical testing at high dimensional sensitivity we used an AFM with an integrated light microscopy unit. This allowed us to identify cells with a modified IF network and directly probe the nanomechanical consequences of desmin expression in living cells.

3.3 Materials and Methods

Cell culture and preparation of cells for AFM

Rat-2 fibroblasts were grown in Dulbecco's modified Eagle's medium (DMEM, Sigma Aldrich, Switzerland) supplemented with 2mML-glutamine (Sigma Aldrich, Switzerland), 100 IU/ml penicillin/ 100 µg/ml streptomycin (Gibco, Switzerland), and 10% fetal calf serum (FCS GOLD; PAA Tissue Culture Company, USA; DFCS) at 37 ºC in a humidified atmosphere containing 5% CO2. Cells were subcultured weekly up to 10 passages. For experimental cultures, ~10^5 cells were plated in DFCS either on glass bottom dishes or coverslips.

Cloning and transient transfection of Rat-2 cells

GFP-tagged full-length desmin wild-type and mutant constructs were obtained by inserting corresponding PCR fragments at the HindIII/BamHI site into the pEGFP-C1 vector (BD Biosciences Clontech) using the following primers: 5'-CCAAGCTTCGATGGCCCAGGCCTACTCGTCCAG-3' (sense) and 5'-GGGATCCTTACAGCACTTCATGTTGTTGCTGTG-3' (antisense). Constructs were verified by DNA sequencing. Rat-2 fibroblast cells were grown for 24 hours on 50 x 40mm x 0.17 mm glass-bottom WillCo™ dishes (GWSt-5040, Intracell LTD, UK) or glass coverslips in a 24-well plate and then transfected with DNA plasmids using FuGENE 6 (Roche, Switzerland) following the standard protocol. Twenty-four hours after transfection, the cells were processed either for AFM experiments or confocal imaging.

Confocal laser scanning microscopy (CLSM)

For immunofluorescence, transfected cells were fixed for 15 min in phosphate-buffered saline (PBS) with 4% formaldehyde at RT. After rinsing with modified Hank's buffer (MHB; Hank's buffer without Ca2+, containing 2 mM EGTA, 5 mM 2-morpholino-ethanesulfonic acid, 0,005 % NaN3, pH 6.2-6.4), coverslips (diameter = 12 mm, thickness = 0.17 mm, Manzel-Glaser, Thermo Scientific, Germany) were permeabilized for 2 min in 0.2% TritonX100, rinsed in MHB and incubated with Cy3-conjugated vimentin antibody (mouse monoclonal 1:1000, Sigma-Aldrich) for 45' at RT in a humidified chamber. After several washes with MHB, coverslips were mounted in Mowiol 1188 (Hoechst). Where indicated, cells were incubated with 647-phalloidin (1:250, Invitrogen) or a α-tubulin mouse monoclonal antibody (1:2000, Boehringer, Germany) followed by a secondary donkey anti mouse antibody coupled to Alexa 488 (1:800, Molecular probes, Switzerland). Confocal sections were recorded with a Leica TCS 4-D CLSM and processed with Imaris software (Bitplane, Switzerland) and Adobe Photoshop version 10.0.. Confocal sections were recorded with a Leica TCS 4-D CLSM and processed with Imaris software (Bitplane, Zurich, Switzerland) and Adobe Photoshop version 10.0.

Mechanical probing by indentation AFM

All AFM experiments were carried out under physiological conditions at 37 ºC using a commercial AFM (Nanowizard I AFM, JPK Instruments, Germany) placed on a Zeiss Axiovert 135 TV microscope (Zeiss, Germany) equipped with 20_ and 40_ objectives and a GFP-fluorescence filter. Bright field and fluorescence signals were monitored using a grayscale digital camera (ANDOR SOLIS CCD-375; ANDOR Technology, Northern Ireland). We used standard triangular silicon nitride cantilevers with a spring constant between 0.04 and 0.08 N/m and a nominal tip radius of 20 nm (DNP-S, Vecco probes, Veeco Instruments, USA). The experimental value for the spring constant of each cantilever was determined by thermal tune method (Sader et al., 1995) using the JPK Nanowizard 1.1 calibration tool. For cell stiffness measurements, the AFM was operated in the ''Force-Volume Mode''. Briefly, arrays of force–displacement curves were recorded in a regular grid over a selected sample surface of 100 lm2. Each of the 128 _ 64 force–displacement curves consists of 1024 sampling points. All indentations were performed with the maximum load set to 1.8 nN at a scan rate of _15 lm/s. AFM stiffness maps were completed within 2–3 h. During the measurements, culture dishes were replenished with fresh DFCS saturated with 5% CO2 to maintain physiological conditions and compensate for evaporation. In the course of an experiment, the pH ranged between 7.4 and 7.5.

Analysis of indentation data

For the analysis of AFM force curves, a method described in Loparic et al. was modified (Loparic et al., 2010). Briefly, we developed software in LABWIEV (National Instruments, USA) for the automated analysis of the force–volume data. The contact point was determined by applying a polynomial fit to raw force curves according to a published algorithm (Lin et al., 2007). Force-indentation data were obtained by the indentation h, which corresponds to the difference between piezo displacement and cantilever deflection, and by multiplying cantilever deflection *d* with the spring constant *k* to obtain load *F*. The slope of each data point is calculated by performing a linear fit to the upper 50% of the unloading force curve. Slope values were spatially plotted to yield a stiffness map using Igor Pro (Wavemetrics, LakeOswego, USA). Gaussian distributions were computed from the stiffness values of individual cells. The mean slope value from the Gaussian fit was then used for calculating elastic modulus (*Es*) for each cell type according to the Oliver and Pharr theory (Oliver and Pharr, 1992) applied by Loparic and coworkers (Stolz et al., 2004; Loparic et al., 2010). In the Eq. (1) where Er represents the measured relative dynamic elastic modulus, Es is the elastic modulus of the sample and Ei of the indenter

$$\frac{1}{E_r} = \frac{1-\upsilon_s{}^2}{E_s} + \frac{1-\upsilon_i^2}{E_i} \tag{1}$$

where υ_s and υ_i are Poisson's ratios of sample and indenter. Assuming that the elastic modulus of biological specimens is orders of magnitude smaller than that of the indenter ($E_i >> E_s$), equation (1) reduces to

$$\frac{1}{E_r} \cong \frac{1-\upsilon_s^2}{E_s} \tag{2}$$

The Poisson's ratio of cells is assumed to be $\upsilon_s = 0.5$ (45). The slope stiffness of the sample is defined as the linear fit between the maximum load $F_2 = 1.8$ nN and the minimum load $F_1 = 0.9$ nN (3). The indentation depth is denoted by *h*.

$$S = \left[\frac{\Delta p}{\Delta h}\right]_{F_1}^{F_2} = \left[\frac{\Delta d \cdot k}{\Delta h}\right]_{d_1}^{d_2} \tag{3}$$

Subsequently, the relative elastic modulus E_r is defined by the following equation:

$$E_r = \frac{\sqrt{\pi}}{2} \frac{S}{\sqrt{A_c(h_c)}} \tag{4}$$

where *Ac(hc)* is the projection of the contact area as a function of the tip angle (θ) and the contact indentation depth *hc*. Assuming hc to correspond to the total depth of indentation *h* yields the following relation for a 4-sided pyramidal tip

$$A_c(h_c) = (2h\tan\Theta)^2 \tag{5}$$

By combining Eqs. (2-5) the elastic modulus of the sample E_s can be calculated:

$$E_s = \frac{\sqrt{\pi}}{2}\left(1-\upsilon_s^2\right)\frac{1}{\sqrt{A_c(h_c)}}\left[\frac{\Delta d \cdot k}{\Delta h}\right]_{d_1}^{d_2} \tag{6}$$

Statistical analysis

Histograms were plotted at bin value of 50 and data are given as mean ± standard deviation (SD). Statistical analysis was performed using paired t-tests. Statistical significance was tested at $p = 0.05$ and $p = 0.0001$. Mean values were calculated from $n = 59$ independent measurements for untransfected cells, $n = 12$ for *DesWT*, $n = 15$ for *DesA213V*, and $n = 19$ for *DesL345P*.

3.4 Results

In order to examine the contribution of the IF network to the mechanical response in living cells, we used an AFM setup with integrated light microscopy features. This allowed us to optically monitor the cells mounted under the fluid cell of the AFM during stiffness measurements over several hours (Fig. 3-1A). Moreover, the cantilever is clearly visible, such that the AFM tip can be precisely positioned to scan a defined area of interest. Another essential feature of the combined microscope is the option of epifluorescence (Fig. 3-1B), which allows the overlay of corresponding fluorescence and bright field images, as well as their direct correlation with AFM stiffness maps. Based on the optical images, transfected cells that are expressing GFP-tagged constructs are readily identified and can be probed in parallel with non-transfected Rat-2 cells.

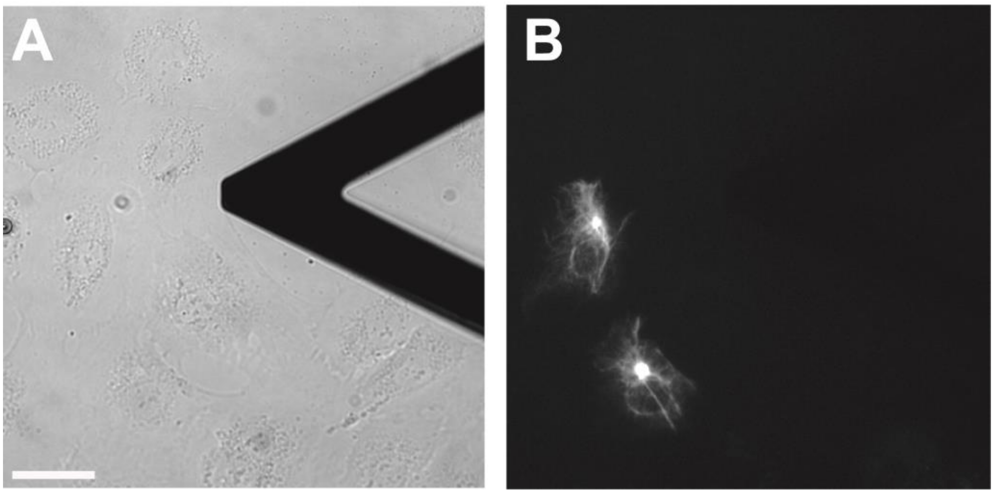

Figure 3-1. Combining AFM with optical microscopy for imaging Rat-2 fibroblasts transfected with GFP-desmin variants under native conditions. (A) The viability of the cells can be monitored in the bright field signal during the experiment by a CCD camera. (B) Fluorescence filters allow for epifluorescence detection of cells that express transfected GFP-desmin. Scale bar, 50 μm.

Transfected desmin differentially interacts with the endogenous vimentin

To specifically address the role of the IF system in cellular elasticity,we have transiently transfected Rat-2 fibroblasts with GFPdesmin wild-type and mutant constructs and examined their effects on the endogenous vimentin network. As illustrated in Fig. 3-2A, CLSM of Rat-2 cells transfected with GFP-DesWT revealed a prominent network of desmin filaments that spans the entire cell. Comparison of transfected and untransfected cells immunolabeled with a vimentin antibody (red) showed that the expression of exogenous GFP-DesWT does not affect the supramolecular organization of the endogenous vimentin network. The extensive co-localization of GFP-DesWT and vimentin in the overlay suggests that the wild-type desmin might have co-assembled with endogenous vimentin IFs, as has been demonstrated for isolated desmin and vimentin in vitro (Wickert et al., 2005). Similarly, cells transfected with GFP-DesA213V (Fig. 3-2B), which contains a single point mutation localized in the alpha-helical desmin domain, displayed a filamentous network that mostly colocalized with the endogenous vimentin IF network. In contrast, the GFP-tagged desmin mutant DesL345P (Fig. 3-2C), which contains a single point mutation in the highly conserved coiled-coil rod domain involved in the desmin assembly process, failed to form filamentous networks in Rat-2 cells. Instead, transfectants exhibited an accumulation of small, dot-like aggregates in the perinuclear region. More importantly, expression of GFP-DesL345P caused striking changes in the organization of the endogenous IF network. Immunofluorescent staining revealed that the vimentin network is disrupted and ‘‘collapsed’’ at the sites where desmin aggregates have accumulated. To ensure that the expression of the exogenous desmin does not significantly affect the other major components of the cytoskeleton, we have stained transiently transfected Rat-2 cells with a tubulin antibody (red) and phalloidin (blue), which binds to filamentous actin. As shown in Fig. 3-3, microtubules and the actin filament network of transfected cells were comparable to that of untransfected cells, even if the endogenous IF system was perturbed bymutant desmin. The immunofluorescence data from transiently transfected, fixed cells shows that by expressing desmin mutants, we can specifically modulate the endogenous IFs with minimal effects on the overall cytoarchitecture of Rat-2 fibroblasts. To ensure that the expression of the exogenous desmin does not significantly affect the other major components of the cytoskeleton, we have stained transiently transfected Rat-2 cells with a tubulin antibody (red) and phalloidin (blue), which binds to filamentous actin. As shown in figure 3-3, microtubules and the actin filament network of transfected cells were comparable to that of untransfected cells, even if the endogenous IF system was perturbed by mutant desmin. The immunofluorescence data from transiently transfected, fixed cells shows that by expressing desmin mutants, we can specifically modulate the endogenous IFs with minimal effects on the overall cytoarchitecture of Rat-2 fibroblasts.

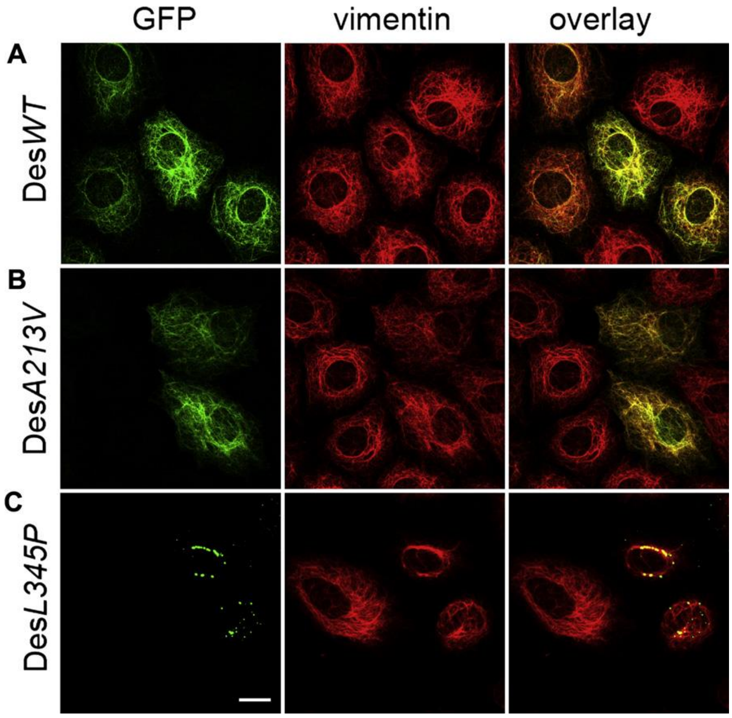

Figure 3-2. Fluorescence microscopy of the IF system in untransfected and transfected cells. Rat-2 cells were transfected with GFP-DesWT, -DesA213V or -DesL345P for 24 h, fixed, and immunolabeled with a vimentin-Cy3 antibody (red). Transfectants are identified by the GFP signal. (A) The overlay shows extensive integration of DesWT into the endogenous vimentin network in transfected cells. (B) The filament forming DesA213V mutant similarly co-localizes with the vimentin network. (C) The DesL345P mutant forms perinuclear aggregates (left panel) which induce a collapse of the vimentin network (middle panel). The overlay reveals a partial colocalization in the perinuclear region. Scale bar, 20 μm.

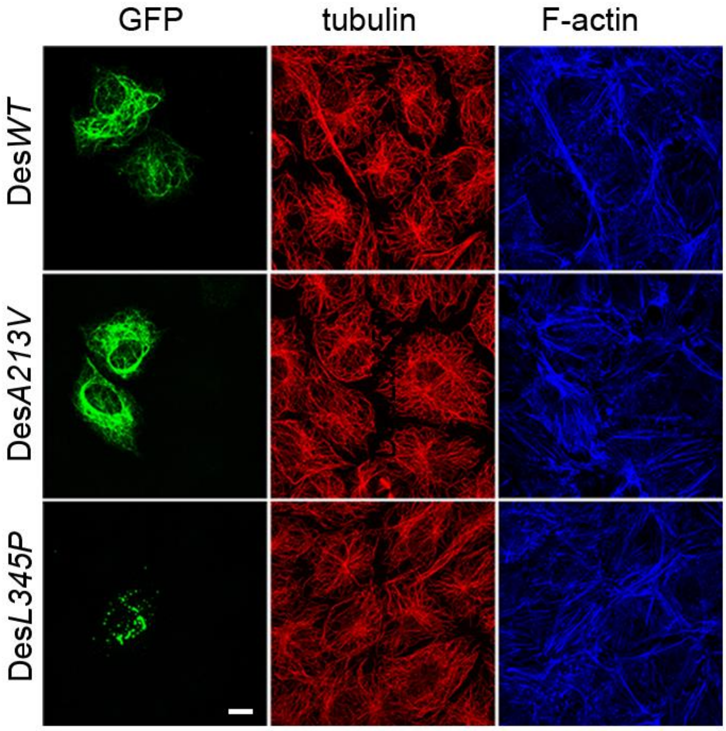

Figure 3-3. Transfection of desmin variants does not rearrange the actin and tubulin cytoskeleton. The GFP signal reveals DesWT (top row), DesA213V (middle row), and DesL345P (bottom row) in transfected cells. Cells were stained with 647-phalloidin (blue) to identify filamentous actin and immunolabeled with b-tubulin antibody (red) to reveal microtubules. Scale bar, 20 μm.

Stiffness mapping by AFM reveals nanomechanical changes in desmin expressing Rat-2 cells

To probe the consequences of modulating the IF system on the mechanical properties of Rat-2 cells by indentation-type AFM; we identified transfectants that express GFP-tagged desmin variants in the fluorescence mode of the combined AFM/light microscope (Fig. 3-4A, insets). Cells were transfected with GFP tagged wild-type desmin (DesWT), mutant desmin DesA213V, or mutant desmin DesL345P. Based on the overlay of bright field and fluorescence image, individual AFM scan areas were specifically selected to comprise transfected and untransfected control cells. In order to minimize the adverse effects of GFP-desmin overexpression, transfectants with moderate intensities were chosen based on the fluorescence intensity signal. The viability and overall cell morphology was optically monitored by bright field microscopy. For DesWT and DesA213V, we did not observe significant morphological differences between untransfected and transfected cells, while cells transfected with DesL345P mutant appeared larger with protruding nuclei when compared to the untransfected cells. Stiffness maps shown in Fig. 3-4B include transfected (marked by a black asterisk) and untransfected control cells recorded under the same experimental conditions, thus a direct comparison of their mechanical properties is feasible. DesWT and DesA213V transfectants exhibit stiffness maps that reflect the spatial organization of filaments revealed by fluorescence (Fig. 3-4A). In contrast, in DesL345P expressing cells we measured significant stiffening localized in areas around the nucleus where fluorescence indicates an accumulation of the mutant desmin.

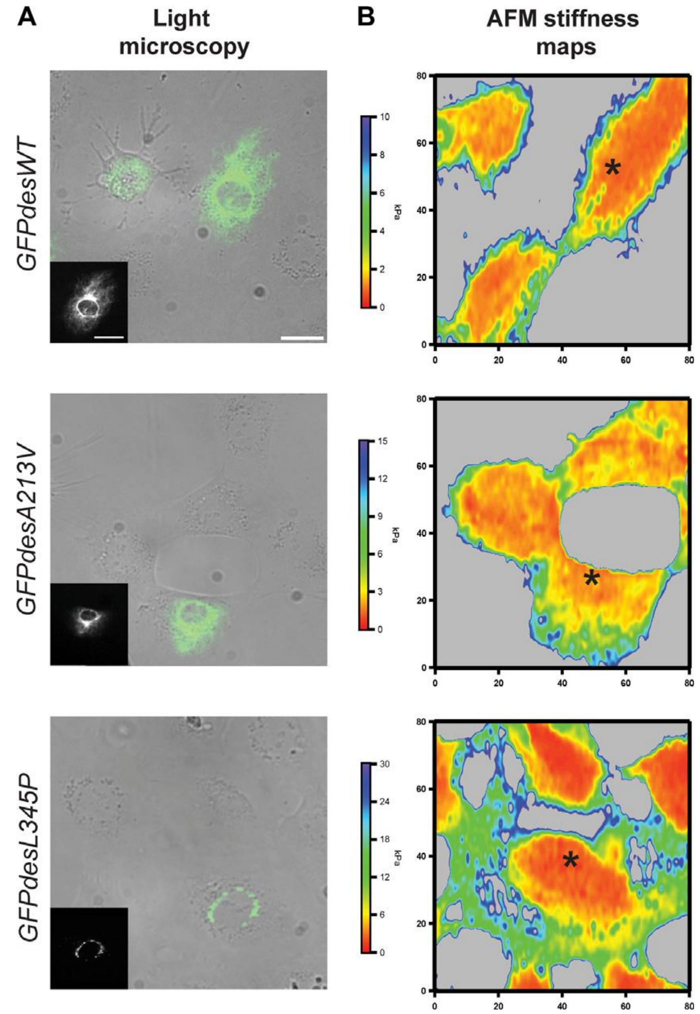

Figure 3-4. Imaging and stiffness mapping of Rat-2 cells by LM/AFM. (A) Overlay of bright field and fluorescence images reveals the location of untransfected and transfected Rat-2 cells for DesWT (top row), DesA213V (middle row), and DesL345P (bottom row). Scale bar, 50 lm. Insets, fluorescence images of the transfectants marked with an asterisk in the stiffness maps. Scale bar, 20 µm. (B) Stiffness maps representing 8192 force curves reveal differences in nanomechanical properties between different desmin variants. The cell expressing DesWT (top panel) exhibits a similar stiffness profile as its untransfected neighbors. The cell expressing DesA213V (middle panel) comprised much stiffer regions than untransfected cells. The DesL345P expressing cell (bottom panel) shows distinct stiffening in the perinuclear region. The stiffness values are indicated by the gradient in the vertical bar.

A quantitative analysis of stiffness distribution is presented as histograms in Fig. 5. Untransfected Rat-2 (Fig. 5A) and transfectants expressing DesWT (Fig. 5B) fall within a narrow range of stiffness values, albeit the latter is slightly softer. In contrast, DesA213V (Fig. 5C) and DesL345P (Fig. 5D) transfectants showed a very broad Gaussian distribution compared to untransfected cells, indicating that interactions between the mutant desmin and the endogenous vimentin induced structural changes in the network that contributed to stiffness heterogeneity. While the distribution is broad for both mutants, only DesL345P fits a bimodal distribution where the stiffer peak represents sites of collapsed IF network (shaded histogram) and the other peak (solid histogram) regions whose stiffness resembles that of untransfected cells. Regions resembling untransfected stiffness values were also found in DesA213V. As illustrated in Fig. 5E, representative force-indentation curves that were calculated from the measured force–displacement curves show distinct slopes for untransfected and transfected cells. Elastic modulus Es values were calculated from the stiffness measurements and presented in Fig. 5F. Untransfected cells exhibit an elastic modulus of $E_{untransfected}$ = 2.55 ± 0.99 kPa, while DesWT cell exhibit E_{DesWT} = 1.64 ± 0.61 kPa. For DesA213V filament forming mutant, the $E_{DesA213V}$ = 6.10 ± 1.82 kPa indicates a twofold stiffening compared to the untransfected cell. Consistent with the co-localized aggregation of DesL345P and vimentin near the nucleus and the bimodal stiffness distribution, transfectants exhibited two distinct stiffness values: $E_{DesL345P\text{-}perinuclear}$ 8.16 ± 3.33 kPa in the perinuclear region and $E_{DesL345P}$ = 2.51 ± 0.83 kPa in the rest of the cell.

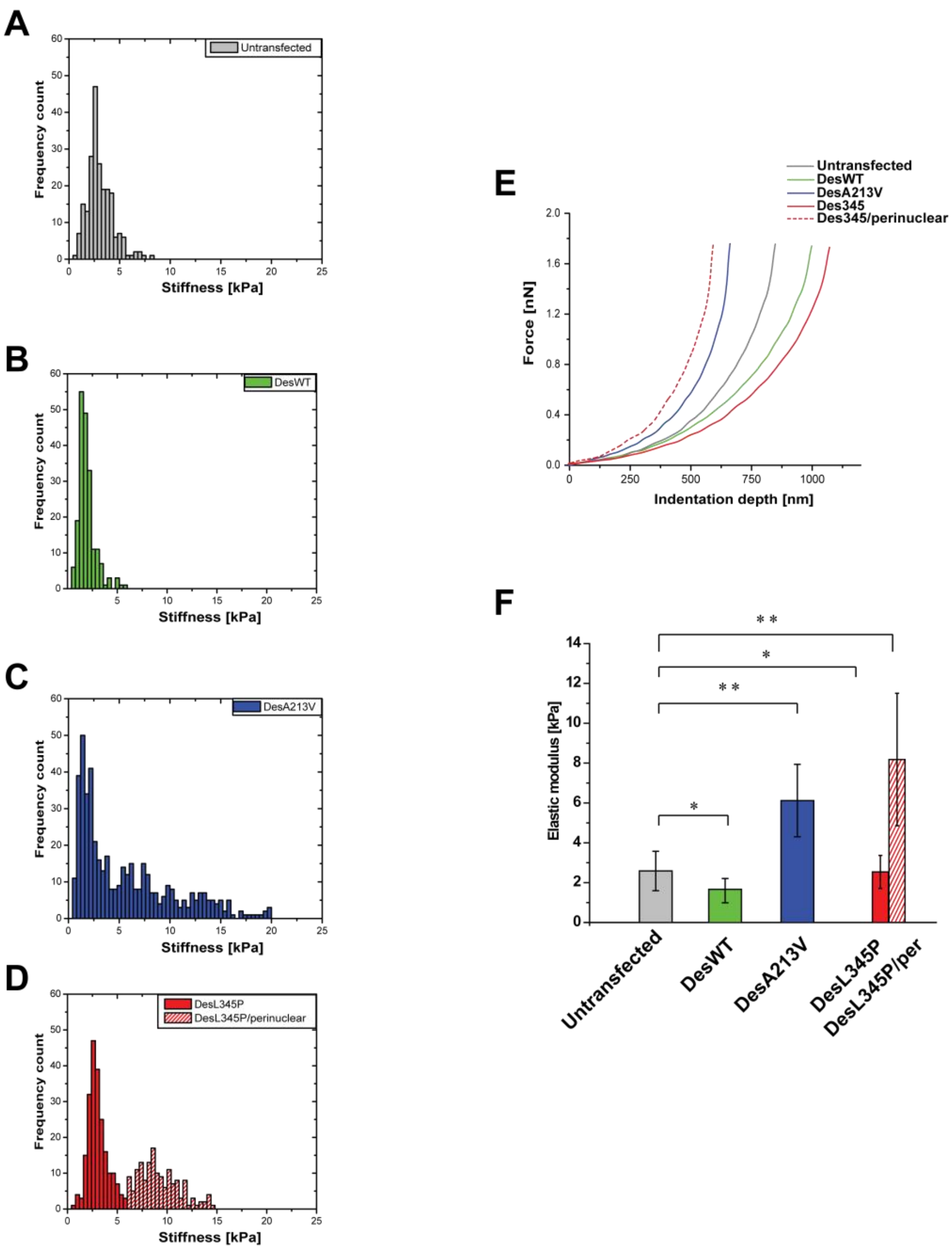

Figure 3-5. Analysis of nanomechanical properties. (A)–(D) Gaussian distribution of stiffness values. (A) Untransfected cells exhibit a uniform distribution. (B) DesWT transfectants exhibit a distribution with a maximum close to that of untransfected cells. (C) For DesA213V expressing cells, the distribution is very broad. (D) DesL345P transfectants are characterized by a bimodal stiffness distribution. The solid peak comprises stiffness values that are typical for untransfected cells. The broader Gaussian distribution (shaded bars) contains the higher stiffness values associated with the perinuclear sites of DesL345P aggregation. (E) Representative unloading force indentation curves for each cell type. (F) The elastic modulus Es for every cell type was calculated using average slope stiffness values. The statistical analysis shows mean values of Es and standard deviation. Stars indicate statistically significant differences (/$p < 0.05$, //$p < 0.0001$).

3.5 Discussion

Relating the effects of IF tuning to the nanomechanical behavior in living cells

In this study, we present comprehensive mechanical probing of living cells by indentation-type AFM using a setup with integrated light microscopy. Besides a precise positioning of the AFM tip at any site of interest and continuous optical assessment of the cell morphology during the stiffness mapping, the epifluorescence mode allowed us to easily identify cells that express GFP-tagged desmin variants within areas chosen for nanomechanical testing. In addition, we were able to measure the relative fluorescence intensities of transfected cells. Because cells that express very high levels of GFP-desmin variants had the tendency to round up and detach, we specifically choose transfectants with similar, moderate levels of GFP-desmin expression. Moreover, captured fluorescence images can be superimposed on corresponding stiffness maps. Thus, changes in the specific mechanical response of the transfectants can be directly related to the structural changes caused by transgene expression.

Data accuracy is improved by an internal reference

The range of elastic moduli reported from AFM elasticity measurements on living cells is rather broad (Janmey and McCulloch, 2007). Besides the cell type, the most obvious reasons for these variations are differences in the spring constant of the cantilevers and in the shape of the tip used, and in the data analysis employed. Specifically, errors intrinsic to these parameters cause significant variations in the absolute stiffness values determined in individual experiments. By using GFP-desmin variants to tune the IF network and a combined AFM/light microscope, we could largely avoid experimental variations between measurements because each stiffness map includes at least one transfected and one untransfected cell. Thus, relative differences in stiffness between normal cells Thus, relative differences in stiffness between normal cells and cells expressing GFP-desmin variants are instantly revealed within the same stiffness map.

Structural complexity of cells requires statistical analysis

Most studies conducted so far have fitted the force curves to the Hertz model, which assumes that living cell is a homogeneous, isotropic, and linear elastic sample with infinite thickness. However, as schematically illustrated in Fig. 3-6, living cells in terms of their mechanical properties are inhomogeneous, highly anisotropic, and multi-layered structures with a complex cytoarchitecture (Peeters et al., 2004). As a result, the elastic modulus of a cell is not constant over the whole range of indentation (Roduit et al., 2009) and also varies with the site of measurement. Consequently, data based on single-point measurements yield a rather biased view of the mechanical properties of a given cell. In contrast, the large number of force curves in our stiffness measurements represents an unbiased spatial sampling of a particular cell, and using sharp pyramidal tips reveals local variations of cell stiffness. By employing two distinct indentation regimes, Kasas et al. Have found that, from a mechanical point of view, a living cell can be considered a multilayered structure (Kasas et al., 2005); the lower segment of the force curve, which corresponds to an indentation depth of 100–200 nm, predominantly represents the stiffness contribution of the actin cytoskeleton below the plasma membrane, whereas the upper segment of the force curve more likely represents the deeper, basket-like IF network around the nucleus, and microtubules. A schematic representation of the relation between structural and mechanical ‘layers’ is illustrated in Fig. 3-6. Following the notion of Kasas and colleagues, we used the upper segment of the force curve, specifically 50% of the maximum force, to characterize the viscoelastic properties of the endogenous or modulated IF system (Fig. 3-6C).

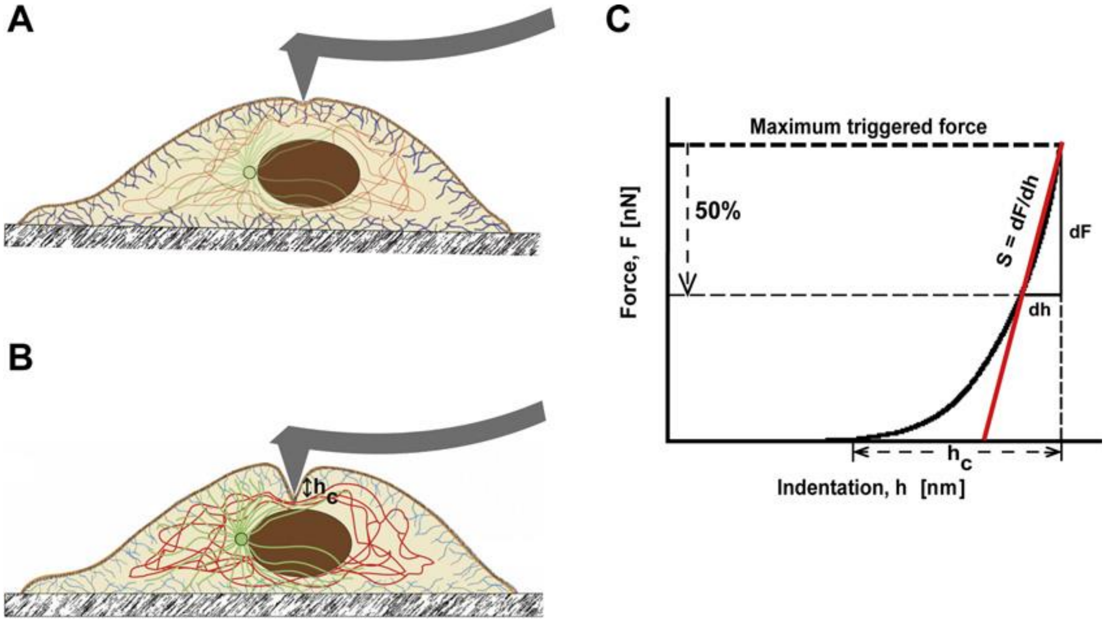

Figure 3-6. Model of the AFM indentation regime for analyzing IF nanomechanics in cells. (A) When indenting a cell, the AFM tip first encounters the actin cytoskeleton (blue) below the plasma membrane and then (B) the intermediate filament network (red). (C) The retracting AFM force curve specifies the cell’s response to the force F applied for indenting the cell to an indentation depth hc. The force curve can be divided into two main segments. The lower segment corresponds to the response of the actin cytoskeleton beneath the plasma membrane to F, whereas the upper segment of the curve predominantly represents the response of the deeper intermediate filament network. The linear fit to the upper 50% of the force curve (red) is used for determining the slope S from which the elastic modulus is calculated.

Expression of GFP-tagged desmin mutants induces changes in the architecture of the endogenous vimentin

Vimentin and muscle-specific desmin are members of the sequence homology class III IF proteins and are very similar in their structural organization as they exhibit more than 70% sequence identity in various vertebrate species (Schaffeld, 2001). Point mutations located in the central α-helical coiled-coil rod domain of desmin cause severe autosomal dominant forms of myofibrilar myopathy (Bar, Strelkov et al. 2004; Bar, Mucke et al. 2005). Many of these mutant desmin variants are able to assemble into seemingly normal IFs *in vitro* whereas others interfere with the assembly process at different stages (Bar, 2006). For example, *DesA213V*, which harbors a point mutation in coil 1B, is capable of forming filaments *in vitro*, but it is maturation-deficient as the filaments are unable to compact radially. Consistently, GFP-tagged *DesA213* formed a filamentous network similar to that observed with GFP-DesWT in transfectants and appeared to largely integrate into the endogenous vimentin IF network without causing major rearrangements. Immunofluorescence studies have previously shown a colocalization of transfected wild-type desmin and the *DesA213V* variant with the endogenous vimentin network in murine 3T3 fibroblasts (Bar, Kostareva et al. 2006).

In contrast, expression of the *GFP-DesL345P* mutant resulted in aggregates in the perinuclear region. More significantly, expression of this mutant led to an apparent collapse of the endogenous vimentin IF network around the nucleus. A similar antimorphic effect on the organization of the endogenous vimentin (Carlsson, Fischer et al. 2002; Bar, Kostareva et al. 2006) or desmin network (Bar, Goudeau et al. 2007) has been previously observed for this mutant.

In a number of studies, reorganization of the IF network in cells has been achieved by treatment with acrylamide (Faigle, Colucci-Guyon et al. 2000) or cisplatin (Evans and Simpkins 1998). However, these drugs simultaneously affect multiple cellular functions, as well as overall protein synthesis. More specifically, treatment with these drugs irreversibly modified other cytoskeletal elements that are linked to the IF network by cytolinkers or motor protein complexes (Liao and Gundersen, 1998). Although we cannot entirely rule out that the IF rearrangements caused by the expression of mutant desmin variants might have subtle effects on the organization of the actin and/or microtubule network, our immunofluorescence data suggest that these cytoskeleton constituents are similarly organized in transfected and untransfected cells. Even in the case of mutant DesL345P where the endogenous vimentin network was severely perturbed, both actin microfilaments and microtubules appeared largely unaffected (see Fig. 3). Hence, we conclude that the expression of mutant desmin variants represents a selective means to specifically modify the vimentin IF system.

Desmin variants provide a tool to assess the contribution of vimentin IFs to the nanomechanical properties of cells

Mechanical measurements complemented by time-resolved electron microscopy (EM) show that desmin and vimentin IF networks assembled in vitro from purified proteins are much more flexible than actin filaments (Storm, 2005). Among IFs, rheology measurements revealed desmin filaments to be stiffer (persistence length $l_{(p)} \approx$ 900nm) than vimentin filaments ($l_{(p)} \approx$ 400 nm). Moreover, filament bundling is more pronounced for desmin than for vimentin. Notably, *in vitro* formed heteropolymers between desmin and vimentin were shown to exhibit intermediary mechanical properties compared those of the homo-polymeric filaments (Schopferer, Bar et al. 2009). Based on data from *in vitro* studies, and the extensive colocalization of vimentin and desmin in *GFP-DesWT* transfectants, one might have assumed that desmin expression leads to a stiffening of the cell. However, AFM stiffness maps revealed *DesWT* transfectants to be slightly softer than the untransfected cells. It is conceivable that this softening is related to specific interactions of vimentin and desmin subunits in the hetero-filaments. Consistently, a recent publication demonstrates end-to-end annealing and intercalary subunit exchange in living cells (Colakoglu and Brown 2009). Such a subunit exchange with *GFP-DesWT* may destabilize and/or slightly reduce the stiffness of the final heteropolymeric network.

In contrast to the wild-type, expression of the filament-forming A213V mutant caused a two-fold stiffening of transfected cells. Because this mutation interferes with a late stage of IF assembly, the final steps of heteropolymeric network formation are likely to be affected in the transfectants. Recent AFM studies of isolated desmin filaments have shown specific point mutations to be related to changes in mechanical properties (Kreplak and Bar 2009). It was suggested that the distinct intra-filamentous structure of the mutant desmin was responsible for the modified force–bearing properties of the filament. Consistent with this notion, structural changes induced by the incorporation of *DesA213V* might be responsible for the significant stiffening of transfected cells.

Expression of the non-filament forming mutant *DesL345P* drastically changed the IF network and the mechanical response of the transfectants. The DesL345P mutation has been shown to affect filament assembly at an early stage and form aggregates rather than filamentous structures (Bar, Kostareva et al. 2006). Consistently, fluorescence data of

DesL345P transfectants indicates that the mutant desmin did not integrate into vimentin filaments. Instead, *DesL345P* expression induced a collapse of the endogenous vimentin system in the perinuclear region, which caused drastic localized cell stiffening in this area. At the same time, cytoplasm exhibited overall stiffening while the stiffness of the nuclear region was comparable to the untransfected cells and the nucleus was protruding out. This is not an unexpected result since the basketlike IF network stabilizes the nucleus, thus by collapsing in the perinuclear region, the nucleus becomes more exposed and the influence on the stiffness from the rest of the cytoskeleton may become more prominent. It has been shown in transgenic mice that tissues expressing *L345P* mutant desmin exhibit changes in the proximal, bulbar and facial muscles that are connected with mechanical weakness (Sjoberg, Saavedra-Matiz et al. 1999). In our system, cells transfected with desmin mutant L345P clearly exhibited severely impaired mechanical function at specific sites within an individual cell. Finally, the accumulation of cells with altered mechanical properties over an extended period of time would most likely result in the complete mechanical dysfunction of the affected tissue.

3.6 Conclusions

In conclusion, we show that desmin variants represent a valuable tool to specifically examine the contribution of the intermediate filament network to the mechanical function of living cells under native conditions. By using a combination of AFM and optical microscopy, we were able to identify cells transfected with desmin variants and measure their nanomechanical properties in direct comparison to untransfected cells at high spatial resolution. Depending on the desmin variant expressed an overall or localized cell stiffening was observed. Our study demonstrates that the alterations in the IF filament structure and architecture have a direct impact on the nanomechanical properties of living cells. Finally, our data show that IFs play an important role not only at large deformations but that they contribute to the mechanical properties also at the nanometer scale. This indicates that molecular changes at the single cell level, which are frequently associated with disease, trigger specific nanomechanical responses.

3.7 Acknowledgements

This work was supported by an NCCR program grant on “Nanoscale Science” awarded by the Swiss National Science Foundation to CAS, the M. E. Müller Foundation of Switzerland

and the Canton Basel-Stadt. H.H. was supported by the German Research Foundation (DFG; HE 1853 and BA 2186/3-1). We gratefully acknowledge Lydia Lussi for the drawing in figure 6, Sandra Mitrovic for advice on transfections, Janne Hyothyla and Roderick Lim for helpful discussions on data analysis.

3.8 References

Bar, H., B. Goudeau, et al. (2007). "Conspicuous involvement of desmin tail mutations in diverse cardiac and skeletal myopathies." Human Mutation **28**(4): 374-386.

Bar, H., A. Kostareva, et al. (2006). "Forced expression of desmin and desmin mutants in cultured cells: Impact of myopathic missense mutations in the central coiled-coil domain on network formation." Experimental Cell Research **312**(9): 1554-1565.

Bar, H., N. Mucke, et al. (2005). "Severe muscle disease-causing desmin mutations interfere with in vitro filament assembly at distinct stages." Proceedings of the National Academy of Sciences of the United States of America **102**(42): 15099-15104.

Bar, H., N. Mucke, et al. (2006). "Impact of disease mutations on the desmin filament assembly process." Journal of Molecular Biology **360**(5): 1031-1042.

Bar, H., S. V. Strelkov, et al. (2004). "The biology of desmin filaments: how do mutations affect their structure, assembly, and organisation?" Journal of Structural Biology **148**(2): 137-152.

Carlsson, L., C. Fischer, et al. (2002). "Cytoskeletal derangements in hereditary myopathy with a desmin L345P mutation." Acta Neuropathologica **104**(5): 493-504.

Colakoglu, G. and A. Brown (2009). "Intermediate filaments exchange subunits along their length and elongate by end-to-end annealing." Journal of Cell Biology **185**(5): 769-777.

Eckes, B., D. Dogic, et al. (1998). "Impaired mechanical stability, migration and contractile capacity in vimentin-deficient fibroblasts." Journal of Cell Science **111**: 1897-1907.

Eckes, B., P. Martin, et al. (1998). "Disruption of tensegrity in vimentin-deficient fibroblasts causes delayed wound healing in fetal and adult mice." Journal of Investigative Dermatology **110**(4): 592-592.

Evans, R. M. and H. Simpkins (1998). "Cisplatin induced intermediate filament reorganization and altered mitochondrial function in 3T3 cells and drug-sensitive and -resistant Walker 256 cells." Experimental Cell Research **245**(1): 69-78.

Faigle, W., E. Colucci-Guyon, et al. (2000). "Vimentin filaments in fibroblasts are a reservoir for SNAP23, a component of the membrane fusion machinery." Molecular Biology of the Cell **11**(10): 3485-3494.

Kreplak, L. and H. Bar (2009). "Severe Myopathy Mutations Modify the Nanomechanics of Desmin Intermediate Filaments." Journal of Molecular Biology **385**(4): 1043-1051.

Kreplak, L. and D. Fudge (2007). "Biomechanical properties of intermediate filaments: from tissues to single filaments and back." Bioessays **29**(1): 26-35.

Kreplak, L., H. Herrmann, et al. (2008). "Tensile properties of single desmin intermediate filaments." Biophysical Journal **94**(7): 2790-2799.

Liao, G. J. and G. G. Gundersen (1998). "Kinesin is a candidate for cross-bridging microtubules and intermediate filaments - Selective binding of kinesin to detyrosinated tobulin and vimentin." Journal of Biological Chemistry **273**(16): 9797-9803.

Ofek, G., D. C. Wiltz, et al. (2009). "Contribution of the Cytoskeleton to the Compressive Properties and Recovery Behavior of Single Cells." Biophysical Journal **97**(7): 1873-1882.

Pelling, A. E., D. W. Dawson, et al. (2007). "Distinct contributions of microtubule subtypes to cell membrane shape and stability." Nanomedicine-Nanotechnology Biology and Medicine **3**(1): 43-52.

Prasad, S., V. A. Soldatenkov, et al. (1999). "Intermediate filament proteins during carcinogenesis and apoptosis (Review)." International Journal of Oncology **14**(3): 563-570.

Qin, Z., L. Kreplak, et al. (2009). "Nanomechanical properties of vimentin intermediate filament dimers." Nanotechnology **20**(42): -.

Rotsch, C. and M. Radmacher (2000). "Drug-induced changes of cytoskeletal structure and mechanics in fibroblasts: An atomic force microscopy study." Biophysical Journal **78**(1): 520-535.

Sager, P. R. (1989). "Cytoskeletal Effects of Acrylamide and 2,5-Hexanedione - Selective Aggregation of Vimentin Filaments." Toxicology and Applied Pharmacology **97**(1): 141-155.

Schopferer, M., H. Bar, et al. (2009). "Desmin and Vimentin Intermediate Filament Networks: Their Viscoelastic Properties Investigated by Mechanical Rheometry." Journal of Molecular Biology **388**(1): 133-143.

Sjoberg, G., C. A. Saavedra-Matiz, et al. (1999). "A missense mutation in the desmin rod domain is associated with autosomal dominant distal myopathy, and exerts a dominant negative effect on filament formation." Human Molecular Genetics **8**(12): 2191-2198.

Steinbock, F. A., B. Nikolic, et al. (2000). "Dose-dependent linkage, assembly inhibition and disassembly of vimentin and cytokeratin 5/14 filaments through plectin's intermediate filament-binding domain." Journal of Cell Science **113**(3): 483-491.

Wang, N., J. P. Butler, et al. (1993). "Mechanotransduction across the Cell-Surface and through the Cytoskeleton." Science **260**(5111): 1124-1127.

Wang, N. and D. Stamenovic (2000). "Contribution of intermediate filaments to cell stiffness, stiffening, and growth." American Journal of Physiology-Cell Physiology **279**(1): C188-C194.

Wickert, U., N. Mucke, et al. (2005). "Characterization of the in vitro co-assembly process of the intermediate filament proteins vimentin and desmin: mixed polymers at all stages of assembly." European Journal of Cell Biology **84**(2-3): 379-391.

Chapter 4

Morphology and cytoarchitecture regulate nanomechanical properties of tumor spheroids

M. Plodinec[1], G. Schweighauser[1], R. Sütterlin[1], E. Oberman[2], U. Aebi[1], C.-A. Schönenberger[1]

1. Maurice E. Müller Institute, Core program Structural Biology& Biophysics, Biozentrum, University of Basel, 4056 Basel, Switzerland

2. Department of Pathology, University Hospital Basel, CH-4031 Basel, Switzerland

* Correspondence: cora-ann.schoenenberger@unibas.ch

Keywords: transformation, actin, 3D culture, hypoxia core, periphery, cytoskeleton, extracellular matrix, stiffness, atomic force microscopy

4.1 Abstract

Cells within tissues continuously encounter mechanical challenges to which they respond by remodeling their cytoskeleton. Cellular interactions as well as the microenvironment orchestrate the cell’s mechanical response under physiological and pathological conditions. Altered expression of components of the cell cytoskeleton can contribute to cellular transformation and tumorigenesis. Moreover, active remodeling of the cytoskeleton is essential for tumor cell invasion and metastasis. We are employing atomic force microscopy (AFM) in combination with light microscopy to probe the nanomechanical properties of cells in relation to changes in cytoarchitecture and microenvironmental conditions that are associated with tumorigenesis. Stiffness maps of living Rat2 fibroblasts and Rat2sm9, a derivative that has been rendered tumorigenic by expression of a Gly245Asp mutant actin, reveal that modification of the cytoskeleton did not alter the stiffness of the transformed cells on glass substrates. To exclude any impact of the substrate attachment on the organization of the cytoskeleton, we probed the stiffness of normal and tumorigenic Rat2 cells grown as 3D spheroids. On day 3, tumor spheroids exhibited a gradual softening from the periphery to the core consistent with the reduction of filamentous actin and vimentin. Moreover, the core region was significantly softer than that of normal spheroids. Consistently, increased HIF-1α expression in the core of tumor spheroids indicated extensive hypoxia compared to normal spheroids. To specifically examine the influence of hypoxia on spheroid nanomechanics and the related changes of the cytoskeleton and extracellular matrix changes (ECM), we exposed spheroid cultures to low oxygen tension. Hypoxic conditions caused only tumor but not normal spheroids to disseminate and differentially affected their nanomechanical properties. Our data suggest that a hypoxia-induced decrease in cell stiffness is conducive to the dissemination of tumor cells.

4.2 Introduction

Primary solid tumors are thought to arise from cells that became unable to respond to normal growth regulatory mechanisms, presumably through various mutations and/or altered gene expression (Osada and Takahashi 2002). This genetic instability enables tumor heterogeneity by causing continuous malignant alterations, including cell clustering in a primary tumor mass, angiogenesis and finally metastatic spread. Tumor progression arises within a three-dimensional microenvironment that consists of cellular and non-cellular components. Experimental data obtained so far show that tumor associated cellular stroma components such as activated endothelial and lymphatic cells, infiltrating immune cells, modified adipocytes and altered fibroblasts have a key role in either enhancing or restricting tumor progression (Barcellos-Hoff and Ravani 2000; Wiseman and Werb 2002; Burdelya, Komarova et al. 2006). For example, during the malignant transformation, cell-cell contacts become damaged and cells undergo epithelial to mesenchymal transition (EMT) including activation of fibroblasts comprising cancer stroma and alterations in actin and intermediate filaments cytoarchitecture and ECM synthesis and regulation (Tlsty and Hein 2001). In particular, fibroblasts from surrounding stroma are associated with cancer cells at all stages of cancer progression, and their structural and functional contributions to this process are beginning to emerge (Mueller and Fusenig 2004). On the other hand, the ECM, nutrient and oxygen supply are non-cellular components which have been shown to contribute to tumor progression either by disrupting tissue integrity and promoting tumor cell motility and invasion or by inducing angiogenesis and promoting survival and selection of the aggressive cell phenotypes ((Erler and Giaccia 2006).

Essentially all tumors start with an avascular stage of growth where nutrient supply occurs simply through diffusion from the nearby microenvironment. Before establishing a blood supply, tumors are not capable of acquiring sufficient nutrients to ensure continued exponential growth (Walenta, Doetsch et al. 2000). The restricted supply of critical nutrients such as oxygen and glucose results in marked gradients within the cell mass (Vaupel 2004). The tumor cells respond by alterations in physiology and metabolism as well as through altered gene and protein expression (Dang and Semenza 1999; Allinen, Beroukhim et al. 2004; Klaunig and Kamendulis 2004). In fact, many of the later manifestations of the malignancy, including invasion and angiogenesis, are thought to be caused and/or enhanced by the oxygen and nutrient gradients that develop in the initial tumor mass. Local environmental conditions can activate tumor fibroblasts to release cytokines, growth factors and ECM degrading enzymes (Erler and Weaver 2009) important for malignant progression.

Tumor microenvironment yields profound effects on cell and cancer tissue mechanical properties that include modification of both tension and compression forces excreted by these cells in the attempt to disseminate from the primary tumor and invade the surrounding tissues (Kumar and Weaver 2009). Clearly, cancer cells undergo marked changes of their mechanical phenotype during cancer progression. Although, remodelling of cell and tissue structure are essential factors in the mechanic response, the influence of the microenvironment conditions such as low oxygen (hypoxia) on the mechanical phenotype should not be neglected. For example, the loss of tissue compactness caused by the lack of oxygen in the deeper regions of the small avascular tumor, will promote the cells to invade surrounding and distant tissues. The effects of hypoxia on cell and tissue mechanics are of clinical relevance, since hypoxia is associated with increased with an aggressive cancer phenotype and poor patient outcome (Wouters, Weppler et al. 2002; Milani and Harris 2008; Hu, Fan et al. 2009). However, until now, there is no experimental data available on the effects of hypoxia on the mechanical features of small avascular tumor and their potential impact on cancer progression.

One approach of investigating the effects of a heterogeneous tumor microenvironment including tumor stroma is to culture cells as three-dimensional (3D) spheroids. Spheroids are aggregates of cells that can be grown under controlled external conditions. In contrast to monolayer cells grown on plastic or glass substrates in a two-dimensional plane (2D), spheroids are able to develop many of the hallmark features of tumors *in vivo,* including proliferation arrest, altered metabolism and gene expression, growth kinetics and therapy resistance (Ghosh, Spagnoli et al. 2005). In a spheroid culture, no unilateral restriction is imposed on the cell. Instead, the cell shape is mainly governed by the intrinsic cell-cell adhesive interactions, specific microenvironmental conditions and by the nature of extracellular matrix produced by the particular cell type comprising the spheroid. With increasing size most spheroids exhibit proliferation gradients from the periphery towards the core and specific nutrient supply patterns, such as centripetal oxygen gradient (Muellerklieser and Sutherland 1982; Casciari, Sotirchos et al. 1992) which makes them superior to other 3D cultures with respect to mimicking physiologically relevant 3D tumor environment. Thus, as the aggregate grows, it develops nutrient and oxygen deprived inner regions similary to avascular tumors *in vivo*. Until now, spheroids from a broad range of cell types have been reproducibly produced by various techniques and used for quantitative or qualitative assessment of tumor growth, invasion and therapy response (Feder-Mengus, Ghosh et al. 2007; Pampaloni, Reynaud et al. 2007; Feder-Mengus, Ghosh et al. 2008).

Even though mechanical properties have been recognized as an important hallmark of tumor progression, 3D spheroid cultures have not yet been explored for the mechanical testing. This is particularly surprising, since a variety of techniques for studying cell and tissue mechanics exist (Suresh 2007) that could be easily applied to 3D spheroid cultures. Bearing in mind that tissue-specific cytoarchitecture and microenvironment including cell-cell, and cell-ECM matrix interactions can influence the state of a cell (i.e. healthy vs. diseased), our objective was to study how correlating changes in these factors that re associated with tumorigenesis affect the mechanical properties of cells in a 3D model tissue system. Towards this goal, we have successfully grown both normal Rat2 wild-type (WT) fibroblasts and its derivative Rat2sm9, which has been rendered tumorigenic by a Gly245Asp actin mutation, as 3D spheroids on Poly (2-Hydroxyethyl methacrylate) (Poly-HEMA)-coated substrates (Folkman and Moscona 1978). We have applied an established atomic force microscopy (AFM) nanomechanical testing procedure (Stolz, Raiteri et al. 2004; Stolz, Gottardi et al. 2009), which has allowed us to correlate the nanomechanical properties with structural, morphological and biochemical effects of the oxygen gradient on the cell cytoskeleton and the extracellular environment for normal and tumorigenic fibroblasts. Our findings demonstrate that hypoxic conditions differentially alter mechanical properties of tumor spheroids and that hypoxia induced cell softening accompanied by structural changes in the actin and vimentin cytoskeleton and by ECM degradation. It is conceivable that the profuse softening of the tumor spheroids promotes dissemination of cells from the primary spheroid similar to the invasion processes found *in vivo*. Importantly, data obtained on Rat2sm9 tumor spheroids strengthen the connection between hypoxia and specific nanomechanical phenotype of tumor stroma.

4.3 Materials and Methods

Cell culture

Rat2-WT and Rat2sm9 were routinely passaged in conventional as conventional 2D cultures in Dulbecco's Modified Eagle's Medium (DMEM, Sigma-Aldrich, Switzerland) supplemented with 10% fetal calf serum (FCS, PAA, USA), 100µg/ml of Streptomycin (Invitrogen, Germany) and 20ml 200mM of L-glutamine (Invitrogen, Germany) per 500 ml of medium at 37 °C in a humidified atmosphere containing 5% CO_2. Cells were subcultured weekly up to 15 passages.

Preparation of 3D spheroid cultures

Poly-HEMA crystals (600 mg) were dissolved in 5 ml 95% EtOH by rotating over night at 37°C. This stock solution was diluted by adding 7 ml of 95% EtOH. 96-well plates were coated with 50 µl/ well (0.1 ml /cm^2) and then dried overnight at room temperature in a sterile environment. Plates could be stored for extended period of time prior to use. For 3D spheroid cultures, 250µl of cell suspension solution ($2.4 \cdot 10^5$ cells/ml) were added added to each well of a Poly-HEMA coated 96 well plate yielding 60'000 cells per well. Cells were cultured for 72 hours under normoxic (20 % oxygen) and hypoxic (2% oxygen) conditions. At day 3, Rat2 cells had formed a single spheroid per well.

Total protein extraction from 2D cultures

The culturing medium was removed and the cells were first washed with the PBS pre-warmed to 37°C before 2ml of ice-cold PBS was added. Cells were scraped from the bottom of the dish using a Teon-coated scraper, collected in an Eppendorf tube and centrifuged for 1min at speed of 13'000 rpm at 4°C. The supernatant was removed and the pellet re-suspended in 250 µl of ice cold RIPA buffer (150mM NaCl,1% Triton X-100, 0.5% sodium salt of Deoxycholic acid, 0.1% Sodium dodecyl sulphate, 50mM Tris, pH=8 containing 1 tablet of protease inhibitor cocktail (Roche, Switzerland) diluted per 10 ml of RIPA buffer). The cells were extracted for 20 min on ice. Subsequently, the lysate was centrifuged at 13'000 rpm for 30min at 4°C. The supernatant was immediately used for immunobloting or stored at – 80°C until further use.

Total protein extraction from 3D spheroid cultures

All spheroids from a 96-well plate were collected and subsequently washed with PBS as described above. The ice cold PBS was removed and 250 µl of RIPA buffer was added. Spheroids were homogenized in RIPA buffer using a homogenizer (IKA Ultra Turrax® T25, Germany) at 12'000rpm for 20 s on ice. Next, the suspension was incubated for 20min on ice with frequent vortexing and subsequently centrifuged at 13'000 rpm for 30 min at 4°C. The supernatant containing cell lysate was either immediately used for immunobloting or stored at -80°C until use.

Immunoblot analysis

Equal amounts of extracted proteins were separated on SDS-PAGE gels and analysed by immunoblotting against actin (1 F1 mAb 1/10; (Schroeder, Graff et al. 2009), (tubulin 1/5000; Sigma Aldrich, Switzerland), vimentin (1/5000; courtesy of Prof. H. Herrmann, Heidelberg, Germany) and mutant actin245Asp (1/20) and detected with a chemiluminescence system (Bucher Biotec, Germany).

Histological procedure

Spheroids were collected and centrifuged for 10 min at 2500 rpm/min. The supernatant was removed and the pellet containing spheroids was further proceessed. After vortexing for 1 min at RT, „Thrombin Reagent“ (Diagnotec AG, Switzerland) was added and vortexing repeated for 1 min at RT. When the coagulation process was complete, coagulated material containing spheroids was fixed in 4% formalin, embedded in paraffin, and sectioned (5 µm thick). Sections were consequently stained with Hematoxylin and Eosin (H&E) according to a standard protocol and analysed for hypoxia and proliferation.

Bromodeoxyuridine (BrdU) staining

Standard BrdU (BD Biosciences, UK) incorporation was used to assess cell proliferation. Prior to spheroid collection, each well of a 96-well plate was incubated for 20 min with 0.02 mM of BrdU in PBS at RT followed by histological procedure. The paraffin-embedded tissue sections were completely dewaxed and rehydrated with PBS followed by microwave antigen retrieval according to the manufacturer's protocol. Sections were incubated in 0.3% H_2O_2 in methanol for 10 min to inhibit endogenous peroxidase activity and rinsed in PBS. After blocking with bovine serum albumin (BSA) at room temperature, the sections were incubated with primary anti-BrdU antibody (1/25 in PBS; Sigma Aldrich, Switzerland) overnight at 4°C in a humidified chamber followed by washing in PBS. After incubation with biotin-conjugated rabbit anti-mouse IgG secondary antibody (Sigma Aldrich, Switzerland) and HRP (horseradish peroxidase)-linked streptavidin for 1 hr. at room temperature each, sections were washed in PBS and developed with DAB. After mounting with Crystal/Mount (Fischer Scientific, USA), sections were examined under a light microscope.

Mounting spheroids on glass slides

Multicellular spheroids were placed on glass coverslips coated with 5% collagen I (BD Biosciences, UK) and left to attach for approximately 2.5 hrs. in a humidified atmosphere containing 5% CO_2 in a humidified chamber. To gain access to inner spheroid regions, the top of the spheroid was removed by using a customized razor blade mounted on a micromanipulator (Eppendorf micromanipulators, USA). After a washing step in pre-warmed culture medium, spheroids were incubated for another 1.5 hrs. at 37°C in either 2% or 20 % oxygen tension with 5% CO_2. Subsequently, spheroids were either used for nanomechanical testing or fixed and processed for immunofluorescence.

Immunofluorescence analysis

Cell monolayers were grown on glass coverslips for 48 h, at 37°C in humidified air with 5% CO_2, fixed with formalin solution (Sigma Aldrich, Switzerland) for 15 min at RT, washed three times with modified Hanks' buffer times with modified Hank's buffer (MHB: Ca-free, containing 2 mM EGTA, 5 mM MES (2-morpholino-ethanesulfonic acid) and 0.005% NaN3, pH 6.2-6.4 (Baschong, Duerrenberger et al. 1999) and then incubated for 1hr with the primary antibody diluted in MHB. Spheroid samples were prepared as described above and fixed for 60 min with formalin solution (Sigma Aldrich, Switzerland), washed several times with MHB and incubated for 2hr with the primary antibody diluted in MHB. Primary antibodies were directed against Collagen I (1:50; rabbit polyclonal, Abacam), beta-tubulin (1:50; mouse monoclonal, Böhringer), fibronectin (1:100; rabbit polyclonal, Calbiochem), and vimentin-Cy3 (1:3000; Cy3 conjugated anti-vimentin mouse monoclonal, Sigma Aldrich, Switzerland). Subsequently, samples were washed twice with MHB and then incubated for 60 min with the corresponding secondary antibody. Secondary antibodies were Cy3-donkey anti-rabbit (1:3000; Jackson Immuno Research Lab), 488-donkey anti-mouse (1:800; Molecular Probes). Filamentous actin was detected with Alexafluor 488 phalloidin (1:400: Molecular probes, Eugene, OR) or 647-Phalloidin (1:200). Confocal images were recorded on SP5 laser scanning confocal microscope (Leica Microsystems, Germany) using a 20× objective. Identical imaging settings were chosen to allow for direct comparison of staining patterns. Digitized confocal images were processed with software from Leica, Imaris 4.1 (Bitplane AG) and Adobe Photoshop.

The nanomechanical AFM testing

For nanomechanical AFM testing, monolayers and spheroids were grown on WillCo glass bottom dishes (Intracell LTD, UK). All AFM experiments were carried out under physiological conditions at 37°C using commercial AFMs (Nanowizard I AFM, JPK Instruments, Germany) which was placed on an inverted microscope Zeiss Axiovert 135 TV (Zeiss, Germany) equipped with 10× and 20× objective. Bright field signals were monitored using a grayscale digital camera (ANDOR SOLIS CCD-375; ANDOR Technology, USA). For certain experiments involving cell monolayers, a Multimode AFM (Veeco Instruments, USA) was used. To compensate for evaporation from the AFM fluid cell and maintain physiological conditions, the culture medium was continuously exchanged during experiments. We used standard triangular silicon nitride cantilevers with a spring constant between 0.04-0.08 N/m and a nominal tip radius of 20 nm (DNP-S, Vecco probes, Veeco Instruments, USA). The experimental value for the spring constant of each cantilever was determined by thermal tune method (Sader, Larson et al. 1995). For cell stiffness measurements, the AFM was operated in the "Force-Volume Mode". Briefly, arrays of 64×64 or 16×16 force displacement curves were recorded in a regular grid over a selected cell or spheroid surface. Individual force displacement curves consisted of 512 sampling points. All indentations were applied with the maximum load set to 1 or 1.8 nN at scan rate of 10 µm/s. Analysis of force data was performed as described in Chapter 3.

Statistical analysis

All data are given as mean ± standard deviation (s.d.). Statistical significance was tested using a paired student's t-test in Origin 7.5 (OriginLab). Statistical significance was set at $P \leq 0.05$.

4.4 Results

Structural and nanomechanical characterization of Rat2WT and Rat2sm9 in 2D culture

The actin cytoskeleton is known to play an important role in cell mechanics as well as in transformation and tumor progression. Expression of a Gly245Asp actin mutant, which is polymerization deficient *in vitro* (Taniguchi, Sagara et al. 1988) in wild-type Rat2 fibroblasts (Rat2WT) yielded the tumorigenic derivative Rat2sm9 (Kakunaga, Hamada et al. 1982). In this study, we tested the effects of the Gly245Asp actin-related transformation on the nanomechanical properties of living Rat2WT and Rat2sm9 cells. When cultured as 2D monolayers the overall morphology of normal and transformed cells appeared very similar (Figure 1a) despite the expression of the mutant actin in Rat2sm9 cells (Figure 1b).

Next, we performed AFM imaging and testing under physiological conditions. The AFM images of living cells showed that Rat2sm9 appear slightly more elongated in comparison to Rat2WT (Figure 1c). However, the overall nanomechanical properties did not significantly differ between the two cells lines, with both exhibiting an average stiffness of 3.4 ± 1.1 kPa (n = 15) (Figure 1d).

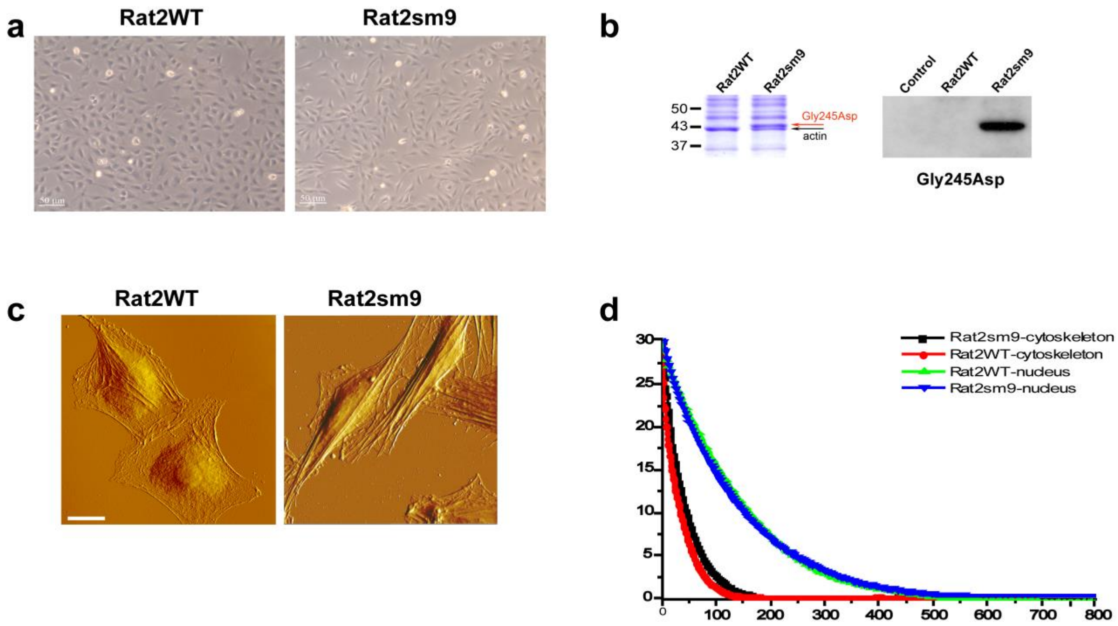

Figure 4-1. Rat2WT and Rat2sm9 cell features in 2D monolayer cultures. (a) Light microscopy reveals morphological appearance of Rat2WT (left panel) and Rat2sm9 (right panel) monolayers. Scale bars, 50 µm (b) Total protein extracts from Rat2WT and Rat2sm9 analysed on 12% SDS page cells (left panel). The band corresponding to the Gly245Asp mutant actin is only present in Rat2sm9. Immunoblot with an antiserum that specifically reacts with actin245Asp identifies transformed actin (right panel). (c) AFM images of living Rat2WT (left panel) and Rat2sm9 cells (right panel) cultured at low density on glass substrates. Scale bar, 10 µm. (d) Averaged force curves representing nanomechanical AFM testing of different areas of Rat2 and Rat2sm9 cells

The consequences of mutant actin expression on cytoarchitecture were examined by immunofluorescence. As illustrated in figure 2, only Rat2sm9 cells (Fig. 2a) expressed the mutant actin, whereas it was absent in Rat2WT (Figure 2a). High levels of Gly245Asp mutant actin clearly accumulated in the filopodia extensions of tumorigenic Rat2sm9. In these peripheral regions, the cell thickness is approximately 100 nm and thus, AFM measurements may reflect contributions from the underlying glass surface and/or the mutant actin.

To assess the changes in cytoarchitecture that are brought on by the tumorigenic transformation, we compared the F-actin, vimentin and microtubule staining pattern in Rat2WT and Rat2sm9 cells (Figure 2c and 2d, respectively). Immunofluorescence did not reveal any significant difference in the structural appearance of the F-actin (left panel), vimentin (middle panel) or microtubules (right panel) between Rat2WT (Figure 2c) and Rat2sm9 fibroblasts (Figure 2d). Consistently, the nanomechanical response of the two cell types was comparable in 2D cultures.

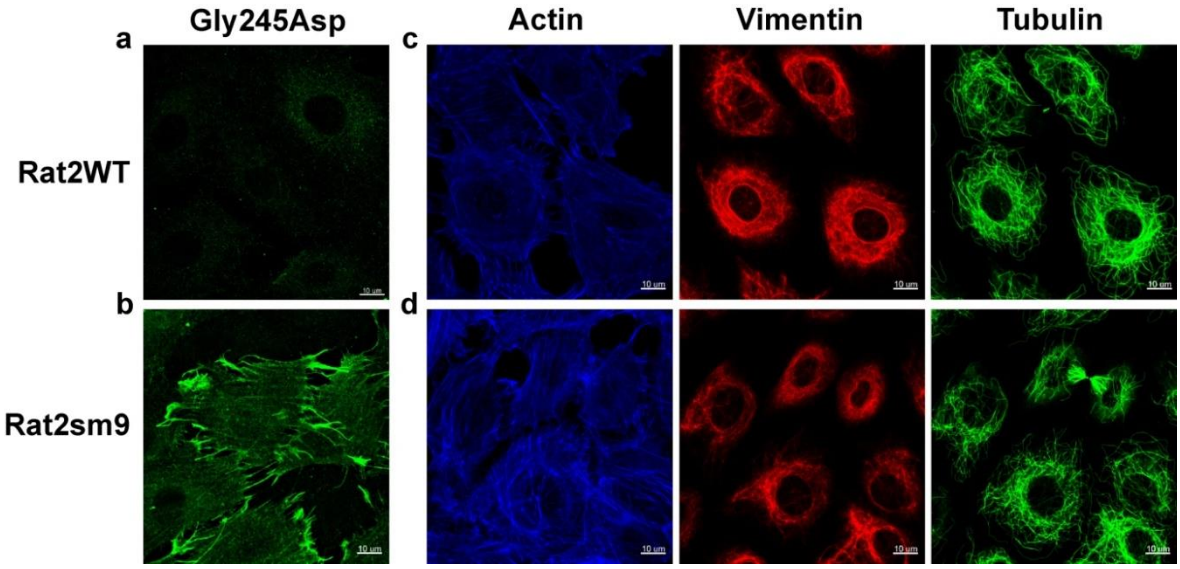

Figure 4-2. Cytoskeletal organization in Rat2WT and Rat2sm9 monolayers. (a, b) Immunolabeling with an antibody that specifically detects Gly245Asp mutant actin. The mutant actin is absent in Rat2WT, whereas Rat2sm9 filopodial extensions strongly express the mutant actin. (c, d) Alexafluor® 647-phalloidin reveals prominent actin stress fibers in Rat2wt and Rat2sm9. The fibroblast marker vimentin (red) forms a similar intermediate filament network in both cell lines. Likewise, tubulin staining (green) reveals comparable microtubule organization in normal and transformed cells. Scale bars, 10 µm.

The tumor-related actin mutation does not modify extracellular matrix (ECM) components in 2D cultures

To evaluate possible contributions of the ECM to malignant transformation (Paszek, Zahir et al. 2005) we tested 2D cultures of Rat2WT and Rat2sm9 for the expression of collagen I and fibronectin (Figure 3). Collagen I seemed to be absent in Rat2WT (Figure 3a, left panel) and in Rat2sm9 (Figure 3b, left panel). In contrast, fibronectin levels and structural appearance were similar in both cells types (Figure 3a and 3b, right panel). From these data we conclude that ECM components are inadequately synthesized and organized in 2D culture systems and thus are not suited for studying the contribution of ECM to cell stiffness.

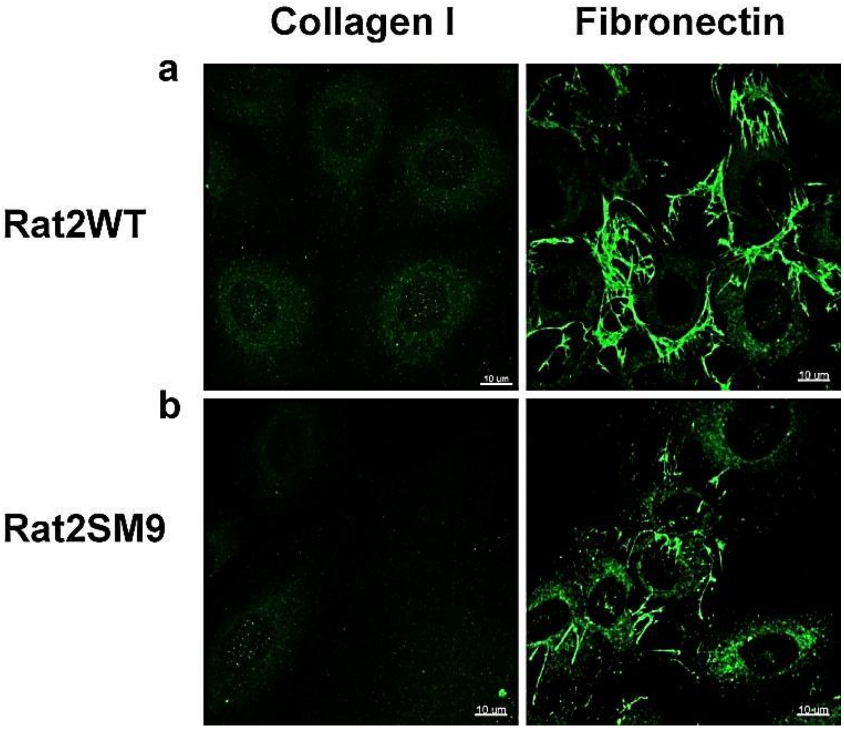

Figure 4-3. Immunofluorescent localization of key extracellular matrix components collagen I and fibronectin in Rat2WT and Rat2sm9 2D cultures. Collagen I synthesis cannot be detected by immunofluorescent labelling of Rat2WT (a, left panel) or Rat2sm9 (b, left panel) in 2D cultures. Fibronectin staining (right panels) of Rat2WT (a) and Rat2sm9 (b) monolayers shows discrete areas that correspond to intercellular spaces. Scale bars, 10 µm.

Morphology and nanomechanical properties of Rat2WT and Rat-2sm9 spheroids

To determine whether cell culture conditions affect the nanomechanical response of cells, we have seeded normal Rat2WT and tumorigenic Rat2sm9 in Poly (2-Hydroxyethyl methacrylate) (Poly-HEMA)-coated 96-well plates. Cells did not attach to Poly-HEMA, but formed a single regular spheroid per well within 24 hours (Figure 4a). At this stage each spheroid displayed a diameter of 400-500 µm. Because AFM is a tool that probes surface properties of immobilized samples, nanomechanical testing of spheroids required minimal sample adaptations. These included letting spheroids attach to a collagen-coated surface for immobilization and a horizontal cut that removes the top part so that the AFM probe gains access to inner (core) and outer (periphery) spheroid regions (Figure 4b).

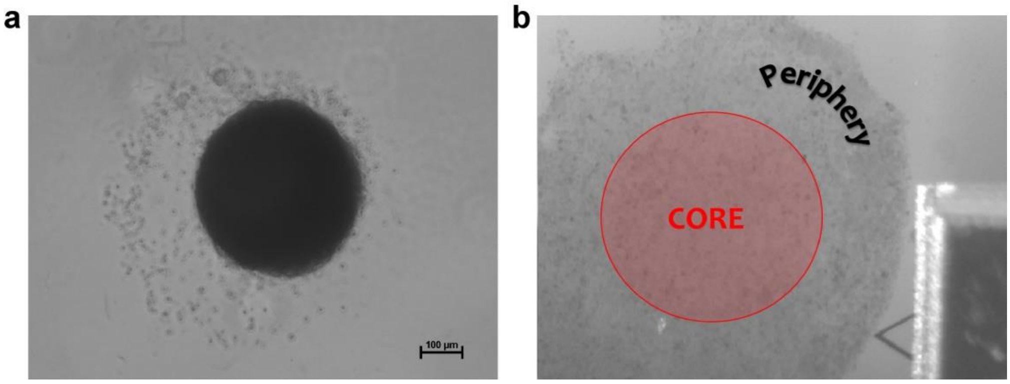

Figure 4-4. Rat2WT and Rat2sm9 form 3D spheroids. (a) Cells cultured on Poly-HEMA coated 96-well plates give rise to multicellular spheroids. At day3, a single spheroid of approximately 400µm in diameter is detected in each well. Scale bar, 100 µm. (b) If spheroids are horizontally cut in half, the AFM tip seen in the right hand corner, gains access to distinct areas throughout the spheroid , for example the core region.

After 3 days of culture, Rat2 spheroids exhibited a uniform morphology with continuous borders (Figure 5a, left panel) whereas tumor spheroids had a more oval appearance with a less regular surface (Figure 5b, left panel).

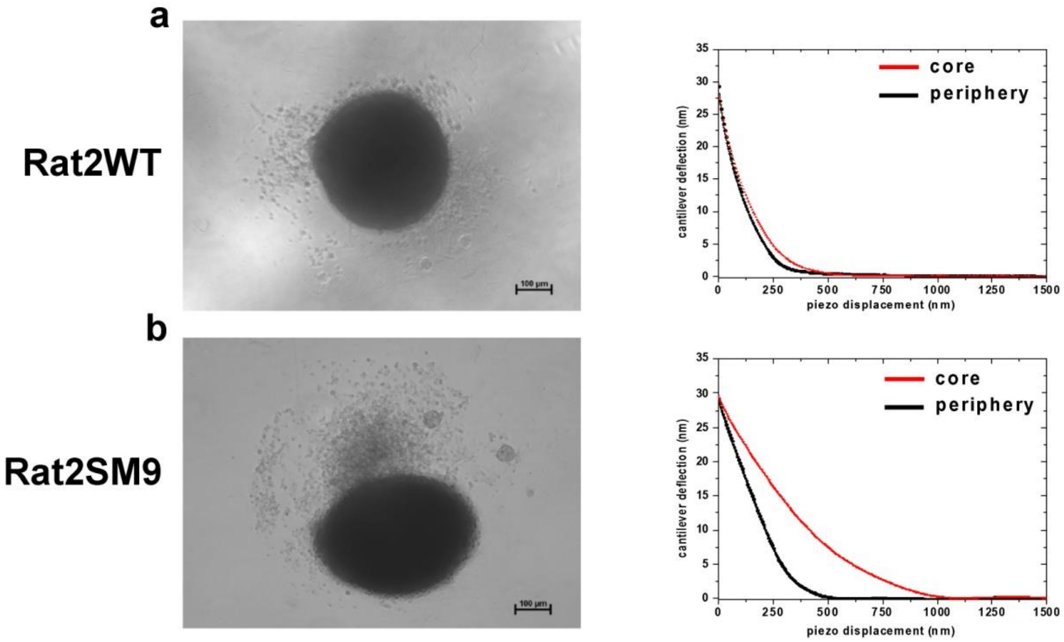

Figure 4-5. Nanomechanical properties of Rat2WT and Rat-2sm9 spheroids. (a, left panel) Optical image of Rat2 spheroid Scale bar, 100 µm. (a, right panel) Average AFM force curves representing stiffness in core and peripheral regions of Rat2 spheroids (b, left panel) Rat2sm9 spheroid exhibits oval shape (left panel). Scale bar, 100 µm. (b, right panel) Average AFM force curves (n=9) from core and peripheral regions of Rat2sm9 demonstrate centripetal softening from periphery to the core.Nanomechanical testing showed that Rat2WT spheroids exhibit similar stiffness E = 6.0 ± 1.3 kPa (n=7) over the entire spheroid cross-section (Figure 5a, right panel). In contrast, Rat2sm9 tumor spheroids showed incremental softening from the periphery with E = 6.7 ± 1.7 kPa to the core with E = 1.0 ± 0.4 kPa (n=9) (Figure 5b, right panel).

Unlike the AFM measurements on 2D cultures, which revealed a similar stiffness for Rat2WT and Rat2sm9, the nanomechanical response of spheroids was markedly different between normal and tumor spheroids.

The morphological indications of differential stiffness spheroids were stained with H&E. As shown in figure 6, spheroids exhibit a "tissue-like phenotype" where cells with nuclei stained in dark blue are surrounded by ECM stained in rose. No significant difference in the spheroid morphology was observed between Rat2WT (Figure 6a, left panel) and Rat2sm9 (Figure 6b, left panel). In addition, BrdU staining of nuclei indicated proliferation in Rat2WT (Figure 6a, right panel) and Rat2sm9 (Figure 6b, right panel) spheroids with virtually no sign of necrosis.

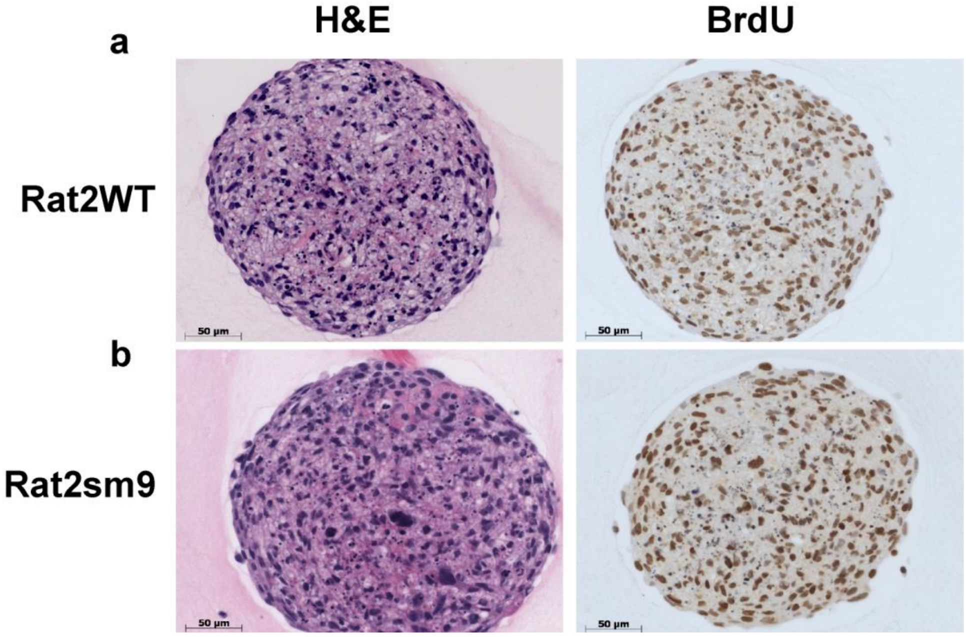

Figure 4-6. Histological phenotype of Rat2WT and Rat2sm9 spheroids (a) Light microscopy image of histological section representing Rat2WT spheroids stained with eosin and haematoxylin (left panel). Immunohistochemical staining of spheroid sections with the BrdU antibody indicates proliferation in all regions of Rat2WT spheroids. (b) The histological phenotype of Rat2sm9 spheroids (left panel) is similar to Rat2WT. BrdU uptake (right panel) reveals proliferating cells with larger nuclei than Rat2WT Scale bars, 50 µm.

Correlating spheroid cytoarchitecture with nanomechanical properties

We explored the effects of 3D culture on spheroid cytoarchitecture to determine whether centripetal softening observed in Rat2sm9 spheroids is associated with changes in the structural organization of the actin, vimentin and microtubule cytoskeleton. Rat2WT spheroids exhibited a rather homogeneous distribution of F-actin (Figure 7a, left panel), vimentin (middle panel) and microtubules (right panel). These findings are consistent with the homogeneous stiffness measured for Rat2WT spheroids. In contrast, Rat2sm9 spheroids, predominantly in the core region, exhibited less F-actin than normal spheroids (Figure 7b, left panel), which is in agreement with the inability of the mutant actin to polymerize. Furthermore, the actin cytoskeleton appeared less dense than in Rat2WT spheroids. Transformation-associated changes in the vimentin filament and microtubule organization were also most obvious in the core region of tumor spheroids (Figure 7b, middle and right panel respectively). The strongly perturbed cytoarchitecture in the core of Rat2sm9 spheroids correlate with the centripetal softening measured by AFM.

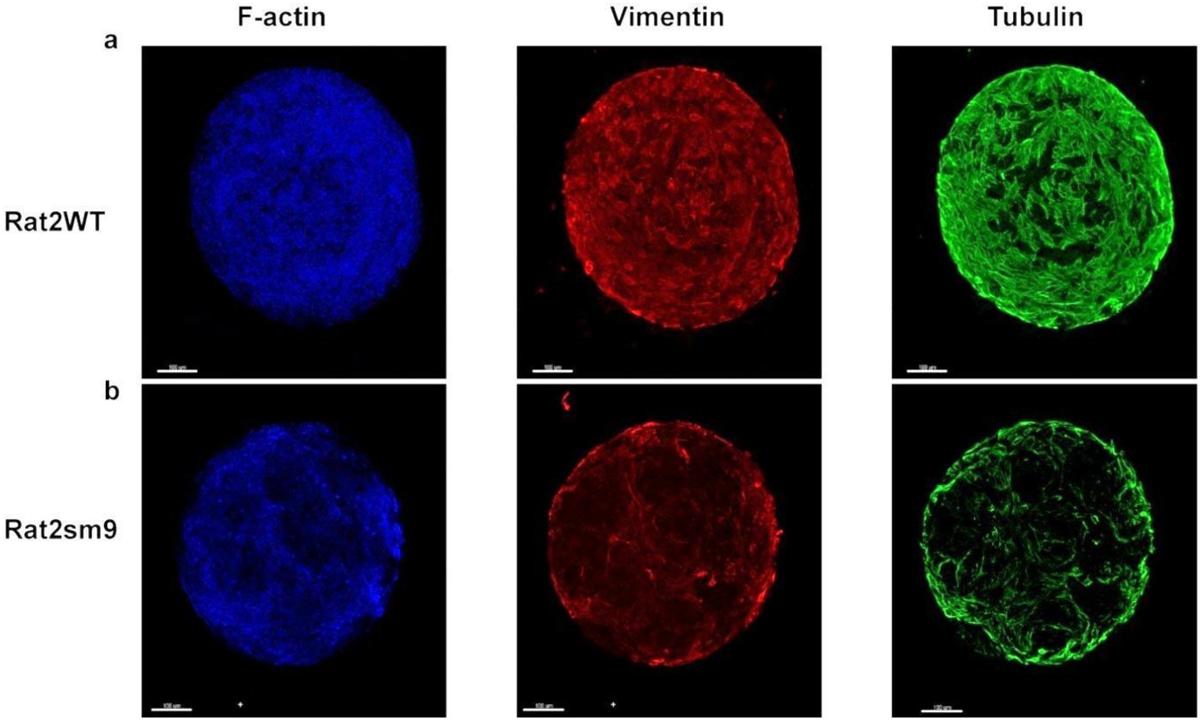

Figure 4-7. Cytoskeletal architecture of Rat2WT and Rat2sm9 spheroids. (a) Confocal sections of Rat2WT spheroids showing phalloidin-stained F-actin network (left panel), the intermediate filament network stained with a vimentin antibody (middle panel), and tubulin labelling (right panel). The staining pattern for the three cytoskeletal systems is quite regular in normal spheroids. (b) In Rat2sm9 spheroids, core regions exhibit less dense staining patterns for actin, vimentin, and tubulin. Scale bars, 100 µm.

Contribution of the ECM to nanomechanical properties of Rat2WT and Rat2sm9 spheroids

One advantage of 3D spheroid cultures is that cells are able to produce their own specific extracellular matrix (Bolli, Ghosh et al. 2005). Therefore, we examined whether the structural features of the ECM are different in normal versus Rat2sm9 spheroids. The expression and organization of fibronectin in the ECM seems to be similar in Rat2WT and Rat2ms9 of (Figure 8a and Figure 8b, left panels respectively). However, collagen I assembled a dense fibrous meshwork in Rat2WT spheroids of (Figure 8a, right panel) while in Rat2sm9 spheroids we observed significantly less fibrous collagen. The significance of the conspicuous ring-like structure that lines a central area lacking collagen fibers is unclear (Figure 8b, right panel). Conclusively, collagen I that significantly contributes to tissue stiffness (Wolf, Alexander et al. 2009) seems to be degraded and reduced in the core of tumor spheroids. It is conceivable that this altered collagen structure contributes to the decrease in stiffness that we observed in the core of Rat2sm9 spheroids.

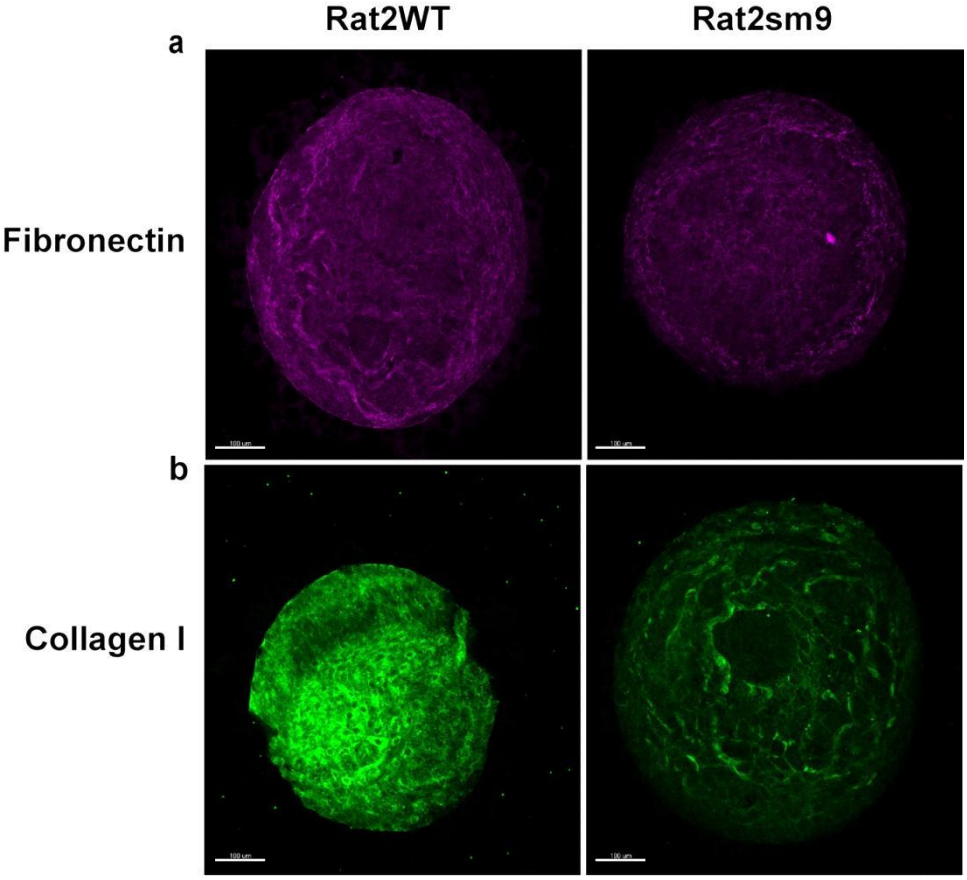

Figure 4-8. Immunostaining of collagen I and fibronectin in spheroids. (a) Rat2WT spheroids show regular, dense fibrillar fibronectin staining (left panel). The collagen I antibody reveals fibril-like structures (right panel). (b) In Rat2sm9, fibronectin staining is (left panel) homogeneous throughout the spheroid. Fibril-like collagen structures (right panel) occur at the periphery, whereas the core shows a more fine disperse collagen I staining. Scale bars, 100 µm.

Hypoxia induces changes in the morphology and nanomechanics properties of tumorigenic Rat-2sm9 spheroids

To determine if the hypoxia differentially alters structural and nanomechanical properties of tumor spheroids we have grown Rat2WT and Rat2sm9 spheroids under hypoxic (2% oxygen tension) conditions. At the light microscopic level, the morphology of Rat2WT spheroids appeared slightly more oval after 3 day of hypoxic culture conditions (Figure 9a, left panel) similar to Rat2sm9 under normoxic conditions (Figure 6b, left panel).

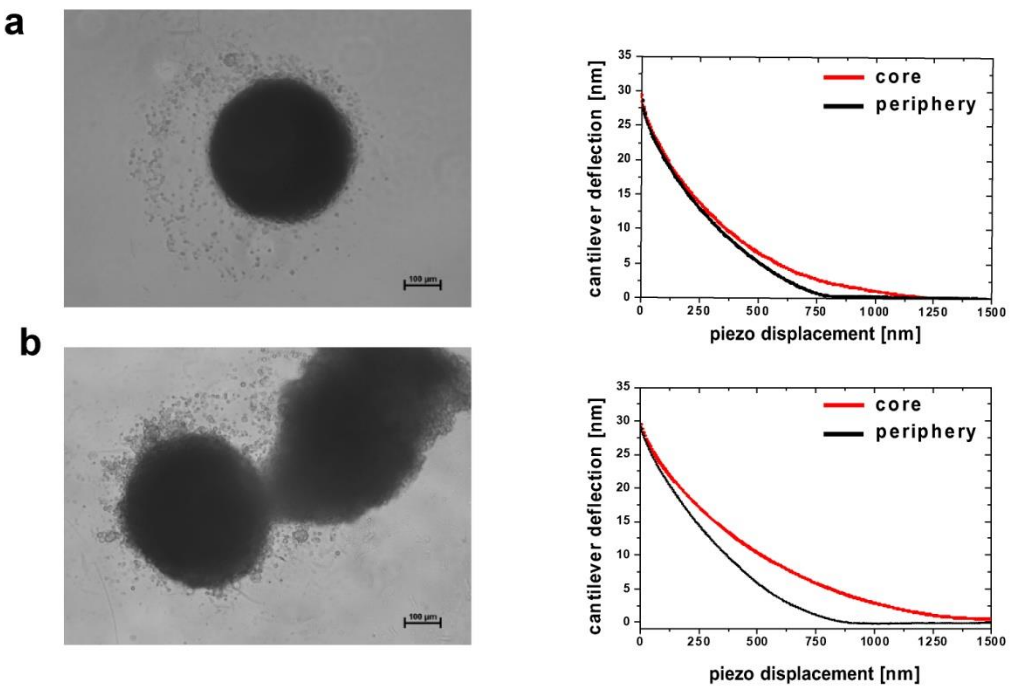

Figure 4-9. Hypoxia alters spheroid morphology and nanomechanical properties. (a) Morphology of hypoxic Rat2WT spheroids (left panel) Scale bar, 100 µm. Average force curves (n=5) reveal comparable stiffness in the periphery and core of the normal spheroid. (b) Under hypoxic conditions, Rat2sm9 forms large satellite structures in addition to the primary spheroid (left panel). Average force curves (n=5) reveal a distinct softening of the core compared to the periphery (right panel). Tumor spheroids are overall softer than Rat2sm9.

Nanomechanical testing of spheroids grown under hypoxic conditions again showed a quite uniform stiffness throughout the spheroid cross-section of E = 2.3 ± 0.4 kPa (n=5). However, the overall stiffness decreased in comparison to E = 6.0 ± 1.3 kPa normoxic conditions (Figure 9a, right panel). In Rat2sm9 spheroids, hypoxia typically induced with the appearance of a satellite spheroid that was disseminating from the primary spheroid (Figure 9b, left panel). Primary Rat2sm9 tumor spheroids exhibited an overall decrease in stiffness but the centripetal softening found under normoxic conditions remained (Figure 9b, right panel). The stiffness decreased from E=1.4 ± 0.2 kPa (n=5) measured at the periphery of spheroids to E=0.5±0.4 kPa (n=5) in the core.

To examine in detail viability and morphology throughout hypoxic spheroids, we performed H&E staining of paraffin sections (Figure 10). Images revealed dead cells to be randomly distributed in Rat2WT spheroids (Figure 10a, left panel). This most likely reflects the inability of normal cells to adapt to the stressful microenvironment. H&E staining of the Rat2sm9 spheroids showed increased necrosis in the center of the primary spheroid but (Figure 10b, left panel) not the satellite (inset). BrdU staining indicated proliferating cells at one rim in Rat2WT spheroids and an increase in dead cells compared to normoxic conditions (Figure 10a, right panel). In Rat2sm9 primary spheroids, cells surrounding the central necrosis were proliferating (Figure 10b, right panel). Interestingly, proliferation occurred in all regions of satellite spheroids (inset).

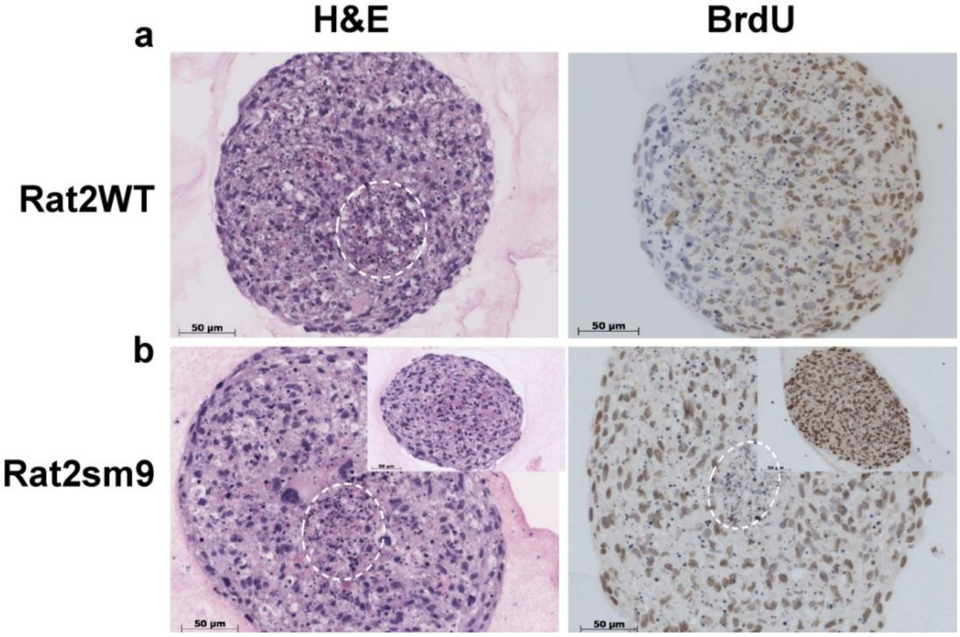

Figure 4-10. Histological analysis of spheroid morphology under hypoxic conditions. (a) H&E staining reveals hypoxia-induced of cell death in Rat2WT (left panel). BrdU staining (brown) indicates decrease in cell proliferation within the hypoxic spheroid (right panel). (b) H&E shows central necrosis in Rat2sm9 spheroid (left panel). The tissue morphology of the satellite spheroid (inset) is indistinguishable. BrdU incorporation (right panel) is excluded from the center in the primary tumor spheroid but not in the satellite. Scale bars, 50 µm..

Hypoxia-induced changes in the cytoskeleton correlate to spheroid softening

Hypoxic Rat2WT spheroids exhibited an organized cytoarchitecture with regular patterns of microfilaments (Figure 11a, left panel), intermediate filaments (Figure 11a, middle panel) and microtubules (Figure 11a, right panel), consistent with a homogeneous nanomechanical response. However, the overall decrease in stiffness remains unaccounted for. In contrast, in Rat2sm9 spheroids F-actin structures were conspicuously missing both in the core and satellites (Figure 11b, left panel). Vimentin structures (Figure 11b, middle panel) and to lesser extent microtubules, were similarly affected by hypoxia (Figure 11b, right panel). These findings indicate that hypoxic conditions cause a severe disorganization of the cytoskeleton, and thereby promote tissue softening.

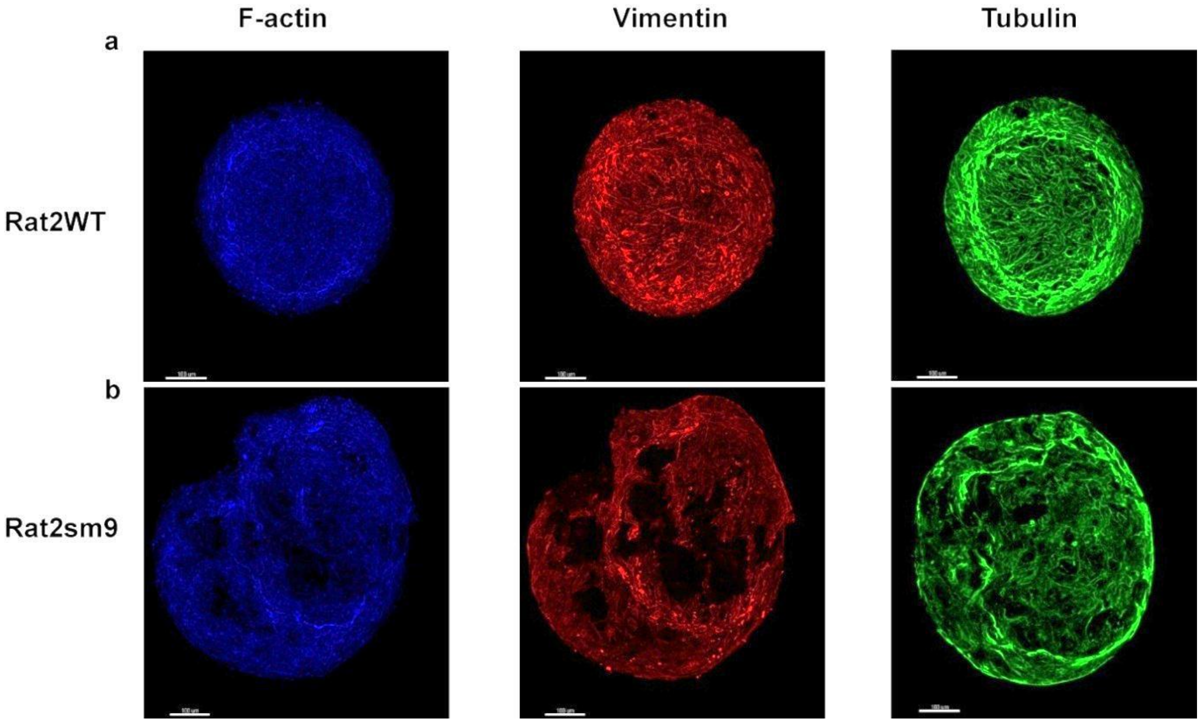

Figure 4-11. Hypoxia-induced reorganization of the cytoskeleton (a) Confocal section showing the phalloidin-stained F-actin network (left panel), the vimentin-positive intermediate filaments (middle panel), and microtubles (right panel). Overall cytoarchitecture appears compact within normal spheroids. (b) The cytoskeleton in hypoxic Rat2sm9 spheroids appears less compact and disorganized. The core region exhibits a loss of cytoskeletal structure. Scale bars, 100 µm.

To determine whether the protein levels of cytoskeletal actin and vimentin in spheroids were influenced by hypoxic conditions, we quantitatively analyzed total protein extracts from normoxic and hypoxic Rat2WT and Rat2sm9 spheroids by immunobloting (Figure 12). Biochemical analysis revealed that expression levels of actin and vimentin normalized against tubulin were not significantly different in normoxic versus hypoxic Rat2WT and Rat2sm9 spheroids, respectively. Conclusively, data substantiate that regional structural differences are a key cause centripetal softening of tumorigenic spheroids.

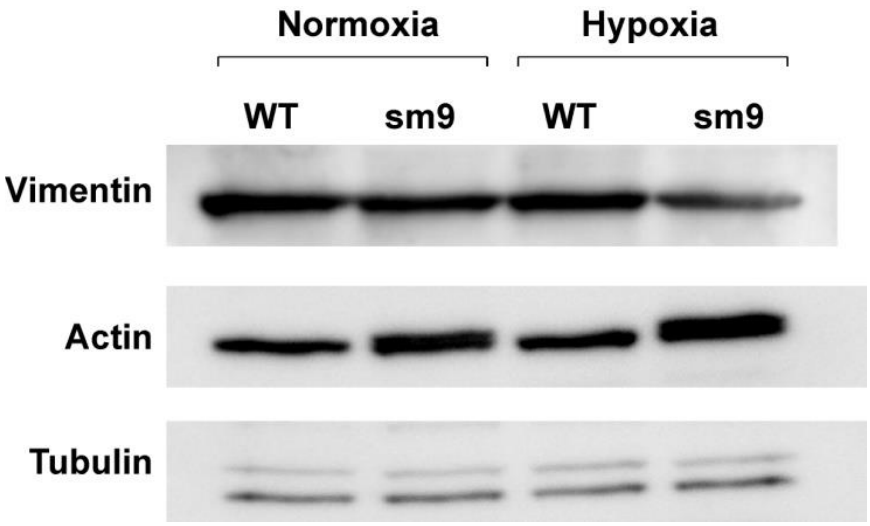

Figure 4-12. Biochemical analysis of spheroid cytoskeleton components in normoxia and hypoxia. Total protein extracts from Rat2WT and Rat2sm9 under normoxic and hypoxic conditions respectively, analysed on 12% SDS page cells, immunoblotted with specific antibody against actin and vimentin and normalized against tubulin.

Hypoxia differentially alters structure and expression of ECM components in spheroids

We explored the relationship between hypoxia and changes in the ECM with respect to tumorigenic transformation by immunohistochemistry. Confocal images revealed that spheroids exhibit distinct fibronectin and collagen I patterns (Figure 13). Remarkably, in the core of Rat2sm9 tumor spheroids, we observed a significant degradation of the collagen structure (Figure 13b, right panel) and possibly a reduced fibronectin signal (Figure 13b, left panel). Taken together these data indicate that controlled hypoxia has a much greater impact on the ECM structure in tumor spheroids than in normal spheroids.

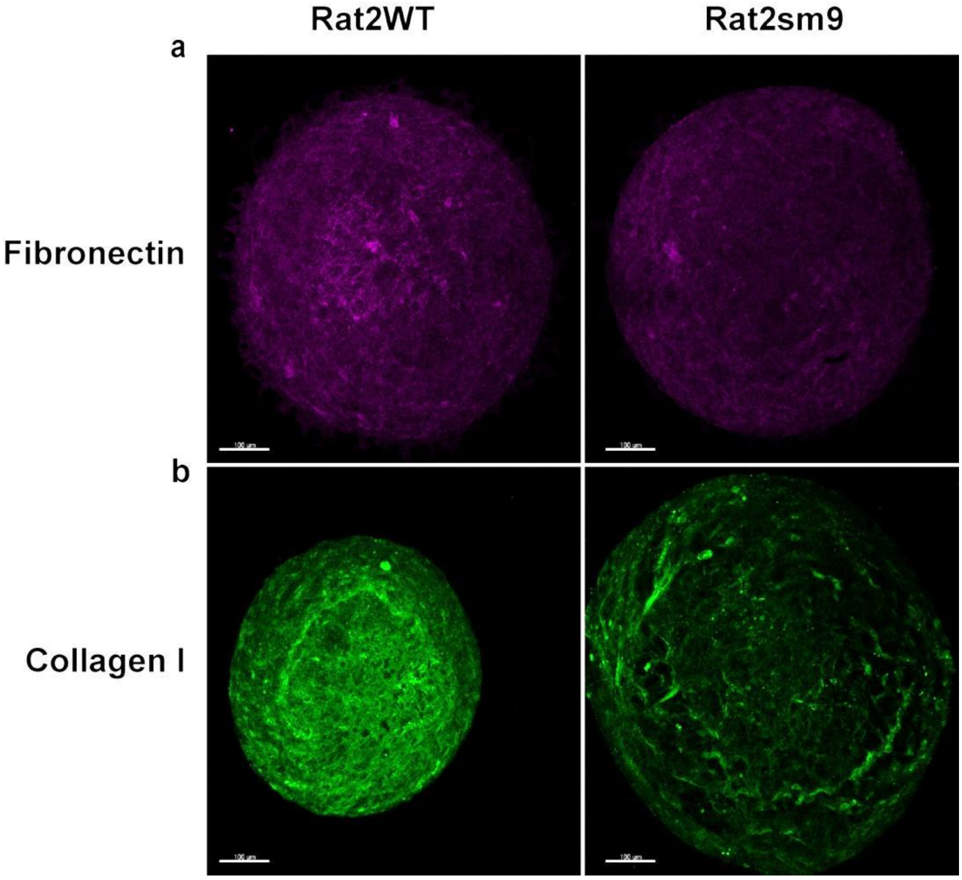

Figure 4-13. ECM components of RatWT and Rat2sm9 spheroids respond differentially to hypoxia (a) Confocal projection images demonstrate uniform pattern (magenta, left panel) and uniform fibrillar pattern for collagen I (green, right panel). (b) In contrast Rat2sm9 spheroids exhibit overall decrease in fibronectin (magenta, left panel) and degradation of collagen I localized in the large inner area (green, right panel) Scale bars, 100 µm.

Correlation of HIF-1α with actin and collagen I in spheroids in normoxic versus hypoxic conditions

Hypoxia regulated HIF-1α signaling involves downstream rearrangement of the actin cytoskeleton (Aitken, Tolg et al. 2010) and collagen remodeling (Erler and Weaver 2009). To provide further evidence that hypoxia-induced signaling cascades eventually lead to a softening of tumor spheroids via changes in the cytoskeleton and ECM, we investigated the expression of HIF-1α transcription factor in Rat2sm9 spheroids (Figure 14). Under normoxic conditions HIF-1α was localized to distinct structures around the core region (Figure 14a), whereas under hypoxic conditions, HIF-1α staining increased and extended over a broader area (Figure 14b). These data are consistent with the increased softening of tumor spheroids under hypoxia, particularly the pronounced softening of the extended core region that mostly consists of hypoxic cells.

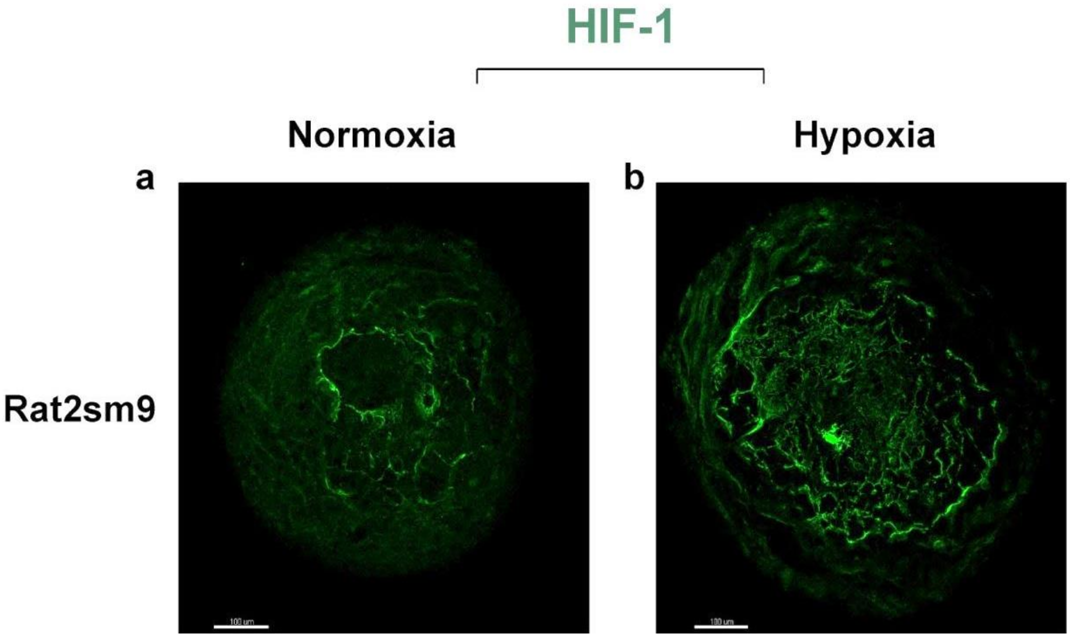

Figure 4-14. Hypoxic conditions induce HIF-1α expression in Rat2sm9 spheroids. (a) Under normoxic conditions, Rat2sm9 spheroid express HIF-1α in a ring-like pattern around the center. (b) Hypoxic conditions strongly increase HIF-1α expression, predominantly in the inner region of the spheroid. Scale bar, 100 µm.

4.5 Discussion

The mechanical behavior of a single cell is governed by the constituency of its cytoskeleton (Heidemann and Wirtz 2004), integrins that connect the cytoskeleton with the ECM (Baker, Lu et al. 2010) and the forces exerted on a cell by the surrounding ECM (Paszek and Weaver 2004). Increasingly cancer cells are becoming the focus of studies that explore the effect of the extracellular environment on cellular homeostasis (Paszek, Zahir et al. 2005; Baker, Bonnecaze et al. 2009; Tilghman, Cowan et al. 2010) and cellular viscoelasticity (Cross, Jin et al. 2008; Hou, Li et al. 2009; Cai, Xing et al. 2010). While significant progress has been made in discovering the molecular mechanisms and signaling pathways that underline cancer development and progression, much less is known about associated mechanical properties. It has long been established that cancerous tissue exhibits elevated stiffness compared to healthy tissues (Paszek, Zahir et al. 2005), while stiffness of individual cells with high metastatic potential significantly decreases in comparison to normal ones (Cross, Jin et al. 2007). However, the relationship between the cell and tissue microenvironmental conditions and cell mechanics has not been systematically investigated. In order to investigate the interplay between the microenvironmental conditions and cell mechanics we have utilized

AFM to measure nanomechanical response of living rat fibroblasts in monolayer (2D) and tissue (3D) culturing conditions. The transformed fibroblasts (Rat2sm9) exhibited mutation in the actin gene which is disabling actin polymerization and renders them tumorigenic (Leavitt, Ng et al. 1987). Moreover they are directly derived from the Rat2WT parental cell line and thus can be directly compared. In the first part of the study we have focused on comparing the nanomechanical properties of individual normal and cancer cells and correlating them with the cell cytoarchitecture. To our surprise obtained data have shown no difference in the nanomechanical properties between the mutant Rat2sm9 and normal Rat2WT cells (Figure 1d) although both biochemical and immunofluorescence data confirmed the presence of the mutant actin in Rat2sm9 cells (Figure 2b). Results were particularly surprising since it has been shown that cytoskeleton reorganization and in particular the actin microfilaments play a crucial role in cell proliferation, migration and viscoelastic properties during malignant transformation and progression ((Decloitre, Cassingena et al. 1991; Lamarche, Tapon et al. 1996; Lozano, Betson et al. 2003; Suresh 2007). However in most of these studies the measured normal versus cells were not of the same origin, therefore the direct comparison of was impossible. This was the advantage in our system because the origin of tumor cells was well known and they could have been directly compared to the wild-type counterpart. Our data suggest that a specific mutation alone, even in the cell cytoskeleton is not enough to alter nanomechanical behaviour of cells with respect to malignant transformation. Obtained results imply that most likely additional factors such as microenvironmental conditions and ECM that are not utilized in a 2D culture might play a significant role in altered mechanical properties of tumor cells.

To investigate the effect of microenvironmental conditions on cell mechanical properties, we established an *in vitro* 3D tumor spheroid model that exhibits microenvironmental conditions representative of tumors *in vivo* (Hirschhaeuser, Menne et al. 2010) and allowed us to study nanomechanical properties of tumor cells in physiologically relevant system. Nanomechanical data have shown that Rat2sm9 spheroids exhibit distinct centripetal softening from periphery to the central core in comparison to Rat2WT spheroids that exhibited homogeneous stiffness over the entire spheroid surface (Figure 6). Accordingly the structural examination of actin, vimentin and microtubule cytoarchitecture has shown that Rat2sm9 spheroids exhibit altered cytoarchitecture with respect to the WT spheroids and are less compact. Our data suggest that softening found in tumor spheroids, alterations in cell cytoskeleton and loss of compactness might be associated with the tendency of cells to disseminate from the primary tumor and more easily invade surrounding tissues (Suresh 2007) most likely through cooperative interactions with the surrounding ECM.

ECM structure and organization are considered as key players in determining the malignant progression (Levental, Yu et al. 2009). The same study determined that collagen stiffening and increase in cross-linked fibrillar collagen in 3D tumor cultures determines tumor stiffening thereby forcing tumor progression. In contrast, observed inhomogeneity in collagen and lack of structured organisation in our tumor spheroid model supports the measured softening. Conversely, this data alone do not provide explanation to what has actually caused the cytoskeleton and ECM structural irregularities and lack of compactness in center of tumor spheroids. Initially we considered that central necrosis often found in avascular 3D spheroids exhibiting sizes between 400-500 µm (Groebe and MuellerKlieser 1996) might account for this behaviour. However, histology and BrdU data demonstrated that neither tumor nor normal spheroids display signs of necrosis and exhibit high viability and proliferation of cells within spheroids (Figure 6). On the other hand, it is well know that tumor spheroids over time in culture start to exhibit pathophysiological gradients, lacking oxygen and nutrients in inner regions comparable to the situation in avascular primary tumors and micrometastases (MuellerKlieser 1997; Friedrich, Seidel et al. 2009). It has been shown recently in spheroids that pathophysiological gradients can alter mechanical compression inserted by tumor cells on their surroundings while changing their shape from round to more oval at the sites of higher compression (Cheng, Tse et al. 2009). Accordingly, the tumor spheroids examined here exhibited more oval shape at the periphery when compared to the WT spheroids. This would suggest that cells from the inner spheroid regions under stressful microenvironmental conditions acquire aggressive phenotype and by exerting compressive forces on the periphery try to escape the primary tumor. Also, emerging evidences suggest that hypoxic cells from inner tumor regions tend to acquire metastatic character and resistance to cancer therapy (Teicher 1994; Sullivan and Graham 2007). Taken together, our data suggest oxygen gradient as a possible factor that might profoundly alter complex 3D network of cell-cell and cell-ECM interactions hence inducing central softening in tumor spheroids.

Because of the possibility to culture spheroids under controlled hypoxic conditions (2 % oxygen), we were able to examine systematically the effects of hypoxia on nanomechanical response of spheroid cultures. We have found that under hypoxic conditions both normal and tumor spheroids exhibit significant decrease in stiffness, however tumor spheroids maintained the centripetal softening pattern (Figure 9). In agreement with previous findings our results further demonstrate that hypoxia drastically influences tumor growth and proliferation since tumor spheroid under hypoxia have shown complete loss of compactness and massive dissemination into satellite structures. These observations strengthen our previous findings and indicate that the decreased regional stiffness concomitant with increased tumor dissemination during hypoxia might be mediated by hypoxia induced cytoskeleton (Cannito, Novo et al. 2010) and ECM remodelling (Noel, Jost et al. 2008). Consistent with this, we noted significantly less actin and vimentin structures within tumor spheroids associated with decreased density (Figure 11) and altered collagen and fibronectin in the central region in comparison to normoxic conditions and WT spheroids (Figure 13). Furthermore, adapting to the hypoxic microenvironment is predominantly achieved by activation of the HIF-1 signalling pathway (Semenza 2002). More specifically HIF-1α which is maintained at low levels in most cells under normoxic conditions and it is known to be upregulated in tumors where it controls the proliferation, migration and ECM remodelling (Favaro, Nardo et al. 2008). Therefore, we compared the expression and spatial distribution of HIF-1α transcription factor in tumor spheroids under normoxic and hypoxic conditions. Immunofluorescence data demonstrated localized distinct expression of HIF-1 α in the core region of the spheroid under normoxic conditions and increase in the distribution and expression under hypoxic conditions in Rat2sm9 spheroids (Figure 14). Results were consistent with observed the central softening and increased cell dissemination of tumor cells. Thus, we propose that regional variations in oxygen concentrations initiate cellular adaptations and nanomechanical changes necessary for emergence of cancer cell invasion.

4.6 Conclusions

We have developed an AFM based nanomechanical analysis to analyze individual cells and 3D culture models. To our knowledge, this is a first study that reports on data obtained on 3D avascular spheroid models in order to examine the effect of tumorigenesis on nanomechanical properties of early tumors. Our data have demonstrated that in monolayer cultures both normal and corresponding tumor fibroblasts exhibited similar nanomechanical properties. In contrast, in 3D cultures WT and tumor spheroids showed distinct nanomechanical responses. Rat2WT spheroids revealed similar stiffness throughout the spheroid corresponding to homogeneous, dense cytoarchitecture and ECM distribution, whereas tumor spheroids exhibited centripetal softening from the periphery to the core associated with cytoskeleton and matrix heterogeneity. Importantly our data have point towards hypoxia as a key factor in regulating the nanomechanical response of tumor spheroids. Experiments performed on spheroids cultured under hypoxic conditions imply that cytoskeleton and collagen degradation conducive with central softening in tumor spheroids is endorsed by hypoxia. Whereas hypoxia undoubtedly induces tumor cell invasion and metastasis, at this stage we do not know the exact mechanism by which HIF-1 pathway regulates this processes thereby modifying nanomechanical responses within tumor tissue, therefore in our future experiments we want to address this issue. Also in terms of collagen degradation, it has been shown that hypoxic conditions increase the expression and activity of MMP-1,3,14 in cancer cells (Egeblad and Werb 2002; Kondo, Kubota et al. 2002; Cha, Ahn et al. 2003; Kan, Abe et al. 2003). Correlation of the HIF-1 α expression and the proteolytic activity of MMPs might provide explanation for observed regional differences in collagen structure in tumor spheroids that were correlated to hypoxia.

4.7 Acknowledgments

The authors thank Surabh Ghosh for helpful advices on spheroid culture, Francine Wolf for the technical support with histology and oxygen controlled incubators, Marko Loparic, Ivan Martin and Giulio Spagnioli for helpful discussions regarding the project.

4.8 References

Aitken, K. J., C. Tolg, et al. (2010). "Mammalian Target of Rapamycin (mTOR) Induces Proliferation and De-Differentiation Responses to Three Coordinate Pathophysiologic Stimuli (Mechanical Strain, Hypoxia, and Extracellular Matrix Remodeling) in Rat Bladder Smooth Muscle." American Journal of Pathology **176**(1): 304-319.

Allinen, M., R. Beroukhim, et al. (2004). "Molecular characterization of the tumor microenvironment in breast cancer." Cancer Cell **6**(1): 17-32.

Baker, E. L., R. T. Bonnecaze, et al. (2009). "Extracellular Matrix Stiffness and Architecture Govern Intracellular Rheology in Cancer." Biophysical Journal **97**(4): 1013-1021.

Baker, E. L., J. Lu, et al. (2010). "Cancer Cell Stiffness: Integrated Roles of Three-Dimensional Matrix Stiffness and Transforming Potential." Biophysical Journal **99**(7): 2048-2057.

Barcellos-Hoff, M. H. and S. A. Ravani (2000). "Irradiated mammary gland stroma promotes the expression of tumorigenic potential by unirradiated epithelial cells." Cancer Research **60**(5): 1254-1260.

Baschong, W., M. Duerrenberger, et al. (1999). "Three-dimensional visualization of cytoskeleton by confocal laser scanning microscopy." Confocal Microscopy **307**: 173-189.

Bolli, M. K., S. Ghosh, et al. (2005). "Culture of melanoma cells in three-dimensional architectures results in impaired immunorecognition by cytotoxic T lymphocytes specific for Melan-A/MART-1 tumor associated antigen." Journal of the American College of Surgeons **201**(3): S79-S79.

Burdelya, L. G., E. A. Komarova, et al. (2006). "Inhibition of p53 response in tumor stroma improves efficacy of anticancer treatment by increasing antiangiogenic effects of chemotherapy and radiotherapy in mice." Cancer Research **66**(19): 9356-9361.

Cai, X. F., X. B. Xing, et al. (2010). "Connection between biomechanics and cytoskeleton structure of lymphocyte and Jurkat cells: An AFM study." Micron **41**(3): 257-262.

Cannito, S., E. Novo, et al. (2010). "Epithelial-Mesenchymal Transition: From Molecular Mechanisms, Redox Regulation to Implications in Human Health and Disease." Antioxidants & Redox Signaling **12**(12): 1383-1430.

Casciari, J. J., S. V. Sotirchos, et al. (1992). "Variations in Tumor-Cell Growth-Rates and Metabolism with Oxygen Concentration, Glucose-Concentration, and Extracellular Ph." Journal of Cellular Physiology **151**(2): 386-394.

Cha, H. S., K. S. Ahn, et al. (2003). "Influence of hypoxia on the expression of matrix metalloproteinase-1,-3 and tissue inhibitor of metalloproteinase-1 in rheumatoid synovial fibroblasts." Clinical and Experimental Rheumatology **21**(5): 593-598.

Cheng, G., J. Tse, et al. (2009). "Micro-Environmental Mechanical Stress Controls Tumor Spheroid Size and Morphology by Suppressing Proliferation and Inducing Apoptosis in Cancer Cells." Plos One **4**(2): -.

Cross, S. E., Y. S. Jin, et al. (2007). "Nanomechanical analysis of cells from cancer patients." Nature Nanotechnology **2**(12): 780-783.

Cross, S. E., Y. S. Jin, et al. (2008). "AFM-based analysis of human metastatic cancer cells." Nanotechnology **19**(38): -.

Dang, C. V. and G. L. Semenza (1999). "Oncogenic alterations of metabolism." Trends in Biochemical Sciences **24**(2): 68-72.

Decloitre, F., R. Cassingena, et al. (1991). "Concomitant Alterations of Microfilaments and Microtubules in Human Epithelial-Cells (Hbl-100) in Relation to Their Malignant Conversion." Tumor Biology **12**(2): 111-119.

Egeblad, M. and Z. Werb (2002). "New functions for the matrix metalloproteinases in cancer progression." Nature Reviews Cancer **2**(3): 161-174.

Erler, J. T. and A. J. Giaccia (2006). "Lysyl oxidase mediates hypoxic control of metastasis." Cancer Research **66**(21): 10238-10241.

Erler, J. T. and V. M. Weaver (2009). "Three-dimensional context regulation of metastasis." Clinical & Experimental Metastasis **26**(1): 35-49.

Favaro, E., G. Nardo, et al. (2008). "Hypoxia inducible factor-1 alpha inactivation unveils a link between tumor cell metabolism and hypoxia-induced cell death." American Journal of Pathology **173**(4): 1186-1201.

Feder-Mengus, C., S. Ghosh, et al. (2008). "New dimensions in tumor immunology: what does 3D culture reveal?" Trends in Molecular Medicine **14**(8): 333-340.

Feder-Mengus, C., S. Ghosh, et al. (2007). "Multiple mechanisms underlie defective recognition of melanoma cells cultured in three-dimensional architectures by antigen-specific cytotoxic T lymphocytes." British Journal of Cancer **96**(7): 1072-1082.

Folkman, J. and A. Moscona (1978). "Role of Cell-Shape in Growth-Control." Nature **273**(5661): 345-349.

Friedrich, J., C. Seidel, et al. (2009). "Spheroid-based drug screen: considerations and practical approach." Nature Protocols **4**(3): 309-324.

Ghosh, S., G. C. Spagnoli, et al. (2005). "Three-dimensional culture of melanoma cells profoundly affects gene expression profile: A high density oligonucleotide array study." Journal of Cellular Physiology **204**(2): 522-531.

Groebe, K. and W. MuellerKlieser (1996). "On the relation between size of necrosis and diameter of tumor spheroids." International Journal of Radiation Oncology Biology Physics **34**(2): 395-401.

Heidemann, S. R. and D. Wirtz (2004). "Towards a regional approach to cell mechanics." Trends in Cell Biology **14**(4): 160-166.

Hirschhaeuser, F., H. Menne, et al. (2010). "Multicellular tumor spheroids: An underestimated tool is catching up again." Journal of Biotechnology **148**(1): 3-15.

Hou, H. W., Q. S. Li, et al. (2009). "Deformability study of breast cancer cells using microfluidics." Biomedical Microdevices **11**(3): 557-564.

Hu, Z. Y., C. Fan, et al. (2009). "A compact VEGF signature associated with distant metastases and poor outcomes." Bmc Medicine **7**: -.

Kakunaga, T., H. Hamada, et al. (1982). "A Point Mutation in Actin Gene and Transformation of Human-Cells." Proceedings of the American Association for Cancer Research **23**(Mar): 75-75.

Kan, C., M. Abe, et al. (2003). "Hypoxia-induced increase of matrix metalloproteinase-1 synthesis is not restored by reoxygenation in a three-dimensional culture of human dermal fibroblasts." Journal of Dermatological Science **32**(1): 75-82.

Klaunig, J. E. and L. M. Kamendulis (2004). "The role of oxidative stress in carcinogenesis." Annual Review of Pharmacology and Toxicology **44**: 239-267.

Kondo, S., S. Kubota, et al. (2002). "Connective tissue growth factor increased by hypoxia may initiate angiogenesis in collaboration with matrix metalloproteinases." Carcinogenesis **23**(5): 769-776.

Kumar, S. and V. Weaver (2009). "Mechanics, malignancy, and metastasis: The force journey of a tumor cell." Cancer and Metastasis Reviews **28**(1-2): 113-127.

Lamarche, N., N. Tapon, et al. (1996). "Rac and Cdc42 induce actin polymerization and G1 cell cycle progression independently of p65(PAK) and the JNK/SAPK MAP kinase cascade." Cell **87**(3): 519-529.

Levental, K. R., H. M. Yu, et al. (2009). "Matrix Crosslinking Forces Tumor Progression by Enhancing Integrin Signaling." Cell **139**(5): 891-906.

Lozano, E., M. Betson, et al. (2003). "Tumor progression: small GTPases and loss of cell-cell adhesion." Bioessays **25**(5): 452-463.

Milani, M. and A. L. Harris (2008). "Targeting tumour hypoxia in breast cancer." European Journal of Cancer **44**(18): 2766-2773.

Mueller, M. M. and N. E. Fusenig (2004). "Friends or foes - Bipolar effects of the tumour stroma in cancer." Nature Reviews Cancer **4**(11): 839-849.

MuellerKlieser, W. (1997). "Three-dimensional cell cultures: from molecular mechanisms to clinical applications." American Journal of Physiology-Cell Physiology **42**(4): C1109-C1123.

Muellerklieser, W. F. and R. M. Sutherland (1982). "Oxygen-Tensions in Multicell Spheroids of 2 Cell-Lines." British Journal of Cancer **45**(2): 256-264.

Noel, A., M. Jost, et al. (2008). "Matrix metalloproteinases at cancer tumor-host interface." Seminars in Cell & Developmental Biology **19**(1): 52-60.

Osada, H. and T. Takahashi (2002). "Genetic alterations of multiple tumor suppressors and oncogenes in the carcinogenesis and progression of lung cancer." Oncogene **21**(48): 7421-7434.

Pampaloni, F., E. G. Reynaud, et al. (2007). "The third dimension bridges the gap between cell culture and live tissue." Nature Reviews Molecular Cell Biology **8**(10): 839-845.

Paszek, M. J. and V. M. Weaver (2004). "The tension mounts: Mechanics meets morphogenesis and malignancy." Journal of Mammary Gland Biology and Neoplasia **9**(4): 325-342.

Paszek, M. J., N. Zahir, et al. (2005). "Tensional homeostasis and the malignant phenotype." Cancer Cell **8**(3): 241-254.

Sader, J. E., I. Larson, et al. (1995). "Method for the Calibration of Atomic-Force Microscope Cantilevers." Review of Scientific Instruments **66**(7): 3789-3798.

Schroeder, U., A. Graff, et al. (2009). "Peptide Nanoparticles Serve as a Powerful Platform for the Immunogenic Display of Poorly Antigenic Actin Determinants." Journal of Molecular Biology **386**(5): 1368-1381.

Semenza, G. L. (2002). "HIF-1 and tumor progression: pathophysiology and therapeutics." Trends in Molecular Medicine **8**(4): S62-S67.

Stolz, M., R. Gottardi, et al. (2009). "Early detection of aging cartilage and osteoarthritis in mice and patient samples using atomic force microscopy." Nature Nanotechnology **4**(3): 186-192.

Stolz, M., R. Raiteri, et al. (2004). "Dynamic elastic modulus of porcine articular cartilage determined at two different levels of tissue organization by indentation-type atomic force microscopy." Biophysical Journal **86**(5): 3269-3283.

Sullivan, R. and C. H. Graham (2007). "Hypoxia-driven selection of the metastatic phenotype." Cancer and Metastasis Reviews **26**(2): 319-331.

Suresh, S. (2007). "Biomechanics and biophysics of cancer cells." Acta Materialia **55**(12): 3989-4014.

Suresh, S. (2007). "Nanomedicine - Elastic clues in cancer detection." Nature Nanotechnology **2**(12): 748-749.

Taniguchi, S., J. Sagara, et al. (1988). "Deficient Polymerization Invitro of a Point-Mutated Beta-Actin Expressed in a Transformed Human Fibroblast Cell-Line." Journal of Biochemistry **103**(4): 707-713.

Teicher, B. A. (1994). "Hypoxia and Drug-Resistance." Cancer and Metastasis Reviews **13**(2): 139-168.

Tilghman, R. W., C. R. Cowan, et al. (2010). "Matrix Rigidity Regulates Cancer Cell Growth and Cellular Phenotype." Plos One **5**(9): -.

Tlsty, T. D. and P. W. Hein (2001). "Know thy neighbor: stromal cells can contribute oncogenic signals." Current Opinion in Genetics & Development **11**(1): 54-59.

Vaupel, P. (2004). "Tumor microenvironmental physiology and its implications for radiation oncology." Seminars in Radiation Oncology **14**(3): 198-206.

Walenta, S., J. Doetsch, et al. (2000). "Metabolic imaging in multicellular spheroids of oncogene-transfected fibroblasts." Journal of Histochemistry & Cytochemistry **48**(4): 509-522.

Wiseman, B. S. and Z. Werb (2002). "Development - Stromal effects on mammary gland development and breast cancer." Science **296**(5570): 1046-1049.

Wolf, K., S. Alexander, et al. (2009). "Collagen-based cell migration models in vitro and in vivo." Seminars in Cell & Developmental Biology **20**(8): 931-941.

Wouters, B. G., S. A. Weppler, et al. (2002). "Hypoxia as a target for combined modality treatments." European Journal of Cancer **38**(2): 240-257.

Chapter 5

The nanomechanical signature of hypoxia-induced breast cancer progression in mice and human patient samples

M. Plodinec[1, 2], E. Obermann[3], U. Müller[5], R. Sütterlin[1, 2], R. Zanetti[4], U. Aebi[2], M. Bentires-Alj[5], and C-A. Schoenenberger[1,2]

1. Core program Structural Biology and Biophysics, Biozentrum, University of Basel, 4056 Basel, Switzerland
2. Maurice E. Mueller Institute for Structural Biology, Biozentrum, University of Basel, 4056 Basel, Switzerland
3. Department of Pathology, University Hospital Basel, 4031 Basel, Switzerland
4. Breast Center, University Women`s Hospital Basel, 4031 Basel, Switzerland
5. Growth Control, Friedrich Miescher Institute for Biomedical Research, 4058 Basel, Switzerland

* Correspondence: cora-ann.schoenenberger@unibas.ch

Keywords: mammary gland, cancer, mouse, human, hypoxia, cytoskeleton, extracellular matrix, stiffness, atomic force microscopy, nanomechanical properties

5.1 Abstract

Hypoxia (low levels of oxygenation) is a common characteristic of solid tumors that has been associated with poor therapeutic response and, more recently, with malignant progression, i.e., an increasing probability of recurrence, local spread, and distant metastasis. Emerging evidence indicates that the effect of hypoxia on tumor progression is mediated by a series of hypoxia-induced genetic and proteomic changes that enable tumor cells to survive or escape their oxygen-deficient environment. Conceivably, the mechanical response of cancer cells to environmental conditions might also vary considerably and thus affect the progression of malignancy. We are employing atomic force microscopy (AFM) to probe with high sensitivity nanomechanical properties of fresh breast tissue biopsies obtained from human patients and MMTV-PyMT (mouse mammary tumor virus-polyoma middle-T antigen) transgenic mice. AFM stiffness maps revealed a gradual softening from the periphery to the core in human and murine cancer tissues while stromal tissue at the tumor periphery was stiffer than the underlying tumor. Pimonidazole staining of murine tissues confirmed that the core of ductal carcinomas in situ (DICS) exhibited extensive hypoxia compared to normal mammary gland. AFM stiffness measurements revealed a correlation between tissue softening and hypoxia. Consistent with this notion, subsequent immunohistochemistry showed collagen degradation and changes in the actin and vimentin cytoskeleton in hypoxic regions. At late stages of tumor progression, the soft and hypoxic phenotypes were increasingly present at the tumor periphery. Moreover, even distant metastatic lesions in the lung displayed a hypoxic phenotype. AFM testing of fresh human breast biopsies revealed distinct nanomechanical signatures associated with different stages of tumor progression. Interestingly, comparison of the nanomechanical properties with the histopathological diagnosis suggests a high ratio of soft versus stiff areas to be an indication of a more aggressive phenotype. Hence, AFM stiffness maps might prove valuable prognostic markers for cancer progression with significant implications for treatment.

5.2 Introduction

The cytoskeleton, a supramolecular network comprised of actin filaments, intermediate filaments and microtubules, is dynamically remodelled during cell adhesion, migration, proliferation and differentiation (Ingber, Dike et al. 1994). In addition, the cytoskeleton network plays structural and functional roles in maintaining cell morphology, signalling and intracellular transport (Janmey 1998). Many of these fundamental cellular processes are modulated by mechanical forces. Correspondingly, tumorigenesis which results from changes in these fundamental processes is associated with alterations in biomechanics. To gain insight into how physical and chemical forces shape and govern the emergence and behaviour of cancer is a new and exciting frontier for cancer research (Needham 1991; Paszek and Weaver 2004; Kumar and Weaver 2009). Biophysical techniques such as atomic force microscopy (AFM) (Lekka, Laidler et al. 1999; Rosenbluth, Lam et al. 2006; Cross, Jin et al. 2007), micropipette aspiration (Ward, Li et al. 1991), microfluidics (Lam, Rosenbluth et al. 2007) and optical tweezers (Guck, Schinkinger et al. 2005) have been used to probe the mechanical properties of cancer cells. More specifically, cell elasticity and/or deformability have been recognized as a marker for the phenotypic consequences of alterations in cytoarchitecture and adhesion that are associated with malignant transformation (Suresh 2007). For example, nanomechanical analysis of single cells isolated from pleural fluid of cancer patients revealed that metastatic cells are softer than corresponding normal cells (Cross, Jin et al. 2007). However, stiffness was measured at one specific site only, and thus does not appropriately reflect the structural heterogeneity of a cell. Also the absence of the native tissue environment is likely to have had an influence on the mechanical behaviour.

Force changes that arise from interactions with the microenvironment play a significant role in triggering genetic changes that induce tumorigenesis. It has been shown that the mechanical properties of living cells are highly dependent on many factors present in their three-dimensional 3D microenvironment (Park, Bissell et al. 2000). This involves both the cell population heterogeneity and extracellular matrix (ECM) components (Kass, Erler et al. 2007). Studies performed on 3D mammary cell cultures and mouse mammary glands have suggested that increased matrix deposition and crosslinking consistent with ECM stiffening promotes the development and progression of cancer (Paszek, Zahir et al. 2005; Levental, Yu et al. 2009). In this case, cancer detection has been achieved by unconfined compression of the whole mammary gland (Sinkus, Lorenzen et al. 2000; Butcher, Alliston et al. 2009) (Paszek, Zahir et al. 2005). However, this approach only considered the peripheral region of the tumor, while the bulk of the underlying cancer was not accessible for testing. Nevertheless, the relative stiffening of the peripheral tumor stroma compared to the adjacent normal mammary gland tissue has led to the widespread assumption that breast cancer is stiffer than the normal mammary gland tissue or benign lesions. The inconsistency of stiffness data obtained on individual cells in culture and on tissues *in situ* emphasizes the importance of taking into account both the measuring approaches, but even more other microenvironmental factors that are present in a 3D tissue context.

A variety of biochemical gradients develops during tumor development and progression within the tissue. Oxygen and pH are considered as the key microenvironmental factors in the development and growth of tumors and their response to treatment (Helmlinger, Yuan et al. 1997). In particular, the hypoxia (low oxygen), as a constituent of the tumor cell microenvironment is a prominent feature of malignant tumors by modifying the pathways that regulate cell proliferation, angiogenesis and cell death (Giatromanolaki and Harris 2001), Cancer cells have the ability to adapt to reduced oxygen conditions, moreover to survive and even grow in these conditions. The correlation between the extent of hypoxia and tumor aggressiveness has been addressed in many studies in great detail (Graeber, Osmanian et al. 1996; Giaccia, Koumenis et al. 1999; Williams, Telfer et al. 2002). In particular, the presence of hypoxic regions within the cancer tissue is often an indication of resistance to radiation therapy and poor prognosis. Cells in the interior of a tumor mass experience a lower oxygen tension microenvironment and lower fluid velocities than those at the edges in proximity with a functional blood vessel, and are prompted to produce different biochemical signals (Tredan, Galmarini et al. 2007). All of these differential responses affect tumor cell fate—that is, whether a cell will live or die, and whether it will be able to detach and migrate to secondary sites in the body. Expression profiling studies have highlighted that genes regulated by hypoxia and HIF-1α are for example angiogenic factors, proliferation and cell-adhesion genes (Denko, Schindler et al. 2000; Koong, Denko et al. 2000; Lal, Peters et al. 2001). This was corroborated by a recent report on quantitative proteomics which revealed that under hypoxia tumor cells secreted proteins involved in angiogenesis, focal adhesion, extracellular matrix-receptor interaction, and immune cell recruitment (Park, Sen Tan et al. 2010). An interesting finding of this study was that the secreted proteins were predominantly cytoplasmic and membrane proteins. Also studies performed on focal adhesion kinase (FAK) expression in hypoxic cells and the effect of FAK siRNA on cytoskeletal arrangement of induced by hypoxia have shown that hypoxia-treated cells displayed a large degree of cell detachment (Saenz-Morales, Escribese et al. 2006). Thus, hypoxic cells exhibit enhanced angiogenic and metastatic potential such as reduced cell-cell and cell-extracellular matrix (ECM) adhesion. Emerging data show that signalling pathways activated by hypoxia modify cytoskeletal and contractile proteins that might alter the biomechanical properties of cells. This is accompanied by remodelling of actin (Wojciak-Stothard, Tsang et al. 2006) and vimentin networks (Liu, Guevara et al. 2010). Consistent with these observations, it has been shown that hypoxia induced stimulation of HIF-1 pathway promotes epithelial-to-mesenchymal transition and fibrinogenesis (Higgins, Kimura et al. 2007). Moreover, hypoxia induced activity of MMPs to degrade and modify the extracellular matrix enables aggressive cancer cells to migrate and invade surrounding tissue (Munoz-Najar, Neurath et al. 2006) and possibly alters their mechanical response. Notably, physical properties of cell cytoskeleton and extracellular matrix in which cells are embedded might be influenced by hypoxia in tumors *in vivo*. However, mechanical properties of cancer cells and/or tissues in the context of hypoxia have not yet been evaluated. The tools applied so far have either included mechanical measurements of extracted cancer cells from the primary tissue or just measured tumor periphery which has provided limited insight into the structural and mechanical heterogeneity of a tumor tissue.

To test the feasibility of AFM nanomechanical testing on soft cancer tissues we probed with high sensitivity nanomechanical properties of fresh breast tissue biopsies obtained from human patients and MMTV-PyMT (mouse mammary tumor virus-polyoma middle T antigen) transgenic mice. This model has been shown to exhibit short period of latency, high tissue penetrance and metastatic cells colonizing the lungs similarly as with human invasive ductal breast carcinoma. It allows with high reproducibility to follow all stages of tumor progression from the primary tumor to the metastatic cancer similar to human breast cancer (Lin, Jones et al. 2003). Obtained data revealed a centripetal softening from the periphery to the core in early breast carcinoma tissue from MMTV-PyMT mice. The periphery of the malignant tissue was significantly stiffer to that measured in normal mammary gland tissue which is confirming previously published observations (Paszek, Zahir et al. 2005). Remarkably, hypoxia staining of murine tissues showed that the core of carcinoma *in situ* exhibited extensive hypoxia compared to normal mammary gland, hence AFM measurements revealed a correlation between central softening and hypoxia. Consistent with this notion, subsequent immunohistochemistry showed ECM degradation and changes in the cell cytoarchitecture in the hypoxic regions. Unexpectedly, at late stages of tumor progression, the soft and hypoxic phenotypes were increasingly present at the tumor periphery and in lung metastasis. To confirm the clinical relevance of the obtained data we performed nanomechanical testing of fresh human breast biopsies. Measurements revealed distinct nanomechanical changes following stages of tumor progression. Our results show direct correlation between the tumor core softening and hypoxia marker. Therefore, AFM stiffness testing might prove valuable prognostic markers for detection of soft hypoxic cancer regions, thereby predicting tumor progression and prognosis.

5.3 Materials and Methods

Mammary tissue samples from MMTV-PyMT mice

All procedures involving mice were conducted in accordance with the Swiss laws regulating the use and care of experimental animals and have been approved by the Swiss animal use committee. To obtain female mice heterozygous for the PyMT transgene, male PyMT mice on a C3H/B6 x FVB-C3H/B6 background were randomly bred with C3H/B6 females lacking the PyMT transgene. Mice were palpated twice weekly to assess mammary tumor onset. Tumor volume was calculated following caliper measurement as width × length × 0.4. Mice were euthanized by CO_2 inhalation. MMTV-PyMT transgenic mice exhibit multiple tumor sites and several glands were removed. They were immediately placed in ice-cold sterile Ringer’s solution supplemented with glucose and a protease inhibitor cocktail (Complete, Boehringer Mannheim). For nanomechanical AFM testing, cylindrical specimens that represent a cross-section of the entire tumor were obtained by a biopsy punch with an inside diameter of 2 mm. Stiffness mapping was started within 1 h after biopsy and continued for up to two days. The mechanical properties of mammary tissue samples remained unchanged during this time period.

Measuring hypoxia *in situ*

Tumor bearing mice were injected intraperitoneally with pimonidazole hydrochloride at 100mg/ml in 0.9 % sterile saline solution (120 mg/kg, hypoxyprobe-1, HPI, Burlington, MA, US**A**). After 90 minutes mice were sacrificed and biopsies taken for nanomechanical testing as described above. Subsequently, hypoxia was assessed by immunohistochemical analysis of pimonidazole incorporation.

Human breast samples

Patient recruitment and stiffness analysis was carried out in accordance with ethical requirements and without previous knowledge of clinical data. The ultrasound-guided core biopsy of the conspicuous lesion removed a radial, cylindrical specimen that was directly transferred to a vial containing ice-cold sterile Ringer's solution supplemented with glucose and a protease inhibitor cocktail (Complete, Boehringer Mannheim, Germany). As for murine tissues, AFM testing started within 1 h after biopsy. Mechanical properties of specimens did not change during this time period.

Nanomechanical AFM testing

For the analysis of the mammary gland tissue samples by AFM (Multimode AFM, Veeco, USA) biopsies were glued onto a round Teflon disk using 2-component glue (Devcon, USA). The mounted specimens were kept in ice-cold Ringer's solution until nanomechanical testing, which was performed at 37°C. Stiffness (elastic modulus, *E*) measurements of biopsies were derived as follows; we recorded load–displacement curves at a given site in an oriented manner during both loading and unloading. An individual set of data consisted of 1,024 load–displacement curves, 512 data points each at a sampling rate of 1.5 Hz. For sharp pyramidal tips (200-mm-long silicon nitride cantilevers, nominal cantilever spring constant $k = 0.06$ N m^{-1}; Veeco, USA), the load–displacement curves were set to a defined trigger deflection (that is, maximum applied load) of 30 nm, which corresponds to an applied load of ~1.8 nN and indentation of ~150–3000 nm. For calculating elastic modulus *E*, experimental force curves were processed using custom software. Stiffness values were calculated from AFM unloading curves. By using unloading rather than loading curves any irreversible (e.g., plastic) deformation or other extraneous displacement effects are avoided. The slopes derived from AFM unloading curves collected in a given square grid were represented as slope histograms. The slope corresponding to the maximum stiffness value was set to one. The bin width was set by dividing the maximum value = 1/50 bars. The subsequent calculation of elastic moduli (E) from the slope data was performed as previously described (Plodinecet al., submitted).

Histology and immunohistochemistry

After the AFM testing, all samples were formalin-fixed and paraffin-embedded following standard histological procedures. Sections of 4 micrometer thickness were cut and transferred onto glass slides. The first and last slide of a series was routinely stained with Haematoxylin & Eosin. Subsequent histopathological examination included assessing the nature of the lesion, the specific type of lesion (invasive ductal carcinoma, DCIS, fibroadenoma etc.) as well as a number of additional histopathological markers (extent of tumor infiltration, fibrosis, necrosis, and lymphocytic infiltration). The remaining slides were used for immunohistochemical analysis using antibodies against the extracellular matrix proteins, collagen I (1:80; Abcam, USA), fibronectin (1:2500; Dako Cytomation, Denmark) and laminin (1:25; Thermo Scientific, USA). Tissue cytoarchitecture was assessed by staining the sections with antibodies against smooth muscle actin, vimentin and desmin. All three antibodies were purchased pre-diluted for experiments (100 µl in 10 mM PBS, pH 7.6 and 0.1% Sodium azide/sample section, Ventana Medical Systems Inc., USA). Immunohistochemical analysis was performed according to a standard protocol. In some cases, sections were first subjected to heat-induced epitope retrieval or treated with Dako Cytomation target retrieval solution at high pH or with 10mM Tris buffer, 1mM EDTA, pH 9.0. For collagen staining, tissues were pre-treated with 2 mg/mL hyalouronidase for 15 minutes at RT. Immunostaining was visualized with horseradish peroxidase (HRP)-conjugated secondary antibodies (DakoCytomation, Denmark). Sections were examined with an upright light microscope (Carl Zeiss, Germany) using 10×, 20× and 40× objectives.

Statistical analysis

All data are given as mean ± standard deviation (s.d.). Statistical significance of differences in mean values was assessed with the paired Student’s t test- in Origin 7.5 (OriginLab). Statistical significance was set at $P \leq 0.05$.

5.4 Results

Nanomechanical testing of soft tissue biopsies by AFM

We have developed an efficient method to assess nanomechanical properties of soft breast tissue biopsies under physiological buffer conditions by AFM (Figure 5-1). For validation of the AFM method in a biologically relevant model system, we measured nanomechanical properties of mammary gland tissues from MMTV-PyMT transgenic mouse and from human breast tissue biopsies. The sample used for AFM testing, was excised from the mammary gland in shape of a radial, cylindrical biopsy (Figure 5-1a). In these samples, 3D tissue integrity and heterogeneity is preserved and the corresponding structural and nanomechanical information throughout the entire specimen is presented in a 2D plain to the AFM probe (Figure 5-2). This allowed us to measure the nanomechanical response in an oriented manner from the most inner part of the sample (core) to the periphery.

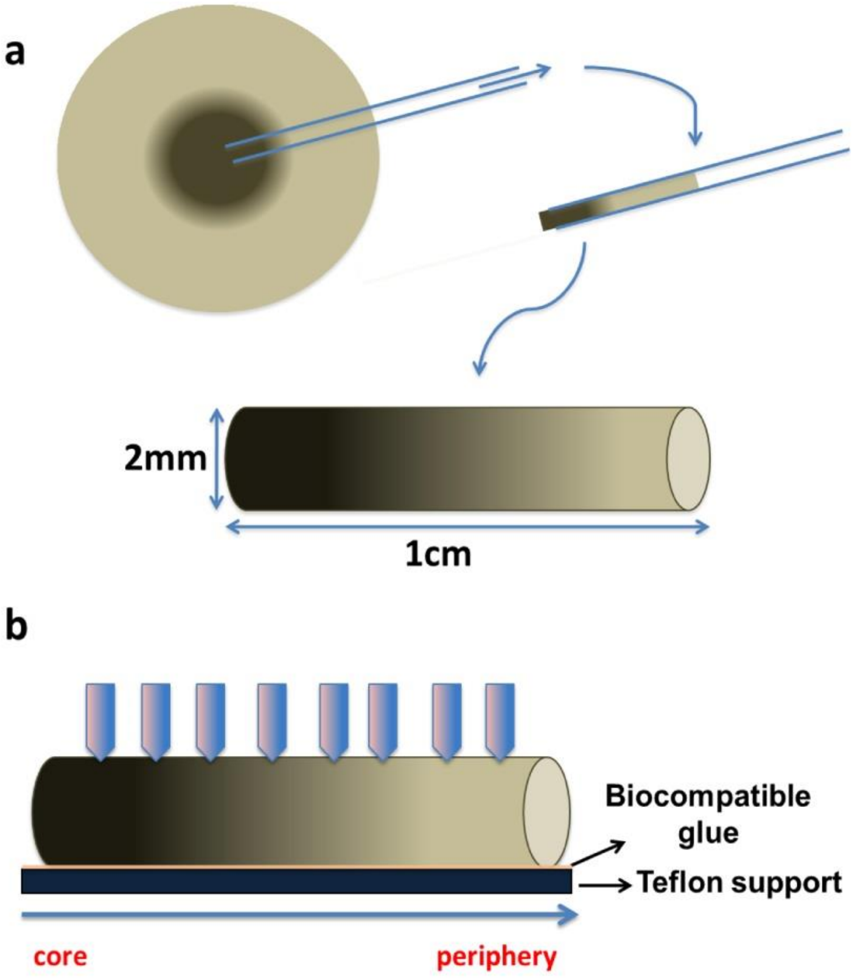

Figure 5-1. Schematic representation of experimental approach in nanomechanical AFM testing biopsies. (a) A representative cylindrical tissue sample exhibiting a distinct orientation from core to the periphery. (b) Fresh tissue samples are stably attached to a solid Teflon support with biocompatible glue an oriented manner. Samples are kept in Ringer’s solution at all times.

Correlating histopathological findings with the nanomechanical response in the MMTV-PyMT mouse model

To assess the nanomechanical changes associated with tumor progression, we have removed tissue samples from mammary glands of MMTV-PyMT transgenic mice at different tumor stages. AFM measurements of normal mouse mammary gland revealed a homogeneous distribution of stiffness with an elastic modulus E=1.28±0.12 kPa (Figure 5-2a, top panel). Correlative histology examination of the specimen confirmed a normal, healthy mammary gland tissue appearance with high amounts of fat tissue that most likely contributes to the low stiffness values (Figure 5-2b, top panel). In the premalignant lesion, the stiffness distribution remained uniform (Figure 5-2a, middle panel) but stiffness increased to E=4.38±0.55 kPa. Histology revealed a densely packed, hyper-proliferating breast epithelium that correlates well with increased tissue stiffness (Figure 5-2b, middle panel).

However, the uniform stiffness distribution is lost in primary cancerous lesions and instead, carcinomas in situ exhibit a bimodal stiffness distribution (Figure 5-2a, bottom panel). In these early stages of tumor development, the E =0.54±0.13 kPa of core regions is 8-fold lower than that of benign lesions and 3-fold lower than normal tissue stiffness. The soft core is surrounded by significantly stiffer areas of E=16.97±6.89 kPa Although the bimodal stiffness distribution of carcinomas *in situ* suggests two distinct populations of cells in the tumor, the histological appearance of the tissue section does not reveal any significant morphological differences among the cancer cells that could contribute to bimodal stiffness distribution (Figure 5-2b, bottom panel). In the carcinoma *in situ*, the loss of tissue organization and the presence of cancer cells within individual ducts are clearly visible. However, cancer cells look cytologically similar. It is noteworthy that in carcinoma *in situ* the surrounding stroma appears unaltered compared to myoepithelium.

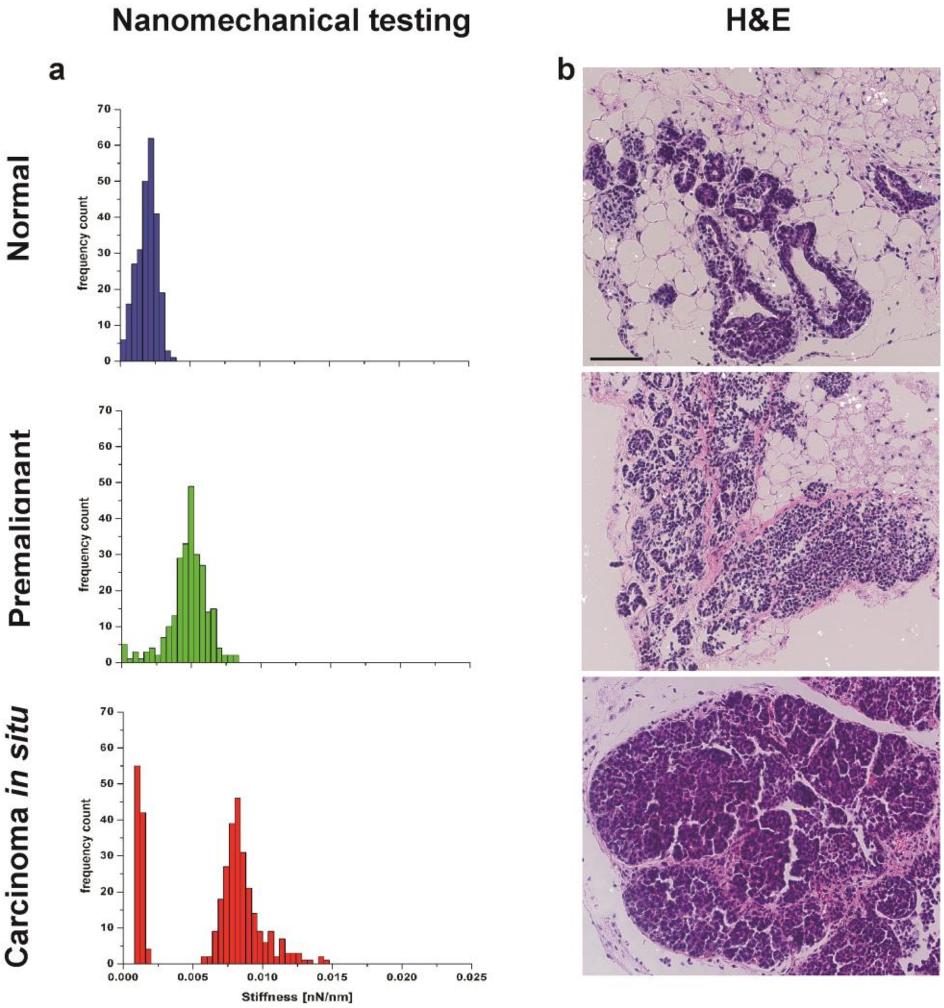

Figure 5-2. Correlating the nanomechanical response with histology in MMTV-PyMT mouse mammary gland tissues. (a) Histograms show frequency distribution of stiffness values from AFM measurements. Normal mouse mammary gland (top panel) exhibits a uniform Gaussian distribution. The stiffness distribution for premalignant hyperplasia (middle panel) is broader but still unimodal Gaussian. The primary cancerous tumor (bottom panel) is characterized by a bimodal stiffness distribution indicative of two distinct mechanical phenotypes. (b) Histology of the respective mouse mammary tissue sections after AFM measurements. Top panel shows inactive (non-lactating) normal mouse mammary gland with a duct surrounded by stromal and adipose tissue. The premalignant lesion (middle panel) displays large proliferation of epithelial cells. In primary cancerous lesions (bottom panel, carcinoma in situ) that are organized in clearly delineated ducts with intact basement membrane, uniform proliferation of tumor cells is seen. Scale bars, 50 µm.

In conclusion, correlative comparison of AFM stiffness measurements with histology allowed us to establish an association between the nanomechanical response of mouse mammary tissues and malignant transformation; Tissue morphology did not provide an apparent explanation for the bimodal stiffness distribution and the soft core region of primary cancerous lesions.

Hypoxia-induced tissue softening in breast cancer of -MMTV-PyMT

Tumor hypoxia caused by inefficient vascularization has been described for a wide range of solid tumors. It is associated with poor prognosis following radiation, chemotherapy, and surgery (Tatum, Kelloff et al. 2006). Interest in the hypoxic status of tumors has further increased with the discovery that hypoxia regulates dozens of genes that alter cellular behaviour and result in a more malignant tumor phenotype (Vaupel and Harrison 2004). Because a hypoxic core is known as a crucial feature of aggressive cancer progression (Guppy 2002), we examined whether the bimodal stiffness distribution observed from the periphery to the core of the primary cancer lesion is related to reduced oygenation . To directly correlate hypoxia and tissue stiffness in staged tumor samples, we injected MMTV-PyMT mice with pimonidazole agent that selectively binds to oxygen-starved cells prior to tumor excision. Subsequently, the nanomechanical properties of the tissue samples were tested by AFM and tissues were later processed for hypoxia assessment. As illustrated in figure 3, immunohistochemical staining revealed that normal glands and benign lesions are negative for hypoxia (Figures 5-3a and 5-3b), whereas primary tumors exhibit clear hypoxia in the core (Figure 5-3c) that correlates well with the significant decrease of stiffness.

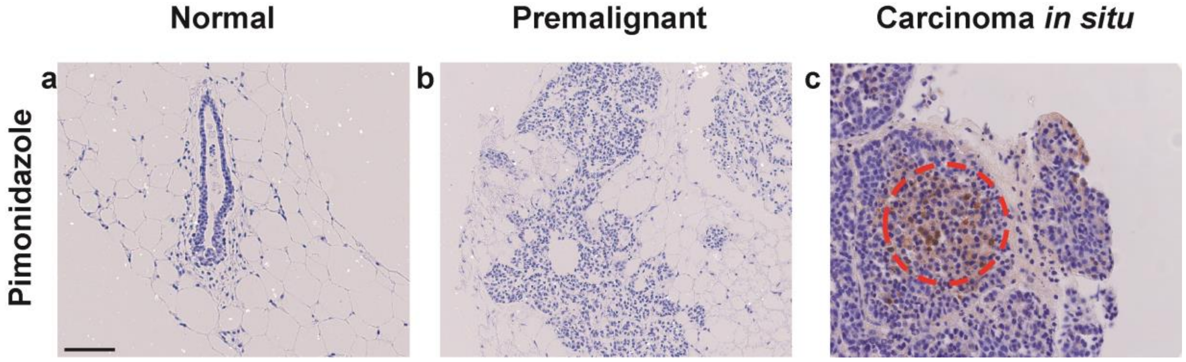

Figure 5-3. Detection of hypoxia during tumor development in MMTV-PyMT-mice. Paraffin-embedded sections of mammary gland tissues from pimonidazole-treated MMTV-mice at different stages were immunolabeled. (a) Normal mouse mammary gland shows no pimonidazole labelling which indicates the absence of hypoxia. (b) The benign lesion is also negative for the hypoxia marker. (c) Primary breast cancer tissue exhibits a positive signal for central hypoxia (dashed red circle) in the ductal structure Scale bar, 50 µm.

Upon progression of malignancy to the invasive metastatic stage (Figure 5-4), a pronounced spread of hypoxia occurred. In addition to the extensive hypoxia in the core (Figure 5-4a zoom in, right panel), this stage is characterized by a progressive dissemination of hypoxic cancer cells (stained brown) to the surrounding tissue. In particular, blood vessels were lined with hypoxic cells (Figure 5-4a, zoom in, middle panel) suggesting intravasation and ultimately invasion at distant sites and hypoxic cells spread to the peripheral tumor stroma (Figure 4a, zoom in, right panel). Corresponding AFM measurements show that invasive carcinomas no longer exhibit two distinct stiffness peaks but rather a broad stiffness distribution with gradual stiffening from the core to the tumor periphery. The softness of the core region and the general broadening of the stiffness distribution (Figure 5-4b) are consistent with immunohistochemical hypoxia assessment which shows hypoxic cells disseminated from the core to/and at the periphery. Interestingly, lung metastases found in MMTV-PyMT mice with invasive carcinoma also contain hypoxic cells (Figure 5-4c). This finding suggests that hypoxia is indeed associated with an invasive, more aggressive phenotype that retains its hypoxic characteristics even in a new microenvironment.

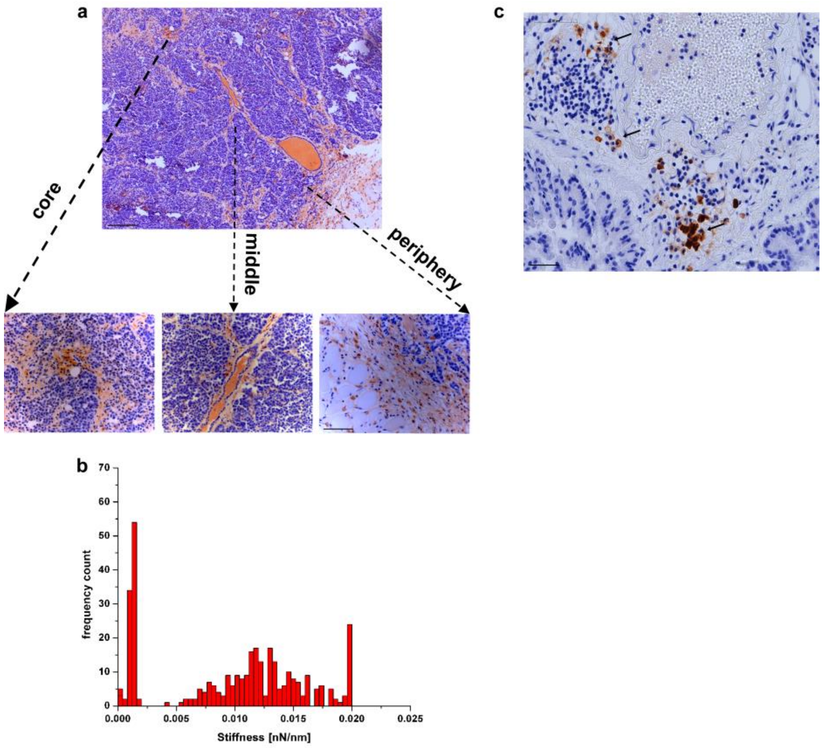

Figure 5-4. Hypoxia-related stiffness heterogeneity in invasive breast cancer of MMTV-PyMT mice. (a) At low magnification, the immunolabeled tissue section of invasive breast cancer from pimonidazole-treated mice shows different hypoxic areas (brown signal). Zooming-in reveals a more detailed view. Hypoxic cells are abundant in the core region of the tumor (left panel), are streaming towards tumor blood vessels (middle panel), and have disseminated to the tumor periphery (right panel, marked by dashed lines). Scale bars 200 µm and 50 µm, respectively. (b) Histogram displaying stiffness measurements exhibits a bimodal distribution. There is an increase in stiffness from the core to the periphery where the stiffness values are broadly distributed. (c) Metastasizing cells found in the lungs (indicated by black arrows) exhibit the hypoxic phenotype Scale bar, 50 µm.

Our AFM stiffness measurements indicate that mechanical aspects are valuable markers for cancer progression. Based on the corresponding hypoxia assessment one might conclude that tumor hypoxia induces a softening of malignant cells that renders them more aggressive.

Following structural changes in the extracellular matrix and cytoarchitecture during breast cancer progression in the mouse model

To gain insight into the molecular mechanisms underlying the nanomechanical changes associated with tumor development we explored structural changes in extracellular matrix components. Collagen I and fibronectin are key components of the extracellular matrix and essential determinants of the tissue stiffness. Collagen expression (brown staining) could not be detected in normal and premalignant mammary tissues (Figure 5-5a and 5-5b, top panel). Normal and premalignant mammary tissues express fibronectin in the tissue stroma surrounding the mammary epithelium (Figures 5-5a and 5-b, middle panel). In the carcinoma *in situ* collagen signal is present only in the stroma surrounding the neoplastic glandular tissue (Figure 5-5c), at the same time the overall fibronectin expression appears increased although the fibrillar structure is similar to normal gland and it is also localized in the stroma. (Figure 5-5c, middle panel). Collagen expression is increased in the stroma of the invasive cancer, in particular spanning the large area at the tumor periphery (Figure 5-5d). Normal and premalignant mammary tissues express fibronectin in the tissue stroma surrounding the mammary epithelium (Figures 5-5a and 5-b, middle panel). In the carcinoma *in situ*, overall fibronectin expression appears increased although the fibrillar structure is similar to normal gland and it is also localized in the stroma. (Figure 5-5c, middle panel). Fibronectin expression and fibrillar structure is drastically altered in the stroma of the invasive cancer, especially at the tumor periphery. It is accompanied by elevated fibronectin expression and a dense fibrous appearance (Figure 5-5d, middle panel). Laminin is one of the major proteins of the basement membrane, thus in the healthy mammary gland it separates the myoepithelium from the tissue stroma (Figure 5-5a, bottom panel). In the premalignant lesion, hyper-proliferation of the luminal epithelium leads to higher expression of the basal laminin, however the structural appearance of the basement membrane is not perturbed. (Figure 5-5b, bottom panel). In carcinoma *in situ* laminin structure remains intact while separating the neoplastic mammary myoepithelium from the adjacent stroma (Figure 5-5c, bottom panel); however in the invasive cancer its structural organization is completely lost (Figure 5-5d, bottom panel).

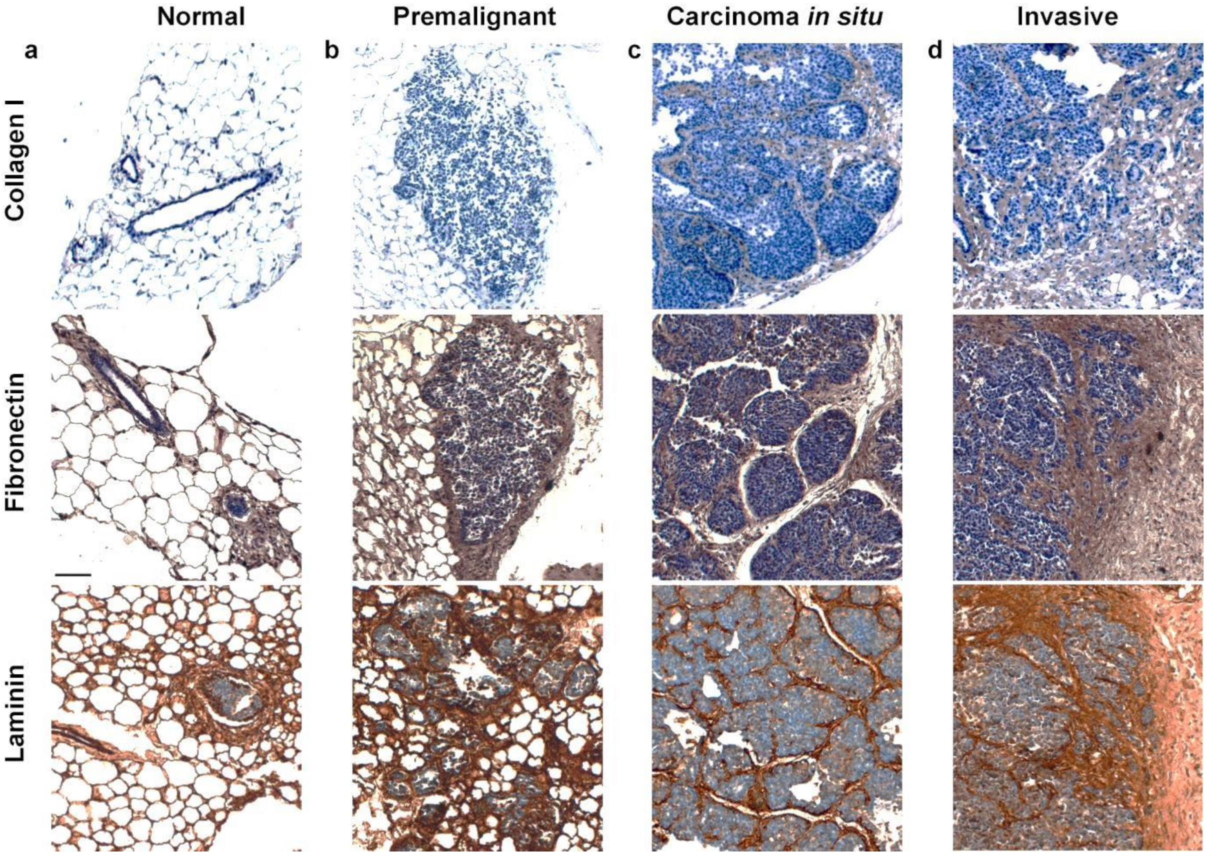

Figure 5-5. Structural changes in the extracellular matrix components during breast cancer progression in the mouse model. (Top panel) (a) Normal and (b) benign mammary tissues do not express collagen I. (c) In carcinoma *in situ* collagen staining (brown staining) is visible surrounding the basement membrane and denoting the presence of tumor stroma, (d) In the invasive cancer, increased collagen staining can be clearly distinguished at the tumor periphery. (Middle panel) Fibronectin staining in brown displayed for the normal (a) and benign (b) mammary tissue shows presence of the normal breast stroma without degradation. Staining of the carcinoma *in situ* (c) indicates defined fibronectin staining lining the intact basement matrix surrounding the localized tumor regions while in the case of invasive cancer (d) fibronectin staining becomes more prominent and diffuse indicating invasion of the cancer cells and recruiting of the tumor stroma. (Bottom panel) Laminin (orange staining), the key component of the basement membrane, is shown for (a) healthy mammary gland and (b) hyperplastic lesion. (c) In the carcinoma *in situ* cancer cells are still maintained within the borders of the intact membrane. In the invasive cancer the basement membrane is completely broken and cancer cells are invading the surrounding tissue (d). Scale bar, 100 µm.

Next, we assessed the effect of tumorigenic transformation on the tissue cytoarchitecture by examining the spatial organization and expression of smooth muscle (SM)-actin, and two mesenchymal markers vimentin and desmin (Figure 5-6). In the normal tissue (Figure 5-6a top panel) and benign lesions (Figure 5-6b top panel), SM-actin (dark brown signal) is found in the myoepithelium whereas in carcinomas *in situ* a significant increase in expression and a loss of structural organization is observed (Figure 5-6c, top panel). In central areas, SM-actin staining is mostly absent which suggests that hypoxia might occur. At later stages of tumor progression, blood vessels appear disorganized and spread throughout the tumor (Figure 5-6d, top panel). This finding is consistent with the tumor invasiveness. Examination of the intermediate filament proteins vimentin and desmin also revealed changes in expression and spatial organization during cancer progression. While only little vimentin and desmin staining was observed in the epithelial cells of normal tissue and benign lesions (Figures 5-6a and 5-6b, middle and bottom panels respectively) , carcinoma *in situ* showed a marked increase of vimentin and desmin signal at the tumor periphery (Figure 5-6c, middle and bottom panels respectively). This finding is consistent with the epithelial mesenchymal transition that is typical for malignant transformation. At the invasive cancer stage, expression and spatial distribution of both vimentin and desmin further increased (Figure 6d, middle and bottom panels respectively).

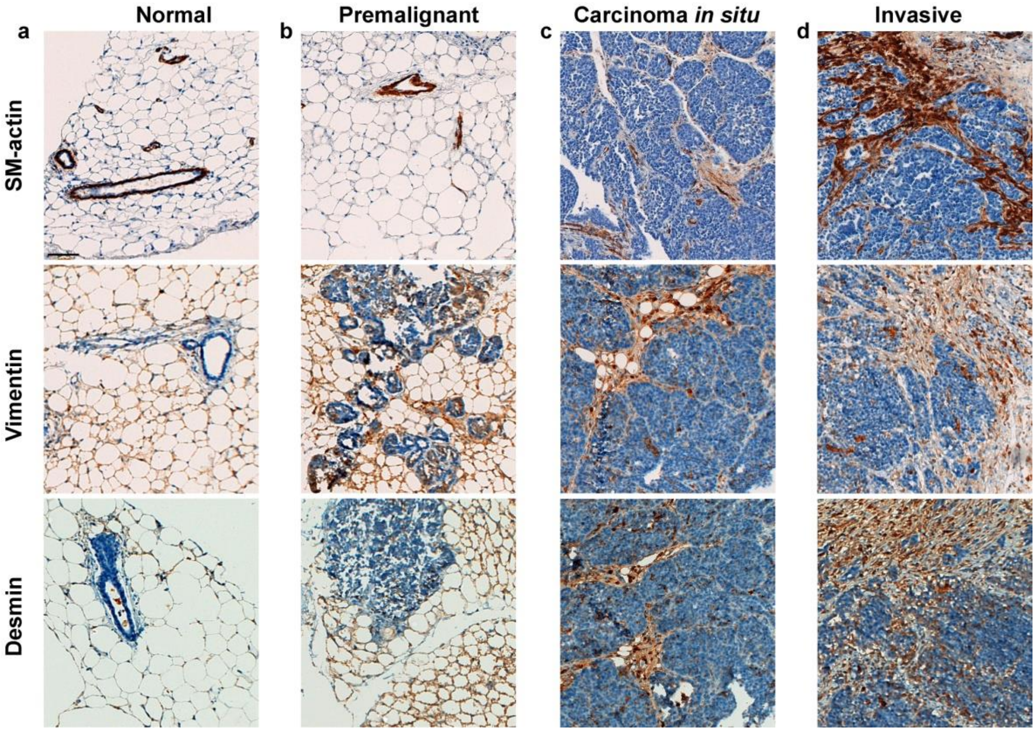

Figure 5-6. Cytoarchitecture of the mouse mammary gland during cancer progression. (Top panel) The expression of smooth muscle actin (SMA) is restricted to myoepithelial cells in the (a) normal gland and (b) benign lesion Tumor vascularization results in an increased SMA staining of blood vessels in (c) primary cancer lesions and more extensively, in (d) invasive cancer tissue. (Middle panel) Vimentin expression is limited to few stromal cells in (a) normal tissue and (b) benign lesion. (c) Carcinoma *in situ* exhibits increased levels of vimentin staining with prominent clusters around cystic structures. Vimentin-positive spindle cells marking myofibroblasts are prominent in the invasive cancer (d). (Bottom panel) Desmin staining surrounds the glandular (c) structures in the normal gland and the (b) benign lesion. (c) In the carcinoma *in situ* and invasive cancer tissue (d) there is a pronounced staining of the mesenchymal marker desmin. Scale bar, 100 µm.

Our immunohistochemical data indicate that degradation and spatial reorganization of ECM components are associated with tumor progression. At the same time, structural changes of SM-actin, vimentin and desmin within the localized primary tumor indicate significant changes in the cytoarchitecture. As the tumor progresses the structural heterogeneity further increases. We conclude that changes in ECM organization and cytoarchitecture affect the nanomechanical response of cells and thus tumor progression is characterized by an increase in the stiffness heterogeneity.

The nanomechanical signature of human breast biopsies

To elucidate the diagnostic and prognostic potential of the nanomechanical tissue properties in human breast cancer we have carried out AFM stiffness measurements of fresh human breast biopsies (Figure 5-7a). Normal mammary gland tissue from a 20year old patient exhibits a narrow range of stiffness values with a peak of E= 1.83±0.69 kPa (Figure 5-7a, top panel). H&E staining of a section from the same sample revealed the typical histology of healthy mammary gland tissue from a young female. In the lobular structure, the acini consist of uniform epithelial cells that are separated by a small amount of connective tissue (Figure 5-7b). The narrow stiffness distribution measured by AFM correlates well with the homogeneous histomorphological appearance. However, because of the young age and premenopausal state of the patient, it is possible that this particular nanomechanical signature is not characteristic for all normal mammary gland tissues. A rather narrow range of stiffness was also found in samples that proved to be benign lesions, although the E=4.07±1.39 kPa indicated an increase in stiffness in the 20 samples tested compared to the normal mammary gland. Consistent with this nanomechanical signature, histological examination of the benign lesion from a 60-year old patient demonstrates fairly uniform, predominantly fibrotic tissue with sporadic lobules typical for fibroadenoma (Figure 5-7b, middle panel). Similar tissue stiffening has been measured in benign lesions of MMTV-PyMT mice. A number of human biopsies (n=12) probed by AFM showed a significantly broader range of stiffness values with two distinct peaks as shown in the bottom panel of Fig 5-7b. Histological examination of this biopsy after AFM measurement confirmed an invasive ductal carcinoma, which represents the most common type of breast cancer in women, as shown for the 70-year old patient (Figure 5-7b, bottom panel). The central areas are dominated by tumor cells that infiltrate in a cord-like pattern into the dense fibrotic tissue at the tumor periphery. By correlating AFM measurements with histology, we identified the cancer cells from the inner regions of the tumor as the main contributors to the soft peak with E=0.87±0.65 kPa. Areas characterized by increased stiffness with a peak at E=11.26±1.90 kPa are mainly situated at the tumor periphery and thus correspond to fibrotic stroma.

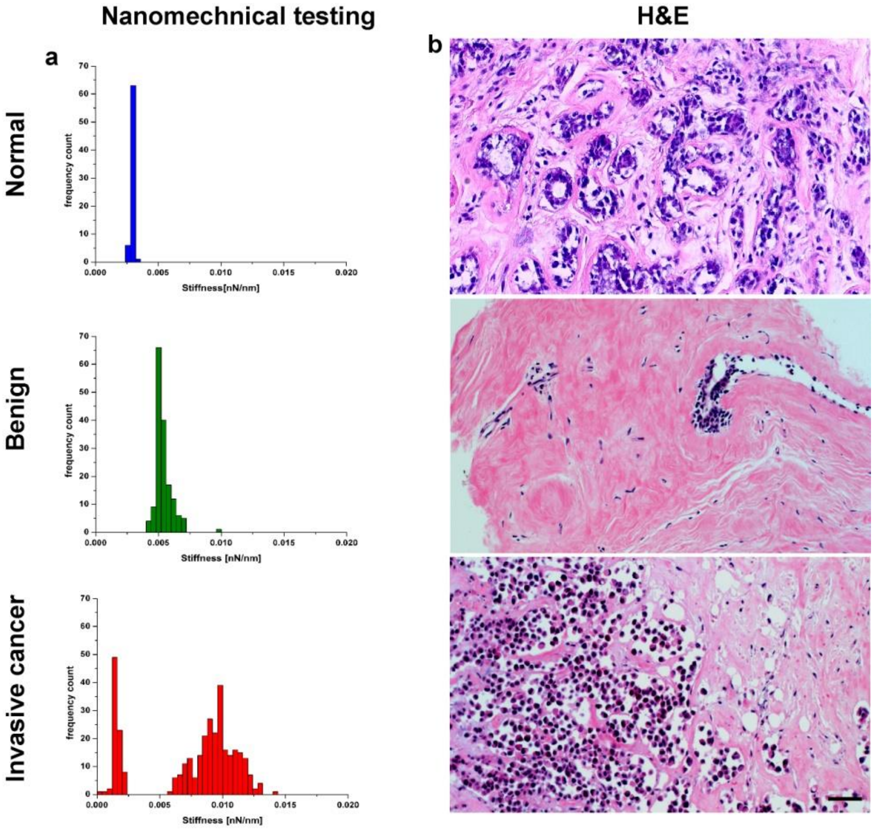

Figure 5-7. Nanomechanical signature of human breast tissue. (a) Stiffness distribution in human breast biopsies. Normal mammary gland tissue of a 20y old female (top panel) exhibits only small variations in the AFM stiffness values measured. A slightly broader but unimodal stiffness distribution with a small increase in overall stiffness is typical for benign lesions (middle panel). In contrast, cancer tissue exhibits a bimodal stiffness distribution with two peaks representing soft and relatively stiff regions of the tumor. (b) Histopathological assessment of tissue samples after AFM testing. (Top panel) Histology reveals the terminal ductal lobular unit of a normal mammary gland fenced by interstitial fibrous connective tissue and more distant adipose tissue. (Middle panel) Benign tumor exhibits mostly uniform proliferation of fibrous tissue typical for fibroadenomas. (Bottom panel) Invasive ductal breast carcinoma with infiltrating nests of cancer cells that have evoked a dense fibrous tissue response. Scale bar, 100 µm.

Importantly, the data on human breast biopsies are consistent with findings observed in the PyMT-MMTV mouse model. They provide evidence that the nanomechanical properties of tissue biopsies may be used as a reliable marker to detect malignant transformation and tumor progression in human patients.

ECM and cytoarchitecture in human breast cancer progression

Perturbations in the expression and structure of cytoskeleton and ECM components are considered features of malignant transformation in the human mammary gland (Kass, Erler et al. 2007). To determine whether we can likewise associate similar changes with the nanomechanical signature we have examined the effect of tumor progression on ECM and cytoarchitecture in human patients. Figure 5-8 illustrates changes in the distribution and structural appearance of the ECM components; collagen I (top panel), fibronectin (middle panel), and laminin (bottom panel) in the biopsies tested for stiffness. In the sample of a healthy mammary gland fibrillar collagen I is homogeneously distributed in the stroma whereas laminin is localized in the basement membrane surrounding the individual ducts in an organized manner. Fibronectin is present only in semi-periodic clusters in the basement membrane and is homogeneously distributed in the surrounding stroma. Consistent with the hypercellular stroma in fibroadenomas, we found an increased density and homogeneous distribution of collagen I and fibronectin in benign lesions (Figures 5-8b, top and middle panel respectively). Conceivably, these changes contribute to their increased stiffness. Because the glandular or ductal part is usually very small in fibroadenomas, laminin is only sparsely detected in few remaining normal ducts at the periphery (Figure 5-8b, bottom panel). Invasive carcinoma exhibits a heterogeneous collagen distribution with more marked collagen phenotype with (Figure 5-8c, top panel). For example, in the inner tissue region which is largely populated with cancer cells, collagen I appears completely degraded, and while at the periphery we found that the irregular fiber appearance is associated with an increase in collagen I expression, fibronectin behaves similarly to collagen, substantiating that two distinct structural phenotypes are present within the malignant tissue. This is in good agreement with the bimodal stiffness distribution measured in carcinomas by AFM. Furthermore, laminin is markedly disorganized and reveals the loss of epithelial polarity is consistent with malignancy and invasiveness.

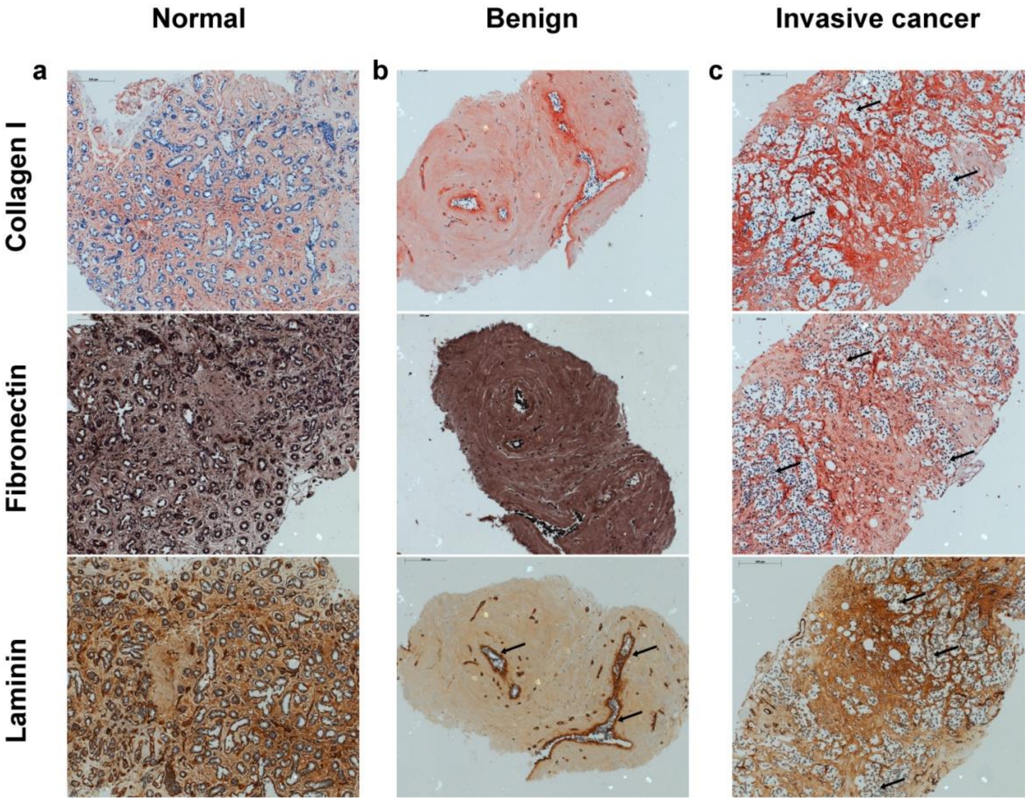

Figure 5-8. Structural changes of the major extracellular matrix components in mammary tissues with distinct nanomechanical signatures. (Top panel) (a) In normal mammary gland tissue, collagen I staining indicates healthy stromal tissue surrounding the ducts. (b) In the benign fibroadenoma, almost the entire tissue section exhibits pronounced collagen staining. (c) In the invasive cancer, the expression of collagen I is heterogeneous. Areas enriched for tumor cells and macrophages are largely devoid of collagen (black arrows) whereas tumor stroma exhibits strong collagen I staining with an irregular structure. (Middle panel) (a) In the normal gland, fibronectin staining marks the healthy stroma surrounding the glandular tissue. (b) In the benign lesion, fibronectin staining has a homogeneous appearance over the entire tissue. (c) Fibronectin staining of invasive cancer is heterogeneous and its expression is low in regions with abundant tumor cells. (Bottom panel) Laminin is a constituent of the basement membrane of healthy ducts and delineates the (a) normal glandular tissue. (b) In the benign lesion, laminin staining reveals only few normal ducts (black arrows). (c) In the invasive cancer, laminin staining is irregular. The tumor is not confined and the border between the tumor stroma and glandular tissue is lost (black arrows). Scale bar, 200 µm.

Next, we compared the cytoarchitecture between normal tissue, and benign and cancerous neoplasias. As expected for normal mammary gland tissue, smooth muscle actin was detected in external ductal and lobular myoepithelium and absent in the luminal epithelial cells (Figure 5-9a, top panel). Moreover, the surrounding stromal cells stained positive for the mesenchymal marker protein vimentin and was negative for desmin (Figures 5-9a, middle and bottom panels respectively). In benign lesions, SM-actin labelling was restricted to the few preserved epithelial ducts (Figure 5-9b, top panel). Consistent with the dominant appearance of the ECM components collagen I and fibronectin in the fibrotic tissue shown in figure 8 which is consistent with the typical fibroadenoma morphology for postmenopausal patients exhibiting predominantly matric components (Kuijper, Mommers et al. 2001), vimentin is marking few stromal cells (Figure 5-9b, middle panel), while sample is negative for desmin (Figure 9b, bottom panel). Invasive cancer tissue samples showed increased SM-actin staining in an irregular pattern typical of tumor vascularization (Figure 5-9c, top panel). In addition, most of the cancer cells stained positive for both vimentin and desmin (Figures 5-9c, middle and bottom panel respectively).

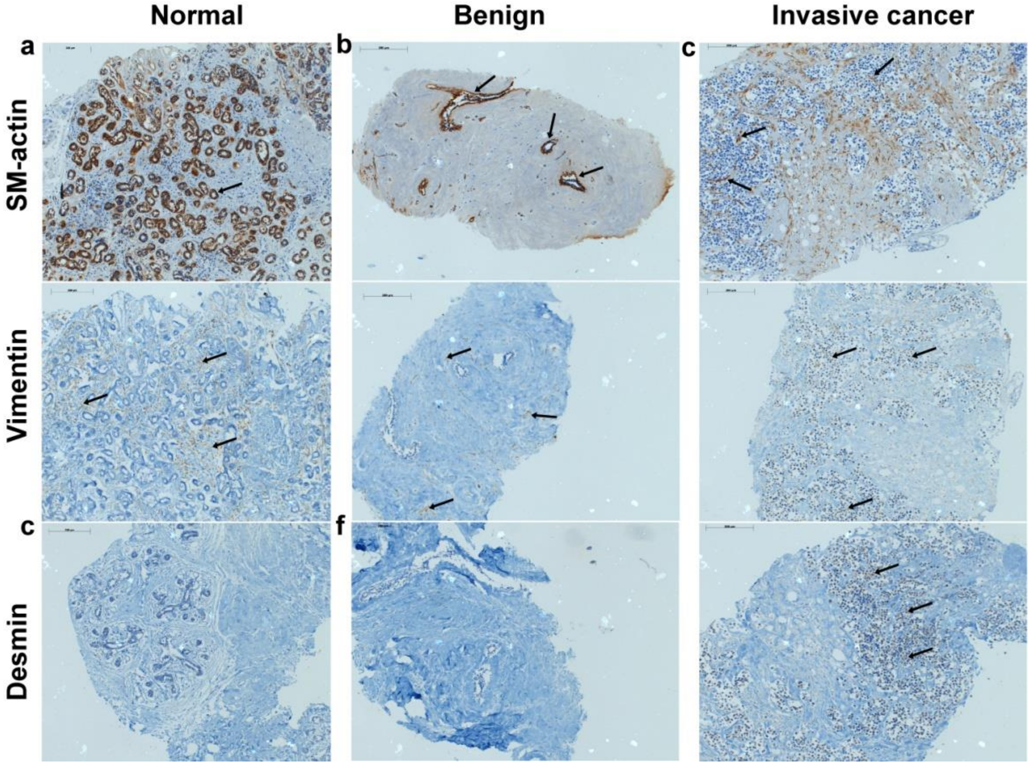

Figure 5-9. Cytoarchitecture of human biopsies. (Top panel) Smooth muscle (SM-) actin is present in the basal cell layers of glandular tissue in (a) normal mammary gland and (b) benign lesions. (c) In the invasive cancer SM-actin staining indicates myofibroblasts and an increased amount of blood vessels present at the sites of invasion (black arrows). (Middle panel) Vimentin expression is restricted to mesenchymal cells in the stroma of (a) normal mammary gland and (b) benign lesion (black arrows). A large number of malignant cells stain positive for vimentin (black arrows) in sections from (c) invasive carcinoma. (Bottom panel) Both the (a) normal gland tissue and the (b) benign lesion do not express desmin. Desmin staining is detected at infiltration sites (black arrows) in the (c) invasive cancer.

These data represent a clear indication of epithelial to mesenchymal transition of the mammary cells that is associated with malignancy and an increasingly aggressive phenotype (Zajchowski, Bartholdi et al. 2001). In particular, the large number of desmin-positive cells suggest poor differentiation and tumor aggressiveness (Ma, Peng et al. 2009). Moreover, since both intermediate filament proteins have an influence on the mechanical behaviour of cells (Plodinec et al., submitted), their abundant expression could contribute to the softening measured in invasive tumors.

5.4 Discussion

The complexity of cancer calls for improved biomarkers for the detection and analysis of the disease. This study has important implications for the use of nanomechanical properties as a novel biomarker for sensing and evaluating changes in native tumour tissues that eventually could be translated into clinical settings.

With our experimental AFM approach we can clearly distinguish between normal tissue and benign lesions such as fibroadenomas. Although both types of tissue typically exhibit a uniform stiffness that is consistent with the respective homogenous morphological appearance, the stiffness of benign lesions is significantly higher than of normal mammary gland tissue. This apparent stiffening is most likely due to fibrocystic hyperplasia which results in a high content of fibrotic tissue that extends into and alters ductal myoepithelium (RonnovJessen, Petersen et al. 1996). In contrast, nanomechanical AFM testing of 14 mammary gland tissue samples obtained from 6 MMTV-PyMT mice and 36 human biopsies demonstrates that malignant lesions are not characterized by a specific stiffness, but rather a radial gradient of stiffness that is related to the aggressive malignant phenotype.

The reports on tumor stiffness evaluation in the literature are diverging. Measurements performed on tissue biopsies by classical rheology led to the widely accepted notion that cancer tissue is generally stiffer than its surroundings (Butcher, Alliston et al. 2009). Similarly, unconfined compression testing performed by Paszek et al. (Paszek, Zahir et al. 2005) have described tumors to be stiffer than normal tissues. In addition, a recent study showed that tissue fibrosis induced by collagen crosslinking, modulated integrin activity (Levental, Yu et al. 2009) and elevated focal adhesions (Cabodi, Tinnirello et al. 2006; Madan, Smolkin et al. 2006) promotes stiffening of the tumor stroma (Levental, Yu et al. 2009). In contrast, a number of studies using different single-cell *in vitro* biomechanical assays report a decrease of stiffness in isolated cancer cells with increasing metastatic efficiency (Guck, Schinkinger et al. 2005; Suresh, Spatz et al. 2005; Darling, Zauscher et al. 2007). For example, it was recently shown by Gimzewski and co-workers. (Cross, Jin et al. 2007) that metastatic cells isolated from cancer patients exhibit 70% lower stiffness than normal cells in the same sample. However, isolated and/or cultured cells lack the complex cell-cell and cell-matrix interactions that occur in tissues. By testing fresh tissue samples we retain both tissue architecture and ECM structure. Moreover, our measurements represent a sampling of the entire tumor cross-section and thus account for the heterogeneity that is typical for tumors. Thus, our AFM stiffness data partially reconcile these discrepancies in that they do not represent a single stiffness but rather a distinct nanomechanical signature. For example, similar to the increased stiffness measured by unconfined compression (Paszek, Zahir et al. 2005), AFM testing also revealed the stromal tumor tissue at the periphery to be relatively stiff; however, the underlying tumor is considerably softer. Because cancer is extremely diverse with respect to cell morphology and biochemistry, a common stiffness modulus for all tumor regions can hardly be expected. Our data offer a new paradigm for understanding how cancer stiffness and aggressive phenotype are influenced by tumor cell heterogeneity.

Hypoxia is amongst the microenvironmental conditions that influence tumor progression by altering the expression of numerous gene products that are conducive to the survival and expansion of cancer cells in an oxygen deficient environment (Knowles and Harris 2001). These processes include angiogenesis, apoptosis, glycolysis, cell cycle control and most interestingly, migration. Our AFM measurements of MMTV-PyMT mammary tissue provide evidence that hypoxia also modulates the nanomechanical properties of cancer tissue. In particular, hypoxia-related softening appears to promote an aggressive, metastatic phenotype. Our findings support the emerging concept that the tumor microenvironment regulates biophysical properties at the cell and/or tissue level (Salaita, Nair et al. 2010). In the case of neoplastic mammary epithelial cells, the resulting downstream cellular response results in cell softening consistent with an increased metastatic potential (Fritsch, Hockel et al. 2010). Consistently, cells with a hypoxic phenotype that were spreading from the core to the periphery in invasive cancer tissues resulted in a corresponding shift of the stiffness distribution. Although we did not measure hypoxia directly in the human samples, the softness of the core suggests that these areas are also hypoxic.

Recently, it has been suggested that modification of the tumor microenvironment through ECM stiffening induced by lysyl oxidase (LOX) mediated collagen crosslinking promotes tumor invasiveness and metastasis (Levental, Yu et al. 2009). Hypoxia upregulates LOX expression and most of all, its catalytic activity which results in a degradation of collagen and drives poorly invasive breast cancer cells toward a more aggressive phenotype (Postovit, Abbott et al. 2008; Kakkad, Solaiyappan et al. 2010). It has been reported previously that hypoxia, through remodelling of ECM and the cytoskeleton (Erler, Bennewith et al. 2006) influences cell stiffness, and that these stiffness changes promote cell invasion and metastasis. We noted prominent degradation of collagen and fibronectin rather than an increase in fibrillar collagen in regions with a high abundance of cancer cells. Similarly, MMP-dependent ECM degradation has been reported to accompany cancer progression

(Page-McCaw, Ewald et al. 2007). Our data indicate a strong correlation between hypoxia, collagen degradation, and tissue softening in invasive carcinomas, although we measured a ~15-fold increase in stiffness in the tumor stroma adjacent to hypoxic cells. It is conceivable that hypoxia-related tissue softening rather the ECM stiffening promotes tumor progression. The presence of lung metastases in MMTV-PyMT mice that have retained their hypoxic phenotype provides further support for this notion.

It is well known that hypoxia induces tumor angiogenesis via chemical and possibly mechanical signals (Shweiki, Itin et al. 1992; Liu and Agarwal 2010). Accordingly, we observed an elevated SM-actin expression in invasive carcinomas. At the same time, hypoxia promotes tumor cell invasiveness which entails that cells cross the endothelial basement membrane during entry into and exit from blood vessels. At the transition from *in situ* to invasive carcinoma, structural degradation of the basement membrane is observed microscopically which coincides with tumour cell invasion. Breaking of the basement membrane as the "last line of defence" before the tumor will spread (Liotta, Tryggvason et al. 1980) most likely causes an additional increase in regional tissue softening and contributes to overall stiffness heterogeneity. Consistently, hypoxic cells were detected not only in the core but also near blood vessels in invasive carcinomas, adding to the characteristic heterogeneous stiffness pattern.

By making originally layered epithelial cells behave like motile fibroblasts, epithelial-mesenchymal transition (EMT) and overexpression of mesenchymal markers are key elements in tumor progression (Frixen, Behrens et al. 1991). Expression of vimentin and desmin dramatically increased with the tumor progression both in MMTV-PyMT mice and human biopsies, thereby contributing to the heterogeneous stiffness phenotype. Coexpression of vimentin and desmin indicates cellular de-differentiation (Franke, Schmid et al. 1981) which might be conducive to adaptation to hypoxia. Expression and behavior of these markers during EMT on the other hand are affected by hypoxia (Mani, Guo et al. 2008). This might explain how the aggressive hypoxic phenotype is maintained even in well oxygenated environment such as blood vessels and lungs.

The exact mechanisms that regulate invasive behaviour are still not well understood. Nevertheless, our data provide evidence that hypoxia-induced changes in the mechanical response of cancer cells are essential for tumor invasion.

5.5 Conclusions and perspectives

The data of this study provide evidence that the soft hypoxic phenotype plays a key role in cancer progression Comparison of the nanomechanical signature of human tissue samples with the corresponding histopathological diagnosis suggests a high ratio of soft versus stiff regions to be an indication of a more aggressive phenotype. The heterogeneity of tumor stiffness was found to be associated with the degradation of ECM components and overexpression of mesenchymal markers, both of which are signs of hypoxia.. To gain insight into the molecular mechanisms by which hypoxia modulates the nanomechanical response of tissues, one need to elucidate and compare genetic profiles of both mouse and human tissues at all stages of tumor progression.

Last, but not least, the ability to detect hypoxia-induced structural and mechanical changes during cancer progression in mouse and patient tissues at the nanometer scale by AFM has opened up the exciting prospect of developing a simple nanodevice into a clinical tool.

5.6 Acknowledgements

The authors thank Sandro Erni and Benjamin Bircher for their help with AFM measurements of human breast tissue biopsies.

5.7 References

Butcher, D. T., T. Alliston, et al. (2009). "A tense situation: forcing tumour progression." Nature Reviews Cancer **9**(2): 108-122.

Cabodi, S., A. Tinnirello, et al. (2006). "p130Cas as a new regulator of mammary epithelial cell proliferation, survival, and HER2-Neu oncogene-dependent breast tumorigenesis." Cancer Research **66**(9): 4672-4680.

Cross, S. E., Y. S. Jin, et al. (2007). "Nanomechanical analysis of cells from cancer patients." Nature Nanotechnology **2**(12): 780-783.

Darling, E. M., S. Zauscher, et al. (2007). "A thin-layer model for viscoelastic, stress-relaxation testing of cells using atomic force microscopy: Do cell properties reflect metastatic potential?" Biophysical Journal **92**(5): 1784-1791.

Denko, N., C. Schindler, et al. (2000). "Epigenetic regulation of gene expression in cervical cancer cells by the tumor microenvironment." Clinical Cancer Research **6**(2): 480-487.

Erler, J. T., K. L. Bennewith, et al. (2006). "Lysyl oxidase is essential for hypoxia-induced metastasis." Nature **440**(7088): 1222-1226.

Franke, W. W., E. Schmid, et al. (1981). "Differentiation-Related Patterns of Expression of Proteins of Intermediate-Size Filaments in Tissues and Cultured-Cells." Cold Spring Harbor Symposia on Quantitative Biology **46**: 431-453.

Fritsch, A., M. Hockel, et al. (2010). "Are biomechanical changes necessary for tumour progression?" Nature Physics **6**(10): 730-732.

Frixen, U. H., J. Behrens, et al. (1991). "E-Cadherin-Mediated Cell Cell-Adhesion Prevents Invasiveness of Human Carcinoma-Cells." Journal of Cell Biology **113**(1): 173-185.

Giaccia, A. J., C. Koumenis, et al. (1999). "The influence of tumor hypoxia on malignant progression." Tumor Hypoxia: 115-124

Giatromanolaki, A. and A. L. Harris (2001). "Tumour hypoxia, hypoxia signaling pathways and hypoxia inducible factor expression in human cancer." Anticancer Research **21**(6B): 4317-4324.

Graeber, T. G., C. Osmanian, et al. (1996). "Hypoxia-mediated selection of cells with diminished apoptotic potential in solid tumours." Nature **379**(6560): 88-91.

Guck, J., S. Schinkinger, et al. (2005). "Optical deformability as an inherent cell marker for testing malignant transformation and metastatic competence." Biophysical Journal **88**(5): 3689-3698.

Guppy, M. (2002). "The hypoxic core: a possible answer to the cancer paradox." Biochemical and Biophysical Research Communications **299**(4): 676-680.

Helmlinger, G., F. Yuan, et al. (1997). "Interstitial pH and pO(2) gradients in solid tumors in vivo: High-resolution measurements reveal a lack of correlation." Nature Medicine **3**(2): 177-182.

Higgins, D. F., K. Kimura, et al. (2007). "Hypoxia promotes fibrogenesis in vivo via HIF-1 stimulation of epithelial-to-mesenchymal transition." Journal of Clinical Investigation **117**(12): 3810-3820.

Ingber, D. E., L. Dike, et al. (1994). "Cellular Tensegrity - Exploring How Mechanical Changes in the Cytoskeleton Regulate Cell-Growth, Migration, and Tissue Pattern during Morphogenesis." International Review of Cytology - a Survey of Cell Biology, Vol 150 **150**: 173-224.

Janmey, P. A. (1998). "The cytoskeleton and cell signaling: Component localization and mechanical coupling." Physiological Reviews **78**(3): 763-781.

Kakkad, S. M., M. Solaiyappan, et al. (2010). "Hypoxic Tumor Microenvironments Reduce Collagen I Fiber Density." Neoplasia **12**(8): 608-617.

Kass, L., J. T. Erler, et al. (2007). "Mammary epithelial cell: Influence of extracellular matrix composition and organization during development and tumorigenesis." International Journal of Biochemistry & Cell Biology **39**(11): 1987-1994.

Knowles, H. J. and A. L. Harris (2001). "Hypoxia and oxidative stress in breast cancer - Hypoxia and tumourigenesis." Breast Cancer Research **3**(5): 318-322.

Koong, A. C., N. C. Denko, et al. (2000). "Candidate genes for the hypoxic tumor phenotype." Cancer Research **60**(4): 883-887.

Kuijper, A., E. C. M. Mommers, et al. (2001). "Histopathology of fibroadenoma of the breast." American Journal of Clinical Pathology **115**(5): 736-742.

Kumar, S. and V. Weaver (2009). "Mechanics, malignancy, and metastasis: The force journey of a tumor cell." Cancer and Metastasis Reviews **28**(1-2): 113-127.

Lal, A., H. Peters, et al. (2001). "Transcriptional response to hypoxia in human tumors." Journal of the National Cancer Institute **93**(17): 1337-1343.

Lam, W. A., M. J. Rosenbluth, et al. (2007). "Chemotherapy exposure increases leukemia cell stiffness." Blood **109**(8): 3505-3508.

Lekka, M., P. Laidler, et al. (1999). "Elasticity of normal and cancerous human bladder cells studied by scanning force microscopy." European Biophysics Journal with Biophysics Letters **28**(4): 312-316.

Levental, K. R., H. M. Yu, et al. (2009). "Matrix Crosslinking Forces Tumor Progression by Enhancing Integrin Signaling." Cell **139**(5): 891-906.

Lin, E. Y., J. G. Jones, et al. (2003). "Progression to malignancy in the polyoma middle T oncoprotein mouse breast cancer model provides a reliable model for human diseases." American Journal of Pathology **163**(5): 2113-2126.

Liotta, L. A., K. Tryggvason, et al. (1980). "Metastatic Potential Correlates with Enzymatic Degradation of Basement-Membrane Collagen." Nature **284**(5751): 67-68.

Liu, J. and S. Agarwal (2010). "Mechanical Signals Activate Vascular Endothelial Growth Factor Receptor-2 To Upregulate Endothelial Cell Proliferation during Inflammation." Journal of Immunology **185**(2): 1215-1221.

Liu, T. G., O. E. Guevara, et al. (2010). "Regulation of vimentin intermediate filaments in endothelial cells by hypoxia." American Journal of Physiology-Cell Physiology **299**(2): C363-C373.

Ma, Y. L., J. Y. Peng, et al. (2009). "Proteomics Identification of Desmin as a Potential Oncofetal Diagnostic and Prognostic Biomarker in Colorectal Cancer." Molecular & Cellular Proteomics **8**(8): 1878-1890.

Madan, R., M. B. Smolkin, et al. (2006). "Focal adhesion proteins as markers of malignant transformation and prognostic indicators in breast carcinoma." Human Pathology **37**(1): 9-15.

Mani, S. A., W. Guo, et al. (2008). "The epithelial-mesenchymal transition generates cells with properties of stem cells." Cell **133**(4): 704-715.

Munoz-Najar, U. M., K. M. Neurath, et al. (2006). "Hypoxia stimulates breast carcinoma cell invasion through MT1-MMP and MMP-2 activation." Oncogene **25**(16): 2379-2392.

Needham, D. (1991). "Possible Role of Cell Cycle-Dependent Morphology, Geometry, and Mechanical-Properties in Tumor-Cell Metastasis." Cell Biophysics **18**(2): 99-121.

Page-McCaw, A., A. J. Ewald, et al. (2007). "Matrix metalloproteinases and the regulation of tissue remodelling." Nature Reviews Molecular Cell Biology **8**(3): 221-233.

Park, C. C., M. J. Bissell, et al. (2000). "The influence of the microenvironment on the malignant phenotype." Molecular Medicine Today **6**(8): 324-329.

Park, J. E., H. Sen Tan, et al. (2010). "Hypoxic Tumor Cell Modulates Its Microenvironment to Enhance Angiogenic and Metastatic Potential by Secretion of Proteins and Exosomes." Molecular & Cellular Proteomics **9**(6): 1085-1099.

Paszek, M. J. and V. M. Weaver (2004). "The tension mounts: Mechanics meets morphogenesis and malignancy." Journal of Mammary Gland Biology and Neoplasia **9**(4): 325-342.

Paszek, M. J., N. Zahir, et al. (2005). "Tensional homeostasis and the malignant phenotype." Cancer Cell **8**(3): 241-254.

Postovit, L. M., D. E. Abbott, et al. (2008). "Hypoxia/reoxygenation: A dynamic regulator of lysyl oxidase-facilitated breast cancer migration." Journal of Cellular Biochemistry **103**(5): 1369-1378.

RonnovJessen, L., O. W. Petersen, et al. (1996). "Cellular changes involved in conversion of normal to malignant breast: Importance of the stromal reaction." Physiological Reviews **76**(1): 69-125.

Rosenbluth, M. J., W. A. Lam, et al. (2006). "Force microscopy of nonadherent cells: A comparison of leukemia cell deformability." Biophysical Journal **90**(8): 2994-3003.

Saenz-Morales, D., M. M. Escribese, et al. (2006). "Requirements for proximal tubule epithelial cell detachment in response to ischemia: Role of oxidative stress." Experimental Cell Research **312**(19): 3711-3727.

Salaita, K., P. M. Nair, et al. (2010). "Restriction of Receptor Movement Alters Cellular Response: Physical Force Sensing by EphA2." Science **327**(5971): 1380-1385.

Shweiki, D., A. Itin, et al. (1992). "Vascular Endothelial Growth-Factor Induced by Hypoxia May Mediate Hypoxia-Initiated Angiogenesis." Nature **359**(6398): 843-845.

Sinkus, R., J. Lorenzen, et al. (2000). "High-resolution tensor MR elastography for breast tumour detection." Physics in Medicine and Biology **45**(6): 1649-1664.

Suresh, S. (2007). "Biomechanics and biophysics of cancer cells." Acta Materialia **55**(12): 3989-4014.

Suresh, S., J. Spatz, et al. (2005). "Connections between single-cell biomechanics and human disease states: gastrointestinal cancer and malaria." Acta Biomaterialia **1**(1): 15-30.

Tatum, J. L., G. J. Kelloff, et al. (2006). "Hypoxia: Importance in tumor biology, noninvasive measurement by imaging, and value of its measurement in the management of cancer therapy." International Journal of Radiation Biology **82**(10): 699-757.

Tredan, O., C. M. Galmarini, et al. (2007). "Drug resistance and the solid tumor microenvironment." Journal of the National Cancer Institute **99**(19): 1441-1454.

Vaupel, P. and L. Harrison (2004). "Tumor hypoxia: Causative factors, compensatory mechanisms, and cellular response." Oncologist **9**: 4-9.

Ward, K. A., W. I. Li, et al. (1991). "Viscoelastic Properties of Transformed-Cells - Role in Tumor-Cell Progression and Metastasis Formation." Biorheology **28**(3-4): 301-313.

Williams, K. J., B. A. Telfer, et al. (2002). "A protective role for HIF-1 in response to redox manipulation and glucose deprivation: implications for tumorigenesis." Oncogene **21**(2): 282-290.

Wojciak-Stothard, B., L. Y. F. Tsang, et al. (2006). "Rac1 and RhoA as regulators of endothelial phenotype and barrier function in hypoxia-induced neonatal pulmonary hypertension." American Journal of Physiology-Lung Cellular and Molecular Physiology **290**(6): L1173-L1182.

Zajchowski, D. A., M. F. Bartholdi, et al. (2001). "Identification of gene expression profiles that predict the aggressive behavior of breast cancer cells." Cancer Research **61**(13): 5168-5178.

Chapter 6

Conclusions and perspectives

6.1 Atomic force microscopy for biological imaging and mechanical testing across length scales

The atomic force microscope (AFM) offers the researcher a unique opportunity to visualize, manipulate, and quantitatively assess structural and mechanical aspects of native biological samples with nanometer resolution (Bustamante, Rivetti et al. 1997; Fotiadis, Scheuring et al. 2002) An exceptional advantage of the AFM over other high-resolution microscopes is that biological specimens, ranging from tissues to cells and even individual molecules, can be investigated in physiologically relevant aqueous environments (Kasas, Thomson et al. 1997). Combining an light microscope (LM) with an AFM makes it possible to directly correlate structural/nanomechanical changes with optical/fluorescence images and provides a powerful tool to address nanomechanical and biochemical effects simultaneously(Lehenkari, Charras et al. 2000) (Figure 6-1).

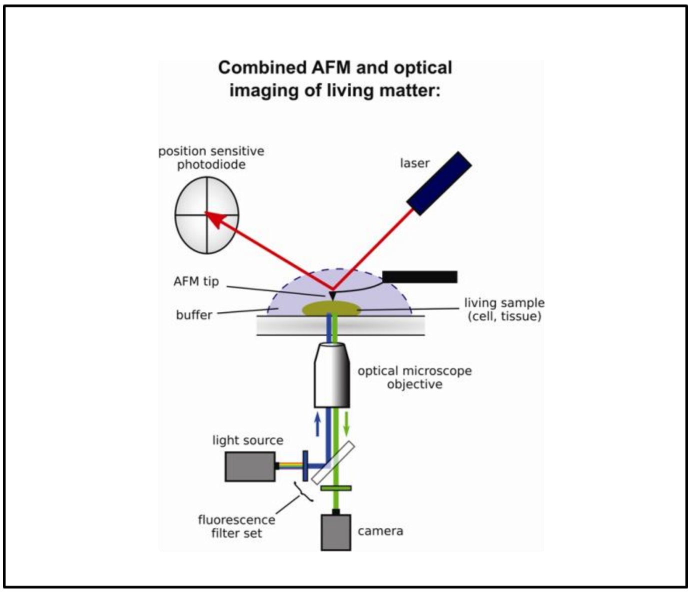

Figure 6-1. Schematic of the LM-AFM setup. The AFM is mounted on inverted optical microscope equipped with high resolution objective. Illumination with a light source together with fluorescence filters allow for simultaneous fluorescence microscopy that is recorded via a CCD camera. The AFM probe scans the surface of living samples (cells, tissues) maintained in buffer culture medium. Surface corrugations are recorded from a laser beam that is reflected from the spring (cantilever) onto a photodetector.

We have used cartilage tissue, live fibroblast cells and individual collagen assemblies to demonstrate how AFM is applicable to a diversity of biological studies (Chapter 2).

Future technical developments in novel microscope elements, such as high speed AFM, AFM sensing and actuation, and new fluorescence dyes will open new avenues in biomedicine and nanoscience.

6.2 The nanomechanical properties of rat fibroblasts are modulated by interfering with the vimentin intermediate filament system.

The contribution of the intermediate filament (IF) network to the mechanical response of cells has so far received little attention, possibly because the assembly and regulation of IFs are not as well understood as that of the actin cytoskeleton or of microtubules (Herrmann, Bar et al. 2007). The mechanical role of IFs has been mostly inferred from measurements performed on individual filaments or gels *in vitro* (Kreplak and Fudge 2007; Wagner, Rammensee et al. 2007).

These observations prompted us to explore the contribution of vimentin IFs to the nanomechanical properties of living cells by employing AFM under native conditions (Chapter 3). To specifically target and modulate the vimentin network, Rat-2 fibroblasts were transfected with GFP-desmin variants. By using a combination of AFM and optical microscopy, we were able to identify cells transfected with desmin variants and measure their nanomechanical properties in direct comparison to untransfected cells at high spatial resolution. Depending on the variant desmin, transfectants were either softer or stiffer than untransfected fibroblasts. Expression of the non-filament forming GFP-DesL345P mutant led to a collapse of the endogenous vimentin network in the perinuclear region that was accompanied by localized stiffening. Correlative confocal microscopy indicated that the expression of desmin variants specifically targets the endogenous vimentin IF network without major rearrangements of other cytoskeletal components. Our study demonstrated that the alterations in the IF filament structure and architecture have a direct impact on the nanomechanical properties of living cells.

Taken together, our data show that IFs play an important role in cell mechanical response not only at large deformations, but they can contribute to the mechanical properties also at the nanometer scale. Moreover, this indicates that molecular changes at the single cell level, which are frequently associated with disease (Omary 2009), trigger specific nanomechanical responses. Hence, future studies should aim at elucidating the mechano-signalling pathways that regulate the nanomechanical behaviour of IFs in related diseases.

6.3 Hypoxia induced changes in morphology and cytoarchitecture regulate nanomechanical properties of tumor spheroids

Biochemical, environmental, and structural factors determine the mechanical form and function of cells. A disease such as cancer, which results from perturbations in these factors, underscores the importance of correlating inter- and intra-cellular effects to the mechanical properties of cells (Suresh 2007). Interpretation of experimental *in vitro* and *in vivo* tumor models is largely based on two-dimensional (2D) cultures which at best, only marginally represent the physiological environments encountered by a cell in a living organism (Pampaloni, Reynaud et al. 2007).

Thus, our objective was to study tumorigenesis and its effects by correlating changes in cell cytoarchitecture and extracellular matrix (ECM) to the mechanical properties of cells. For this purpose, we employed AFM in combination with light microscopy to probe the nanomechanical properties of cells cultured in two-dimensional (2D) monolayer versus three-dimensional (3D) spheroid culture conditions (Chapter 4). Nanomechanical testing of living Rat2 fibroblasts and Rat2sm9, a derivative which has been rendered tumorigenic by expression of a Gly245Asp actin mutant (Leavitt, Ng et al. 1987), reveal that modification of the cytoskeleton did not alter the stiffness of the transformed cells. By culturing cells as 3D spheroids, we have shown that normal spheroids exhibit uniform stiffness distribution, while tumor spheroids exhibited a gradual softening from the periphery to the core consistent with the reduction of filamentous actin and vimentin and fibrillar collagen I in the core. Moreover, the core region was significantly softer than that of normal spheroids. Consistently, increased HIF (hypoxia inducible factor) -1α signal in the core of tumor spheroids indicated extensive hypoxia compared to normal spheroids. To specifically examine the influence of hypoxia on spheroid nanomechanics and associated cytoskeleton and extracellular matrix (ECM) changes, we cultured spheroids under hypoxic conditions. This has triggered only tumor, but not normal spheroids, to disseminate and differentially affected their mechanical properties. Our findings suggest that a hypoxia-induced decrease in cell stiffness favours the dissemination of tumor cells.

We are now facing the challenge of elucidating the key molecular mechanisms by which mechanical force and hypoxia regulate tumor progression in human tissues (Semenza 2008). Also, further developments of 3D *in vitro* systems to study cancer cell interactions with other cells from the vasculature or immune system or even to study 3D cell behaviour in a well-controlled gradient of growth factors or chemokine are crucial. By resolving these issues we will be able to gain a detailed understanding of the interactions between cancer cells and their physical and biochemical environment which are essential for the development of novel cancer therapies.

6.4 The nanomechanical signature of hypoxia-induced breast cancer progression in mice and human patient samples

Emerging evidence indicates that the effect of hypoxia on tumor progression is mediated by a series of hypoxia-induced genetic and proteomic changes that enable tumor cells to survive or escape their oxygen-deficient environment (Semenza 2007). Conceivably, the mechanical response of cancer cells within the tumor tissue might also vary considerably in response to environmental conditions and thus affect the progression of malignancy. Despite the unique potential of the AFM to probe tissue nanomechanics under physiological conditions (Stolz, Gottardi et al. 2009), this technique has so far not been applied to intact tumor tissues, which the most appropriately reflect the *in vivo* characteristics of cancer.

To test the feasibility of AFM nanomechanical testing on organized tissues, we probed with high sensitivity nanomechanical properties of fresh breast biopsies obtained from human patients and MMTV-PyMT (mouse mammary tumor virus-polyoma middle-T antigen) transgenic mice (Guy, Cardiff et al. 1992) (Chapter 5). AFM stiffness maps revealed a gradual softening from the periphery to the core in human and murine cancer tissues while stromal tissue at the tumor periphery was stiffer than the underlying tumor. Hypoxia staining of murine tissues confirmed that the core of carcinomas *in situ* exhibited extensive hypoxia compared to normal mammary gland and AFM stiffness measurements revealed a correlation between tissue softening and hypoxia. We established that the heterogeneity of tumor stiffness is associated with the degradation of ECM components and overexpression of mesenchymal markers, both of which are signs of hypoxia. Remarkable finding was that at late stages of tumor progression, the soft and hypoxic phenotypes were increasingly present at the tumor periphery and even distant metastatic lesions in the lung displayed a hypoxic phenotype.

Comparison of the nanomechanical signature of human tissue samples with the corresponding histopathological diagnosis suggested a high ratio of soft versus stiff regions to be an indication of a more aggressive phenotype. This confirms our hypothesis that the soft hypoxic phenotype plays a key role in cancer progression. Finally, the exceptional ability to detect hypoxia-induced structural and mechanical changes during cancer progression in mouse and patient tissues at the nanometer scale by AFM has opened up the exciting prospect of developing a simple nanodevice into a diagnostic tool.

6.5 Summary and perspectives

The work presented in this thesis provides essential insights into the role of microenvironment on cell and tissue mechanical responses in healthy and diseased state. Combining the AFM with an optical microscope allowed us directly correlate structural with nanomechanical changes in individual cells and 3D tissue cultures. A natural progression of our AFM work involved studying human carcinoma, where we measured the stiffness profiles (absolute value, distribution) of intact human breast tumor biopsies with a force sensitivity and spatial resolution that is unmatched by any state-of-the-art technique. This is underscored by our results, where we discovered that malignant lesions are characterized by a gradient of stiffness relating to the degree of malignancy. While we have shown that the above mentioned findings are in agreement with the conventional form of diagnosis such as histology (Figure 6-2), the use of AFM technology in cancer diagnostics is advantageous with regards to expediting disease detection and may provide additional pre-symptomatic information relevant to prognosis of disease and treatment which is not possible by current methods. This is critical given that standard histological diagnostics is very slow (a few days are needed for diagnosis per patient) and requires extensive experience and training in the field.

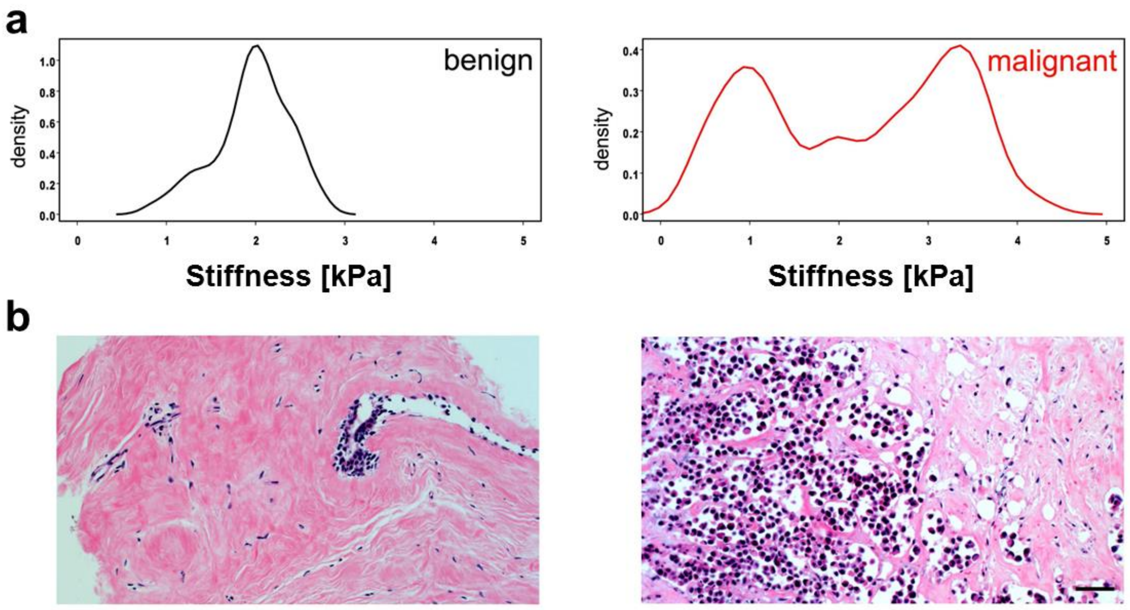

Figure 6-2. Nanomechanical response as diagnostic feature. (a) AFM stiffness distribution of benign breast lesions (left panel) exhibit a similar stiffness over the probed area, whereas malignant specimens (right panel) are characterized by a bimodal stiffness distribution. (b) Histological examination of the corresponding

specimen revealed that the uniform stiffness correlates with the rather homogenous histology typical for benign lesions. In this case, stromal tissue and lobules are present (left panel). Two distinct peak stiffness values are detected in the malignant lesion (right panel). In this poorly differentiated invasive carcinoma, areas dominated by tumor cells, which infiltrate in a cord-like pattern and they are softer than the dense fibrotic tissue in the periphery. Scale bar, 200µm.

By translating fundamental insights from this work into the development of an Automated and Reliable Tissue Diagnostic Tool (ARTIDIS), promises to revolutionize tissue diagnostics based on its sensitivity, accuracy, unbiased detection and bench to the clinic “ease-to-use” applicability.

6.6 References

Bustamante, C., C. Rivetti, et al. (1997). "Scanning force microscopy under aqueous solutions." Current Opinion in Structural Biology **7**(5): 709-716.

Fotiadis, D., S. Scheuring, et al. (2002). "Imaging and manipulation of biological structures with the AFM." Micron **33**(4): 385-397.

Guy, C. T., R. D. Cardiff, et al. (1992). "Induction of Mammary-Tumors by Expression of Polyomavirus Middle T-Oncogene - a Transgenic Mouse Model for Metastatic Disease." Molecular and Cellular Biology **12**(3): 954-961.

Herrmann, H., H. Bar, et al. (2007). "Intermediate filaments: from cell architecture to nanomechanics." Nature Reviews Molecular Cell Biology **8**(7): 562-573.

Kasas, S., N. H. Thomson, et al. (1997). "Biological applications of the AFM: From single molecules to organs." International Journal of Imaging Systems and Technology **8**(2): 151-161.

Kreplak, L. and D. Fudge (2007). "Biomechanical properties of intermediate filaments: from tissues to single filaments and back." Bioessays **29**(1): 26-35.

Leavitt, J., S. Y. Ng, et al. (1987). "Expression of Transfected Mutant Beta-Actin Genes - Transitions toward the Stable Tumorigenic State." Molecular and Cellular Biology **7**(7): 2467-2476.

Lehenkari, P. P., G. T. Charras, et al. (2000). "Adapting atomic force microscopy for cell biology." Ultramicroscopy **82**(1-4): 289-295.

Omary, M. B. (2009). ""IF-pathies": a broad spectrum of intermediate filament-associated diseases." Journal of Clinical Investigation **119**(7): 1756-1762.

Pampaloni, F., E. G. Reynaud, et al. (2007). "The third dimension bridges the gap between cell culture and live tissue." Nature Reviews Molecular Cell Biology **8**(10): 839-845.

Semenza, G. L. (2007). "Hypoxia and cancer." Cancer and Metastasis Reviews **26**(2): 223-+.

Semenza, G. L. (2008). "Hypoxia, HIF-1, and cancer." Clinical & Experimental Metastasis **25**: 20-20.

Stolz, M., R. Gottardi, et al. (2009). "Early detection of aging cartilage and osteoarthritis in mice and patient samples using atomic force microscopy." Nature Nanotechnology **4**(3): 186-192.

Suresh, S. (2007). "Biomechanics and biophysics of cancer cells." Acta Biomaterialia **3**(4): 413-438.

Wagner, O. I., S. Rammensee, et al. (2007). "Softness, strength and self-repair in intermediate filament networks." Experimental Cell Research **313**(10): 2228-2235.

Apendix

Plodinec and Schoenenberger *Breast Cancer Research* 2010, **12**:308
http://breast-cancer-research.com/content/12/4/308

Breast Cancer
RESEARCH

VIEWPOINT

Spatial organization acts on cell signaling: how physical force contributes to the development of cancer

Marija Plodinec and Cora-Ann Schoenenberger*

Abstract

Cells constantly encounter physical forces and respond to neighbors and circulating factors by triggering intracellular signaling cascades that in turn affect their behavior. The mechanisms by which cells transduce mechanical signals to downstream biochemical changes are not well understood. In their work, Salaita and coworkers show that the spatial organization of cell surface receptors is crucial for mechanotransduction. Consequently, force modulation that disrupts the mechanochemical coupling may represent a critical step in cancerogenesis.

Background

The ability of cells to respond to mechanical signals from the environment plays an essential role in a myriad of biologically relevant functions such as cell migration [1], growth and differentiation [2]. In general, we can differentiate cellular responses to physical force into a purely mechanical response predominantly consisting of the cell's load-bearing deformation of cytoskeletal structures [3], and into biochemical signaling cascades where force propagation is relayed through membrane proteins or protein complexes to intracellular chemical signaling networks. Alterations in mechanotransduction often result in diseases such as cancer [4], arthritis [5] or atherosclerosis [6]. Resolving the mechanisms underlying mechanochemical coupling is therefore of fundamental importance.

One emerging mechanism through which mechanical forces may affect downstream signal transduction pathways involves the spatial organization of cell surface receptors [7]. A special case is that of juxtacrine interactions; for example, ephrin-A1 on one cell binds to EphA2 receptor tyrosine kinase on the apposed cell surface, which will induce assembly of higher-order clusters that trigger bidirectional signaling cascades in interacting cells [8,9]. Because EphA2 is overexpressed in 40% of mammary carcinomas and is functionally impaired in many other types of cancer [10], unveiling the mechanism by which the spatial organization of EphA2 receptors can affect the downstream cellular response to ephrin ligands is essential. Recent advances using nanolithography provide new insights into how the ephrin–Eph signaling system responds to different mechanical aspects of interacting cells [11]. These findings represent an important step towards understanding mechanochemical coupling and give us a glimpse into the significance of mechanical force in health and disease.

Article

In their recent study, Salaita and colleagues have established a procedure for investigating spatiomechanical concepts involved in the EphA2 signaling pathway [11]. The authors managed to reconstitute *in vitro* the juxtacrine signaling geometry between living cells expressing the EphA2 receptor tyrosine kinase and the laterally mobile ephrin-A1 ligand displayed on a fluid lipid bilayer supported on a glass substrate. Furthermore, by employing nanolithography the researchers were able to set physical barriers to the ligand mobility on the supported membrane. Their work shows that the mechanical ligand restriction extends to the spatial organization of EphA2 receptor at cell surface junctions and alters the cellular response to ephrin-A1.

Salaita and coworkers scrutinized two experimental conditions: one in which EphA2-expressing cells are interacting with ephrin-A1 ligand that has an unrestricted lateral mobility on a fully saturated lipid bilayer, and a second where ephrin is presented on a fluid membrane that is physically constrained by an underlying pattern of nanofabricated metal lines. In the first scenario, ephrin-A1–EphA2 interaction triggered spatial reorganization of the receptor on the cell membrane into

---

*Correspondence: Cora-ann.schoenenberger@unibas.ch
M.E.Müller Institute for Structural Biology, Biozentrum, University of Basel, Klingelbergstrasse 50/70, CH-4056 Basel/Switzerland

microclusters that undergo inward radial transport. In contrast, when the cells expressing EphA2 receptors contact what the authors call spatial mutations, the receptor and associated signaling molecules became equally constrained as the boundaries impede radial transport of Eph–ephrin microclusters. Local receptor activation, however, occurred irrespective of the substrate geometry.

Total internal reflection microscopy tracking of unrestricted fluorescently labeled ephrin-A1 and green fluorescent protein-labeled actin revealed an annular association of F-actin with the EphA2 clusters. Moreover, actomyosin contractility was shown to be the driving force of radial cluster movement. Consistent with an association of F-actin with EphA2, restriction of receptor movement changed the cytoskeleton to a spread morphology with filamentous actin predominantly concentrated in lamellopodia at the cell periphery.

To establish whether the propensity to radially transport the EphA2 receptor can be used to characterize breast cancer cell lines, Salaita and colleagues determined a radial distribution function for 26 mammary cancer cell lines with different molecular and phenotypic signatures in neoplasia. The spatial organization phenotypes were then correlated with genomic and proteomic data available from these lines. There was no correlation to the mRNA and protein expression levels of EphA2; however, an association between radial EphA2 transport and signaling pathways that are associated with invasiveness – such as ErbB, p53, integrin and mitogen-activated protein kinase – became apparent. In addition, more aggressive cell lines exhibited larger complex clusters. The authors conclude that the spatial organization of the EphA2 receptor, which is modulated by mechanical aspects of the microenvironment, could serve as a marker for cancer progression.

Viewpoint

By mechanically restricting the movement of cell surface molecules, Salaita and coworkers have convincingly shown that external physical forces alone are sufficient to modify downstream cellular activities. In their system, the EphA2/ephrin-A1 complex acts as a force sensor that, by radial movement and molecular clustering, transduces mechanical signals from the environment to a chemical response of the cell. Notably, the signaling pathways affected upon force modulation are those that play a role in the onset and progression of cancer.

Specific physical parameters of the environment, such as the texture or geometry of the surrounding tissue, have previously been shown to be important phenotypic determinants of mammalian cells [12]. Given the sensitivity to mechanical restriction displayed by the EphA2/ephrin-A1 signaling complexes, one could imagine that force measurements in general could be valuable markers for tumor characterization. Consistent with this notion, recent findings emphasize force being a key factor in cancer progression [13]. The kind and length scale of forces a cell needs to experience to first transform into a cancer cell and later on assume a more aggressive phenotype, however, remains an enigma.

In the near future we will hopefully learn about the fine-tuning of mechanical stimuli that promote a switch from the normal to the malignant phenotype and *vice versa*. Considering that the force-sensing mechanisms could be sites for therapeutic intervention, the relevance of gaining knowledge on mechanotransduction is more than obvious. Moreover, by resolving the downstream signaling pathways involved in a mechanically induced switch of phenotype, targets for anti-cancer therapeutic agents that can counteract the applied force might be identified. Possibly, drugs that are administered for other diseases could act on the mechanical coupling step as well.

In conclusion, linking mechanical aspects to biochemical approaches is a promising way to gain knowledge on tumorigenesis, and thus opens new avenues for cancer therapies in the future.

Competing interests

The authors declare that they have no competing interests.

Acknowledgements

The authors are supported by the National Center of Competence in Research Nanoscale Science, the Swiss National Science Foundation, and the M.E. Müller Foundation.

Published: 23 August 2010

References

1. Janmey PA, McCulloch CA: **Cell mechanics: integrating cell responses to mechanical stimuli.** *Annu Rev Biomed Eng* 2007, **9**:1-34.
2. Discher DE, Janmey P, Wang YL: **Tissue cells feel and respond to the stiffness of their substrate.** *Science* 2005, **310**:1139-1143.
3. Kasza KE, Rowat AC, Liu J, Angelini TE, Brangwynne CP, Koenderink GH, Weitz DA: **The cell as a material.** *Curr Opin Cell Biol* 2007, **19**:101-107.
4. Paszek MJ, Zahir N, Johnson KR, Lakins JN, Rozenberg GI, Gefen A, Reinhart-King CA, Margulies SS, Dembo M, Boettiger D, Hammer DA, Weaver VM: **Tensional homeostasis and the malignant phenotype.** *Cancer Cell* 2005, **8**:241-254.
5. Millward-Sadler SJ, Wright MO, Lee H-S, Caldwell H, Nuki G, Salter DM: **Altered electrophysiological responses to mechanical stimulation and abnormal signalling through $\alpha_5\beta_1$ integrin in chondrocytes from osteoarthritic cartilage.** *Osteoarthritis Cartilage* 2000, **8**:272-278.
6. Hahn C, Schwartz MA: **The role of cellular adaptation to mechanical forces in atherosclerosis.** *Arterioscler Thromb Vasc Biol* 2008, **28**:2101-2107.
7. Shen K, Thomas VK, Dustin ML, Kam LC: **Micropatterning of costimulatory ligands enhances CD4$^+$ T cell function.** *Proc Natl Acad Sci U S A* 2008, **105**:7791-7796.
8. Qi Murai KK, Pasquale EB: **'Eph'ective signaling: forward, reverse and crosstalk.** *J. Cell Sci* 2003, **116**:2823-2832.
9. Marquardt T, Shirasaki R, Ghosh S, Andrews SE, Carter N, Hunter T, Pfaff SL: **Coexpressed EphA receptors and ephrin-A ligands mediate opposing actions on growth cone navigation from distinct membrane domains.** *Cell* 2005, **121**:127-139.
10. Zelinski DP, Zantek ND, Irizarry AR, Kinch MS: **EphA2 overexpression causes tumorigenesis of mammary epithelial cells.** *Cancer Res* 2001, **61**:2301-2306.
11. Salaita K, Nair PM, Petit RS, Neve RM, Das D, Gray JW, Groves JT: **Restriction of receptor movement alters cellular response: physical force sensing by**

EphA2. *Science* 2010, **327**:1380-1385.
12. Vogel V, Sheetz M: Local force and geometry sensing regulate cell functions. *Nat Rev Mol Cell Biol* 2006, **7**:265-275.
13. Kumar S, Weaver VM: Mechanics, malignancy, and metastasis: the force journey of a tumor cell. *Cancer Metastasis Rev* 2009, **28**:113-127.

doi:10.1186/bcr2623
Cite this article as: Plodinec M, Schoenenberger C-A: Spatial organization acts on cell signaling: how physical force contributes to the development of cancer. *Breast Cancer Research* 2010, **12**:308.

Journal of Structural Biology 174 (2011) 476–484

Contents lists available at ScienceDirect

Journal of Structural Biology

journal homepage: www.elsevier.com/locate/yjsbi

The nanomechanical properties of rat fibroblasts are modulated by interfering with the vimentin intermediate filament system

Marija Plodinec [a], Marko Loparic [a], Rosmarie Suetterlin [a], Harald Herrmann [b], Ueli Aebi [a], Cora-Ann Schoenenberger [a,*]

[a] M.E. Müller Institute for Structural Biology, Biozentrum, University of Basel, 4056 Basel, Switzerland
[b] Department of Molecular Genetics, German Cancer Research Center, 69120 Heidelberg, Germany

ARTICLE INFO

Article history:
Received 15 December 2010
Received in revised form 5 March 2011
Accepted 15 March 2011
Available online 21 March 2011

Keywords:
Cytoskeleton
Intermediate filaments
Vimentin
Atomic force microscopy
Nanomechanics
Stiffness
Dynamic elastic modulus

ABSTRACT

The contribution of the intermediate filament (IF) network to the mechanical response of cells has so far received little attention, possibly because the assembly and regulation of IFs are not as well understood as that of the actin cytoskeleton or of microtubules. The mechanical role of IFs has been mostly inferred from measurements performed on individual filaments or gels *in vitro*. In this study we employ atomic force microscopy (AFM) to examine the contribution of vimentin IFs to the nanomechanical properties of living cells under native conditions. To specifically target and modulate the vimentin network, Rat-2 fibroblasts were transfected with GFP-desmin variants. Cells expressing desmin variants were identified by the fluorescence microscopy extension of the AFM instrument. This allowed us to directly compare the nanomechanical response of transfected and untransfected cells at high spatial resolution by means of AFM. Depending on the variant desmin, transfectants were either softer or stiffer than untransfected fibroblasts. Expression of the non-filament forming GFP-DesL345P mutant led to a collapse of the endogenous vimentin network in the perinuclear region that was accompanied by localized stiffening. Correlative confocal microscopy indicates that the expression of desmin variants specifically targets the endogenous vimentin IF network without major rearrangements of other cytoskeletal components. By measuring functional changes caused by IF rearrangements in intact cells, we show that IFs play a crucial role in mechanical behavior not only at large deformations but also in the nanomechanical response of individual cells.

1. Introduction

Living cells are complex heterogeneous systems with specific viscoelastic properties that are dominated by the structure of the three main cytoskeleton components; actin microfilaments, intermediate filaments (IFs) and microtubules. Developments in atomic force microscopy (AFM) allowed for mechanical probing of small volumes such as individual cells (Radmacher, 2007). Mechanical measurements on living cells show that the disruption of the actin or microtubule cytoskeleton results in a decreased cellular stiffness (Rotsch and Radmacher, 2000; Pelling et al., 2007; Ofek et al., 2009). While these studies have provided insight into distinct roles of these cytoskeletal constituents on cellular mechanics, the contribution of the IF system remains elusive. The abundance of IFs in specific cells and the fact that they span the entire cell from the nucleus to the plasma membrane suggest that they play an important mechanical role by providing structural stability and/or by relaying mechanical signals (Steinbock et al., 2000). To date, most of the information on the mechanical function of IFs in cells is inferred from rheological measurements on vimentin, desmin and keratin gels *in vitro* (Janmey et al., 1991; Coulombe et al., 1998; Schopferer et al., 2009). These polymer gels exhibit highly nonlinear stress–strain relationships, characterized by a very low initial stiffness at small strains and relatively high stiffness at large strains. Molecular dynamics simulations support that IFs are rather compliant at low strain and stiffen when a high strain is applied (Qin et al., 2009).

Vimentin is the most widely distributed of all IF proteins. It is essential in early embryonic development and is a hallmark of mesenchymal cells, for example, fibroblasts, leukocytes and endothelial cells. Interestingly, these cell types occur in tissues that experience extensive forces, such as shear, tension and compression (Wang and Stamenovic, 2000; Brown et al., 2001). Moreover, vimentin is frequently overexpressed in many aggressive tumors (Prasad et al., 1999). The mechanical properties of vimentin have been examined by rheometry techniques in vimentin knock-out cells and in drug-treated cells (Sager, 1989; Wang et al., 1993; Eckes et al., 1998a,b; Wang and Stamenovic, 2000). These studies

---

* Corresponding author. Address: Klingelbergstrasse 50/70, CH-4056 Basel, Switzerland. Fax: +41 61 267 21 09.
E-mail address: cora-ann.schoenenberger@unibas.ch (C.-A. Schoenenberger).

1047-8477/$ - see front matter © 2011 Elsevier Inc. All rights reserved.
doi:10.1016/j.jsb.2011.03.011

indicate a significant role of the vimentin network at large deformation, whereas at small deformation, cellular mechanics appear to be unaffected by changes in vimentin.

Despite numerous human diseases that arise from single point mutations in IF genes the nanomechanical function of IFs in individual cells is still an enigma. Mutations in the muscle-specific desmin, which belongs to the same class of IFs as vimentin, are associated with skeletal and cardiac myopathies (Omary et al., 2004). Interestingly, during development and differentiation of muscle cells, vimentin and desmin are co-expressed (Gard and Lazarides, 1980). In addition, vimentin and desmin are able to copolymerize at all stages of filament assembly *in vitro* (Wickert et al., 2005). Transfection experiments using different desmin mutations have shown that the mutant desmin interacts with the endogenous vimentin and affects the architecture of the IF network in the cell (Bar et al., 2006b, 2007).

Recently, the nanoscopic properties of individual vimentin and desmin filaments *in vitro* were examined by AFM (Kreplak and Fudge, 2007; Kreplak et al., 2008). These AFM experiments have shown that individual IFs, both recombinant and authentic, are soft, extensible and very compliant. Although these properties might be reflected in the mechanics of living cells, IFs form a complex network within the cell and thus may exhibit a different elastic behavior compared to isolated filaments. Questions on the nanomechanical function of IFs in a cellular context have so far not been systematically addressed because tools to specifically target IFs have been missing. In this study, we have specifically modified the IF network in Rat-2 fibroblasts by expressing GFP-tagged wild-type desmin and desminopathic mutants and have compared the nanomechanical response of transfected and untransfected cells. For mechanical testing at high dimensional sensitivity we used an AFM with an integrated light microscopy unit. This allowed us to identify cells with a modified IF network and directly probe the nanomechanical consequences of desmin expression in living cells.

2. Materials and methods

2.1. Cell culture and preparation of cells for AFM

Rat-2 fibroblasts were grown in Dulbecco's modified Eagle's medium (DMEM, Sigma Aldrich, Switzerland) supplemented with 2 mM L-glutamine (Sigma Aldrich, Switzerland), 100 IU/ml penicillin/100 μg/ml streptomycin (Gibco, Switzerland), and 10% fetal calf serum (FCS GOLD; PAA Tissue Culture Company, USA; DFCS) at 37 °C in a humidified atmosphere containing 5% CO_2. Cells were subcultured weekly up to 10 passages. For experimental cultures, $\sim 10^5$ cells were plated in DFCS either on glass bottom dishes or coverslips.

2.2. Cloning and transient transfection of GFP-desmin variants

GFP-tagged full-length desmin wild-type and mutant constructs were obtained by inserting corresponding PCR fragments at the HindIII/BamHI site into the pEGFP-C1 vector (BD Biosciences Clontech) using the following primers: 5′-CCAAGCTTCGATG GCCCAGGCCTACTCGTCCAG-3′ (sense) and 5′-GGGATCCTTACAG CACTTCATGTTGTTGCTGTG-3′ (antisense). Constructs were verified by DNA sequencing. Rat-2 fibroblasts were grown for 24 h on 50 × 40 mm × 0.17 mm glass-bottomWillCo™ dishes (GWSt-5040, Intracell Ltd., UK) or glass coverslips in a 24-well plate and then transfected with GFP-desmin variants using FuGENE 6 (Roche, Switzerland) following the standard protocol. Twenty-four hours after transfection, the cells were processed either for AFM experiments or confocal imaging.

2.3. Confocal laser scanning microscopy (CLSM)

For immunofluorescence, transfected cells were fixed for 15 min in phosphate-buffered saline (PBS) with 4% formaldehyde at RT. After rinsing with modified Hank's buffer (MHB; Hank's buffer without Ca^{2+}, containing 2 mM EGTA, 5 mM 2-morpholino-ethanesulfonic acid, 0005% NaN_3, pH 6.2–6.4), coverslips were permeabilized for 2 min in 0.2% TritonX-100, rinsed in MHB and incubated with Cy3-conjugated vimentin antibody (mouse monoclonal 1:1000, Sigma–Aldrich) for 45′ at RT in a humidified chamber. After several washes with MHB, coverslips were mounted in Mowiol 1188 (Hoechst, Germany). Where indicated, cells were incubated with 647-phalloidin (1:250, Invitrogen, Switzerland) or a ®-tubulin mouse monoclonal antibody (1:2000, Boehringer, Germany) followed by a secondary donkey anti mouse antibody coupled to Alexa 488 (1:800, Molecular probes, Switzerland). Confocal sections were recorded with a Leica TCS 4-D CLSM and processed with Imaris software (Bitplane, Switzerland) and Adobe Photoshop version 10.0.

2.4. Mechanical probing by indentation AFM

All AFM experiments were carried out under physiological conditions at 37 °C using a commercial AFM (Nanowizard I AFM, JPK Instruments, Germany) placed on a Zeiss Axiovert 135 TV microscope (Zeiss, Germany) equipped with 20× and 40× objectives and a GFP-fluorescence filter. Bright field and fluorescence signals were monitored using a grayscale digital camera (ANDOR SOLIS CCD-375; ANDOR Technology, Northern Ireland). We used standard triangular silicon nitride cantilevers with a spring constant between 0.04 and 0.08 N/m and a nominal tip radius of 20 nm (DNP-S, Vecco probes, Veeco Instruments, USA). The experimental value for the spring constant of each cantilever was determined by thermal tune method (Sader et al., 1995) using the JPK Nanowizard 1.1 calibration tool. For cell stiffness measurements, the AFM was operated in the "Force-Volume Mode". Briefly, arrays of force–displacement curves were recorded in a regular grid over a selected sample surface of 100 μm^2. Each of the 128 × 64 force–displacement curves consists of 1024 sampling points. All indentations were performed with the maximum load set to 1.8 nN at a scan rate of ~15 μm/s. AFM stiffness maps were completed within 2–3 h. During the measurements, culture dishes were replenished with fresh DFCS saturated with 5% CO_2 to maintain physiological conditions and compensate for evaporation. In the course of an experiment, the pH ranged between 7.4 and 7.5.

2.5. Analysis of indentation data

For the analysis of AFM force curves, a method described in Loparic et al. was modified (Loparic et al., 2010). Briefly, we developed software in LABWIEV (National Instruments, USA) for the automated analysis of the force–volume data. The contact point was determined by applying a polynomial fit to raw force curves according to a published algorithm (Lin et al., 2007). Force-indentation data were obtained by the indentation h, which corresponds to the difference between piezo displacement and cantilever deflection, and by multiplying cantilever deflection d with the spring constant k to obtain load F. The slope of each data point is calculated by performing a linear fit to the upper 50% of the unloading force curve. Slope values were spatially plotted to yield a stiffness map using Igor Pro (Wavemetrics, LakeOswego, USA). Gaussian distributions were computed from the stiffness values of individual cells. The mean slope value from the Gaussian fit was then used for calculating elastic modulus (E_s) for each cell type according to the Oliver and Pharr theory (Oliver and Pharr, 1992) applied by Loparic and coworkers (Stolz et al., 2004; Loparic et al., 2010). In the Eq. (1) where E_r represents the measured relative dynamic elastic modulus, E_s is the elastic modulus of the sample and E_i of the indenter

$$\frac{1}{E_r} = \frac{1-\upsilon_s^2}{E_s} + \frac{1-\upsilon_i^2}{E_i} \tag{1}$$

where υ_s and υ_i are Poisson's ratios of sample and indenter. Assuming that the elastic modulus of biological specimens is orders of magnitude smaller than that of the indenter ($E_i >> E_s$), Eq. (1) reduces to

$$\frac{1}{E_r} \cong \frac{1-\upsilon_s^2}{E_s} \tag{2}$$

The Poisson's ratio of cells is assumed to be $\upsilon_s = 0.5$ (45). The stiffness of the sample S is defined as the linear fit between the maximum load $F_2 = 1.8$ nN and the minimum load $F_1 = 0.9$ nN (3). The indentation depth is denoted by h.

$$S = \left[\frac{\Delta p}{\Delta h}\right]_{F_1}^{F_2} = \left[\frac{\Delta d \times k}{\Delta h}\right]_{d_1}^{d_2} \tag{3}$$

Subsequently, the relative elastic modulus E_r is defined by the following equation:

$$E_r = \frac{\sqrt{\pi}}{2}\frac{S}{\sqrt{A_c(h_c)}} \tag{4}$$

where $A_c(h_c)$ is the projection of the contact area as a function of the tip angle (Θ) and the contact indentation depth h_c. Assuming h_c to correspond to the total depth of indentation h yields the following relation for a 4-sided pyramidal tip

$$A_c(h_c) = (2h\tan\Theta)^2 \tag{5}$$

By combining Eqs. (2)–(5) the elastic modulus of the sample E_s can be calculated:

$$E_s = \frac{\sqrt{\pi}}{2}(1-\upsilon_s^2)\frac{1}{\sqrt{A_c(h_c)}}\left[\frac{\Delta d \times k}{\Delta h}\right]_{d_1}^{d_2} \tag{6}$$

2.6. Statistical analysis

Histograms were plotted at a bin value of 50, and data are given as mean ± standard deviation (SD). Statistical analysis was performed using paired student's *t*-test. Statistical significance was tested at $p = 0.05$ and $p = 0.0001$. Mean values were calculated from $n = 59$ independent measurements for untransfected cells, $n = 12$ for *DesWT*, $n = 15$ for *DesA213V*, and $n = 19$ for *DesL345P*.

3. Results

In order to examine the contribution of the IF network to the mechanical response in living cells, we used an AFM setup with integrated light microscopy features. This allowed us to optically monitor the cells mounted under the fluid cell of the AFM during stiffness measurements over several hours (Fig. 1A). Moreover, the cantilever is clearly visible, such that the AFM tip can be precisely positioned to scan a defined area of interest. Another essential feature of the combined microscope is the option of epifluorescence (Fig. 1B), which allows the overlay of corresponding fluorescence and bright field images, as well as their direct correlation with AFM stiffness maps. Based on the optical images, transfected cells that are expressing GFP-tagged constructs are readily identified and can be probed in parallel with non-transfected Rat-2 cells.

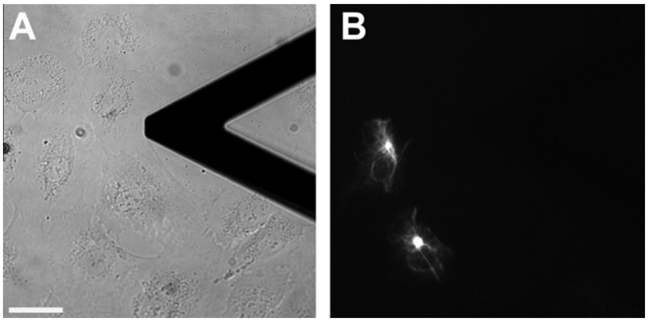

Fig.1. Combining AFM with optical microscopy for imaging Rat-2 fibroblasts transfected with GFP-desmin variants under native conditions. (A) The viability of the cells can be monitored in the bright field signal during the experiment by a CCD camera. (B) Fluorescence filters allow for epifluorescence detection of cells that express transfected GFP-desmin. Scale bar, 50 µm.

3.1. Transfected desmin differentially interacts with the endogenous vimentin

To specifically address the role of the IF system in cellular elasticity, we have transiently transfected Rat-2 fibroblasts with GFP-desmin wild-type and mutant constructs and examined their effects on the endogenous vimentin network. As illustrated in Fig. 2, CLSM of Rat-2 cells transfected with GFP-*DesWT* (top row) revealed a prominent network of desmin filaments that spans the entire cell. Comparison of transfected and untransfected cells immunolabeled with a vimentin antibody (red) showed that the expression of exogenous GFP-*DesWT* does not affect the supramolecular organization of the endogenous vimentin network. The extensive co-localization of GFP-*DesWT* and vimentin in the overlay suggests that the wild-type desmin might have co-assembled with endogenous vimentin IFs, as has been demonstrated for isolated desmin and vimentin *in vitro* (Wickert et al., 2005). Similarly, cells transfected with GFP-*DesA213V* (Fig. 2, middle row), which contains a single point mutation localized in the alpha-helical desmin domain, displayed a filamentous network that mostly co-localized with the endogenous vimentin IF network.

In contrast, the GFP-tagged desmin mutant *DesL345P* (Fig. 2, bottom row), which contains a single point mutation in the highly conserved coiled-coil rod domain involved in the desmin assembly process, failed to form filamentous networks in Rat-2 cells. Instead, transfectants exhibited an accumulation of small, dot-like aggregates in the perinuclear region. More importantly, expression of GFP-*DesL345P* caused striking changes in the organization of the endogenous IF network. Immunofluorescent staining revealed that the vimentin network is disrupted and "collapsed" at the sites where desmin aggregates have accumulated.

To ensure that the expression of the exogenous desmin does not significantly affect the other major components of the cytoskeleton, we have stained transiently transfected Rat-2 cells with a tubulin antibody (red) and phalloidin (blue), which binds to filamentous actin. As shown in Fig. 3, microtubules and the actin filament network of transfected cells were comparable to that of untransfected cells, even if the endogenous IF system was perturbed by mutant desmin. The immunofluorescence data from transiently transfected, fixed cells shows that by expressing desmin mutants, we can specifically modulate the endogenous IFs with minimal effects on the overall cytoarchitecture of Rat-2 fibroblasts.

3.2. Stiffness mapping by AFM reveals nanomechanical changes in desmin expressing Rat-2 cells

To probe the consequences of modulating the IF system on the mechanical properties of Rat-2 cells by indentation-type AFM; we

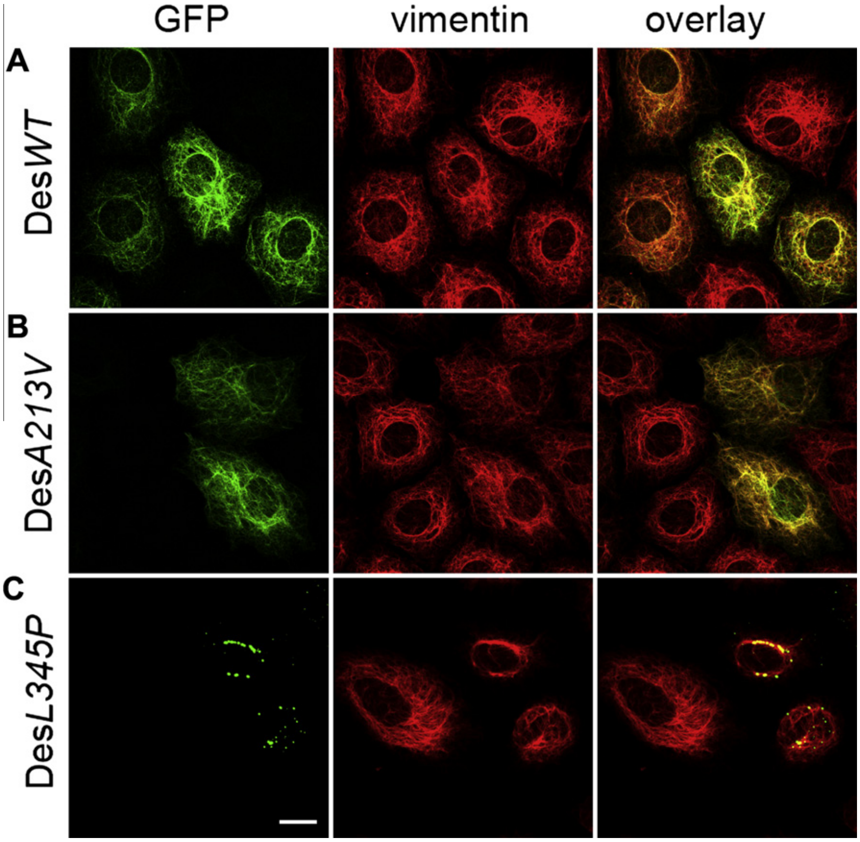

Fig.2. Fluorescence microscopy of the IF system in untransfected and transfected cells. Rat-2 cells were transfected with GFP-*DesWT*, -*DesA213V* or -*DesL345P* for 24 h, fixed, and immunolabeled with a vimentin-Cy3 antibody (red). Transfectants are identified by the GFP signal. (A) The overlay shows extensive integration of *DesWT* into the endogenous vimentin network in transfected cells. (B) The filament forming *DesA213V* mutant similarly co-localizes with the vimentin network. (C) The *DesL345P* mutant forms perinuclear aggregates (left panel) which induce a collapse of the vimentin network (middle panel). The overlay reveals a partial colocalization in the perinuclear region. Scale bar, 20 μm.

identified transfectants that express GFP-tagged desmin variants in the fluorescence mode of the combined AFM/light microscope (Fig. 4A, insets). Cells were transfected with GFP tagged wild-type desmin (*DesWT*), mutant desmin *DesA213V*, or mutant desmin *DesL345P*. Based on the overlay of bright field and fluorescence image, individual AFM scan areas were specifically selected to comprise transfected and untransfected control cells. In order to minimize the adverse effects of GFP-desmin overexpression, transfectants with moderate intensities were chosen based on the fluorescence intensity signal. The viability and overall cell morphology was optically monitored by bright field microscopy. For *DesWT* and *DesA213V*, we did not observe significant morphological differences between untransfected and transfected cells, while cells transfected with DesL345P mutant appeared larger with protruding nuclei when compared to the untransfected cells. Stiffness maps shown in Fig. 4B include transfected (marked by a black asterisk) and untransfected control cells recorded under the same experimental conditions, thus a direct comparison of their mechanical properties is feasible. *DesWT* and *DesA213V* transfectants exhibit stiffness maps that reflect the spatial organization of filaments revealed by fluorescence (Fig. 4A). In contrast, in *DesL345P* expressing cells we measured significant stiffening localized in areas around the nucleus where fluorescence indicates an accumulation of the mutant desmin. A quantitative analysis of stiffness distribution is presented as histograms in Fig. 5. Untransfected Rat-2 (Fig. 5A) and transfectants expressing *DesWT* (Fig. 5B) fall within a narrow range of stiffness values, albeit the latter is slightly softer. In contrast, *DesA213V* (Fig. 5C) and *DesL345P* (Fig. 5D) transfectants showed a very broad Gaussian distribution compared to untransfected cells, indicating that interactions between the mutant desmin and the endogenous vimentin induced structural changes in the network that contributed to stiffness heterogeneity. While the distribution is broad for both mutants, only *DesL345P* fits a bimodal distribution where the stiffer peak represents sites of collapsed IF network (shaded histogram) and the other peak (solid histogram) regions whose stiffness resembles that of untransfected cells. Regions resembling untransfected stiffness values were also found in *DesA213V*.

As illustrated in Fig. 5E, representative force-indentation curves that were calculated from the measured force–displacement curves show distinct slopes for untransfected and transfected cells. Elastic modulus E_s values were calculated from the stiffness measurements and presented in Fig. 5F. Untransfected cells exhibit an elastic modulus of $E_{untransfected} = 2.55 \pm 0.99$ kPa, while *DesWT* cell exhibit $E_{DesWT} = 1.64 \pm 0.61$ kPa. For *DesA213V* filament forming mutant, the $E_{DesA213V} = 6.10 \pm 1.82$ kPa indicates a twofold stiffening compared to the untransfected cell. Consistent with the co-localized aggregation of *DesL345P* and vimentin near the nucleus and the bimodal stiffness distribution, transfectants exhibited two distinct stiffness values: $E_{DesL345P\text{-}perinuclear}$ 8.16 ± 3.33 kPa in the perinuclear region and $E_{DesL345P} = 2.51 \pm 0.83$ kPa in the rest of the cell.

4. Discussion

4.1. Relating the effects of IF tuning to the nanomechanical behavior in living cells

In this study, we present comprehensive mechanical probing of living cells by indentation-type AFM using an instrument setup

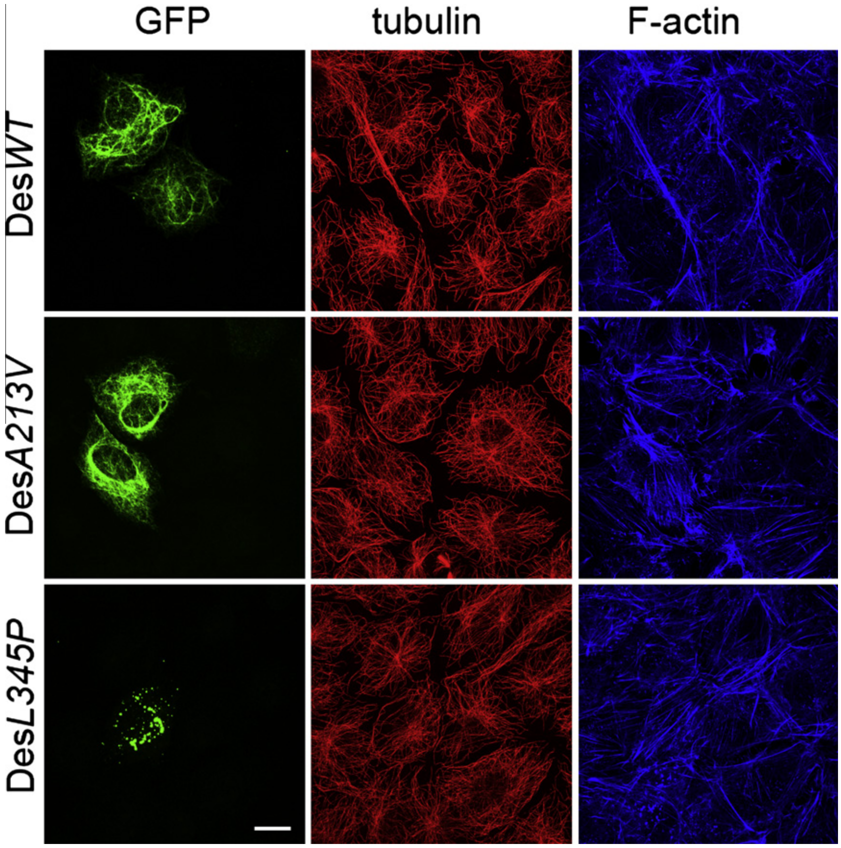

Fig.3. Transfection of desmin variants does not rearrange the actin and tubulin cytoskeleton. The GFP signal reveals *DesWT* (top row), *DesA213V* (middle row), and *DesL345P* (bottom row) in transfected cells. Cells were stained with 647-phalloidin (blue) to identify filamentous actin and immunolabeled with β-tubulin antibody (red) to reveal microtubules. Scale bar, 20 μm.

with integrated light microscopy. Besides a precise positioning of the AFM tip at any site of interest and continuous optical assessment of the cell morphology during the stiffness mapping, the epifluorescence mode allowed us to easily identify cells that express GFP-tagged desmin variants within areas chosen for nanomechanical testing. In addition, we were able to measure the relative fluorescence intensities of transfected cells. Because cells that express very high levels of GFP-desmin variants had the tendency to round up and detach, we specifically choose transfectants with similar, moderate levels of GFP-desmin expression. Moreover, captured fluorescence images can be superimposed on corresponding stiffness maps. Thus, changes in the specific mechanical response of the transfectants can be directly related to the structural changes caused by transgene expression.

4.2. Data accuracy is improved by an internal reference

The range of elastic moduli reported from AFM elasticity measurements on living cells is rather broad (Janmey and McCulloch, 2007). Besides the cell type, the most obvious reasons for these variations are differences in the spring constant of the cantilevers and in the shape of the tip used, and in the data analysis employed. Specifically, errors intrinsic to these parameters cause significant variations in the absolute stiffness values determined in individual experiments. By using GFP-desmin variants to tune the IF network and a combined AFM/light microscope, we could largely avoid experimental variations between measurements because each stiffness map includes at least one transfected and one untransfected cell. Thus, relative differences in stiffness between normal cells and cells expressing GFP-desmin variants are instantly revealed within the same stiffness map.

4.3. Structural complexity of cells requires statistical analysis

Most studies conducted so far have fitted the force curves to the Hertz model, which assumes that living cell is a homogeneous, isotropic, and linear elastic sample with infinite thickness. However, as schematically illustrated in Fig. 6, living cells in terms of their mechanical properties are inhomogeneous, highly anisotropic, and multi-layered structures with a complex cytoarchitecture (Peeters et al., 2004). As a result, the elastic modulus of a cell is not constant over the whole range of indentation (Roduit et al., 2009) and also varies with the site of measurement. Consequently, data based on single-point measurements yield a rather biased view of the mechanical properties of a given cell. In contrast, the large number of force curves in our stiffness measurements represents an unbiased spatial sampling of a particular cell, and using sharp pyramidal tips reveals local variations of cell stiffness. By employing two distinct indentation regimes, Kasas et al. have found that, from a mechanical point of view, a living cell can be considered a multilayered structure (Kasas et al., 2005); the lower segment of the force curve, which corresponds to an indentation depth of 100–200 nm, predominantly represents the stiffness contribution of the actin cytoskeleton below the plasma membrane, whereas the upper segment of the force curve more likely represents the deeper, basket-like IF network around the nucleus, and microtubules. A schematic representation of the relation between structural and mechanical 'layers' is illustrated in Fig. 6. Following

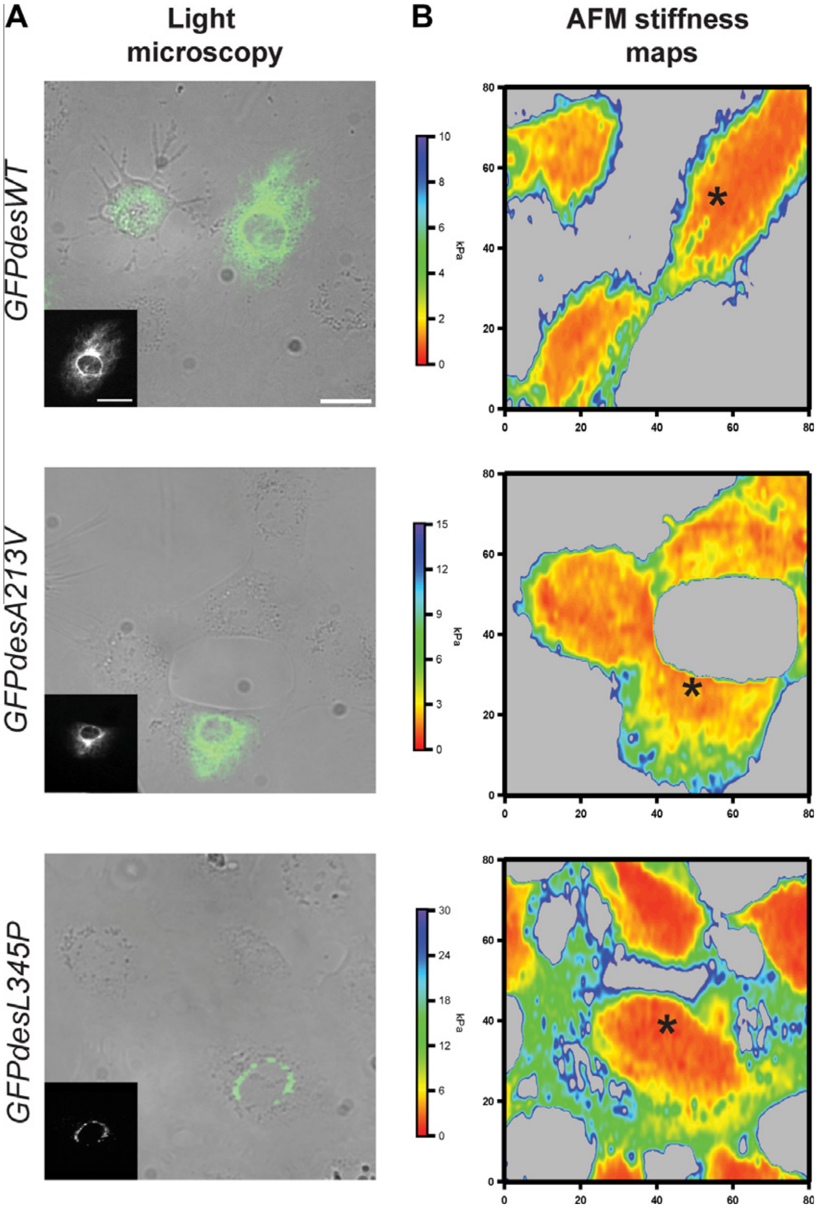

Fig.4. Imaging and stiffness mapping of Rat-2 cells by LM/AFM. (A) Overlay of bright field and fluorescence images reveals the location of untransfected and transfected Rat-2 cells for *DesWT* (top row), *DesA213V* (middle row), and *DesL345P* (bottom row). Scale bar, 50 µm. Insets, fluorescence images of the transfectants marked with an asterisk in the stiffness maps. Scale bar, 20 µm. (B) Stiffness maps representing 8192 force curves reveal differences in nanomechanical properties between different desmin variants. The cell expressing *DesWT* (top panel) exhibits a similar stiffness profile as its untransfected neighbors. The cell expressing *DesA213V* (middle panel) comprised much stiffer regions than untransfected cells. The *DesL345P* expressing cell (bottom panel) shows distinct stiffening in the perinuclear region. The stiffness values are indicated by the gradient in the vertical bar.

the notion of Kasas and colleagues, we used the upper segment of the force curve, specifically 50% of the maximum force, to characterize the viscoelastic properties of the endogenous or modulated IF system (Fig. 6C).

4.4. Expression of GFP-tagged desmin variants induces changes in the architecture of the endogenous vimentin

Vimentin and muscle-specific desmin are members of the sequence homology class III IF proteins and are very similar in their structural organization as they exhibit more than 70% sequence identity in various vertebrate species (Schaffeld et al., 2001). Point mutations located in the central α-helical coiled-coil rod domain of desmin cause severe autosomal dominant forms of myofibrilar myopathy (Bar et al., 2004, 2005). Many of these mutant desmin variants are able to assemble into seemingly normal IFs *in vitro* whereas others exhibit an aberrant assembly process at different stages (Bar et al., 2006b). For example, *DesA213V*, which harbors a point mutation in coil 1B, is capable of forming filaments *in vitro*, but it is maturation-deficient as the filaments are unable to compact radially. Consistently, GFP-tagged *DesA213* formed a filamentous network similar to that observed with GFP-DesWT in transfectants and both appeared to largely integrate into the endogenous vimentin IF network without causing major rearrangements. Similarly, previous immunofluorescence studies in murine 3T3 fibroblasts have shown a colocalization of transfected wild-type desmin and the *DesA213V* variant with the endogenous vimentin network (Bar et al., 2006a).

In contrast, expression of the *DesL345P* mutant resulted in aggregates in the perinuclear region. More significantly, expression

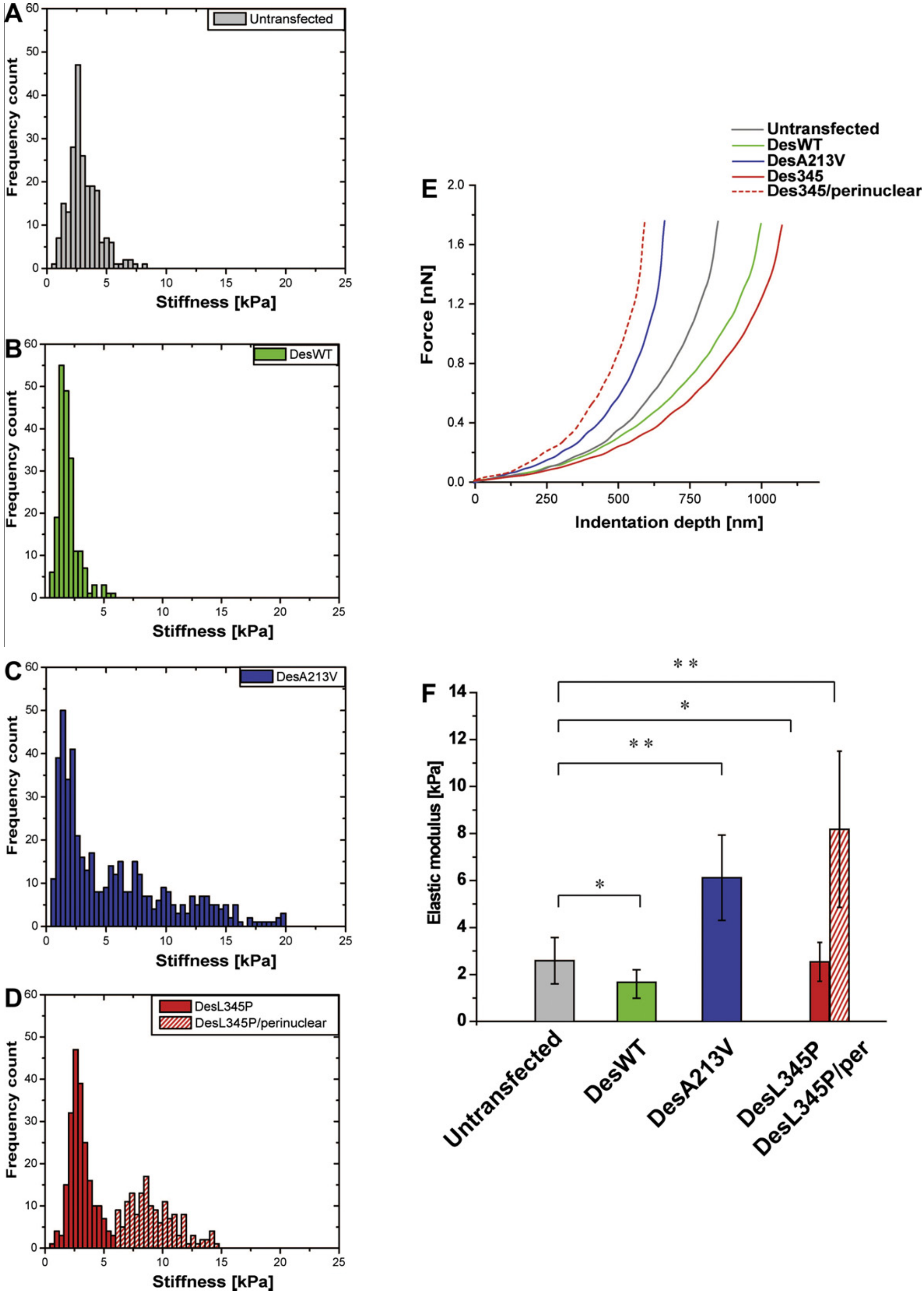

Fig.5. Analysis of nanomechanical properties. (A)–(D) Gaussian distribution of stiffness values. (A) Untransfected cells exhibit a uniform distribution. (B) *DesWT* transfectants exhibit a distribution with a maximum close to that of untransfected cells. (C) For *DesA213V* expressing cells, the distribution is very broad. (D) *DesL345P* transfectants are characterized by a bimodal stiffness distribution. The solid peak comprises stiffness values that are typical for untransfected cells. The broader Gaussian distribution (shaded bars) contains the higher stiffness values associated with the perinuclear sites of *DesL345P* aggregation. (E) Representative unloading force indentation curves for each cell type. (F) The elastic modulus E_s for every cell type was calculated using average slope stiffness values. The statistical analysis shows mean values of E_s and standard deviation. Stars indicate statistically significant differences ($^{*}p < 0.05$, $^{**}p < 0.0001$).

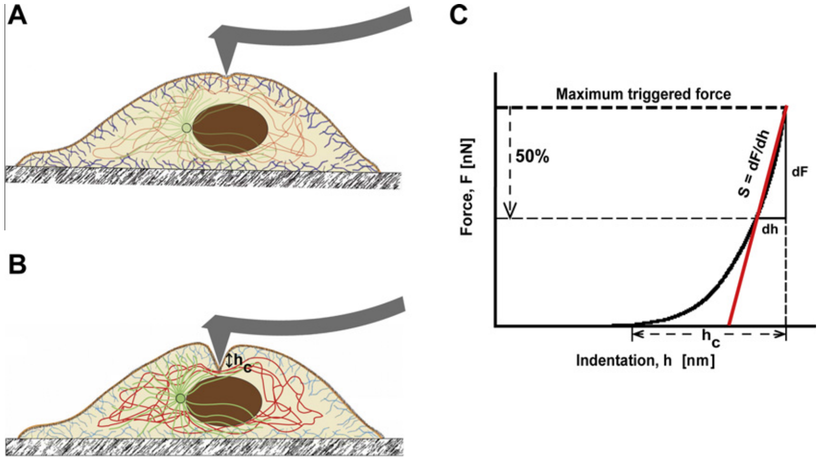

Fig.6. Model of the AFM indentation regime for analyzing IF nanomechanics in cells. (A) When indenting a cell, the AFM tip first encounters the actin cytoskeleton (blue) below the plasma membrane and then (B) the intermediate filament network (red). (C) The retracting AFM force curve specifies the cell's response to the force *F* applied for indenting the cell to an indentation depth h_c. The force curve can be divided into two main segments. The lower segment corresponds to the response of the actin cytoskeleton beneath the plasma membrane to *F*, whereas the upper segment of the curve predominantly represents the response of the deeper intermediate filament network. The linear fit to the upper 50% of the force curve (red) is used for determining the slope *S* from which the elastic modulus is calculated.

of this mutant led to an apparent collapse of the endogenous vimentin IF network around the nucleus. A similar antimorphic effect on the organization of the endogenous vimentin (Carlsson et al., 2002; Bar et al., 2006a) or desmin network (Bar et al., 2007) has been previously observed for this mutant.

In a number of studies, reorganization of the IF network in cells has been achieved by treatment with acrylamide (Faigle et al., 2000) or cisplatin (Evans and Simpkins, 1998). However, these agents simultaneously affect multiple cellular functions as well as overall protein synthesis. More specifically, treatment with these drugs irreversibly modified other cytoskeletal elements that are linked to the IF network by cytolinkers or motor protein complexes (Liao and Gundersen, 1998). Although we cannot entirely rule out that the IF rearrangements caused by the expression of mutant desmin variants might have subtle effects on the organization of the actin and/or microtubule network, our immunofluorescence data suggest that these cytoskeleton constituents are similarly organized in transfected and untransfected cells. Even in the case of mutant *DesL345P* where the endogenous vimentin network was severely perturbed, both actin microfilaments and microtubules appeared largely unaffected (see Fig. 3). Hence, we conclude that the expression of mutant desmin variants represents a selective means to specifically modify the vimentin IF system.

4.5. Desmin variants provide a tool to assess the contribution of vimentin IFs to the nanomechanical properties of cells

Mechanical measurements complemented by time-resolved electron microscopy (EM) show that desmin and vimentin IF networks assembled *in vitro* from purified proteins are much more flexible than actin filaments (Storm et al., 2005). Among IFs, rheology measurements revealed desmin filaments to be stiffer (persistence length $l_{(\mathrm{p})} \approx 900$ nm) than vimentin filaments ($l_{(\mathrm{p})} \approx 400$ nm). Moreover, filament bundling is more pronounced for desmin than for vimentin. Notably, *in vitro* formed heteropolymers between desmin and vimentin were shown to exhibit intermediary mechanical properties compared to those of the homopolymeric filaments (Schopferer et al., 2009). Based on data from *in vitro* studies, and the extensive colocalization of vimentin and desmin in *DesWT* transfectants, one might have assumed that desmin expression leads to a stiffening of the cell. However, AFM stiffness maps revealed *DesWT* transfectants to be slightly softer than the untransfected cells. It is conceivable that this softening is related to specific interactions of vimentin and desmin subunits in the hetero-filaments. Consistently, a recent publication demonstrates end-to-end annealing and intercalary subunit exchange in living cells (Colakoglu and Brown, 2009). Such a subunit exchange with *DesWT* may destabilize and/or slightly reduce the stiffness of the final heteropolymeric network.

In contrast to the wild-type, expression of the filament-forming A213V mutant caused a twofold stiffening of transfected cells. Because this mutation interferes with a late stage of IF maturation, the final steps of heteropolymeric network formation are likely to be affected in the transfectants. Recent AFM studies of isolated desmin filaments have shown specific point mutations to be related to changes in mechanical properties (Kreplak and Bar, 2009). It was suggested that the distinct intra-filamentous structure of the mutant desmin was responsible for the modified force-bearing properties of the filament. Consistent with this notion, structural changes induced by the incorporation of *DesA213V* might be responsible for the significant stiffening of transfected cells.

Expression of the non-filament forming mutant *DesL345P* drastically changed the IF network and the mechanical response of the transfectants. The DesL345P mutation has been shown to affect filament assembly at an early stage and form aggregates rather than filamentous structures (Bar et al., 2006a). Consistently, fluorescence data of *DesL345P* transfectants indicates that the mutant desmin did not integrate into vimentin filaments. Instead, *DesL345P* expression induced a collapse of the endogenous vimentin system in the perinuclear region, which caused drastic localized cell stiffening in this area. At the same time, stiffness in other areas of the cell was comparable to that of untransfected cells.

Our data show that expression of mutant *L345P* desmin leads to severely impaired mechanical function at specific sites within an individual cell. Proximal, bulbar and facial muscles of transgenic mice expressing *L345P* mutant desmin exhibit changes that result in mechanical weakness (Sjoberg et al., 1999). Based on these findings we speculate that the accumulation of cells with altered mechanical properties over an extended period of time will eventually result in the complete mechanical dysfunction of the affected tissue.

5. Conclusions

In conclusion, we show that desmin variants represent a valuable tool to specifically examine the contribution of the intermediate filament network to the mechanical function of living cells under native conditions. By using a combination of AFM and optical microscopy, we were able to identify cells transfected with desmin variants and measure their nanomechanical properties in direct comparison to untransfected cells at high spatial resolution. Depending on the desmin variant expressed, IF-related or localized stiffening was observed. Our study demonstrates that alterations in the IF filament structure and architecture have a direct impact on the nanomechanical properties of living cells. Finally, our data show that IFs play an important role not only at large deformations but that they contribute to the mechanical properties also at the nanometer scale. This indicates that molecular changes at the single cell level, which are frequently associated with disease, trigger specific nanomechanical responses.

Acknowledgments

This work was supported by an NCCR program grant on "Nanoscale Science" awarded by the Swiss National Science Foundation to CAS, the M.E. Müller Foundation of Switzerland and the Canton Basel-Stadt. H.H. was supported by the German Research Foundation (DFG; HE 1853 and BA 2186/3-1). We gratefully acknowledge Lydia Lussi for the drawing in Fig. 6, Sandra Mitrovic for advice on transfections. We are thankful to Martin Stolz, Janne Hyötylä and Roderick Lim for their help with data analysis.

References

Bar, H., Goudeau, B., et al., 2007. Conspicuous involvement of desmin tail mutations in diverse cardiac and skeletal myopathies. Human Mutation 28 (4), 374–386.

Bar, H., Kostareva, A., et al., 2006a. Forced expression of desmin and desmin mutants in cultured cells: impact of myopathic missense mutations in the central coiled-coil domain on network formation. Experimental Cell Research 312 (9), 1554–1565.

Bar, H., Mucke, N., et al., 2005. Severe muscle disease-causing desmin mutations interfere with in vitro filament assembly at distinct stages. Proceedings of the National Academy of Sciences of the United States of America 102 (42), 15099–15104.

Bar, H., Mucke, N., et al., 2006. Impact of disease mutations on the desmin filament assembly process. Journal of Molecular Biology 360 (5), 1031–1042.

Bar, H., Strelkov, S.V., et al., 2004. The biology of desmin filaments: how do mutations affect their structure, assembly, and organisation? Journal of Structural Biology 148 (2), 137–152.

Brown, M.J., Hallam, J.A., et al., 2001. Rigidity of circulating lymphocytes is primarily conferred by vimentin intermediate filaments. Journal of Immunology 166 (11), 6640–6646.

Carlsson, L., Fischer, C., et al., 2002. Cytoskeletal derangements in hereditary myopathy with a desmin L345P mutation. Acta Neuropathologica 104 (5), 493–504.

Colakoglu, G., Brown, A., 2009. Intermediate filaments exchange subunits along their length and elongate by end-to-end annealing. Journal of Cell Biology 185 (5), 769–777.

Coulombe, P.A., Ma, L., et al., 1998. Examining the micromechanical properties of epidermal keratin intermediate filaments. Molecular Biology of the Cell 9, 164a.

Eckes, B., Dogic, D., et al., 1998a. Impaired mechanical stability, migration and contractile capacity in vimentin-deficient fibroblasts. Journal of Cell Science 111, 1897–1907.

Eckes, B., Martin, P., et al., 1998b. Disruption of tensegrity in vimentin-deficient fibroblasts causes delayed wound healing in fetal and adult mice. Journal of Investigative Dermatology 110 (4), 592.

Evans, R.M., Simpkins, H., 1998. Cisplatin induced intermediate filament reorganization and altered mitochondrial function in 3T3 cells and drug-sensitive and -resistant Walker 256 cells. Experimental Cell Research 245 (1), 69–78.

Faigle, W., Colucci-Guyon, E., et al., 2000. Vimentin filaments in fibroblasts are a reservoir for SNAP23, a component of the membrane fusion machinery. Molecular Biology of the Cell 11 (10), 3485–3494.

Gard, D.L., Lazarides, E., 1980. Synthesis and distribution of desmin and vimentin during myogenesis in vitro. Cell 19 (1), 263–275.

Janmey, P.A., Euteneuer, U., et al., 1991. Viscoelastic properties of vimentin compared with other filamentous biopolymer networks. Journal of Cell Biology 113 (1), 155–160.

Janmey, P.A., McCulloch, C.A., 2007. Cell mechanics: integrating cell responses to mechanical stimuli. Annual Review of Biomedical Engineering 9, 1–34.

Kasas, S., Wang, X., et al., 2005. Superficial and deep changes of cellular mechanical properties following cytoskeleton disassembly. Cell Motility and the Cytoskeleton 62 (2), 124–132.

Kreplak, L., Bar, H., 2009. Severe myopathy mutations modify the nanomechanics of desmin intermediate filaments. Journal of Molecular Biology 385 (4), 1043–1051.

Kreplak, L., Fudge, D., 2007. Biomechanical properties of intermediate filaments: from tissues to single filaments and back. Bioessays 29 (1), 26–35.

Kreplak, L., Herrmann, H., et al., 2008. Tensile properties of single desmin intermediate filaments. Biophysical Journal 94 (7), 2790–2799.

Liao, G.J., Gundersen, G.G., 1998. Kinesin is a candidate for cross-bridging microtubules and intermediate filaments – selective binding of kinesin to detyrosinated tobulin and vimentin. Journal of Biological Chemistry 273 (16), 9797–9803.

Lin, D.C., Dimitriadis, E.K., et al., 2007. Robust strategies for automated AFM force curve analysis – I. Non-adhesive indentation of soft, inhomogeneous materials. Journal of Biomechanical Engineering – Transactions of the ASME 129 (3), 430–440.

Loparic, M., Wirz, D., et al., 2010. Micro- and nanomechanical analysis of articular cartilage by indentation-type atomic force microscopy: validation with a gel-microfiber composite. Biophysical Journal 98 (11), 2731–2740.

Ofek, G., Wiltz, D.C., et al., 2009. Contribution of the cytoskeleton to the compressive properties and recovery behavior of single cells. Biophysical Journal 97 (7), 1873–1882.

Oliver, W.C., Pharr, G.M., 1992. An improved technique for determining hardness and elastic-modulus using load and displacement sensing indentation experiments. Journal of Materials Research 7 (6), 1564–1583.

Omary, M.B., Coulombe, P.A., et al., 2004. Mechanisms of disease: intermediate filament proteins and their associated diseases. New England Journal of Medicine 351 (20), 2087–2100.

Peeters, E.A.G., Bouten, C.V.C., et al., 2004. Anisotropic, three-dimensional deformation of single attached cells under compression. Annals of Biomedical Engineering 32 (10), 1443–1452.

Pelling, A.E., Dawson, D.W., et al., 2007. Distinct contributions of microtubule subtypes to cell membrane shape and stability. Nanomedicine – Nanotechnology Biology and Medicine 3 (1), 43–52.

Prasad, S., Soldatenkov, V.A., et al., 1999. Intermediate filament proteins during carcinogenesis and apoptosis (Review). International Journal of Oncology 14 (3), 563–570.

Qin, Z., Kreplak, L., et al., 2009. Nanomechanical properties of vimentin intermediate filament dimers. Nanotechnology 20 (425), 101–108.

Radmacher, M., 2007. Studying the mechanics of cellular processes by atomic force microscopy. Cell Mechanics 83, 347–372.

Roduit, C., Sekatski, S., et al., 2009. Stiffness tomography by atomic force microscopy. Biophysical Journal 97 (2), 674–677.

Rotsch, C., Radmacher, M., 2000. Drug-induced changes of cytoskeletal structure and mechanics in fibroblasts: an atomic force microscopy study. Biophysical Journal 78 (1), 520–535.

Sader, J.E., Larson, I., et al., 1995. Method for the calibration of atomic-force microscope cantilevers. Review of Scientific Instruments 66 (7), 3789–3798.

Sager, P.R., 1989. Cytoskeletal effects of acrylamide and 2,5-hexanedione – selective aggregation of vimentin filaments. Toxicology and Applied Pharmacology 97 (1), 141–155.

Schaffeld, M., Herrmann, H., et al., 2001. Vimentin and desmin of a cartilaginous fish, the shark Scyliorhinusstellaris: sequence, expression patterns and in vitro assembly. European Journal of Cell Biology 80 (11), 692–702.

Schopferer, M., Bar, H., et al., 2009. Desmin and vimentin intermediate filament networks: their viscoelastic properties investigated by mechanical rheometry. Journal of Molecular Biology 388 (1), 133–143.

Sjoberg, G., Saavedra-Matiz, C.A., et al., 1999. A missense mutation in the desmin rod domain is associated with autosomal dominant distal myopathy, and exerts a dominant negative effect on filament formation. Human Molecular Genetics 8 (12), 2191–2198.

Steinbock, F.A., Nikolic, B., et al., 2000. Dose-dependent linkage, assembly inhibition and disassembly of vimentin and cytokeratin 5/14 filaments through plectin's intermediate filament-binding domain. Journal of Cell Science 113 (3), 483–491.

Stolz, M., Raiteri, R., et al., 2004. Dynamic elastic modulus of porcine articular cartilage determined at two different levels of tissue organization by indentation-type atomic force microscopy. Biophysical Journal 86 (5), 3269–3283.

Storm, C., Pastore, J.J., et al., 2005. Nonlinear elasticity in biological gels. Nature 435 (7039), 191–194.

Wang, N., Butler, J.P., et al., 1993. Mechanotransduction across the cell-surface and through the cytoskeleton. Science 260 (5111), 1124–1127.

Wang, N., Stamenovic, D., 2000. Contribution of intermediate filaments to cell stiffness, stiffening, and growth. American Journal of Physiology – Cell Physiology 279 (1), C188–C194.

Wickert, U., Mucke, N., et al., 2005. Characterization of the in vitro co-assembly process of the intermediate filament proteins vimentin and desmin: mixed polymers at all stages of assembly. European Journal of Cell Biology 84 (2–3), 379–391.

nature nanotechnology

ARTICLES

PUBLISHED ONLINE: 21 OCTOBER 2012 | DOI: 10.1038/NNANO.2012.167

The nanomechanical signature of breast cancer

Marija Plodinec[1,2], Marko Loparic[1,2†], Christophe A. Monnier[1†], Ellen C. Obermann[3†], Rosanna Zanetti-Dallenbach[4†], Philipp Oertle[1], Janne T. Hyotyla[1], Ueli Aebi[2], Mohamed Bentires-Alj[5], Roderick Y. H. Lim[1]* and Cora-Ann Schoenenberger[2]

Cancer initiation and progression follow complex molecular and structural changes in the extracellular matrix and cellular architecture of living tissue. However, it remains poorly understood how the transformation from health to malignancy alters the mechanical properties of cells within the tumour microenvironment. Here, we show using an indentation-type atomic force microscope (IT-AFM) that unadulterated human breast biopsies display distinct stiffness profiles. Correlative stiffness maps obtained on normal and benign tissues show uniform stiffness profiles that are characterized by a single distinct peak. In contrast, malignant tissues have a broad distribution resulting from tissue heterogeneity, with a prominent low-stiffness peak representative of cancer cells. Similar findings are seen in specific stages of breast cancer in MMTV-PyMT transgenic mice. Further evidence obtained from the lungs of mice with late-stage tumours shows that migration and metastatic spreading is correlated to the low stiffness of hypoxia-associated cancer cells. Overall, nanomechanical profiling by IT-AFM provides quantitative indicators in the clinical diagnostics of breast cancer with translational significance.

Physical and chemical forces mediate the order by which cells proliferate, differentiate and migrate[1] within the three-dimensional microenvironment of living tissue[2]. Perturbations to this intricate balance[3–5] are known to promote tumorigenesis and progression to metastasis[6]. At the molecular level, tumour initiation and progression are accompanied by complex structural changes in the extracellular matrix (ECM) and cellular architecture, which are anticipated to develop differentiable mechanical responses[7]. However, it has been difficult to reach a consensus as to how such biomechanical heterogeneities occur and what their role might be. This is due to challenges in being able to discriminate between the mechanoresponses of cells and the surrounding ECM within native tumour tissue with adequate spatial/structural resolution and force sensitivity. Not least for its implications in diagnostics and treatment, being able to understand the mechanobiology of tumorigenesis is paramount in revealing its deterministic role in cancer development and metastasis[5].

Long-standing ambiguities exist because efforts to understand cancer biomechanics are largely polarized between tumour-level and single-cell experimentation. In accordance with conventional wisdom (breast palpation), studies on whole mouse mammary glands show that breast tumours are considerably more rigid than the surrounding tissue due to a relative stiffening of the peripheral tumour stroma[7,8]. This notion is consistent with the increase in matrix deposition and crosslinking observed in three-dimensional cell cultures and mouse mammary glands during cancer progression[9,10]. Paradoxically, biophysical techniques[11–16] reveal that single (cultured) cancer cells are more compliant (or 'softer') than their healthy counterparts. This increase in elasticity and/or deformability is accompanied by alterations in the cytoarchitecture that have known associations with malignant transformation[17]. Because of their softness, cancer cells have been detected by indentation-type atomic force microscopy (IT-AFM) in tissue sections from tumours that were surgically removed from patients with advanced cancer[18]. Furthermore, Cross *et al.* found that metastatic cells isolated from the pleural fluid of human patients are softer than normal cells[12], suggesting that metastasis might be promoted by cell compliance. No doubt, criticism is common on both sides of the length-scale divide. On the one hand, the mechanoresponse of whole tumours is arguably dominated by stiff structural elements in the peripheral stroma (for example, collagen[19,20]), leaving potentially more compliant regions in the underlying cancerous core insensitive to detection. On the other hand, the relevance of single cell measurements has been questioned given the lack of a proper three-dimensional tissue environment[21].

The diversity of biomechanical profiles underscores the importance of obtaining a holistic understanding of malignancy and how it manifests in breast tumours. This includes correlating biomechanical and microenvironmental properties at different stages of cancer progression. In this Article, we report on a comprehensive effort to correlate the nanomechanical properties of native human breast biopsies to specific histopathological markers in healthy tissue and in benign and malignant tumours. As a standard animal model, our human biopsy results are validated with systematic experiments on MMTV-PyMT (mouse mammary tumour virus-polyoma middle T antigen) transgenic mice[22], which we follow from early cancer to metastasis. In bridging across length scales, our nanomechanical measurements reconcile tumour-level and single-cell measurements in both humans and transgenic mice and reveal unique mechano-markers that can be used to identify different cancer stages. Moreover, these findings suggest close correlations between cell softening, tumour hypoxia and lung metastasis.

Nanomechanical signatures of human breast biopsies

To elucidate and correlate the respective nanomechanical profiles to pathohistological findings in normal, benign and malignant biopsies, we carried out IT-AFM analyses of *ex vivo* breast tissues under physiological buffer conditions. The experimental approach

---

[1] Biozentrum and the Swiss Nanoscience Institute, University of Basel, 4056 Basel, Switzerland, [2] Maurice E. Mueller Institute for Structural Biology, Biozentrum, University of Basel, 4056 Basel, Switzerland, [3] Institute of Pathology, University Hospital Basel, 4031 Basel, Switzerland, [4] Department of Gynecology and Gynecological Oncology, University Hospital Basel, University of Basel, 4031 Basel, Switzerland, [5] Mechanisms of Cancer, Friedrich Miescher Institute for Biomedical Research, 4058 Basel, Switzerland; † These authors contributed equally to this work. *e-mail: roderick.lim@unibas.ch

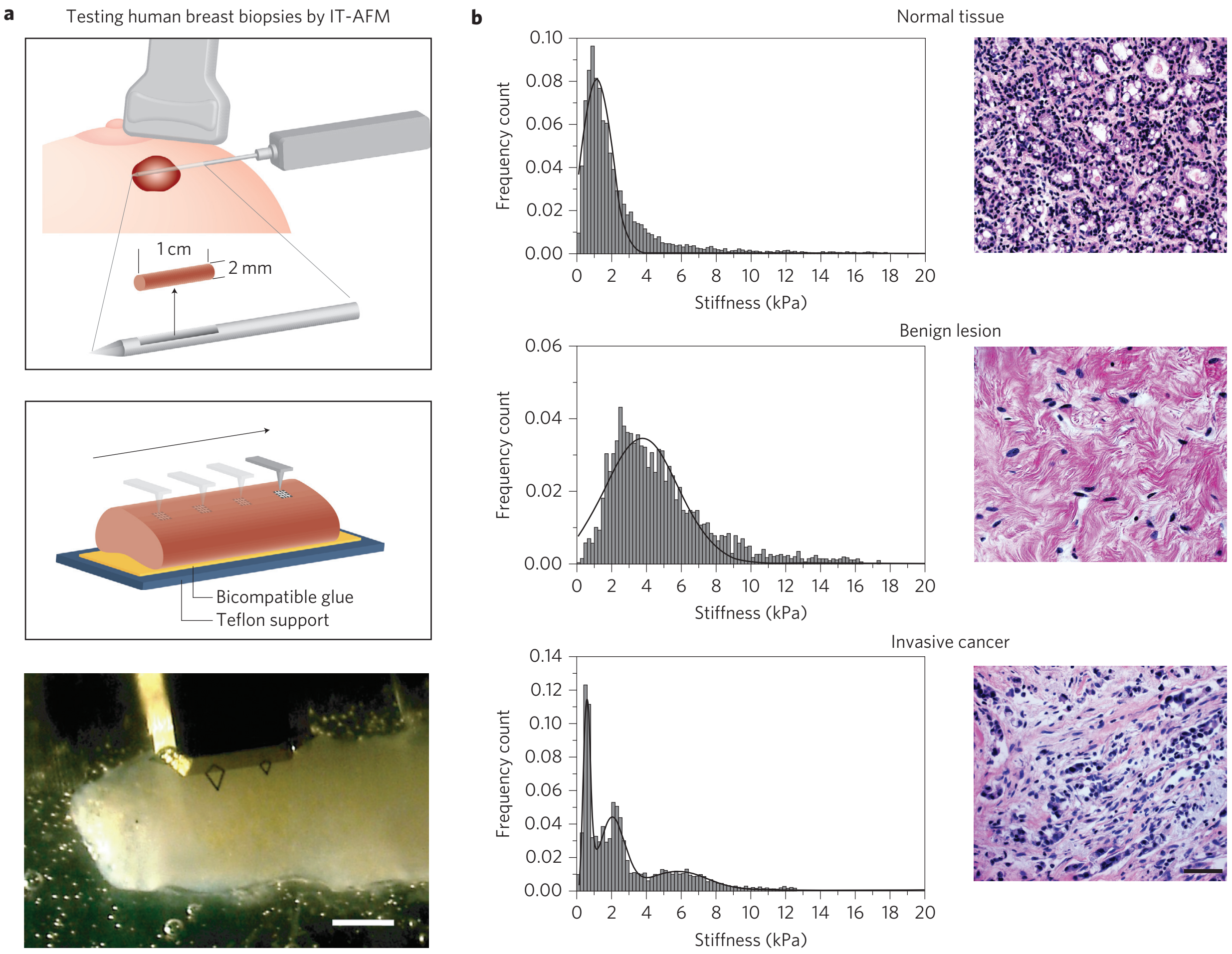

Figure 1 | Nanomechanical signatures of human breast tissue. a, Top: schematic of an ultrasound-guided biopsy from a patient with a suspicious lesion. Middle: multiple stiffness maps (20 × 20 μm each) are recorded in a defined geometrical pattern across the entire specimen. Bottom: top view of an oriented, immobilized biopsy in Ringer's solution with the cantilever positioned for IT-AFM. Scale bar, 500 μm. **b**, Top left: stiffness distribution for normal mammary gland tissue is unimodal. Top right: post-AFM H&E-stained section reveals the terminal ductal lobular unit of a normal mammary gland fenced by interstitial connective tissue. Middle left: biopsy-wide histogram for a benign lesion reveals a unimodal but broader stiffness distribution with an increase in stiffness compared with the healthy biopsy. Middle right: H&E-stained section reveals extensive fibrotic stroma interspersed with fibroblasts typical for fibroadenoma. Bottom left: heterogeneous stiffness distribution with a characteristic soft peak for malignant tumour tissue is consistent with histopathology (bottom right), revealing an invasive breast carcinoma with infiltrating nests of cancer cells that have evoked a dense fibrous tissue response. Scale bar applies to all images, 50 μm.

for obtaining multiple stiffness maps across entire biopsies is described in Fig. 1a. The tissue architecture and surface integrity of the biopsies were confirmed by scanning electron microscopy (SEM; Supplementary Fig. S1). Plotting a histogram of biopsy-wide stiffness values from a healthy specimen reveals a unimodal stiffness distribution of 1.13 ± 0.78 kPa (Fig. 1b, top left). Healthy ducts define the histological appearance in haematoxylin & eosin (H&E)-stained sections of the mapped specimen (Fig. 1b, top right). The benign fibroadenoma with its characteristic highly fibrotic content shows an increased stiffness of 3.68 ± 1.92 kPa (Fig. 1b, middle left). Softer features (<2 kPa) presumably represent individual fibroblasts embedded in the fibrotic stroma. Post-AFM histological examination of the mapped specimen confirmed fibroblasts to be the dominant cell type within the benign lesion[23] (Fig. 1b, middle right).

In comparison, a representative cancer biopsy typically exhibits a bimodal stiffness distribution with two prominent peaks at 0.57 ± 0.16 kPa ('peak 1') and 1.99 ± 0.73 kPa ('peak 2') (Fig. 1b, bottom left). At values stiffer than 2 kPa, a broadening in the distribution indicates a marked mechanical heterogeneity across the sample, with 'peak 3' located at 5.75 ± 1.62 kPa. Post-AFM H&E staining confirmed the dominance of tumour cells that infiltrate the stroma in a cord-like pattern (Fig. 1b, bottom right). We also assigned individual stiffness peaks to specific tissue morphologies by performing more detailed measurements within defined regions of the biopsy (Fig. 2a), in particular in the core (Fig. 2b) and at the periphery (Fig. 2c). The correlation of local AFM data with matching histologies corroborated that the soft peak is typical for cancer cells (Fig. 2b) that are surrounded by stiffer peripheral stroma (Fig. 2c).

Individual biopsy-wide stiffness distributions for 30 human biopsies (8 healthy, 8 benign and 14 malignant) are displayed in Supplementary Fig. S2 and peak stiffness values are summarized in Supplementary Table S1. In general, the nanomechanical signature of healthy breast tissue is characterized by a unimodal distribution with peak stiffness from 1.13 to 1.83 kPa. The stiffness distribution across benign lesions remains uniform; however, stiffness values range from 1.91 to 3.68 kPa and thus indicate a stiffer phenotype. All 14 biopsies with cancer exhibited a characteristic stiffness profile with a dominant peak at 0.31–0.75 kPa, that is, at least factor of two softer than healthy mammary gland epithelium ($P < 0.0001$). The nanomechanical signature of cancer included a second peak between 1.54 and 1.99 kPa. Another feature found in

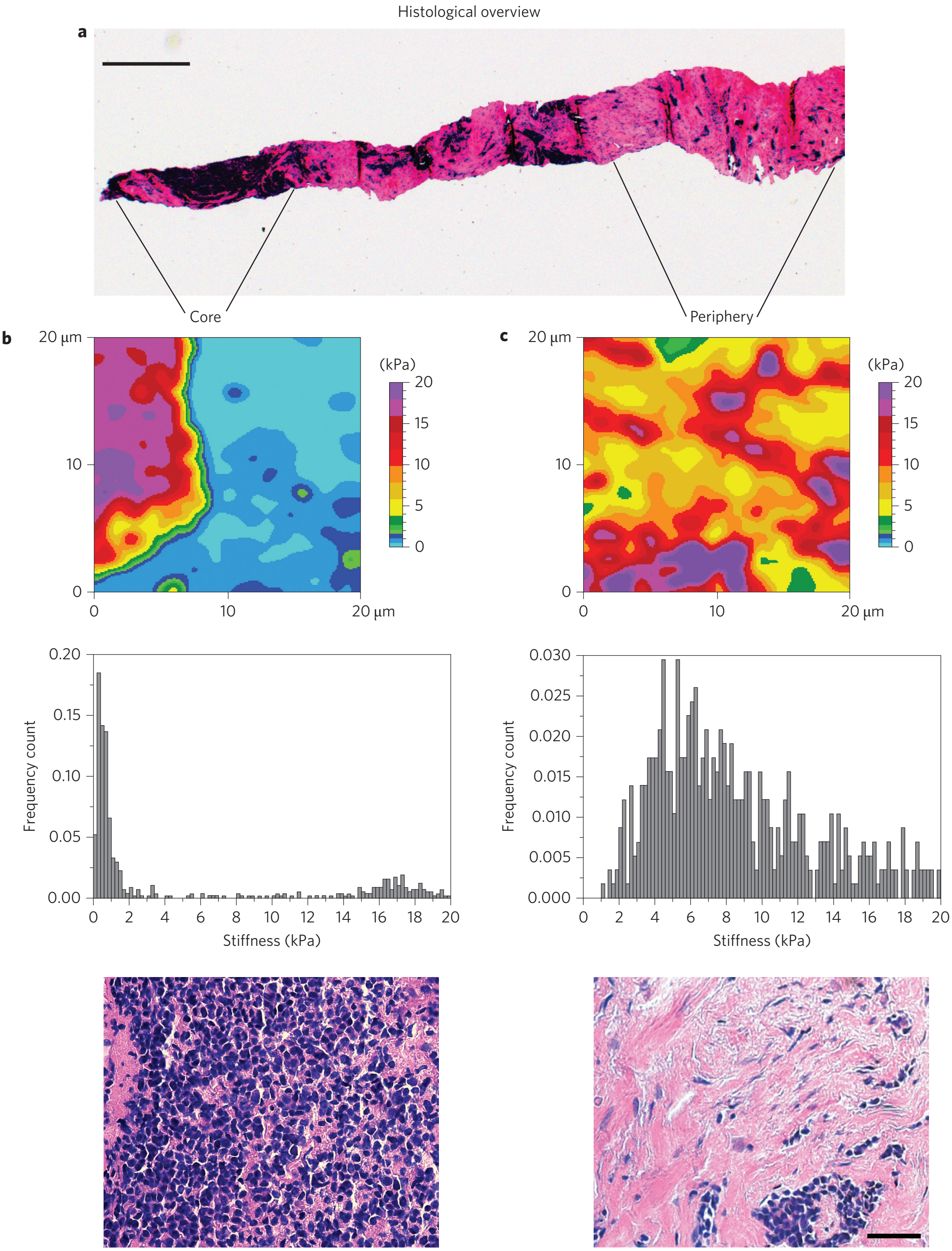

Figure 2 | Stiffness varies from core to periphery in human cancer biopsies. a, Post-AFM histological overview of the entire cancer biopsy with reference to the areas mapped in detail. Scale bar, 500 µm. **b**, Top: representative AFM stiffness map (24 × 24 pixels) of the core region visualizes pronounced softness within a narrow peak of specific stiffness values (middle). Bottom: the local histology shows that the core region is densely populated with cancer cells. **c**, Top: typical stiffness map (24 × 24 pixels) of the tumour periphery demonstrates stiff features. Middle: the corresponding stiffness distribution is broader and shifted towards stiffer values. Bottom: post-AFM histopathology reveals that the tumour periphery predominantly comprises fibrotic tissue. Scale bar, 50 µm (also applies to image in **b**).

several malignant biopsies is that the remaining stiffness values are broadly distributed up to ~20 kPa. This spread is indicative of the overall loss of mammary gland architecture accompanied by tumour vascularization and infiltration, and changes in the invasion-afflicted peripheral ECM[19,24]. Interestingly, cancer biopsies often demonstrate a distinct minimum (~1.1–1.5 kPa, Supplementary Fig. S3) between the primary and secondary peaks. Because it is inversely correlated to the average stiffness value for healthy breast tissue (Supplementary Fig. S3), we interpret the minimum to arise from the malignant transformation of healthy epithelium.

Nanomechanical staging of tumour progression

Because of the genetic and epidemiologic diversity in human patients we turned to MMTV-PyMT transgenic mice, a reliable model for

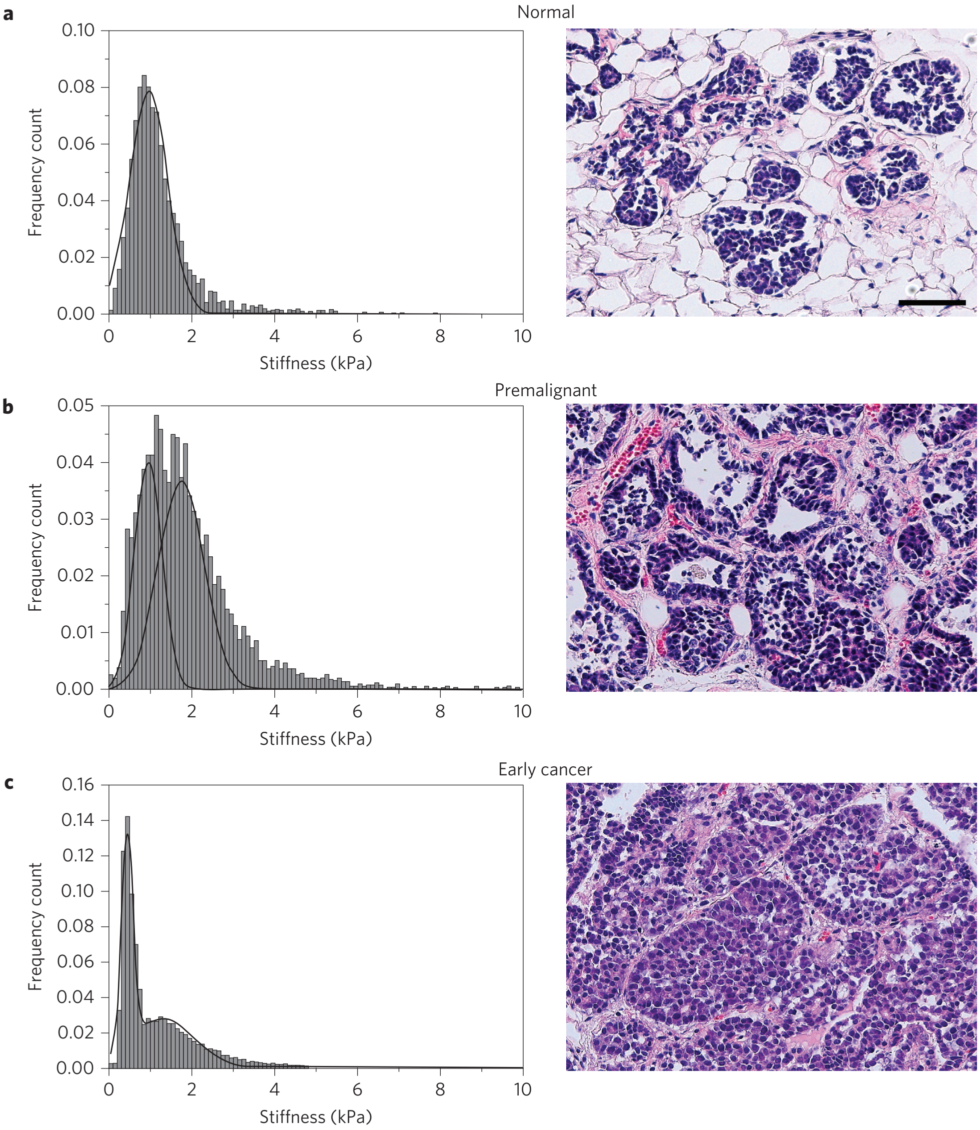

Figure 3 | Correlating the nanomechanical response with tumour progression in MMTV-PyMT mice. a, Left: stiffness values of normal ductal epithelium follow a uniform Gaussian distribution. Right: post-AFM H&E-stained section shows a non-lactating mammary gland with a duct surrounded by adipose tissue. **b**, Left: in the premalignant lesion, the contribution of stiffer features increases, as seen by a broader stiffness distribution with an indication of bimodality. Right: H&E-stained sections of the same tissue show extensive proliferation of epithelial cells and an increase of the surrounding stromal components. **c**, Left: in early cancer, the significant softening produces a characteristic peak that dominates the prominent bimodality of the stiffness distribution. Right: in the H&E section, cancer cells are delineated by stromal tissue. Scale bar in **a** applies to images in **b** and **c**, 50 μm.

human breast cancer, to more systematically elucidate the nanomechanical markers of tumour progression and metastasis[22]. For the corresponding staging of MMTV-PyMT specimens used for stiffness mapping, we monitored the loss of integrin β1 expression, which accompanies tumour progression[22] (Supplementary Fig. S4).

The biopsy-wide histogram across a normal mouse mammary gland revealed a unimodal stiffness distribution with a peak of 1.02 ± 0.42 kPa (Fig. 3a, left) that is characteristic of healthy mammary tissue, with its well-organized arrangement of densely packed epithelial cells (Fig. 3a, right). The uniform stiffness profile is comparable to that of normal human breast. It should be noted, however, that in contrast to human breast tissues, healthy murine mammary glands exhibit extensive amounts of adipose tissue (70–80%) (Supplementary Fig. S5a).

The biopsy-wide histogram of premalignant tissues shows the onset of a bimodal stiffness distribution with peaks at 0.95 ± 0.18 and 1.75 ± 0.27 kPa, as identified by peak-analysing software. The presence of soft and moderately stiffer features correlates with an increase of stromal components surrounding the proliferative cell masses revealed in H&E stained sections (Fig. 3b, right).

In early cancer samples, this trend is more pronounced, resulting from distinct soft and stiff areas (Fig. 3c, left), as demonstrated by the peaks at 0.45 ± 0.12 and 1.29 ± 0.76 kPa, respectively. These correspond to distinct zones of densely packed cancer cells and early stromal invasion, as revealed in H&E stained sections (Fig. 3c, right). A summary of the peak stiffness values that were calculated for murine mammary tissues is presented in Supplementary Table S2.

As mentioned above, adipose tissue is prevalent in murine mammary glands and, because of its softness, could be mistaken for cancer cell clusters. Control experiments on adipose tissues demonstrated that the two cell types could be discriminated by their stiffness (Supplementary Fig. S5). Mammary adipocytes exhibit a stiffness of 0.31 ± 0.13 kPa (Supplementary Fig. S5a, middle), whereas cancer cells have a stiffness peak at 0.75 ± 0.25 kPa (Supplementary Fig. S5b, middle).

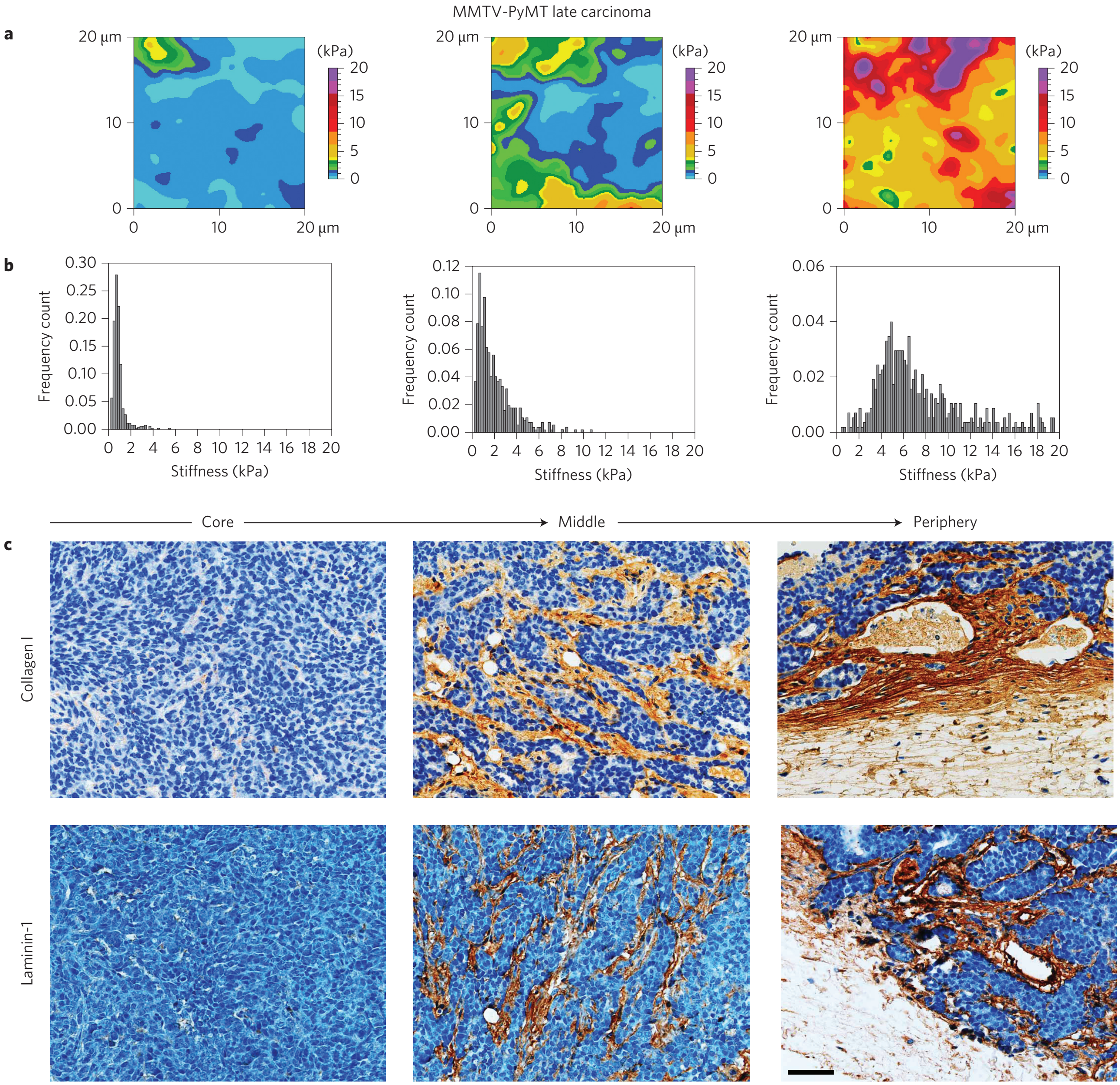

Figure 4 | Correlating local nanomechanical properties and ECM structure in late cancer. a, Consecutive stiffness maps (24 × 24 pixels) across the sample demonstrate a significant increase in stiffness and mechanical heterogeneity from core to periphery (left to right). **b**, Corresponding stiffness distributions change from the core to the periphery. **c**, IHC analysis (brown staining) reveals associated structural and morphological changes in collagen I (top) and laminin-1 (bottom) from core to periphery. Scale bar applies to all images, 50 μm.

Among the most substantial structural changes in mammary gland architecture that occur with the transition from normal mammary gland to early cancer are the degradation of the basement membrane that surrounds normal and premalignant glands (Supplementary Fig. S6, top) and the altered expression and organization of collagen I (Supplementary Fig. S6, bottom). In later stages of tumour progression, stromal contributions increasingly modify cancer behaviour[25]. For example, collagen I, which is the main component of the ECM, is associated with cancer stiffening[19,21]. Therefore, we examined the relation between local nanomechanical profiles and ECM structure in late MMTV-PyMT cancer, which corresponds to invasive ductal carcinomas in humans. Sequential stiffness maps across the specimen demonstrate gradual stiffening from the core to the periphery (Fig. 4a), with peak values shifting from 0.74 ± 0.26 kPa in the core to 5.51 ± 1.70 kPa at the periphery (Fig. 4b). At the same time, mechanical heterogeneity increases and is most extensive at the periphery. These changes appear to be associated with distinct changes in the ECM, as revealed by subsequent immunohistochemistry (IHC) analysis (Fig. 4c).

In particular, collagen I is not detected in the soft core but is increasingly present towards the periphery (Fig. 4c, top). Also, laminin-1 expression is virtually absent from the core (Fig. 4c, bottom left), as expected in advanced cancer where the basement membrane has disintegrated[26]. However, the increased vascularization of the mid and peripheral areas resulted in laminin-1 staining of vessel basement membranes (Fig. 4c, bottom middle and right). We conclude that the absence of laminin-1 and collagen I in the core regions contributes to the soft phenotype of cancer cells. On the other hand, the increased staining of laminin-1 and collagen I towards the periphery marks the increase of stromal invasion related to stiffening in the respective regions. Clearly, IHC analyses show that there is considerable tissue heterogeneity at

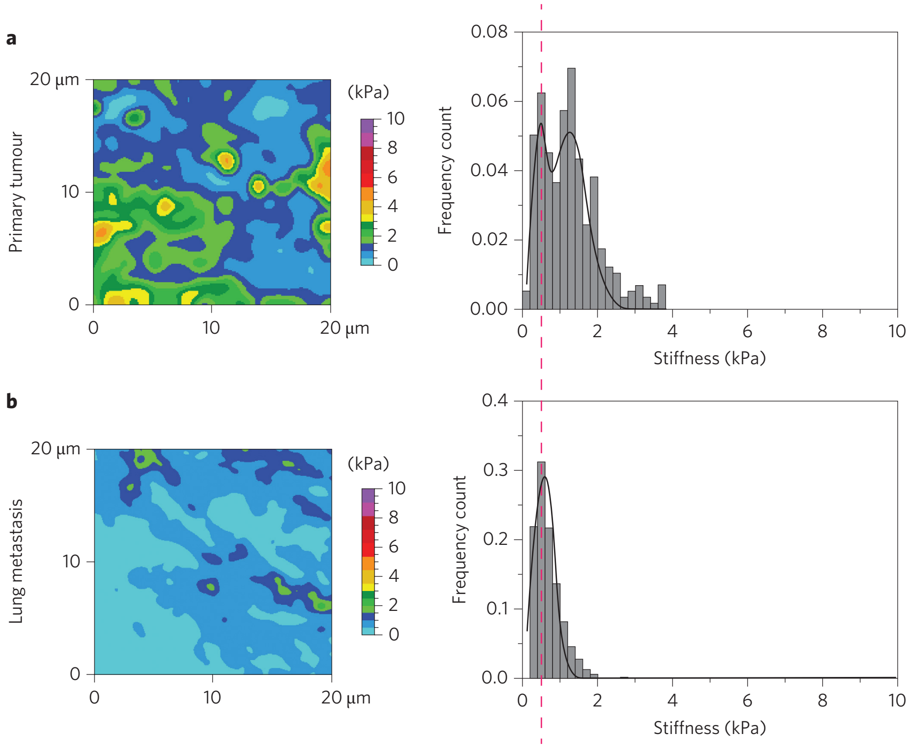

Figure 5 | Stiffness profiles of primary tumour and lung metastasis reveal a common phenotype. a, Left: representative AFM stiffness map (24 × 24 pixels) demonstrates nanomechanical heterogeneity among cancer cells in primary lesions. Right: the corresponding stiffness distribution from the map reveals two peaks representing distinct phenotypes of cancer cells, a softer one at 0.45 ± 0.15 kPa and another at 1.26 ± 0.43 kPa. **b**, Left: representative AFM stiffness map (24 × 24 pixels) of a metastatic lesion and the corresponding stiffness distribution (right) reveal a peak value that is almost identical to the softer peak detected at the primary tumour site (indicated by the red dashed line).

late tumour stages that is reflected in the broad range of stiffness values (Fig. 4b).

The indications that the stiffness signatures are based on distinct changes in the cytoarchitecture and ECM in MMTV-PyMT transgenic mice prompted us to follow up on this correlation in human breast cancer biopsies (Supplementary Fig. S7). Overall, the staining patterns in human biopsies diagnosed with invasive cancer were similar to those observed in the late cancer stage of MMTV-PyMT mammary tissues (Fig. 4, Supplementary Fig. S7). At the cellular level, a distinct expression of desmin and vimentin, both markers of epithelial–mesenchymal transition (EMT), was found in cancer cells, but also in the adjacent stroma of the invasive lobular (Supplementary Fig. S7c) and ductal (Supplementary Fig. S7d) carcinomas. We therefore rationalize that the soft phenotype detected in human cancer biopsies (Supplementary Fig. S2, Table S1) is an indication of tumour progression.

A soft hypoxic cell phenotype is conducive to metastasis

We next asked whether the very soft cancer phenotypes could be associated with the ability to metastasize to distant sites, in particular to the lungs where metastases frequently occur in MMTV-PyMT mice at late stages of tumour progression[27,28]. Stiffness measurements from lungs of mice bearing late-stage tumours reveal an extremely soft peak (Supplementary Fig. S8a) that is absent in healthy lungs (Supplementary Fig. S8b; statistical differences between specimens are presented in Supplementary Table S3). Most importantly, with a stiffness peak of 0.45 ± 0.15 kPa, the softest nanomechanical phenotype present at the primary tumour site (Fig. 5a) closely corresponds to the stiffness of a metastatic lesion obtained from the lungs of the same mouse (0.56 ± 0.26 kPa, Fig. 5b).

Because a hypoxic core is a key feature of aggressive cancers[29], we examined whether the nanomechanical changes associated with cancer progression are related to reduced tumour oxygenation by injecting MMTV-PyMT mice at distinct stages of tumour progression with pimonidazole (a probe that selectively binds to hypoxic cells), 90 min before tumour excision. As expected, normal glands and premalignant lesions were negative for hypoxia (Fig. 6, top left and middle). In contrast, early cancer exhibited central hypoxia (Fig. 6, right) that correlated well with a significant decrease of cell stiffness (Fig. 3c, left; Supplementary Table S2). In late cancer, dissemination of hypoxic cancer cells to areas of stromal invasion and to the tumour periphery (Fig. 6, bottom left) adds to the mechanical heterogeneity observed in these regions (Fig. 4b). Moreover, their presence suggests that a decreased stiffness is able to promote the metastatic spread of soft cells to the lungs (Fig. 5).

The role of mechanical properties in cancer development and progression has prompted high-powered research initiatives worldwide. Several studies in recent years have led to the notion that tumours are generally stiffer than healthy tissue[30] and that continuous tissue stiffening is a promoter of cancer[10,31]. Contrary to this dogma, there are numerous studies reporting that single isolated cancer cells are significantly softer than normal cells[32]. However, two-dimensional systems do not recapitulate the architecture or surrounding forces to which a cell is exposed in its native tissue environment[7,33]. Here, our work resolves the stiffness paradox by exploiting the nanomechanical sensitivity of IT-AFM[34] and its unprecedented spatial resolution to comprehensively investigate the mechanical properties of native breast biopsies from human patients (Supplementary Table S1). The most striking finding is that normal glandular tissue, benign lesions and malignant tumours exhibit qualitatively unique biomechanical signatures that are reproducible across different patients. Malignancies are recognized by two features: (i) mechanical heterogeneity in line with histological appearance and (ii) a characteristic stiffness peak of 0.5–0.8 kPa measured in areas with densely packed tumour cells and little intervening stroma. Normal glandular epithelium and benign solid lesions on the other hand each exhibit a

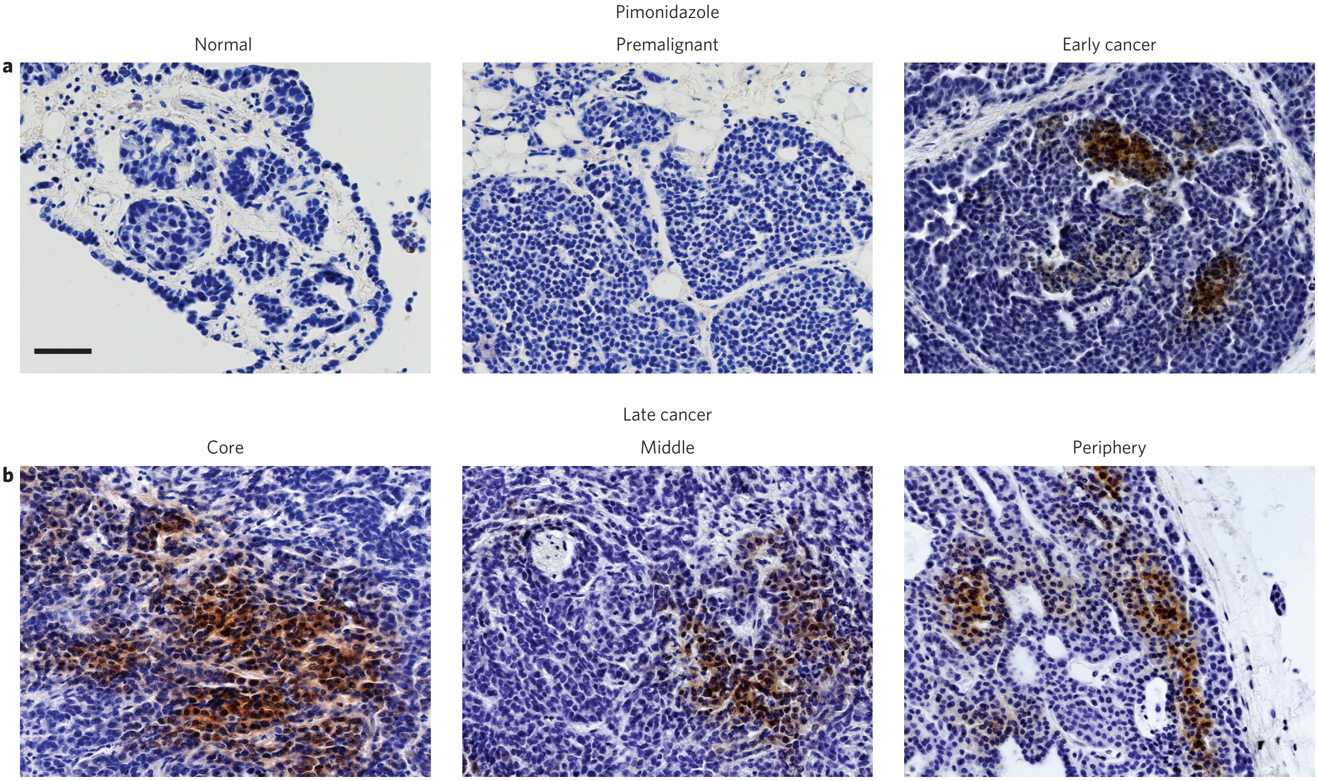

Figure 6 | Dissemination of hypoxic cancer cells increases with tumour progression. Paraffin-embedded sections of mammary gland tissues of pimonidazole (hypoxyprobe)-treated MMTV-PyMT mice at different stages were immunolabelled. **a**, Hypoxia is absent in normal glandular tissue (left) and in premalignant lesions (middle). In contrast, pimonidazole-positive cells (brown staining) reveal central hypoxia in early cancer (right). **b**, In advanced cancer stages, hypoxic cells abundant in the core region (left) are streaming towards tumour blood vessels (middle) and have disseminated to the tumour periphery (right). Scale bar applies to all images, 50 μm.

unimodal stiffness distribution with peaks at ~1 kPa and ~3 kPa, respectively. In fact, signature-based diagnoses in double-blind experiments correlate nearly 100% with conventional histopathology of the same biopsy post-AFM.

Detecting solid breast lesions by differential tissue elasticity is also the underlying principle in sonoelastography, which has emerged as a clinical, non-invasive diagnostic technique in recent years[35]. However, the length scale of this approach does not allow for a reliable distinction of benign and malignant breast masses[36,37]. This challenge is uniquely met by IT-AFM, which is able to differentiate between cancer and benign lesions by correlating stiffness measurements resolved at the nanometre scale across the entire length of a biopsy.

Conclusions

We have resolved the nanomechanical signatures of defined stages of tumour progression, including metastasis. Most notably, high-resolution stiffness mapping has revealed that cancer progression is not limited to matrix stiffening, as previously assumed[10], but is associated with a significant softening of tumour epithelial cells in comparison to normal mammary epithelium. This distinctive softening probably went unnoticed in a recent AFM study[32], because the 5 μm colloidal probe that was used only allowed for bulk measurements that did not provide sufficient resolution to distinguish between the individual tissue components (that is, the cells and ECM[32,38]). Tumour progression to the late, invasive stage accentuates the soft peak and brings about a broadening of the stiffness distribution (Fig. 4) as a result of the cancer cells infiltrating the surrounding tissue, as well as stromal disorganization and tumour vascularization[31].

Recent evidence shows that hypoxia promotes tumour invasion and ultimately metastases, and thus is associated with tumour aggressiveness[38,39]. Also, it has long been hypothesized in the field that metastatic cells need a certain degree of flexibility and deformability to escape their original niche[40–42]. By analysing metastatic lesions in lungs from MMTV-PyMT mice we now provide the first evidence that supports this hypothesis. These data indicate a direct link between cancer cell softening in the primary tumour and aggressive behaviour leading to metastases. In conclusion, soft peaks detected in the primary tumour may serve not only as mechanobiological markers for the onset of cancer but have prognostic qualities as well.

Methods

Human biopsies. Human biopsies were obtained from the outpatient breast clinic, Department of Gynecology and Gynecological Oncology, University Hospital Basel. The study was approved by the institutional review board (ref. no. EK:157/08) and conducted in accordance with ethical guidelines. Patient recruitment was carried out with informed consent. For each patient, one out of five biopsies was used for IT-AFM analysis directly after removal, without previous knowledge of clinical data. The other four biopsies were evaluated by standard pathological procedures. Cylindrical specimens with a diameter of ~0.2 cm and length of 0.2–1 cm were biopsied from suspicious lesions under ultrasound guidance (Fig. 1a). Biopsies were immediately transferred to ice-cold isotonic Ringer solution (6.00 g NaCl, 0.40 g KCl, 50 g anhydric glucose, 0.27 g $CaCl_2$, 3.20 g lactic acid per 1,000 ml of distilled water) supplemented with glucose and a protease inhibitor cocktail (Complete, Boehringer Mannheim; 1 tablet per 10 ml) and kept at 4 °C to minimize tissue degradation. IT-AFM analysis was performed no later than three days after biopsy.

Mammary and lung tissue samples from MMTV-PyMT mice. All procedures involving mice were conducted in accordance with the Swiss laws regulating the use and care of animals in research and have been reviewed and approved by the Federal veterinary office. Female mice heterozygous for the PyMT transgene were obtained by breeding male PyMT mice on a FVB background with FVB females lacking the PyMT transgene. Mice were killed at different time points of tumour development[22], and mammary tissues and lungs from at least six different mice were immediately excised and placed in ice-cold Ringer solution. IT-AFM was performed 1–72 h after tissue removal, after which stiffness profiles were essentially unaltered

(Supplementary Fig. S9) and tissue integrity intact as judged by RNA stability (Supplementary Fig. S9 and Supplementary Information on RNA isolation). For hypoxia assessment, mice were injected intraperitoneally with pimonidazole hydrochloride at 100 mg ml^{-1} in 0.9% sterile saline solution (120 mg kg^{-1}, hypoxyprobe-1, HPI). After 90 min, mice were killed and tissue specimens taken for IT-AFM. Hypoxia was demonstrated by immunohistochemical analysis of pimonidazole incorporation according to a standard protocol[42].

IT-AFM and data analysis. All preparative steps were performed in a sterile buffer environment supplemented with protease inhibitors. Each specimen was immobilized on a plastic dish with a thin layer of two-component fast drying epoxy glue (Devcon). Mechanical manipulations during sample preparation were kept minimal at all times. To level out the surface to be scanned, small wedges were placed under uneven specimens. IT-AFM was carried out with a noise-isolated FlexAFM ARTIDIS (Nanosurf AG) and a Nanowizard I atomic force microscope (JPK Instruments). To compensate for large surface corrugations on such native biological samples, we developed and implemented customized homebuilt hardware and software algorithms for automated levelling, which enabled uninterrupted AFM operation during data acquisition (see Supplementary Information on Automated levelling). A top-down microscope (S8AP0 with Imagesource DFK 31F03, Leica) was used to visually position the AFM cantilever with respect to the specimen. Four-sided pyramidal tips (205-μm-long DNP-S10 triangular silicon nitride cantilevers, resonance frequency (air) $f = 18$ kHz, nominal cantilever spring constant $k = 0.06$ Nm^{-1}, tip radius = 20 nm, half-open angle of the pyramidal face of $\theta \approx 35^\circ$, Bruker) were used. The exact spring constant k of the cantilever was determined before each experiment using the thermal tune method[43] and the deflection sensitivity was determined in fluid using glass substrates as an infinitely stiff reference material. IT-AFM at room temperature involved recording up to 22 different 20 × 20 μm^2 force–volume maps over 24 × 24 point grids (576 force–displacement curves per map and a pixel size of 833 nm) and for high spatial resolution 72 × 72 point grids (5,184 force–displacement curves per map and a pixel size of 277 nm) were recorded. Force–volume maps spaced at 500 μm apart were acquired in a systematic manner across the entire sample surface (Fig. 1a). Individual force curves consisted of 512 data points, with a Z piezo-displacement between 5 and 8 μm, which were collected at 0.8–1 load/unload cycles per second. The maximum applied loading force was set to 1.8 nN, which gave indentation depths that varied approximately between 150 and 3,000 nm depending on the intrinsic mechanical differences within each biopsy (examples are shown in Supplementary Fig. S10). Force curves were analysed using the Oliver and Pharr method[44] as described previously[45–47]. See Supplementary Methods on Oliver and Pharr analysis for further details. The stiffness values (Pa = N m^{-2}) calculated from force curves were spatially plotted to yield colour-coded stiffness maps in Igor Pro 6.22 (Wavemetrics). A two-dimensional spline interpolation was performed on the stiffness maps to smooth the visual presentation of the data.

Statistics. A total of 30 human breast biopsies from female patients (Supplementary Table S1) and 27 mammary glands and 6 lungs obtained from 13 MMTV-PyMT mice were analysed. All individual stiffness values for a specimen were summarized in OriginPro 8.5 (Microcal) to obtain the distribution of stiffness values (henceforth defined as biopsy-wide histogram). The bin width was set to 200 Pa for all mammary gland specimens and 500 Pa for the murine lungs. Counts were normalized according to the total amount of measured stiffness values per specimen. For data fitting, peaks were located with the peak analysis application of OriginPro. Subsequently, a multi-peak fit was applied to the stiffness distribution. All data are given as mean ± standard deviation. The statistical significance of differences in mean values was assessed with the paired Student's t-test in OriginPro 8.5. Statistical significance was set at $P \leq 0.05$.

Immunohistochemical analysis. After IT-AFM, all samples were retrieved, formalin-fixed and paraffin-embedded according to standard histological procedures. Sections with a thickness of ~5 μm were cut and transferred onto coated glass slides. The first and last slides of sequential sections were routinely stained with H&E. Subsequent histopathological examination included assessing the type of lesion (invasive ductal carcinoma, fibroadenoma and so on) and a number of standard histopathological markers (extent of tumour infiltration, fibrosis, necrosis and lymphocytic infiltration). For IHC analysis of the remaining slides of human mammary tissues, the following antibodies were used: anti-collagen I (1:80; Biologo CO2111), anti-laminin (1:25; Thermo RB-082-A, Thermo Scientific), anti-vimentin (prediluted, Ventana 790-2917, Roche Diagnostics), anti-desmin (prediluted, Ventana 760-2513, Roche Diagnostics). IHC analysis of murine tissue sections for laminin was performed in the same manner as for human sections. In addition, murine sections were stained with anti-β1 integrin (1:50, Abcam, ab52971) and anti-mouse collagen I (1:800, Abcam, ab34710). In some cases, sections were treated for antigen retrieval by heat or with 10 mM Tris buffer, 1 mM EDTA, pH 9.0 and citrate buffer, pH 6.0. For collagen staining of human biopsies, sections were pre-treated with pepsin for 30 min at room temperature. Avidin/biotin was used for blocking non-specific binding of the primary antibody. For immunolabelling, sections were incubated with 100 μl antibodies correspondingly diluted in 10 mM PBS, pH 7.6 and 0.1% sodium azide. Staining was visualized with horseradish peroxidase (HRP)-conjugated secondary antibodies (DakoCytomation). Sections were examined with an upright light microscope (Carl Zeiss) at the magnifications indicated.

Received 29 June 2012; accepted 29 August 2012; published online 21 October 2012

References

1. Ingber, D. E. *et al.* Cellular tensegrity—exploring how mechanical changes in the cytoskeleton regulate cell-growth, migration, and tissue pattern during morphogenesis. *Int. Rev. Cytol.* **150,** 173–224 (1994).
2. Park, C. C., Bissell, M. J. & Barcellos-Hoff, M. H. The influence of the microenvironment on the malignant phenotype. *Mol. Med. Today* **6,** 324–329 (2000).
3. Needham, D. Possible role of cell cycle-dependent morphology, geometry, and mechanical-properties in tumor-cell metastasis. *Cell Biophys.* **18,** 99–121 (1991).
4. Paszek, M. J. & Weaver, V. M. The tension mounts: mechanics meets morphogenesis and malignancy. *J. Mammary Gland Biol.* **9,** 325–342 (2004).
5. Kumar, S. & Weaver, V. Mechanics, malignancy, and metastasis: the force journey of a tumor cell. *Cancer Metast. Rev.* **28,** 113–127 (2009).
6. Kass, L., Erler, J. T., Dembo, M. & Weaver, V. M. Mammary epithelial cell: influence of extracellular matrix composition and organization during development and tumorigenesis. *Int. J. Biochem. Cell B* **39,** 1987–1994 (2007).
7. Butcher, D. T., Alliston, T. & Weaver, V. M. A tense situation: forcing tumour progression. *Nature Rev. Cancer* **9,** 108–122 (2009).
8. Sinkus, R. *et al.* High-resolution tensor MR elastography for breast tumour detection. *Phys. Med. Biol.* **45,** 1649–1664 (2000).
9. Paszek, M. J. *et al.* Tensional homeostasis and the malignant phenotype. *Cancer Cell* **8,** 241–254 (2005).
10. Levental, K. R. *et al.* Matrix crosslinking forces tumor progression by enhancing integrin signaling. *Cell* **139,** 891–906 (2009).
11. Rosenbluth, M. J., Lam, W. A. & Fletcher, D. A. Force microscopy of nonadherent cells: a comparison of leukemia cell deformability. *Biophys. J.* **90,** 2994–3003 (2006).
12. Cross, S. E., Jin, Y. S., Rao, J. & Gimzewski, J. K. Nanomechanical analysis of cells from cancer patients. *Nature Nanotech.* **2,** 780–783 (2007).
13. Lekka, M. *et al.* Elasticity of normal and cancerous human bladder cells studied by scanning force microscopy. *Eur. Biophys. J. Biophy.* **28,** 312–316 (1999).
14. Ward, K. A., Li, W. I., Zimmer, S. & Davis, T. Viscoelastic properties of transformed-cells—role in tumor-cell progression and metastasis formation. *Biorheology* **28,** 301–313 (1991).
15. Lam, W. A., Rosenbluth, M. J. & Fletcher, D. A. Chemotherapy exposure increases leukemia cell stiffness. *Blood* **109,** 3505–3508 (2007).
16. Guck, J. *et al.* Optical deformability as an inherent cell marker for testing malignant transformation and metastatic competence. *Biophys. J.* **88,** 3689–3698 (2005).
17. Suresh, S. Biomechanics and biophysics of cancer cells. *Acta Mater.* **55,** 3989–4014 (2007).
18. Lekka, M. *et al.* Cancer cell detection in tissue sections using AFM. *Arch. Biochem. Biophys.* **518,** 151–156 (2012).
19. Weaver, V. M. *et al.* Matrix crosslinking forces tumor progression by enhancing integrin signaling. *Cell* **139,** 891–906 (2009).
20. Erler, J. T. & Weaver, V. M. Three-dimensional context regulation of metastasis. *Clin. Exp. Metastasis* **26,** 35–49 (2009).
21. Weaver, V. M., DuFort, C. C. & Paszek, M. J. Balancing forces: architectural control of mechanotransduction. *Nature Rev. Mol. Cell. Biol.* **12,** 308–319 (2011).
22. Lin, E. Y. *et al.* Progression to malignancy in the polyoma middle T oncoprotein mouse breast cancer model provides a reliable model for human diseases. *Am. J. Pathol.* **163,** 2113–2126 (2003).
23. Lundin, M., Lundin, J., Helin, H. & Isola, J. A digital atlas of breast histopathology: an application of web based virtual microscopy. *J. Clin. Pathol.* **57,** 1288–1291 (2004).
24. Weaver, V. M. *et al.* Tensional homeostasis and the malignant phenotype. *Cancer Cell* **8,** 241–254 (2005).
25. Egeblad, M. & Werb, Z. New functions for the matrix metalloproteinases in cancer progression. *Nature Rev. Cancer* **2,** 161–174 (2002).
26. Albrechtsen, R., Nielsen, M., Wewer, U., Engvall, E. & Ruoslahti, E. Basement membrane changes in breast cancer detected by immunohistochemical staining for laminin. *Cancer Res.* **41,** 5076–5081 (1981).
27. Guy, C. T., Cardiff, R. D. & Muller, W. J. Induction of mammary tumors by expression of polyomavirus middle T oncogene: a transgenic mouse model for metastatic disease. *Mol. Cell Biol.* **12,** 954–961 (1992).
28. Fantozzi, A. & Christofori, G. Mouse models of breast cancer metastasis. *Breast Cancer Res.* **8,** 212 (2006).
29. Guppy, M. The hypoxic core: a possible answer to the cancer paradox. *Biochem. Biophys. Res. Commun.* **299,** 676–680 (2002).
30. Sedwick, C. Valerie Weaver: overcoming cancer's stiff resistance. *J. Cell. Biol.* **193,** 802–803 (2011).
31. Lopez, J. I., Kang, I., You, W. K., McDonald, D. M. & Weaver, V. M. *In situ* force mapping of mammary gland transformation. *Integr. Biol. (Camb.)* **3,** 910–921 (2011).

32. Suresh, S. Biomechanics and biophysics of cancer cells. *Acta Biomater.* **3,** 413–438 (2007).
33. Alcaraz, J. *et al.* Collective epithelial cell invasion overcomes mechanical barriers of collagenous extracellular matrix by a narrow tube-like geometry and MMP14-dependent local softening. *Integr. Biol. (Camb.)* **3,** 1153–1166 (2011).
34. Stolz, M. *et al.* Early detection of aging cartilage and osteoarthritis in mice and patient samples using atomic force microscopy. *Nature Nanotech.* **4,** 186–192 (2009).
35. Thomas, A. *et al.* Real-time elastography—an advanced method of ultrasound: first results in 108 patients with breast lesions. *Ultrasound Obst. Gyn.* **28,** 335–340 (2006).
36. Burnside, E. S. *et al.* Differentiating benign from malignant solid breast masses with US strain imaging. *Radiology* **245,** 401–410 (2007).
37. Xu, H. Y. *et al.* Axial-shear strain imaging for differentiating benign and malignant breast masses. *Ultrasound Med. Biol.* **36,** 1813–1824 (2010).
38. Wong, C. C. L. *et al.* Hypoxia-inducible factor 1 is a master regulator of breast cancer metastatic niche formation. *Proc. Natl Acad. Sci. USA* **108,** 16369–16374 (2011).
39. Erler, J. T. *et al.* Lysyl oxidase is essential for hypoxia-induced metastasis. *Nature* **440,** 1222–1226 (2006).
40. Fritsch, A. *et al.* Are biomechanical changes necessary for tumour progression? *Nature Phys.* **6,** 730–732 (2010).
41. Wirtz, D., Konstantopoulos, K. & Searson, P. C. The physics of cancer: the role of physical interactions and mechanical forces in metastasis. *Nature Rev. Cancer* **11,** 512–522 (2011).
42. Erler, J. T., Jeffrey, S. S. & Giaccia, A. J. Hypoxia promotes invasion and metastasis of breast cancer cells by increasing lysyl oxidase expression. *Breast Cancer Res.* **7,** S57 (2005).
43. Sader, J. E., Larson, I., Mulvaney, P. & White, L. R. Method for the calibration of atomic-force microscope cantilevers. *Rev. Sci. Instrum.* **66,** 3789–3798 (1995).
44. Oliver, W. C. & Pharr, G. M. An improved technique for determining hardness and elastic-modulus using load and displacement sensing indentation experiments. *J. Mater. Res.* **7,** 1564–1583 (1992).
45. Plodinec, M., Loparic, M. & Aebi, U. Atomic force microscopy for biological imaging and mechanical testing across length scales. *Cold Spring Harb. Protoc.* **2010,** pdb top86 (2010).
46. Loparic, M. *et al.* Micro- and nanomechanical analysis of articular cartilage by indentation-type atomic force microscopy: validation with a gel-microfiber composite. *Biophys. J.* **98,** 2731–2740 (2010).
47. Plodinec, M. *et al.* The nanomechanical properties of rat fibroblasts are modulated by interfering with the vimentin intermediate filament system. *J. Struct. Biol.* **174,** 476–484 (2011).

Acknowledgements

The authors thank U. Mueller for excising tissues from MMTV-PyMT mice, T. Nguyen and P. Hirschmann for technical assistance with histology and IHC, and R. Suetterlin for advice on IHC. B. Bircher is acknowledged for his contribution to AFM data analysis, T. Pfändler for logistic support concerning clinical samples and A. Roulier for help with the drawing in Fig. 1. The authors also thank U. Sauder for SEM sample preparation, D. Mathys for SEM imaging and P. Demougin for RNA extraction. This work is funded by the National Centre of Competence in Research 'Nanoscale Science', Swiss National Science Foundation (to C-A.S.), and the Commission for Technology and Innovation (CTI) supporting university–industry partnerships (Project 11977.2 PFNM-NM within the project ARTIDIS 'Automated and Reliable Tissue Diagnostics' awarded to R.Y.H.L in partnership with Nanosurf AG). R.Z.D. is supported by Krebsliga Beider Basel (grant no. 22-2010). The laboratory of M.B-A. is supported by the Novartis Research Foundation, the European Research Council (ERC starting grant no. 243211-PTPsBDC), the Swiss Cancer League and the Krebsliga Beider Basel.

Author contributions

M.P., R.Y.H.L. and C-A.S. conceived the study and designed experiments. M.P., M.L. and R.Y.H.L. developed all customized hardware and software solutions for AFM. M.P. and E.C.O. performed pathohistological and IHC analysis of human and murine tissues. R.Z.D. recruited patients and provided human biopsies. M.P., C.A.M. and P.O. performed AFM experiments. M.P., M.L, C.A.M., J.T.H., P.O. and R.Y.H.L. analysed AFM data. M.B-A. provided MMTV-PyMT mice and was involved in the analysis of murine tissues. M.P., U.A., R.Y.H.L. and C-A.S. wrote the paper. All authors discussed the results and commented on the manuscript.

Additional information

Supplementary information is available in the online version of the paper. Reprints and permission information is available online at http://www.nature.com/reprints. Correspondence and requests for materials should be addressed to R.Y.H.L.

Competing financial interests

The University of Basel has filed patents on the technology and intellectual property related to this work based on the inventions of M.P., M.L. and R.Y.H.L.

nature nanotechnology

SUPPLEMENTARY INFORMATION

DOI: 10.1038/NNANO.2012.167

The nanomechanical signature of breast cancer

Marija Plodinec, Marko Loparic[†], Christophe A. Monnier[†], Ellen C. Obermann[†], Rosanna Zanetti-Dallenbach[†], Philipp Oertle, Janne T. Hyotyla, Ueli Aebi, Mohamed Bentires-Alj, Roderick Y. H. Lim* and Cora-Ann Schoenenberger

* Correspondence to: roderick.lim@unibas.ch

† These authors contributed equally to this work.

Supplementary Methods

Oliver and Pharr analysis. Software was developed in LABVIEW (National Instruments, USA) for the automated analysis of force-volume data. The contact point was determined by applying a polynomial fit to raw force curves according to a published algorithm[1]. Force-indentation data was obtained by the indentation h, which corresponds to the difference between piezo displacement and cantilever deflection, and by multiplying the cantilever deflection d with the spring constant k to obtain load F. The slope of each data point is calculated by performing a linear fit to the upper 50 % of the unloading force curve (i.e., between 0.9 nN and 1.8 nN). This is because the loading curves represent both plastic and elastic deformation that cannot be distinguished, whereas the unloading curves denote the (visco)-elastic recovery of the material when the load is released[2, 3]. Slope values were spatially plotted to yield a stiffness map using Igor Pro (Wavemetrics, USA). Gaussian distributions were computed from the individual stiffness values. The mean slope value from the Gaussian fit was then used for calculating the elastic modulus (E_s) according to Oliver and Pharr theory[3] as applied by Plodinec, Loparic and coworkers[4-6] in the following manner:

In Equation (1), E_r represents the measured relative dynamic elastic modulus, E_s is the elastic modulus of the sample and E_i of the indenter

$$\frac{1}{E_r} = \frac{1-\upsilon_s^{\ 2}}{E_s} + \frac{1-\upsilon_i^2}{E_i} \tag{1}$$

where υ_s and υ_i are Poisson's ratios of sample and indenter. Assuming that the elastic modulus of biological specimens is orders of magnitude smaller than that of the indenter ($E_i >> E_s$), equation (1) reduces to

$$\frac{1}{E_r} \cong \frac{1-\upsilon_s^2}{E_s} \tag{2}$$

The Poisson's ratio of soft tissues is assumed to be $\upsilon_s = 0.5$[7-9]. The stiffness of the sample S is defined as the linear fit between the maximum load $F_2 = 1.8$ nN and the minimum load $F_1 = 0.9$ nN (3). The indentation depth is denoted by h.

$$S = \left[\frac{\Delta p}{\Delta h}\right]_{F_1}^{F_2} = \left[\frac{\Delta d \times k}{\Delta h}\right]_{d_1}^{d_2} \tag{3}$$

Subsequently, the relative elastic modulus E_r is defined by the following equation:

$$E_r = \frac{\sqrt{\pi}}{2}\frac{S}{\sqrt{A_c(h_c)}} \tag{4}$$

where $A_c(h_c)$ is the projection of the contact area as a function of the tip angle (Θ) and the contact indentation depth h_c. Assuming h_c to correspond to the total depth of indentation h yields the following relation for a 4-sided pyramidal tip

$$A_c(h_c) = (2h \tan\Theta)^2 \qquad (5)$$

By combining equations (2), (3), (4) and (5) the elastic modulus of the sample E_s can be calculated:

$$E_s = \frac{\sqrt{\pi}}{2}\left(1-\upsilon_s^2\right)\frac{1}{\sqrt{A_c(h_c)}}\left[\frac{\Delta d \times k}{\Delta h}\right]_{d_1}^{d_2} \qquad (6)$$

Automated levelling. We developed a method to compensate for the limited Z piezo working range (~10 µm) during AFM indentation testing of the biopsies. Often, large height variations on the biopsy surface can exceed this limit thereby restricting measurements and causing errors during force (i.e., stiffness) mapping (where sequential force measurements are obtained within a specific area). To overcome this problem, our method consists of a vertical alignment system, which activates three external step motors to lift or lower the AFM scanner assembly (the so-called "head") in a step-wise manner whenever the Z piezo reaches its limit (i.e., max. extension or max. retraction). In this manner, our method allows for AFM force mapping to proceed uninterrupted and error-free over corrugated surfaces.

Scanning electron microscopy (SEM). Human breast biopsies were transferred to Ringer solution after removal and processed for SEM without delay and in accordance with a previously published protocol[10]. Samples were fixed in 2.5% formaldehyde/2.5% glutaraldehyde (Electron Microscopy Sciences) in 0.1 M sodium cacodylate buffer (Electron Microscopy Sciences) for 1 hr at room temperature (RT), after which samples were placed in fresh fixative and incubated overnight at 4°C. Samples were then washed in cacodylate buffer and postfixed in 1.5% osmium tetroxide (Electron Microscopy Sciences) at RT for 1.5 hrs. Samples were again washed in buffered solution and dehydrated in a graded ethanol series. After critical point drying, samples were sputter-coated with platinum to a nominal thickness of 3–5 nm and examined with a Hitachi S4800 FEG scanning electron microscope at 5 kV accelerating voltage.

Isolation of RNA. Total RNA was isolated post-AFM from normal murine mammary glands after 3 days of storage in Ringer solution supplemented with glucose and a protease inhibitor cocktail (Complete, Boehringer Mannheim; 1 tablet per 10 ml) at 4ºC and from fresh control glands. After the homogenization of the glands in Qiazol (Qiagen Inc) using a tissue homogenizer (Retsch MM301, Haan), total RNA was isolated using miRNeasy Mini Kit (Qiagen Inc.) according to the instructions of the manufacturer. Quantification of the isolated RNA was done by NanoDrop ND-1000 Spectrophotometer (NanoDrop Technologies). The RNA integrity was assessed using the RNA Nano 6000 Chip on 2100 Bioanalyzer (Agilent Technologies and Bioanalysis Systems). The gel-like image generated by the Bioanalyzer software was used to display RNA quality (see Supplementary Fig. S9b).

Supplementary figure legends

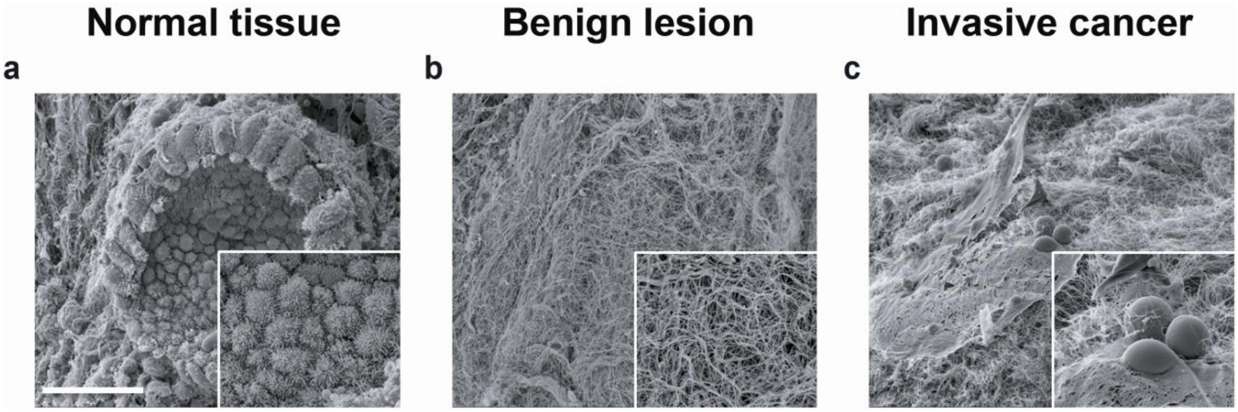

Supplementary Fig. S1. Scanning electron microscopy reveals the surface structure of human breast biopsies. a, SEM image of a normal duct shows uniform cellular organization of intact epithelial cells surrounded by myoepithelial cells. Zooming in reveals submicron brushes on the surface of the epithelial layer (inset). **b,** SEM image of the benign lesion (fibroadenoma) reveals a pronounced collagen meshwork. Higher magnification reveals collagen bundles that vary in thickness and banding pattern (inset). **c,** SEM image of an invasive cancer biopsy showing a lack of structural organization. Individual cancer cells are embedded in the extracellular matrix. Scale bar, 20 μm, insets are 4.5× magnified.

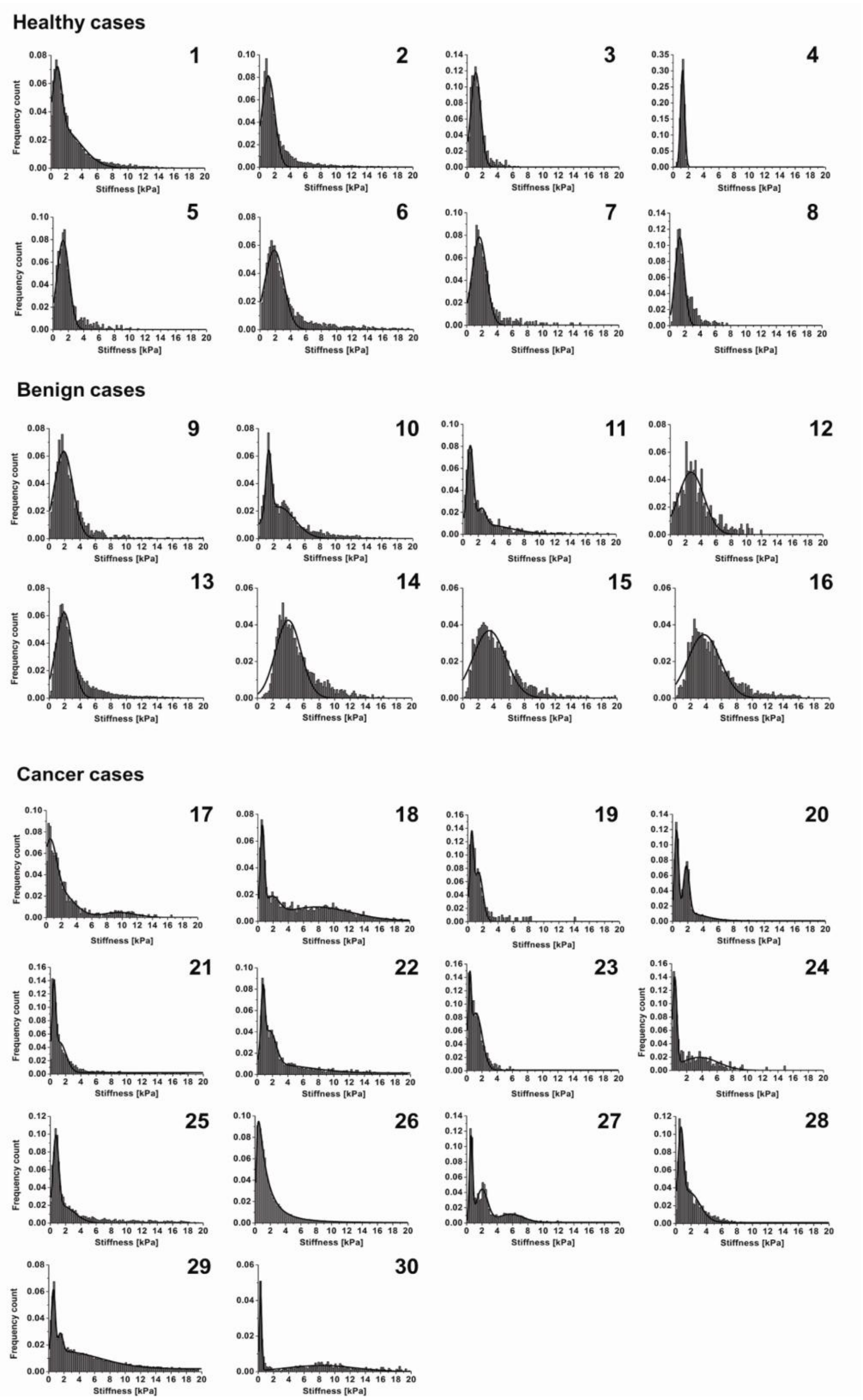
Healthy cases
1
2
3
4
5
6
7
8
Benign cases
9
10
11
12
13
14
15
16
Cancer cases
17
18
19
20
21
22
23
24
25
26
27
28
29
30
Frequency count
Stiffness [kPa]

Supplementary Fig. S2. Biopsy-wide histograms show the stiffness distributions for all human biopsies tested. The counts in each histogram are normalized to the total amount of measured data points per patient biopsy as listed in Supplementary Table S1. The nanomechanical signature of healthy breast tissue is characterized by a unimodal distribution with peak stiffness from 1.13 to 1.83 kPa. In benign lesions, the stiffness distribution is also uniform although it should be noted that stiffness values in fibroadenomas range from 1.91 to 3.68 kPa (cases 12-16). In case 12, there was a high abundance of fibroblasts within the mass of fibrotic tissue, which is reflected in the lower stiffness value (1.91 ± 0.99 kPa). In case 9, the similarity in stiffness to healthy breast biopsies results from the presence of usual ductal hyperplasia (UDH) as shown by pathohistological diagnosis (PHD). In cases 10 and 11, the biopsy-wide distribution revealed two peaks: "peak 1" (1.33 ± 0.32 kPa and 0.95 ± 0.20 kPa, respectively) that corresponds to the stiffness of normal breast tissue, and "peak 2" (2.63 ± 2.06 kPa and 2.45 ± 0.26 kPa, respectively) that falls within the range of fibroadenoma. Consistent with this notion, PHD of case 10 revealed a segment of UDH, in addition to fibroadenoma. Following treatment for invasive ductal carcinoma, the biopsy of patient 11 displayed seemingly normal ducts and fibrosis that resulted in two stiffness peaks. All fourteen biopsies with cancer shared a stiffness profile with a dominant peak at 0.31 to 0.75 kPa. The signature of cancer includes a second peak between 1.54 and 1.99 kPa accompanied by a broad distribution up to ~ 20 kPa.

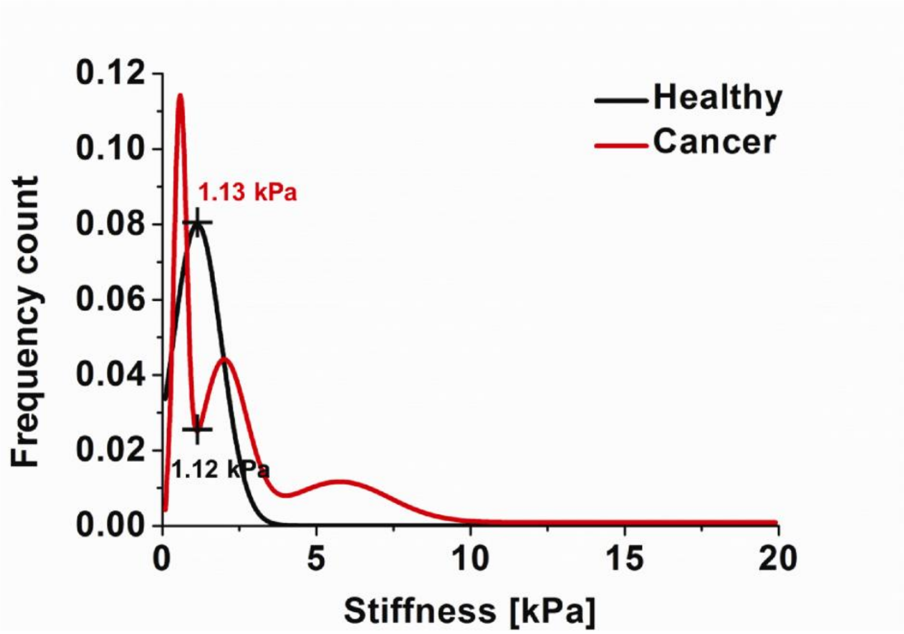

Supplementary Fig. S3. Inverse stiffness correlation between healthy and cancer biopsies. Comparison of healthy and cancer stiffness profiles reveals an inverse correlation between the two.

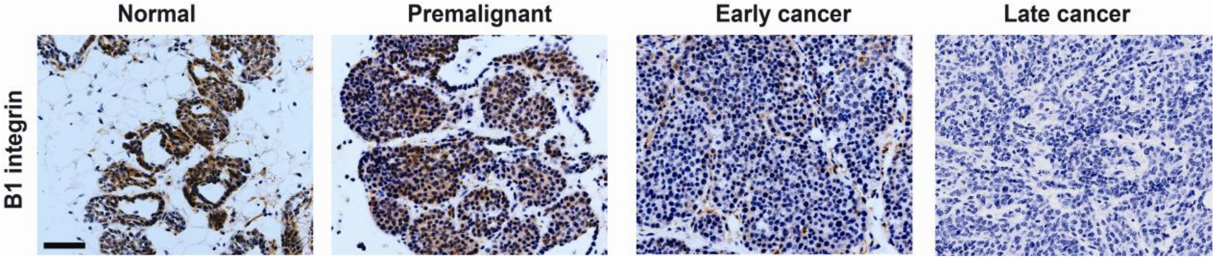

Supplementary Fig. S4. β1-integrin expression as histological marker for tumour progression in MMTV-PyMT mice. Glandular epithelial cells in normal and premalignant tissues stain positive for integrin-β1**.** In early cancer, integrin-β1 staining is significantly reduced, while in late cancer it is no longer detected. Scale bar, 50 µm.

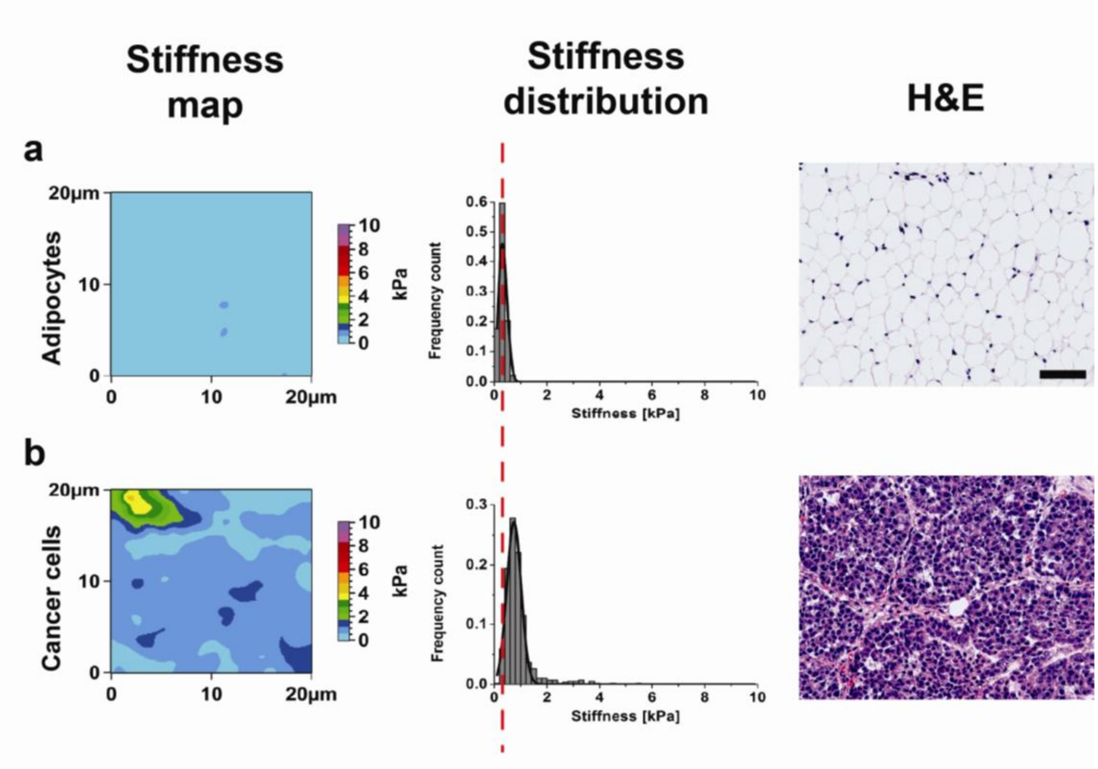

Supplementary Fig. S5. **Murine mammary adipocytes and cancer cells have different nanomechanical signatures. a,** In contrast to human breast tissues, healthy murine mammary glands exhibit extensive amounts of adipose tissue (70-80%). Adipocytes are typically larger than cancer cells. Stiffness maps of mammary gland fat pads devoid of epithelium are homogeneously soft. The corresponding histogram shows a narrow distribution with a mean stiffness value of 0.31 ± 0.13 kPa. In H&E-stained sections, adipocytes can be discerned from all other cell types based on their uniform morphology. **b,** Stiffness maps in areas with sheets of cancer cells exhibit stiffer features with a wider distribution that is spread over a mean stiffness of 0.75 ± 0.25 kPa. The difference between the peak stiffness values of adipose and cancer cells in native tissues is highlighted by the red dashed line. Besides being approximately one third softer than cancer cells, adipocytes can also be discerned by their strong adhesion to AFM tips. Scale bar, 50 µm.

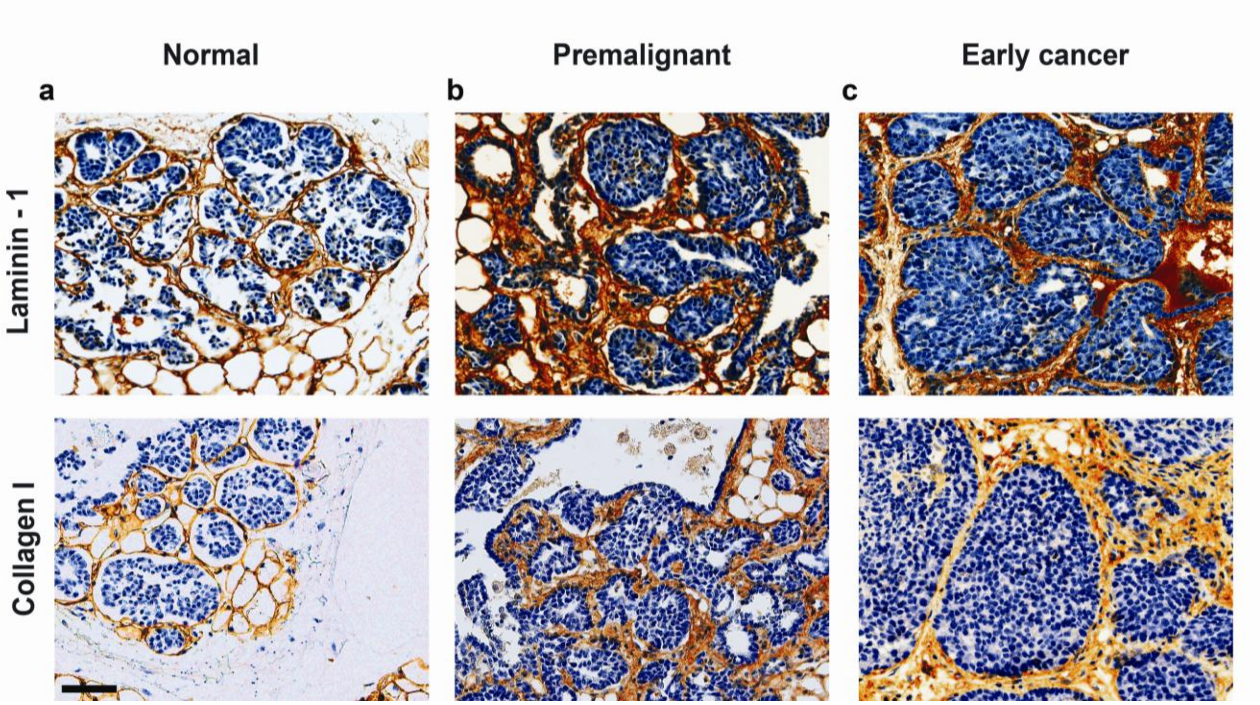

Supplementary Fig. S6. Changes in the organization of extracellular matrix components at varying stages of cancer progression in MMTV-PyMT mice. a, In normal glandular tissue, laminin-1 staining is continuous and circumscribes the epithelium (top) while collagen I is restricted to stromal tissue (bottom). **b,** Laminin-1 staining is detected in the basement membrane of premalignant lesions (top). Collagen I staining is more pronounced indicating an increase of stromal tissue (bottom). **c,** Laminin-1 staining of early cancer reveals that cancer cells remain within the border of the basement membrane that is starting to disintegrate. Collagen I staining is increased in the adjacent tumour stroma. Scale bar, 50 µm.

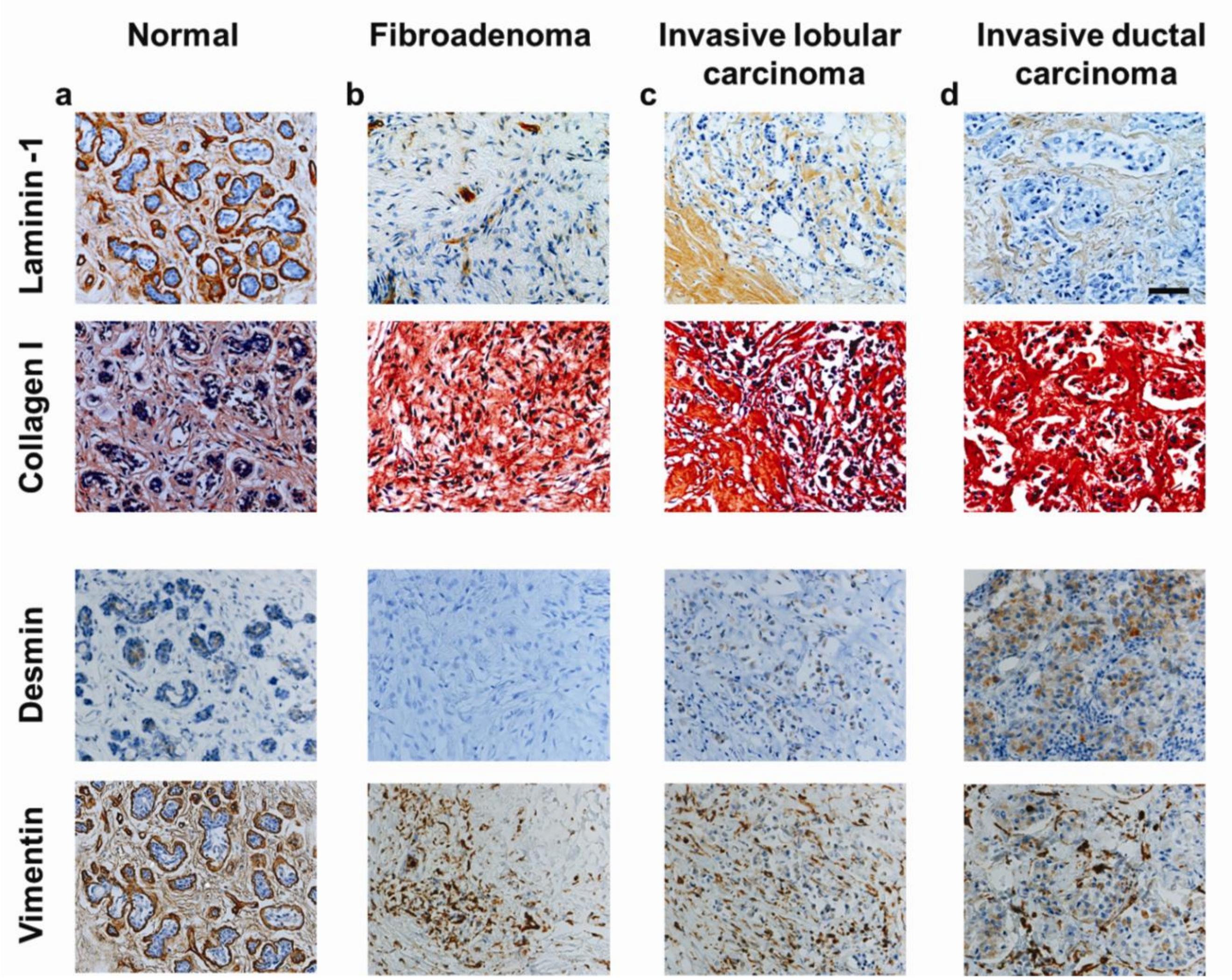

Supplementary Fig. S7. Structural changes in extracellular matrix and cytoarchitecture of human biopsies. The indications that the stiffness profiles of different tumour stages are based on distinct changes in the cytoarchitecture and ECM in MMTV-PyMT transgenic mice prompted us to follow up on this correlation in human breast cancer biopsies. **a,** In normal breast biopsies, laminin-1 delineates healthy ducts from the surrounding ECM (left). Collagen I staining is localized to the stroma adjacent to the ducts. Desmin expression is restricted to the myoepithelium, while vimentin labeling is associated with stromal components i.e., mesenchymal cells. **b,** In the benign lesion (fibroadenoma), laminin-1 staining is limited to a few blood capillaries and collagen I is prominent across the entire section. The fibroadenoma is negative for desmin, while the vimentin staining is limited to blood capillaries and shows a marked expression in fibroblasts. In contrast, the biopsies of invasive lobular and invasive ductal carcinomas largely exhibit disorganized laminin-1, which indicates loss of epithelial polarity that is typically associated with malignancy and invasiveness. **c,** In invasive lobular carcinoma, laminin-1 staining is irregular with a partially preserved structural organization. The tumour is not confined, and expression of collagen I is heterogeneous. A large number of malignant cells stain positive for desmin and vimentin. **d,** In the invasive ductal carcinoma, areas with mostly tumour cells and infiltrating macrophages are largely devoid of laminin-1 and collagen I, whereas tumour stroma exhibits strong collagen I staining with an irregular structure. Desmin and vimentin staining is not only strong in the stroma but also in the cancer epithelium. Scale bar, 50 µm.

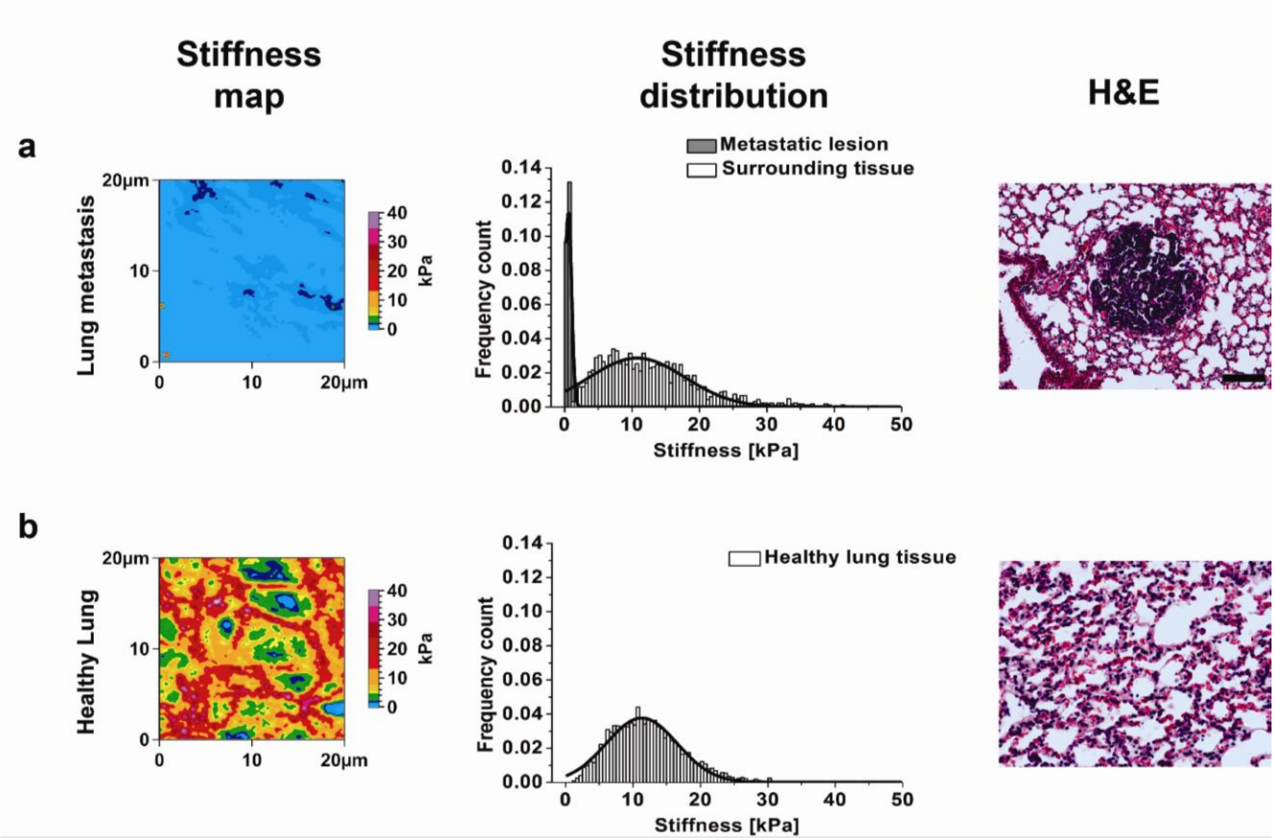

Supplementary Fig. S8. Stiffness profiles of murine lungs reveal a distinct soft phenotype in metastatic lesions. a, Representative AFM stiffness map visualizing the softness of a metastatic lesion in the lung. The biopsy-wide stiffness profile across the entire specimen reveals distinct mechanical phenotypes for the metastasis and the surrounding lung tissue. Histopathological analysis shows the location of a metastatic cluster within seemingly normal alveolar structures. **b,** Representative AFM stiffness map and the biopsy-wide stiffness distribution of healthy lungs. Post-AFM histology reveals normal epithelial lung morphology. Scale bar, 50µm.

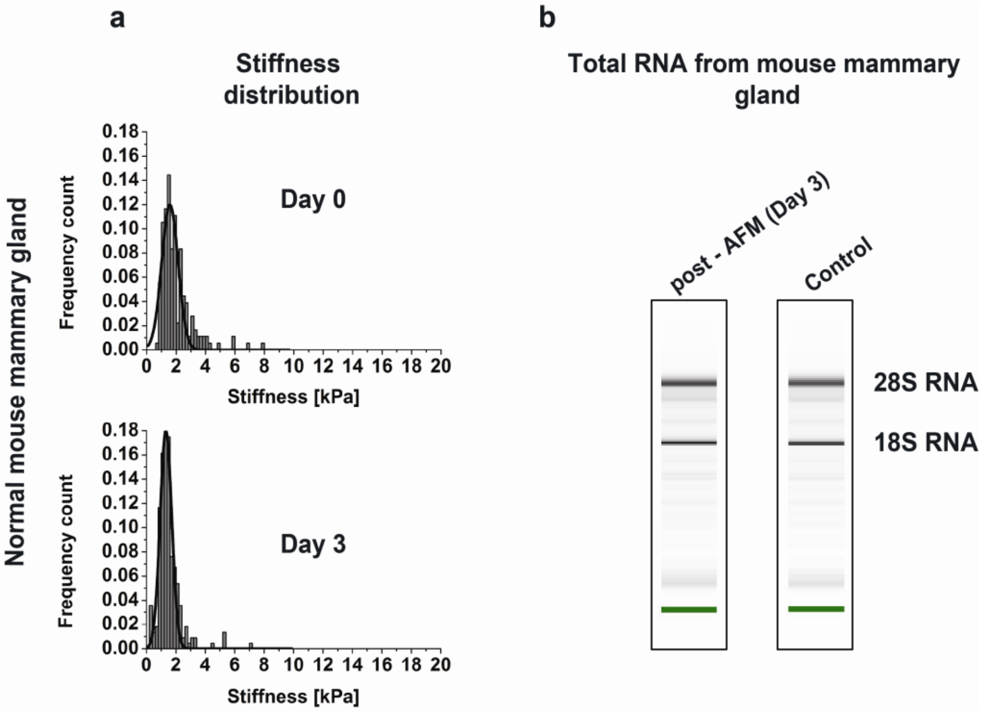

Supplementary Fig. S9. Nanomechanical profiles and RNA stability remain constant over 3 days. a, Stiffness profiles of a normal murine mammary gland recorded immediately after tissue excision (Day 0, top) are unaltered after storage for 3 days at 4°C in a Ringer solution containing protease inhibitors (Day 3, bottom). **b,** Comparison of total RNA extracted from the post-AFM specimen shown in (a) and from freshly excised control mammary glands reveals that the 3 day storage does not affect RNA stability as demonstrated by intact 28S and 18S RNA bands.

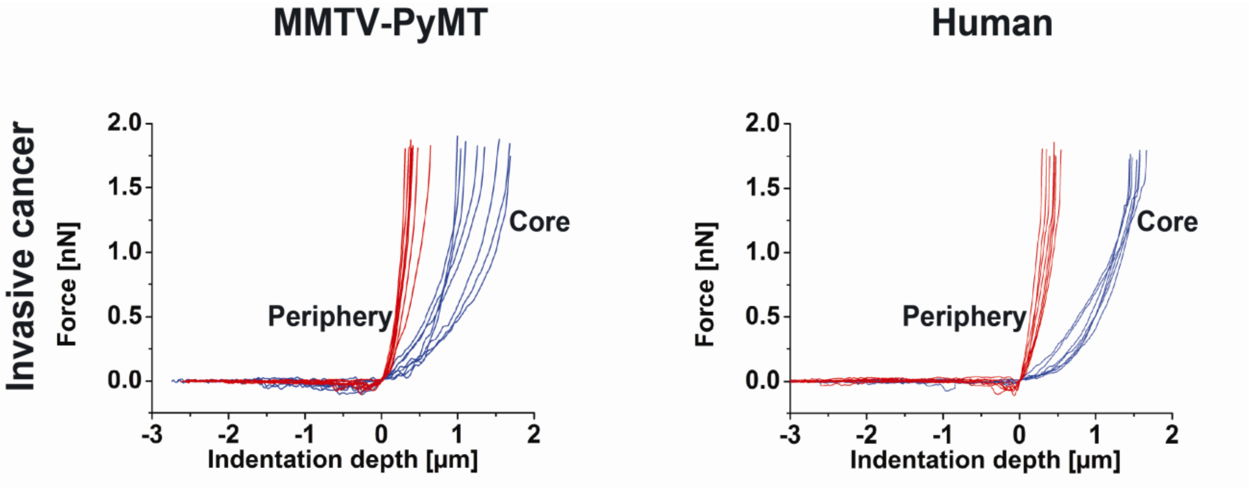

Supplementary Fig. S10. Examples of force curves from murine and human breast cancer biopsies. Representative force curves obtained from mouse and human biopsies with late invasive cancer reveal distinct force profiles that differ between the tumour core and periphery.

Supplementary Table S1. Nanomechanical analysis (Young's modulus *E*, mean ± SD) versus histopathology in different patients. (Note: The corresponding stiffness distributions are shown in Supplementary Fig. S2.)

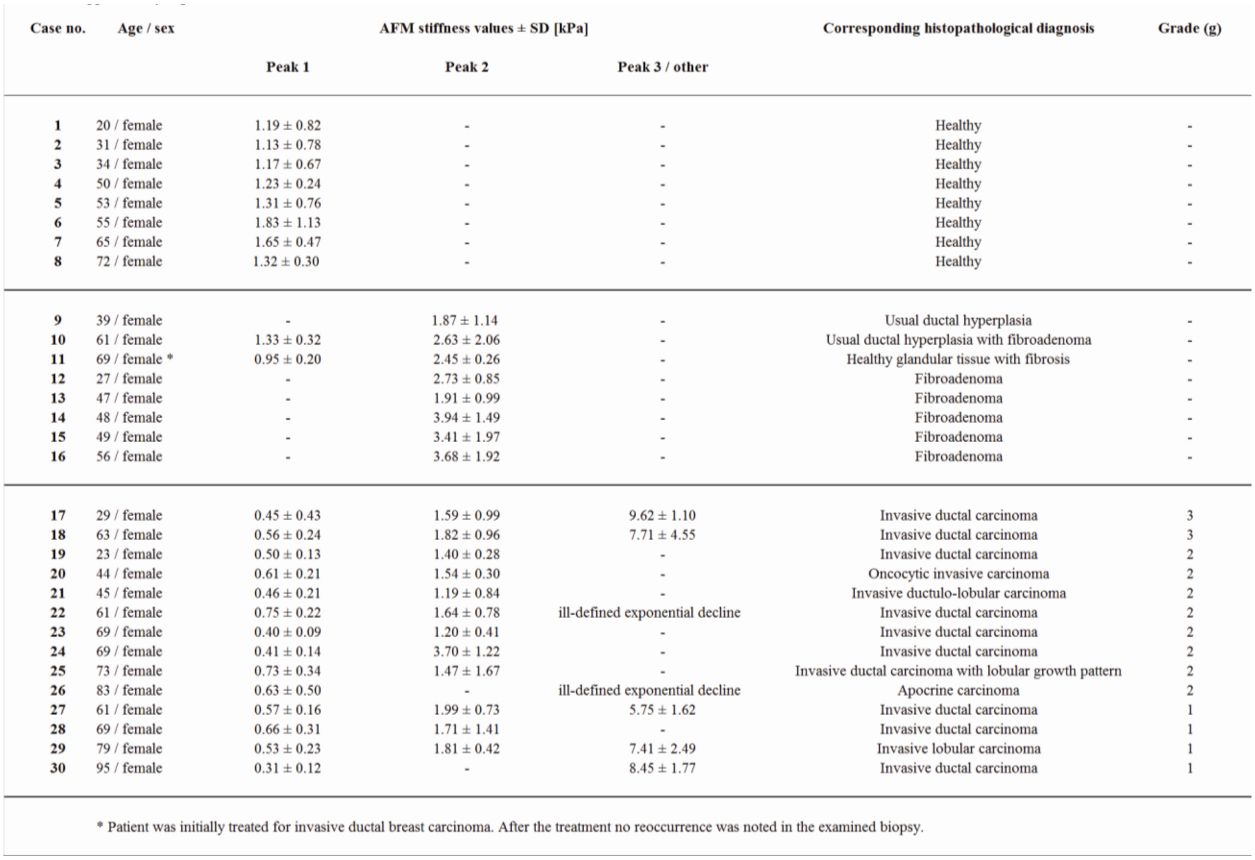

Case no.	Age / sex	AFM stiffness values ± SD [kPa]			Corresponding histopathological diagnosis	Grade (g)
		Peak 1	Peak 2	Peak 3 / other		
1	20 / female	1.19 ± 0.82	-	-	Healthy	-
2	31 / female	1.13 ± 0.78	-	-	Healthy	-
3	34 / female	1.17 ± 0.67	-	-	Healthy	-
4	50 / female	1.23 ± 0.24	-	-	Healthy	-
5	53 / female	1.31 ± 0.76	-	-	Healthy	-
6	55 / female	1.83 ± 1.13	-	-	Healthy	-
7	65 / female	1.65 ± 0.47	-	-	Healthy	-
8	72 / female	1.32 ± 0.30	-	-	Healthy	-
9	39 / female	-	1.87 ± 1.14	-	Usual ductal hyperplasia	-
10	61 / female	1.33 ± 0.32	2.63 ± 2.06	-	Usual ductal hyperplasia with fibroadenoma	-
11	69 / female *	0.95 ± 0.20	2.45 ± 0.26	-	Healthy glandular tissue with fibrosis	-
12	27 / female	-	2.73 ± 0.85	-	Fibroadenoma	-
13	47 / female	-	1.91 ± 0.99	-	Fibroadenoma	-
14	48 / female	-	3.94 ± 1.49	-	Fibroadenoma	-
15	49 / female	-	3.41 ± 1.97	-	Fibroadenoma	-
16	56 / female	-	3.68 ± 1.92	-	Fibroadenoma	-
17	29 / female	0.45 ± 0.43	1.59 ± 0.99	9.62 ± 1.10	Invasive ductal carcinoma	3
18	63 / female	0.56 ± 0.24	1.82 ± 0.96	7.71 ± 4.55	Invasive ductal carcinoma	3
19	23 / female	0.50 ± 0.13	1.40 ± 0.28	-	Invasive ductal carcinoma	2
20	44 / female	0.61 ± 0.21	1.54 ± 0.30	-	Oncocytic invasive carcinoma	2
21	45 / female	0.46 ± 0.21	1.19 ± 0.84	-	Invasive ductulo-lobular carcinoma	2
22	61 / female	0.75 ± 0.22	1.64 ± 0.78	ill-defined exponential decline	Invasive ductal carcinoma	2
23	69 / female	0.40 ± 0.09	1.20 ± 0.41	-	Invasive ductal carcinoma	2
24	69 / female	0.41 ± 0.14	3.70 ± 1.22	-	Invasive ductal carcinoma	2
25	73 / female	0.73 ± 0.34	1.47 ± 1.67	-	Invasive ductal carcinoma with lobular growth pattern	2
26	83 / female	0.63 ± 0.50	-	ill-defined exponential decline	Apocrine carcinoma	2
27	61 / female	0.57 ± 0.16	1.99 ± 0.73	5.75 ± 1.62	Invasive ductal carcinoma	1
28	69 / female	0.66 ± 0.31	1.71 ± 1.41	-	Invasive ductal carcinoma	1
29	79 / female	0.53 ± 0.23	1.81 ± 0.42	7.41 ± 2.49	Invasive lobular carcinoma	1
30	95 / female	0.31 ± 0.12	-	8.45 ± 1.77	Invasive ductal carcinoma	1

* Patient was initially treated for invasive ductal breast carcinoma. After the treatment no reoccurrence was noted in the examined biopsy.

Supplementary Table S2. Nanomechanical characterization of mammary gland tissue from MMTV-PyMT mice (Young's modulus *E*, mean ± SD) versus histopathological diagnosis.

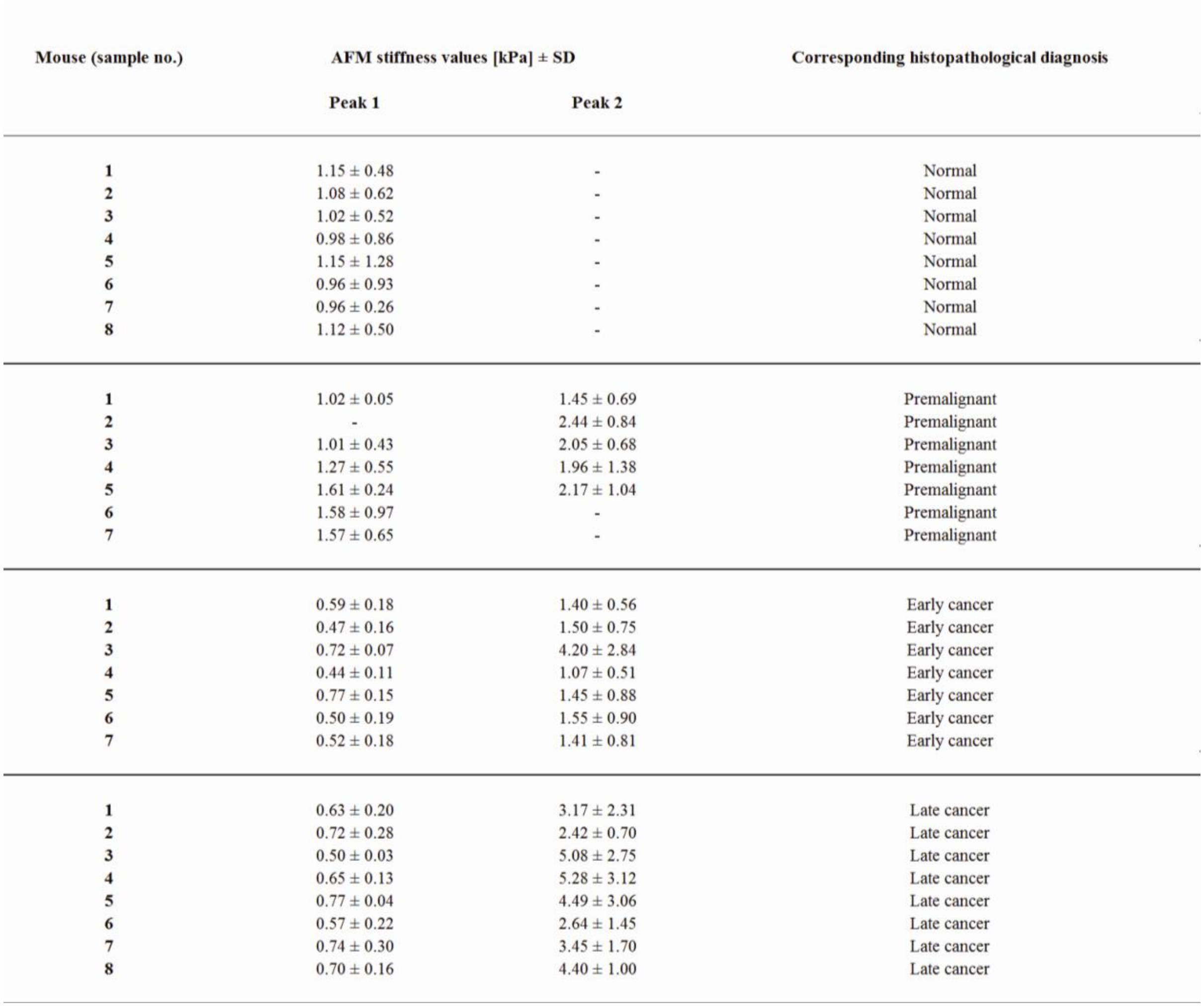

Mouse (sample no.)	AFM stiffness values [kPa] ± SD		Corresponding histopathological diagnosis
	Peak 1	Peak 2	
1	1.15 ± 0.48	-	Normal
2	1.08 ± 0.62	-	Normal
3	1.02 ± 0.52	-	Normal
4	0.98 ± 0.86	-	Normal
5	1.15 ± 1.28	-	Normal
6	0.96 ± 0.93	-	Normal
7	0.96 ± 0.26	-	Normal
8	1.12 ± 0.50	-	Normal
1	1.02 ± 0.05	1.45 ± 0.69	Premalignant
2	-	2.44 ± 0.84	Premalignant
3	1.01 ± 0.43	2.05 ± 0.68	Premalignant
4	1.27 ± 0.55	1.96 ± 1.38	Premalignant
5	1.61 ± 0.24	2.17 ± 1.04	Premalignant
6	1.58 ± 0.97	-	Premalignant
7	1.57 ± 0.65	-	Premalignant
1	0.59 ± 0.18	1.40 ± 0.56	Early cancer
2	0.47 ± 0.16	1.50 ± 0.75	Early cancer
3	0.72 ± 0.07	4.20 ± 2.84	Early cancer
4	0.44 ± 0.11	1.07 ± 0.51	Early cancer
5	0.77 ± 0.15	1.45 ± 0.88	Early cancer
6	0.50 ± 0.19	1.55 ± 0.90	Early cancer
7	0.52 ± 0.18	1.41 ± 0.81	Early cancer
1	0.63 ± 0.20	3.17 ± 2.31	Late cancer
2	0.72 ± 0.28	2.42 ± 0.70	Late cancer
3	0.50 ± 0.03	5.08 ± 2.75	Late cancer
4	0.65 ± 0.13	5.28 ± 3.12	Late cancer
5	0.77 ± 0.04	4.49 ± 3.06	Late cancer
6	0.57 ± 0.22	2.64 ± 1.45	Late cancer
7	0.74 ± 0.30	3.45 ± 1.70	Late cancer
8	0.70 ± 0.16	4.40 ± 1.00	Late cancer

Supplementary Table S3. Nanomechanical characterization of lung tissue from MMTV-PyMT mice (Young's modulus *E*, mean ± SD) versus histopathological diagnosis.

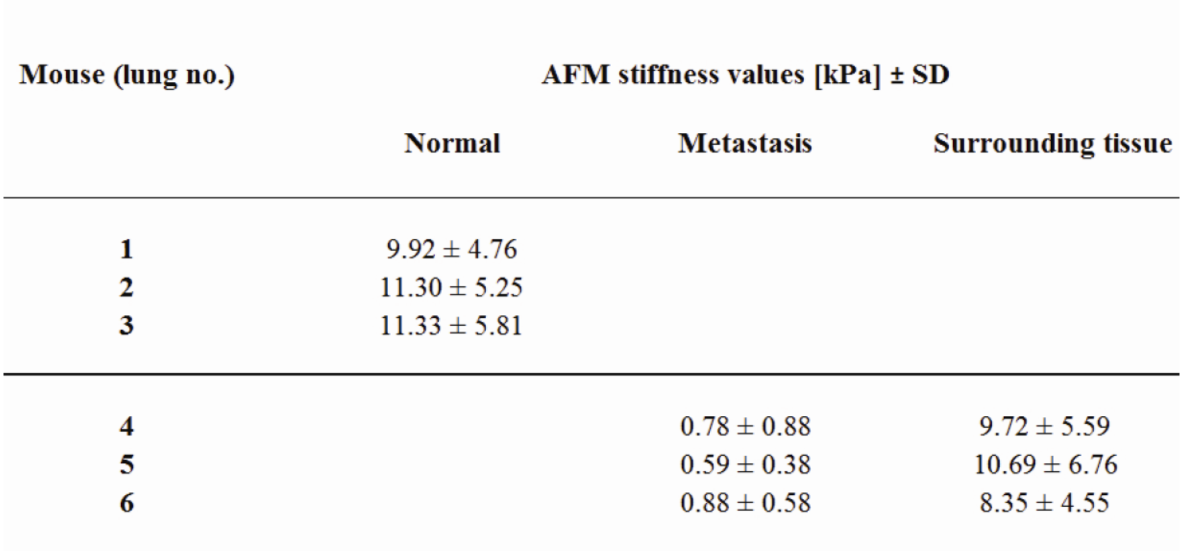

Mouse (lung no.)	AFM stiffness values [kPa] ± SD		
	Normal	Metastasis	Surrounding tissue
1	9.92 ± 4.76		
2	11.30 ± 5.25		
3	11.33 ± 5.81		
4		0.78 ± 0.88	9.72 ± 5.59
5		0.59 ± 0.38	10.69 ± 6.76
6		0.88 ± 0.58	8.35 ± 4.55

References:

1. Lin, D.C., Dmitriadis, E.K. & Horkay, F. Robust strategies for automated AFM force curve Analysis-II: Adhesion-influenced indentation of soft, elastic materials. *J Biomech Eng-T Asme* **129**, 904-912 (2007).
2. Hay, J.C., Bolshakov, A. & Pharr, G.M. A critical examination of the fundamental relations used in the analysis of nanoindentation data. *J Mater Res* **14**, 2296-2305 (1999).
3. Oliver, W.C. & Pharr, G.M. An Improved Technique for Determining Hardness and Elastic-Modulus Using Load and Displacement Sensing Indentation Experiments. *J Mater Res* **7**, 1564-1583 (1992).
4. Plodinec, M., Loparic, M. & Aebi, U. Atomic force microscopy for biological imaging and mechanical testing across length scales. *Cold Spring Harb Protoc* **2010**, pdb top86 (2010).
5. Loparic, M. et al. Micro- and Nanomechanical Analysis of Articular Cartilage by Indentation-Type Atomic Force Microscopy: Validation with a Gel-Microfiber Composite. *Biophysical Journal* **98**, 2731-2740 (2010).
6. Plodinec, M. et al. The nanomechanical properties of rat fibroblasts are modulated by interfering with the vimentin intermediate filament system. *J Struct Biol* **174**, 476-484 (2011).
7. Lekka, M. et al. Cancer cell detection in tissue sections using AFM. *Archives of Biochemistry and Biophysics* **518**, 151-156 (2012).
8. Stolz, M. et al. Early detection of aging cartilage and osteoarthritis in mice and patient samples using atomic force microscopy. *Nat Nanotechnol* **4**, 186-192 (2009).
9. Lopez, J.I., Kang, I., You, W.K., McDonald, D.M. & Weaver, V.M. In situ force mapping of mammary gland transformation. *Integr Biol. (Camb.)* **3**, 910-921 (2011).
10. Provenzano, P.P. et al. Collagen density promotes mammary tumour initiation and progression. *BMC Med* **6**, 11 (2008).

Acknowledgments

I would like to thank to prof. Ueli Aebi for recognizing my motivation for scientific work, for giving me the opportunity to do my PhD in his group and for his admirable support and patience throughout my PhD.

A big thank you goes to my supervisor PD. Dr. Cora-Ann Schoenenberger for the great support over the last two years since we worked together and for teaching me the wonders of cell biology.

Especially, a big hug goes to her for the enourmouse involvement over the last couple of weeks to help me finish this thesis on time. Thanks so much once again, this would not be possible without your tremendous effort.

I am very grateful to Prof. Harald Herrmann who kindly agreed to become Co-Referee, but even more for nice scientific discussions and help with the IF project.

I would like to thank to Prof. Roderick Lim for his motivation, support and many words of wisdom through my Phd. I am very much looking forward to our future project.

I am grateful to Prof. Martin Stolz for introducing me to the world of nanomechanical testing and helping me to start my experiments.

Many thanks to Sourabh Ghosh-very important person in my scientific life because he introduced me to the world of 3D tumor culture which has greatly influenced my scientific work.

Thanks to my dear Lab and Biozentrum friends: Vassiliki-my dear and close friend since I first came to Switzerland, the entire Lim group ….Especially I want to thank Janne, Kai and Bref for the chocolates, pizza, coins- the food and drinsk keept me going in the long working nights. Thanks to Unai, Rosie (thanks for all the help with my projects)….and to all the people that are not any more in the Biozentrum: Yvonne, David, Teba, Sofia. Ellie, Esther, Birthe, Laurent…..

I would also like to thank to all the collaborators for the greats support: Francine Wolf, Dr. Ellen Obermann, Dr. Rosanna Zanetti, Dr. Serenella Eppenberger, Dr. Momo Bentires-Alj, Prof. Ivan Martin and Prof. Giulio Spagnioli.

Thanks to Röbi Wyss, Ursula Sauder, Vesna Oivieri, Roland Buerki, Margit Jenny (computer and Liselotte Walti for their technical support.

Finally, a big thank you goes to my parents for their unlimited love and for giving me the opportunity for education. And for the end a special thank you to my husband - my partner at home and at work, my best friend and the love of my life. And last but not least, a big kiss goes to my daughter-my sweet little princes who spent a lot of evenings in the lab waiting for me or papa to finish some experiments.

Curriculum Vitae

MARIJA PLODINEC

Biozentrum and the Swiss Nanoscience Institute

University of Basel

Klingelbergstrasse 50-70, Basel, Switzerland

Phone number: + 41 61 267 2264

Fax: + 41 61 2672109

e-mail: marija.plodinec@unibas.ch

PERSONAL INFORMATION

Date of Birth: March 16, 1981

Place of Birth: Zagreb, Croatia

Nationality: Croatian

Marital Status: Married, two children

EDUCATION:

1987-1995 Elementary High School, Zagreb

1995-1999 Secondary High School, Zagreb

1999-2005 University of Zagreb, Faculty of Natural Sciences, Zagreb

2005-2010 PhD at the Biozentrum, Department of Structural Biology and Maurice Müller Institute, University of Basel, Basel, Switzerland

FELLOWSHIPS

2001-2003 Fellowship for talented students awarded by Croatian National Ministry of Education and Science

2004 -2005 Fellowship for undergraduate students for performing research in Switzerland awarded by Roche Research Foundation

HONOURS AND ACHIVEMENTS:

2004 Dean’s award from University of Zagreb for the research project:
Forest fires on Croatian islands Brac, Korcula and Rab as an example of
Self organized criticality (SOC) systems

2004 Young researcher award given by Croatian Physical Society

PUBLICATIONS:

Plodinec, M. and Schoenenberger, C. A. (2010). *Breast Cancer Res*, *12*(4), 308. **Spatial organization acts on cell signaling: how physical force contributes to the development of cancer**

Plodinec, M., M. Loparic, et al. (2011). J Struct Biol **174**(3): 476-484. **The nanomechanical properties of rat fibroblasts are modulated by interfering with the vimentin intermediate filament system.**

Plodinec, M., M. Loparic, et al. (2012). Nature Nanotechnology 7, 757-765 doi:10.1038/nnano.2012.167. **The nanomechanical signature of breast cancer.**

Plodinec M., Blache U., et al. *(in preparation).* **Morphology and cytoarchitecture regulate nanomechanical properties of tumor spheroids.**

BOOK CHAPTER:

Plodinec M., Loparic M., Aebi U. (2010). A Laboratory Manual 2nd ed., D.L.S. Robert D. Goldman, Editor. 2010, Cold Spring Harbor Laboratory Press. **Atomic-Force Microscopy for Biological Imaging and Mechanical Testing across Length Scales, in Live Cell Imaging**

PATENTS:

Plodinec M., Loparic M., Lim Roderick Y.H. (2011) (European patent pending-PCT/EP2011/072494). **Method for staging cancer progression by AFM.**

Plodinec M., Loparic M., Lim Roderick Y.H. (2011) (European patent pending-EP11193120.0). **Method, system and device for controlling an scanning probe microscope**

SCIENTIFIC MEETINGS

2002 International Conference for Physics Students (ICPS) in Budapest, Hungary – poster, oral presentation

2003 International Conference for Physics Students (ICPS) In Odense, Denmark- oral presentation

2003 Winter College on Biophotonics: Optical imaging and Manipulation of Molecules and Cells, Abdus Salam Institute, Trieste, Italy

2003 Course on Audition, Language and Communication, MIND and BRAIN III IN Dubrovnik, Croatia

2003 8th International Summer School on Biophysics: Supramolecular structure and function

2006 - 2007 Biovalley Science Days, Basel, Switzerland – poster

Biozentrum symposium, Basel, Switzerland – poster

2008 Biozentrum symposium, Basel, Switzerland – poster

First European Conference on Nanomedicine (CLINAM), Basel, Switzerland –

poster

Symposium of Structural Biology and Biophysics, Biozentrum, Basel,

Switzerland – oral presentation

Mechanisms and Models of Cancer, Cold Spring Harbor Laboratory, New York, USA – poster

Biozentrum symposium, Basel, Switzerland – oral presentation

2009 American Society for Cell Biology 49th Annual Meeting, San Diego, USA – poster presentation

ETH Zurich, Switzerland, Department of Materials – invited oral presentation

2010 Seeing at the Nanoscale VIII, Basel, Switzerland – oral presentation

2011 2nd "Physics of Cancer" International Symposium, Leipzig, Germany – poster presentation

2012 Symposium in honour of Prof. Ueli Aebi, Basel, Switzerland – oral presentation

2012 European Conference on Nanomedicine (CLINAM), Basel, Switzerland –

poster presentation

2012 "From Solid State to Biophysics", Dubrovnik, Croatia – invited oral presentation

2012 International Conference on Nanoscience and Nanotechnology (ICNT), Paris, France – selected for oral presentation

2012 3rd "Physics of Cancer" International Symposium, Leipzig, Germany – poster presentation

2012 American Society for Cell Biology 52th Annual Meeting, San Francisco, USA – poster presentation

INVOLVMENT IN RESEARCH PROJECTS

2008 - Swiss Nanoscience Institute Basel; Module 1 Nanobiology, Project 1.5 "Nanomechanical analysis of cancer cells and tissues"

2010 - 2012 Commission for Technology and Innovation – CTI Project 1977.2 PFNM-NM "ARTIDIS" (Automated and Reliable Tissue Diagnostic)

2012 - Commission for Technology and Innovation – CTI Project 14540.2 PFNM-NM "ARTIDIS+""ARTIDIS" (Automated and Reliable Tissue Diagnostic)

TEACHING EXPERIENCE

2005-2012 – Blockcourses: AFM in Biology II (winter and summer semester)

2008-2009 - Exercises: Methods in Structural Biology (winter semester)

2008-2012 - Supervising four Master thesis projects in Nanoscience and Structural Biology

LANGUAGES:

fluent in English, conversational German